Analysis and Control of Space Systems Dynamics via Floquet Theory, Normal Forms and Center Manifold Reduction

by

Peter Moses Bweya Waswa

A Dissertation Presented in Partial Fulfillment
of the Requirements for the Degree
Doctor of Philosophy

Approved October 2019 by the
Graduate Supervisory Committee:

Sangram Redkar, Chair
Bradley Rogers
Thomas Sugar

ARIZONA STATE UNIVERSITY

December 2019

ABSTRACT

It remains unquestionable that space-based technology is an indispensable component of modern daily lives. Success or failure of space missions is largely contingent upon the complex system analysis and design methodologies exerted in converting the initial idea into an elaborate functioning enterprise. It is for this reason that this dissertation seeks to contribute towards the search for simpler, efficacious and more reliable methodologies and tools that accurately model and analyze space systems dynamics. Inopportunely, despite the inimical physical hazards, space systems must endure a perturbing dynamical environment that persistently disorients spacecraft attitude, dislodges spacecraft from their designated orbital locations and compels spacecraft to follow undesired orbital trajectories. The ensuing dynamics' analytical models are complexly structured, consisting of parametrically excited nonlinear systems with external periodic excitations–whose analysis and control is not a trivial task. Therefore, this dissertation's objective is to overcome the limitations of traditional approaches (averaging and perturbation, linearization) commonly used to analyze and control such dynamics; and, further obtain more accurate closed-form analytical solutions in a lucid and broadly applicable manner. This dissertation hence implements a multi-faceted methodology that relies on Floquet theory, invariant center manifold reduction and normal forms simplification. At the heart of this approach is an intuitive system state augmentation technique that transforms non-autonomous nonlinear systems into autonomous ones. Two fitting representative types of space systems dynamics are investigated; *i)* attitude motion of a gravity gradient stabilized spacecraft in an eccentric orbit, *ii)* spacecraft motion in the vicinity of irregularly shaped small bodies. This investigation demonstrates how to analyze the motion stability, chaos, periodicity and resonance. Further, versal deformation of the normal forms scrutinizes the bifurcation behavior of the gravity gradient stabilized attitude motion. Control laws developed on

transformed, more tractable analytical models show that; unlike linear control laws, nonlinear control strategies such as sliding mode control and bifurcation control stabilize the intricate, unwieldy astrodynamics. The pitch attitude dynamics are stabilized; and, a regular periodic orbit realized in the vicinity of small irregularly shaped bodies. Importantly, the outcomes obtained are unconventionally realized as closed-form analytical solutions obtained via the comprehensive approach introduced by this dissertation.

DEDICATION

To Taraji Waswa.

Kadonye, may this dissertation inspire you to pursue advanced knowledge.

ACKNOWLEDGMENTS

I am very grateful to the advice, teaching, and encouragement that my advisor–Prof. Sangram Redkar graciously provided throughout this research. His insightful and knowledgeable mentoring is indispensable to the success of this research and my doctoral program as a whole. Our frequent interactions have indeed deepened my understanding of nonlinear dynamics. I am also thankful to the following members of my committee for their time and suggestions to improve my dissertation research: Prof. Bradley Rogers and Prof. Thomas Sugar. I thank Prof. Arunachala M. Kannan as well for his time and suggestions to enhance this dissertation.

In addition, I am grateful for all the assistance I received from the Ira A. Fulton Schools of Engineering at the Arizona State University Polytechnic campus. I thank the program chair, Prof. John Rajadas, the staff and all the students in the department that I interacted with.

I am also grateful to the co-chair of ASU Interplanetary Initiative, Prof. Linda Elkins-Tanton and all the staff of Interplanetary Initiative through the School of Earth and Space Exploration for supporting our research efforts.

I most graciously acknowledge the wisdom, guidance and encouragement rendered to me by my mentor, colleague and friend–the late Prof. Calestous Juma of Harvard Kennedy School. Our interactions immensely shepherded my advanced scholarly pursuits.

Finally, I would like to thank all my family, friends and especially my parents for their continued support and prayers throughout my academic pursuits. I dedicate this dissertation to my daughter.

TABLE OF CONTENTS

Page

LIST OF TABLES x

LIST OF FIGURES xi

NOMENCLATURE xiv

PREFACE xvi

CHAPTER

1 INTRODUCTION 1

1.1 Motivation 1

1.2 Parametrically Excited Nonlinear Spacecraft Dynamics With Periodic External Excitation 7

1.2.1 Attitude Motion of a Gravity Gradient Stabilized Spacecraft in an Eccentric Orbit 7

1.2.2 Spacecraft Dynamics in the Vicinity of Irregularly Shaped Small Bodies 8

1.3 Dissertation Scope and Overview 10

2 METHOD OF ANALYSIS 15

2.1 Floquet Theory 18

2.2 Computation of Lyapunov-Floquet Transformation Matrix via Chebyshev Polynomials 21

2.3 Normal Forms 23

2.3.1 Time Independent Normal Form (TINF) 25

2.3.2 Time Dependent Normal Form (TDNF) 27

2.4 Center Manifold Reduction 30

2.4.1 Time Periodic Center Manifold Reduction 32

CHAPTER Page

2.4.2 Constant Coefficients Center Manifold Reduction 36
2.5 Analysis of Nonlinear Systems With External Periodic Excitation... 36
2.5.1 Normal Forms of Nonlinear Systems with External Periodic Excitation 37
2.5.1.1 Systems with Constant Coefficients 39
2.5.1.2 Systems with Periodic Coefficients..... 42
2.5.2 Illustrative Normal Forms Application 43
2.5.2.1 Forced Nonlinear Systems With Constant Coefficients 43
2.5.2.2 Forced Nonlinear Systems With Periodic Coefficients 49
2.5.3 Center Manifold Reduction of Nonlinear Systems with External Periodic Excitation 53
2.5.3.1 Systems with Periodic Coefficients..... 56
2.5.3.2 Systems with Constant Coefficients 59
2.5.4 Illustrative Center Manifold Reduction Application Cases . 60
2.5.4.1 Systems With Periodic Coefficients 60
2.5.4.2 Systems With Constant Coefficients 64
2.6 Summary and Discussion 70
3 GRAVITY GRADIENT ATTITUDE STABILIZATION IN ECCENTRIC ORBIT 76
3.1 Dynamical Model Development 76
3.2 Implicit Time History Analysis 79
3.3 Stability and Chaos 82
3.3.1 Floquet Multipliers and Exponents 84
3.3.2 Poincaré Map 85

CHAPTER Page

3.3.3 Chaos 86
3.3.4 Lyapunov Exponents 86
3.3.5 Stability Charts 88
3.4 Resonance 91
3.5 Versal Deformation of the Normal Form and Bifurcation Analysis . 92
3.5.1 State Augmented System 93
3.5.2 L-F Transformed System 97
3.6 Summary and Discussion 106
4 CONTROL OF GRAVITY GRADIENT STABILIZED ATTITUDE MOTION 108
4.1 Lyapunov-Floquet Transformation 109
4.2 Linear Control 112
4.2.1 State Augmented System 112
4.2.2 L-F transformed System 113
4.3 Nonlinear Control 115
4.3.1 Sliding Mode Control 115
4.3.1.1 State Augmented System 116
4.3.1.2 L-F Transformed System 119
4.3.2 Bifurcation Control 121
4.3.2.1 State Augmented System 123
4.3.2.2 L-F Transformed System 126
4.4 Summary and Discussion 130
5 MOTION IN THE VICINITY OF IRREGULARLY SHAPED SMALL BODIES 134

CHAPTER Page

5.1 Gravitational Potential Models 135
5.1.1 Spherical Harmonics Models 136
5.1.1.1 Types of Spherical Harmonics 138
5.1.1.2 A Simple Harmonic Model 139
5.1.2 Ellipsoidal Harmonics Models 142
5.1.3 Polyhedron Models 143
5.1.4 Other Gravity Field Representations 146
5.2 Dynamical Model Development 147
5.3 Motion Analysis: A case for Asteroid 4179 Toutatis 150
5.3.1 Time History Analysis 158
5.3.2 Stability 163
5.3.2.1 Floquet Multipliers and Exponents 163
5.3.3 Chaos 165
5.3.4 Poincaré Map 165
5.4 Summary and Discussion 166
6 CONTROL OF MOTION IN THE VICINITY OF SMALL IRREGULARLY SHAPED BODIES 170
6.1 Lyapunov-Floquet Transformation 171
6.2 Center Manifold Reduction 174
6.3 Normal Forms Simplification 178
6.4 Nonlinear Control and Periodic Orbit Realization 179
6.5 Summary and Discussion 185
7 CONCLUSIONS AND FUTURE DIRECTIONS 187
7.1 Summary and Contributions 187

CHAPTER Page

7.1.1 Part I: Gravity Gradient Attitude Motion 192

7.1.2 Part II: Motion in the Vicinity of Small Irregularly Shaped Bodies 193

7.2 Future Research Directions 194

REFERENCES 196

APPENDIX

A DETAILED EQUATIONS OF ILLUSTRATIVE EXAMPLE CASES .. 210

B DETAILED EQUATIONS OF THE ISSB MOTION ANALYSIS 215

INDEX 237

LIST OF TABLES

Table Page

1. Stability of Representative $e - \sigma$ Pairs 90

2. Toutatis Orbital Parameters (Courtesy NASA-JPL) 154

3. Periodic Variation of Toutatis Angular velocity Amplitude. 156

LIST OF FIGURES

Figure		Page
1.	Dissertation Road-map	14
2.	Motion Analysis Sequence	16
3.	Motion Analysis and Control Law Development Sequence	17
4.	State Response Comparison for Nonresonant Excitation Case	46
5.	State Response Comparison for Superharmonic Excitation Case	48
6.	State Response Comparison for Subharmonic Excitation Case	50
7.	State Response Comparison for Mathieu-Duffing System	54
8.	Periodic System State Response Comparison	63
9.	Periodic System Phase Portrait	64
10.	2-dof Spring-Mass-Damper System	64
11.	Spring-Mass-Damper System State Response Comparison	68
12.	Spring-Mass-Damper System State Response Comparison	69
13.	Spring-Mass-Damper System State Response Comparison	70
14.	Gravity Gradient Stabilization	77
15.	State Response of the Motion in Original Coordinates	80
16.	State Response of Augmented States System	82
17.	Floquet Multipliers Location	85
18.	Poincaré Section of the Attitude Motion	85
19.	Chaos: Attitude Motion Sensitivity to Initial Conditions	87
20.	Dynamics of Lyapunov Exponents for the Attitude Motion	88
21.	Stability Chart of the Attitude Motion	89
22.	Resonance in Linear and Forcing Terms	91
23.	Poincaré Map of State Augmented Motion Post-Bifurcation Behavior	97

Figure Page

24.L-F Transformed System Implicit Time History Response 98

25.Plot of Elements of the LFT Matrix and Its Inverse 99

26.Augmented System States 99

27.Plot of Elements of the Second LFT Matrix and Its Inverse 102

28.Poincaré Map of L-F Transformed Motion Post-Bifurcation Behavior 105

29.Uncontrolled Attitude Motion 108

30.Linear Control of L-F Transformed State 114

31.Sliding Mode Controlled Actual and Augmented States 118

32.Sliding Mode Controlled States in L-F Transformed Coordinates 121

33.Sliding Mode Controlled States in Original Coordinates 122

34.Uncontrolled Dynamics of the Normalized State Augmented System 124

35.Dynamics of the Bifurcation Controlled State Augmented System 126

36.Dynamics of the Normalized L-F Transformed System 127

37.Back Transformed Normalized Augmented States 128

38.State Response of the Bifurcation Controlled L-F Transformed System 129

39.Preserved Locations of Floquet Multipliers After Bifurcation Control 129

40.Types of Spherical Harmonics: (a) Zonal, (b) Tesseral, and (c) Sectorial (Courtesy MathWorks ®) 139

41.The Reference Sphere and Ellipsoid About Asteroid 4769 Castalia. *(A)* Reference Sphere of Spherical Harmonics.*(B)* Reference Ellipsoid of Ellipsoidal Harmonics (Courtesy: [117]) 143

42.Polyhedron Faces Denoting the Edges, Vertices and Normal Vectors 145

43.Periodic Variation of the Small Body Angular Velocity 151

44.Toutatis Orbit Around the Sun (Courtesy Dominic Ford) 154

Figure Page
45.Toutatis Shape and Coordinate Axes 155
46.States Time-History Responses in the Vicinity of Toutatis 158
47.States Time-History Responses in the Vicinity of Toutatis 159
48.States Time-History Responses in the Vicinity of Toutatis 160
49.States Time-History Responses in the Vicinity of Toutatis 160
50.Phase Portraits of the Motion in the Vicinity of Toutatis 161
51.3-Dimension View of Orbital Motion in the Vicinity of the Small Irregularly Shaped Body 162
52.Additional Elevations of the Orbit Configuration in the Vicinity of the Small Irregularly Shaped Body–Toutatis 163
53.Floquet Multipliers Location for the Uncontrolled Dynamics in the Vicinity of Toutatis 164
54.Chaos: Motion Insensitivity to Initial Conditions 166
55.Poincaré Sections of the Motion in the Vicinity of ISSB 167
56.Motion Analysis and Control Law Development Sequence 171
57.Plot of Half of the Elements of LFT Matrix 175
58.Plot of the Remaining Half of the Elements of LFT Matrix 176
59.Controlled States Responses in the Vicinity of Toutatis 182
60.Controlled States Responses in the Vicinity of Toutatis 183
61.3-Dimension View of Orbital Motion in the Vicinity of the Small Irregularly Shaped Body 183
62.Additional View Angle of the Orbit Shape in the Vicinity of Toutatis 184
63.Additional View Angle and Elevation of the Orbit Shape in the Vicinity of Toutatis 184

NOMENCLATURE

AU	=	astronomical unit, $149,597,870.700\ km$
e	=	Eccentricity
f	=	True anomaly, *radians*
r	=	Orbit radius, m
C_{lm}	=	Gravity field spherical harmonic coefficients
COM	=	Center of Mass
ISSB	=	Irregularly shaped small body
$\boldsymbol{I}$	=	Identity matrix
I_x, I_y, I_z	=	Principal moments of inertia about the roll, pitch and yaw axes respectively, $kg.m^2$
I_{xx}, I_{yy}, I_{zz}	=	Small irregularly shaped body principal moments of inertia, $kg.m^2$
J	=	Jacobi integral
LTI	=	Linear Time Invariant
LVLH	=	Local-Vertical-Local-Horizontal
MOR	=	Model Order Reduction
P	=	Semilatus rectum
P_{lm}	=	Legendre Functions of spherical harmonics gravitational potential
$\boldsymbol{Q}(t)$	=	Lyapunov-Floquet Transformation (LFT) matrix
S_{lm}	=	Gravity field spherical harmonic coefficients
TDNF	=	Time Dependent Normal Forms
TINF	=	Time Independent Normal Forms
U	=	Gravitational potential function
V	=	Effective potential function
μ	=	Gravitational parameter

ω = Spacecraft angular velocity, $^{rad}/_{s}$

ω_ρ = Perturbation frequency, $^{rad}/_{s}$

ω_s = Time scaling frequency, $\sqrt{10^{-6}}\ ^{rad}/_{s}$

ω_T = Small irregularly shaped body angular velocity, $^{rad}/_{s}$

ω_τ = Time-scaled small irregularly shaped body angular velocity, $^{rad}/_{s}$

σ = $^{(I_x - I_y)}/_{I_z}$, Dimensionless ratio of the spacecraft's principal moments of inertia

$\hat{\sigma}$ = $^{(I_{yy} - I_{xx})}/_{(I_{zz} - I_{xx})}$, Dimensionless mass-distribution parameter

Θ = Spacecraft pitch angle, *radians*

Ψ = Spacecraft roll angle, *radians*

Ω = Spacecraft yaw angle, *radians*

$\mathbf{\Phi}(t)$ = State Transition Matrix (STM)

$\mathbf{\Phi}(T)$ = Floquet Transition Matrix (FTM)

PREFACE

This dissertation was submitted at Arizona State University in partial fulfillment of the requirements for the degree of Doctor of Philosophy in Systems Engineering. Parts of this dissertation contain derived works from my journal articles that have already been published, accepted, or under review for publication, and papers presented at conferences. They include:

Published Journal Articles

- Waswa, P. M. B., and Redkar, S. *Control of nonlinear spacecraft attitude motion via state augmentation, Lyapunov-Floquet transformation and normal forms.* Advances in Space Research, vol. 64, no. 3, pp. 668–686, 2019. DOI: doi.org/10.1016/j.asr.2019.05.013.
- Waswa, P. M. B., and Redkar, S. *A survey of space mission architecture and system actualisation methodologies*, International Journal of Space Science and Engineering, vol. 4, no. 3, pp. 234–252, Jul. 2017. DOI: 10.1504/IJSPACESE.2017.085674.

Accepted Journal Articles (In publication process at the time of writing this dissertation.)

- Waswa, P.M.B. and Redkar, S., *A Direct Approach for Simplifying Nonlinear Systems with External Periodic Excitation Using Normal Forms, Journal Nonlinear Dynamics.* Accepted (Sept, 2019).
- Waswa, P.M.B., Redkar, S. and Subramanian, S.C., *Plain center manifold reduc-*

tion for nonlinear systems with external periodic excitation, Journal of Vibration and Control. Accepted (June, 2019)

Journal Articles Under Review (At the time of writing this dissertation.)

- Waswa, P. M. B., and Redkar, S., *Analysis of the Attitude Motion of Gravity Gradient Stabilized Spacecraft in Eccentric Orbit Including Versal Deformation of the Normal Forms*, International Journal of Non-Linear Mechanics.
- Waswa, P. M.B. *Unique Role of Small Satellites in Empowering Spacecraft Formation Flying Missions.* Int. J. Space Science and Engineering.

Book Chapter (In publication process at the time of writing this dissertation.)

- Waswa, P. M. B., and Redkar, S. (2019). *Analysis and Control of Nonlinear Attitude Motion of Gravity Gradient Stabilized Spacecraft via Lyapunov-Floquet Transformation and normal Forms.* In Timothy Sands Editor, Advances in Spacecraft Attitude Control. IntechOpen, UK.

Conference Papers

- Waswa and S. Redkar, *Lucid Analysis of Periodically Forced Nonlinear Systems via Normal Forms,* Proceedings of the ASME 2019 International Design Engineering Technical Conferences and Computers and Information in Engineering Conference IDETC/CIE 2019. August 18-21, 2019, Anaheim, California, USA.

Chapter 1

INTRODUCTION

1.1 Motivation

Space technology plays an indispensable role in many areas of our lives such as telecommunications, navigation, personal entertainment, weather forecasting, farming, security, defense, scientific exploration, research, innovation etc. There are currently over 1,957 satellites in orbit around earth [1] providing such essential services to millions of people. Moreover, over 42 space missions located beyond earth orbit [2] are currently underway and numerous others planned for future launch. Undoubtedly, the prominence of space technology in shaping humanity's future is unequivocal. The success or failure of a given space mission is largely contingent upon the complex system analysis and design methodologies exerted in converting the initial idea into an elaborate functioning enterprise [3]. It is for this reason that reliable and efficacious methodologies and tools are consistently utilized in space mission formulation and implementation. Thus, there is a need to continuously examine the effectiveness of prevailing space mission analysis and design methodologies. This is in order to improve prevailing tools and approaches that shall expedite relatively simpler, more reliable and accurate mission analytical modeling and analysis.

Space systems are required to function nominally in their designated orbital locations, maintain appropriate orientation and conform to planned trajectories despite the ambient perturbing space environment. Strict mission pointing requirements normally constrain spacecraft in orbit around a large body to maintain a fixed stable orbital position and orientation during operation. However, perturbing space-environment torques act to dislodge

positioned spacecraft and disorient stabilized ones [4], [5]. Similarly, spacecraft injected into deep space transit trajectories often require multiple mid-course corrections to offset undue deviations from their planned trajectories caused by prevailing space-environment disturbance torques or inherent inaccuracies in mission design methodologies [6]–[11]. Further, space mission objectives often necessitate elaborate dynamical operations such as rendezvous, docking, hovering, descent, sampling etc in hostile uncertain environments. Modeling, analyzing and controlling dynamics of space systems is therefore a crucial component of space mission design. The quest for relatively simpler, more accurate and more reliable analytical methodologies and tools to represent, scrutinize and manipulate the dynamics of space systems is therefore a worthwhile undertaking.

Inopportunely, dynamics of space systems tend to be commonly represented by coupled analytical models that possess complex structures encompassing nonlinearity, parameter-variant coefficients (parametric excitation) and external periodic excitation terms [12]–[23]. Moreover, such analytical models normally encompass a large number of ordinary differential equations (ODE). The requisite analysis essential to facilitate the understanding of such motion is not a trivial undertaking–except for few special cases, the general solution for such dynamical systems cannot be found. The intricate and complex structures of these analytical models characteristically point to nondeterministic and potentially chaotic systems over a range of initial conditions and system parameters. Therefore, to analyze the space systems dynamical models, we often have to content with non-autonomous, nonlinear and periodic differential equations [24], [25]. This presents an immense analysis challenge. For instance, time-varying eigenvalues of the periodic linear system matrix cannot determine the system stability. Consequently, methods such as; linearization [26], averaging [27] and perturbations techniques [28], [29] have been consistently used to analyze such complex nonlinear, periodic motion. However, the two latter

approaches tend to be limited to minimally excited systems (parameter multiplying the periodic terms is small); while linearization is restricted to small domains about the operating point. Further, such methods are inclined to be relatively cumbersome and normally augmented with numerical approaches to analyze dynamical systems and accomplish real-life applications [30]–[32].

Therefore, this dissertation intends to overcome the above limitations and further obtain more accurate closed-form analytical solutions in a lucid and broadly applicable manner. We shall hence implement a multi-faceted methodology that relies on;

- Floquet theory.
- Normal Form (NF) theory.
- Center manifold reduction.
- System States Augmentation.

At the heart of this approach is the intuitive system state augmentation that transforms non-autonomous nonlinear dynamical systems to autonomous ones.

Fitting use of the aforementioned transformations and techniques, enables dynamical systems analysis and control law development in transformed, parameter-invariant and more tractable coordinates that preserve the original system's Lyapunov stability and bifurcation properties [33], [34]. Consequently, we intend to exploit this propitious attribute in our investigation. Applications of L-F transformations in spacecraft dynamics have been previously investigated by authors such as [16], [35]. The former demonstrates how L-F theory enhances the representation of relative spacecraft dynamics in elliptical orbits; while the latter further proposes an orbit control law based on L-F theory.

The use of normal forms to investigate nonlinear systems with external periodic excitation has been studied by several authors in literature. [36] present a direct methodology that utilizes a 'book-keeping' parameter in conjunction with a set of time-dependent

near-identity transformations to construct the system's normal forms. The authors further demonstrate how their approach is applicable to forced nonlinear systems with both periodic and invariant coefficients. To analyze forced nonlinear systems, [37] augment the differential equations modeling the dynamical systems by introducing new equation variables and detuning parameters. Subsequently, normalization of the system with an expanded dimension is shown. In his approach to normalize the forced oscillations of the Duffing oscillator, [38] introduces an additional state variable to convert the system from two-dimensional non-autonomous to three-dimensional autonomous system. A detuning parameter is similarly included in this methodology to obtain the normal forms of the forced nonlinear system. In the investigation of damped and close to resonance second-order mechanical vibration problems by [39], the authors show that the near-identity transformation is unaffected by the introduction of damping or forcing. Despite the authors utilizing perturbation techniques with a detuning parameter, they show that a book-keeping parameter is not required provided that forcing and damping are considered to be weak. In an earlier investigation, [40] utilize approaches equivalent to those by authors such as [37] and [38] to investigate second-order nonlinear vibration problems via normal forms. [41] show a relatively simpler approach detailing how normal forms expedite nonlinear systems model order reduction via nonlinear normal modes (NNM) to analyze the hardening/softening behavior in forced nonlinear structural systems. By using normal forms, the authors avoid too severe truncation normally attributed to a single mode of a nonlinear system. Subsequently, [42] improves the methodology in [41] by considering damping effects in the MOR. The two foregoing investigations require a small book-keeping parameter as well in their approach to obtain normal forms. [43] use a similar approach to [41] and [42] to show that additional resonance terms do not increase the accuracy of second-order normal form method.

The foregoing methodologies encompass special strategies such as introduction of detuning parameters, 'book-keeping' parameters, *ad-hoc* unsolved ODEs, *ad-hoc* new variables, etc. In general, the aggrandizement of the foregoing parameters seemingly lacks consistent, plain and direct affiliation to the pertinent terms of the nonlinear equations. Consequently, these formulations appear daunting, cumbersome and convoluted. Moreover, the mandatory *ad-hoc* parameters involved hinder seamless suitability of these approaches to broad applications over a wide range of nonlinear systems.

Therefore, as the novelty of our research; we shall formulate a relatively more direct and simpler approach to obtain normal forms of nonlinear systems subjected to external periodic excitation. Additionally, presence of external periodic excitation and/or periodic coefficients in the system dynamics introduces unique challenges that render direct application of the conventional nonlinear order reduction methodologies infeasible.

On the other hand several authors have applied varying techniques to obtain reduced order models of nonlinear systems with external periodic excitation. For instance, stochastic approaches such as Proper Orthogonal Decomposition (POD), for order reduction of self-excited, time-periodic systems are found in [44]. Few other researchers such as [45] and [46] proved the existence of Spectral Sub-manifolds (SSM) and their application for model order reduction for structural analysis.

Using the method of multiple scales to construct NNM, [47] augment the states to address periodic forcing. However, this perturbations technique is only valid for small nonlinearities. [48] and [49] similarly employ NNM to reduce the order of periodically excited systems. The former includes solving partial differential equations (PDEs) via polynomial expansion while the latter numerically solves the PDEs. A detailed review of application of NNM for model reduction in mechanical systems is presented in [50].

The approaches presented by [51] and [52] avoid augmentation of the state-space and

perform order reduction of periodically forced nonlinear systems with periodic and constant coefficients via center manifold reduction. [51] treat the invariant manifold as time modulated nonlinear functions of the dominant states which have a specific structure in terms of temporal and spatial terms. The work by [52] extends ideas of [53] and [51] in order to improve modeling of secondary resonance with external periodic excitation. Moreover, [52] argue that; in general, state augmentation approach is not appealing for order reduction of systems subjected to multi-frequency and/or parametric excitation. This is because each augmented state has a corresponding single increase in the degree of freedom (DOF) of the equivalent system. Therefore construction of invariant manifold could be cumbersome and may invalidate the advantages of order reduction altogether.

As elucidated in the foregoing illustrative examples; several authors have presented different approaches to address the MOR of nonlinear systems subjected to external periodic excitation. Some of the presented approaches incorporate a means to augment the state space by treating the forcing as an additional state (e.g. [47]), while others construct invariant manifolds composed of temporal and spatial state variables (e.g. [51]). Depending on the application, some approaches could be adapted as a generic methodology, whereas others are limited to a narrow application.

However, here, we present an intuitive state space augmentation methodology that simplifies model order reduction on the center manifold for nonlinear systems with external periodic excitation. Our methodology is applicable to parametrically excited and constant coefficient nonlinear systems with external periodic forcing. Moreover, this approach can represent commensurate multifrequency excitations in terms of the delineated state corresponding to the fundamental frequency. In the case of incommensurate multifrequencies, the simplified methodology of reducing the order of periodically forced system far outweighs the aggrandizement of states.

To study the complex dynamics of space systems via the strategies above, we shall consider two fitting representative types of space systems dynamics, *i)* dynamics of a rigid body about its center of mass (COM) while in an eccentric orbit around a central large mass, *ii)* dynamics of a point mass in a non-uniform Newtonian force field. Respectively, we shall therefore apply the aforementioned series approaches to analyze and control:

I. Attitude motion of a gravity gradient stabilized spacecraft in an eccentric orbit.
II. Spacecraft motion in the vicinity of irregularly shaped small bodies (ISSB).

1.2 Parametrically Excited Nonlinear Spacecraft Dynamics With Periodic External Excitation

In this section we introduce the two representative dynamical space systems characterized by nonlinear models with parametric excitation and periodic external excitation. We first describe the attitude motion of a gravity gradient stabilized spacecraft followed by spacecraft motion in the vicinity of irregularly shaped small bodies. The detailed description and dynamical models developments are respectively conducted in Chapters 3 and 5.

1.2.1 Attitude Motion of a Gravity Gradient Stabilized Spacecraft in an Eccentric Orbit

A number of strategies are employed to stabilize spacecraft attitude motion and maintain a desired orientation despite the presence of perturbing torques present in the space environment. The most common attitude control and stabilization approaches are three-axis stabilization, spin stabilization and gravity gradient stabilization. To provide the

determined control input required to offset undesired attitude deviations, these methods employ either active control systems (e.g. thrusters, magnetic torquers, reaction wheels) or passive control systems (e.g. booms). Unlike passive controllers, active controllers utilize an external source of energy to drive the attitude control actuators [31], [54].

Among the stated attitude stabilization methods, gravity gradient stabilization of spacecraft attitude is attractive due to its relatively intrinsic simplicity, reliability and low cost [55]. However, it is mostly feasible in low earth orbit due to its principle of operation as discussed in chapter 3.

The motion about COM of a rigid gravity gradient stabilized spacecraft is libratory about the pitch axis [56]. This axis is normal to the orbital plane in an inverse-square gravity field. The satellite will oscillate about a position of stable relative equilibrium if the work done by external perturbing forces is greater than the rotational kinetic energy. The sufficient conditions for stability of relative equilibrium are explained in chapter 2. The complete formulation of COM motion for a gravity gradient stabilized satellite in eccentric orbit consists of six coupled, nonlinear second-order differential equations. This system of equations is considered analytically unsolvable in closed form [13], [15], [57]–[59].

1.2.2 Spacecraft Dynamics in the Vicinity of Irregularly Shaped Small Bodies

Since its onset, deep space exploration has been traditionally dominated by missions to investigate ascertained planets of our solar system. Additionally, even missions to non-planetary bodies have mostly targeted relatively sizable moons such as Ganymede, Titan, Callisto, Io etc. These destinations remain comparable in size to small planets of the solar

system. Conversely, a relatively meager number of missions (≈10%), have targeted asteroids, comets or other irregularly shaped bodies within the solar system [60].

Notably, a recent trend characterized by rising interest to explore ISSB of our solar system has emerged within the space scientific community. Evidence of this surging affinity is illustrated by the plethora of mission proposals targeting small bodies that dominated entries in the recently concluded 2017 NASA's Discovery Program competition. Over half of the competing mission proposals sought to explore small bodies such as comets, asteroids and small moons. In the end, two missions–PYSCHE and LUCY were selected as winners [61]. Both missions will dispatch spacecraft to visit and investigate asteroids (ISSB) in a quest to assist mankind unravel origins of the universe.

The aforementioned developments reveal a fervent interest within NASA and the space scientific community at large to study small bodies in our solar system. Moreover, numerous proposals of manned-missions to rocky small bodies similarly continue to be formulated and deliberated upon. At the time of writing this dissertation, the OSIRIS-REx spacecraft just went into orbit around asteroid Bennu. This mission has set the record for the smallest body ever orbited by a spacecraft [62]. Undoubtedly, exploration of small bodies in the solar system has emerged to be a sustained priority undertaking for the space science community.

To achieve the designated mission objectives, space systems investigating ISSB may be required to execute a variety of close proximity rendezvous maneuvers such as hovering, descent, orbiting, sampling etc. However, there exist inimitable complex challenges in the the modeling, analysis and control of spacecraft dynamics in the vicinity of ISSB. These exceptional challenges stem from several distinctive factors such as; uncertainty in the small-body mass and orbital parameters, irregularly shaped, weak gravitational forces, strong susceptibility to 3^{rd}-body and solar radiation pressure perturbations etc., [63]–[68]

Therefore, the resulting spacecraft dynamics in the proximity of ISSB are modeled by a large system of coupled astrodynamical ODEs that are nonlinear, parametrically excited with external periodic excitations [22], [63], [69]–[74]. As previously noted, modeling, analysis and control law development for such motion is not a trivial task given that the dynamics equations are unsolvable in closed form. It is hence the intention of this dissertation to address this particular problem.

1.3 Dissertation Scope and Overview

Summarily, this dissertation models, analyzes and controls complex dynamics of space systems. The analytical models of the dynamical systems under consideration possess complex structures encompassing nonlinear differential equations with parameter-variant coefficients and periodic external excitation. Methods such as linearization, averaging and perturbation techniques are commonly used to solve such complex dynamical systems. However, due to the shortcomings inherent in these approaches; we shall utilize state augmentation, L-F transformation and normal forms techniques in our methodologies. The preferred methodologies are not subjected to the constraints and assumptions beleaguering the prevalent methodologies.

Two representative types of motions are considered–motion of a rigid body about its COM in eccentric orbit, and motion of a point mass in a gravity field due to an irregularly shaped small body. As a result, the dissertation problem to be investigated is divided into two major parts:

I. Firstly, our analysis of gravity gradient stabilized spacecraft attitude dynamics will investigate the motion periodicity, quasi-periodicity and chaos. Moreover, the motion structural stability, resonances and bifurcation behavior will similarly be exam-

ined. Requisite assumptions made to facilitate the attitude motion analyses will be explicitly stated and qualified. Attitude motion analyses will be followed by synthesis of suitable control laws that adequately offset the periodic and secular attitude variations due to perturbing ambient environmental torques.

II. Secondly, we shall investigate periodicity, chaos, resonance and stability of the dynamical space system in the vicinity of irregularly shaped small bodies. We intend to further demonstrate how the suitability of our proposed approach in modeling and analysis of the pertinent astrodynamics will similarly facilitate synthesis of appropriate space systems motion controllers via conventional techniques. This is essential in designing successful imperative mission maneuvers such as hovering, orbiting, sampling, descent etc.

To study the problem of dynamics of space systems via Floquet theory, center manifold reduction and normal forms, the remainder of this dissertation is segmented into six chapters. Next, we briefly outline the fundamental objectives of each chapter.

Chapter 2 will present the details of the methodologies and strategies that this dissertation will use to investigate space systems dynamics. The classical theories of normal forms, center manifold reduction and Floquet theory will be summarized. After examining the limitations of these methods in studying nonlinear systems with external periodic excitation, this chapter will introduce the intuitive state augmentation and demonstrate how to extend the Floquet theory, center manifold reduction and normal forms to the analysis of parametrically excited nonlinear systems with external periodic excitation. We shall validate the accuracy of the proposed techniques using numerous illustrative cases of Duffing's and Mathieu-Duffing equations.

Chapter 3 introduces the first part of this dissertation by characterizing the problem of spacecraft gravity gradient attitude stabilization in eccentric orbit. After developing

the dynamical model of this motion, we shall analyze the dynamic's time-history, stability, chaos and periodicity. Further, by investigating the versal deformation of the normal forms, this chapter will scrutinize the bifurcation behavior of a gravity gradient stabilized spacecraft in eccentric orbit.

Chapter 4 completes the first part of this dissertation by demonstrating various means to control the gravity gradient spacecraft. Because the planar pitch attitude motion of a gravity gradient stabilized spacecraft is undesirable for nominal space mission operations, this chapter will explore development strategies for linear and nonlinear control laws capable of stabilizing the spacecraft by countering the prevailing librations. Among the nonlinear control approaches to be applied are sliding mode control and bifurcation control methods. The controller design will be conducted after the system has been transformed from the original coordinates into more tractable forms via L-F transformation, state augmentation and near identity transformation.

Chapter 5 will introduce the second part of this dissertation by characterizing the motion in the vicinity of irregularly shaped small bodies. After examing the unique challenges associated with studying the motion in the vicinity of irregularly shaped small bodies, this chapter will outline the significance of modeling the gravitation potential of an irregularly shaped body and examine the main approaches used to model such a gravitational potential. Using the second degree and order spherical harmonic gravitational model, the dynamical model in the vicinity of an irregularly shaped small body is developed here. Subsequently, we shall study the time-history behavior, stability, periodicity and chaos of the pertinent motion. The analysis will culminate in examining the shape and behavior of orbits around the irregularly shaped small body.

Chapter 6 studies how to control the dynamics in the vicinity of the irregularly shaped small body. This section demonstrates how the series of procedures in our approach i.e. L-

F transformation, state augmentation, center manifold reduction and normal forms simplification enable appropriate nonlinear control laws synthesis aimed at stabilizing our dynamics. The trajectories in the vicinity of irregularly shaped small bodies are erratic and necessitate a means to control them so that they may be conducive to space mission design. Chapter 6 will demonstrate how regular and periodic orbits that are favorable to space mission design can be realized around irregularly shaped small bodies by using asteroid 4179 Toutatis as a case study.

Chapter 7 will constitute the concluding remarks, dissertation contributions to the body of knowledge and future areas of research on this and related topics. We shall outline the contributions this dissertation has made by introducing the lucid and direct approaches of analyzing parametrically excited nonlinear systems with external periodic excitation via center manifold reduction and normal forms. Then, we separately outline the dissertation's contributions in the gravity gradient attitude stabilization problem and in the motion in the vicinity of irregularly shaped small bodies problem. Finally, we make recommendations for future areas of research on the primary theme tackled by this research and other closely related areas.

The dissertation road map culminating from the chapters as outlined above is hence illustrated in the layout schematic shown in figure 1.

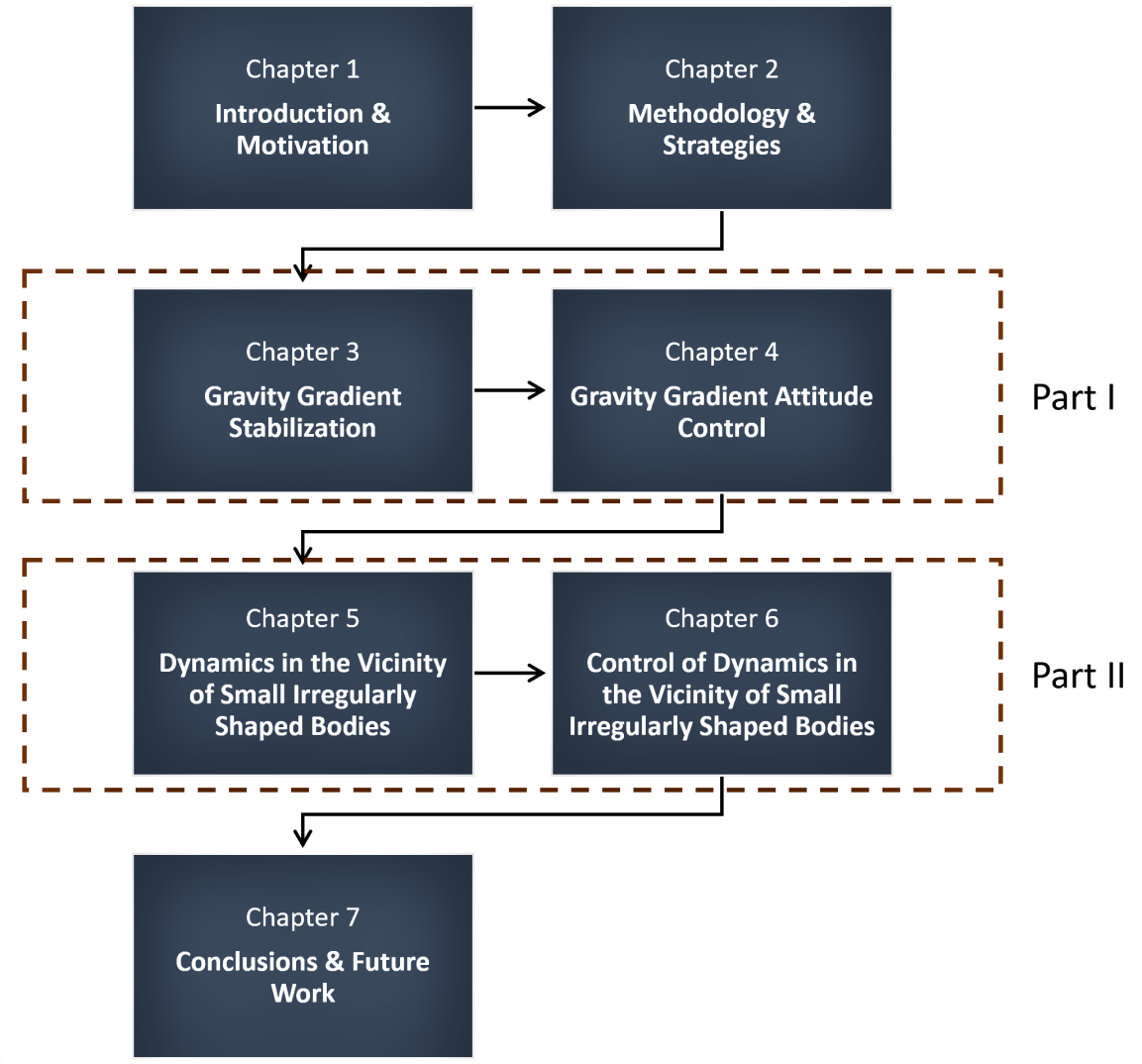

Figure 1: Dissertation Road-map

Chapter 2

METHOD OF ANALYSIS

In general, Floquet theory and Lyapunov-Floquet transformation (LFT) techniques in particular facilitate stability analysis of dynamical systems with periodic coefficients; facilitate solving parametrically excited nonlinear systems and help design full-state feedback control laws. By introducing an intuitive state augmentation technique, we shall augment these capabilities with Model Order Reduction (MOR) techniques and normal forms approaches in our methodology in this dissertation. MOR reduces the dimension of our analytical models while normal forms simplify our nonlinear system into a more tractable form. The intuitive system states augmentation essentially converts our non-autonomous system into an autonomous which avails numerous advantages in our methodology as we shall see. Subsequently, the emanating synergies from the cumulative application of these techniques serve to accomplish the intended analysis of and control of parametrically excited nonlinear space systems dynamics with external periodic excitation.

To analyze the nonlinear motion, we shall first transforms the linear parameter-varying terms of the dynamics equations into parameter-invariant terms using L-F transformation. Then, we subsequently reduce the order of nonlinear terms into their respective simpler normal forms using a near identity transformation. Motion periodicity, resonance and chaos will be investigated in the original coordinates while Floquet theory will facilitate stability analysis. Further, resonance analysis will be undertaken in the L-F transformed coordinates. On the other hand, analyzing the versal deformation of the normal forms will provide insights in to bifurcation behavior within the neighborhood of the critical point. System state augmentation will facilitate normalization of the periodically excited

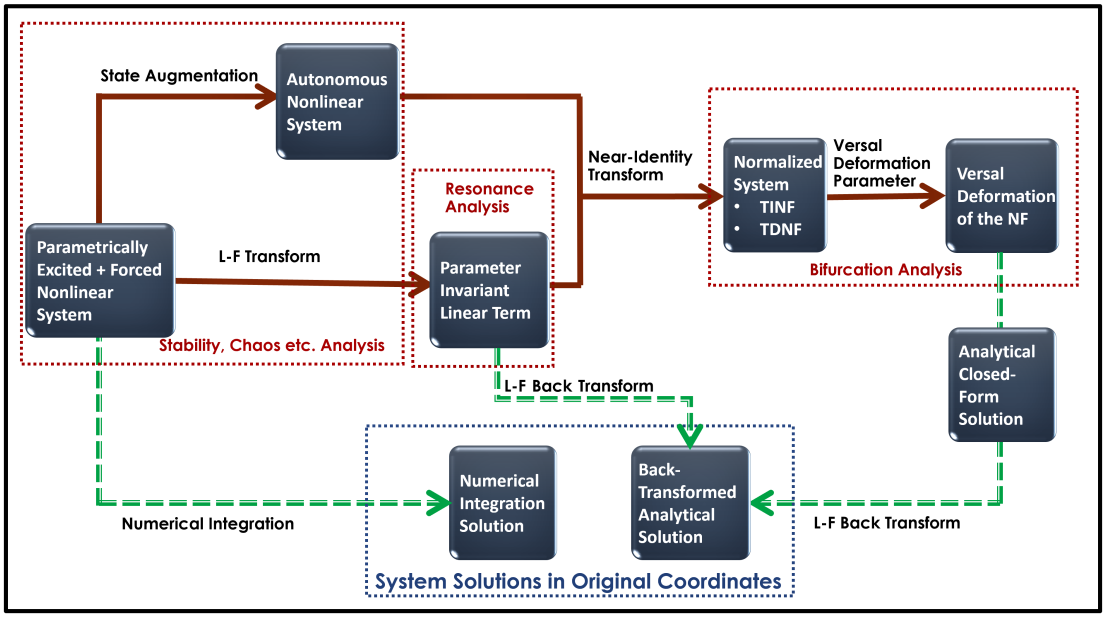

Figure 2: Motion Analysis Sequence

system before constructing the versal deformations. Our approach to analyze this motion is summarily illustrated in the schematic shown in figure 2.

Control law development on the other hand is carried out on dynamics that have been subjected to L-F transformation, state-augmented, dimensional order-reduced and normalized. This is because, the preceding steps transform the dynamical model into a more tractable and conducive form for application of conventional control law synthesis. The motion in the original coordinates consisting of parametric excitation, nonlinearity and external periodic excitation does not readily lend itself to conventional control law synthesis approaches. The control law synthesis sequence we shall follow in this dissertation is as shown in figure 3.

We shall exploit the orthogonal properties of Chebyshev Polynomials to compute the Lyapunov-Floquet transformation (LFT) matrix in closed form in addition to the pre-

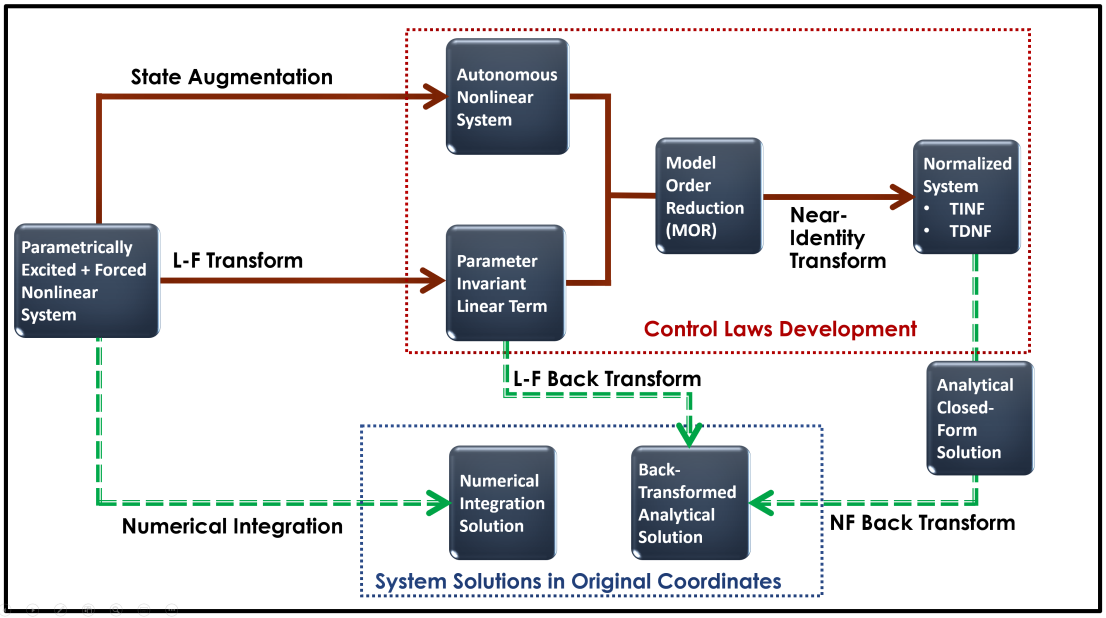

Figure 3: Motion Analysis and Control Law Development Sequence

requisite state transition matrix (STM) and Floquet transition matrix (FTM) as explicit function of the varying parameter. Chebyshev polynomials are preferred because they convert the emanating integral equations into amenable algebraic expressions and have relatively better convergence properties. Elements of the LFT matrix and its inverse in closed form are expressed in terms of truncated Fourier series with the orbit true anomaly, f as the series independent parameter. The LFT matrix will be applied to transform the linear periodic terms of the motion into linear parameter-invariant terms. Thereafter, MOR will be utilized to reduce the model dimension and final normal forms simplification will simplify the nonlinear terms into their simpler forms via a near-identity coordinate transformations. Since the L-F transformed dynamics retain their original Lyapunov stability and bifurcation characteristics [33], [34]; motion analysis and control can still be safely undertaken on the transformed dynamics. The Lyapunov-Floquet and Normal Form approaches stated above are similar to those proposed by [34], [36], [75], [76]. However, we shall extend these approaches and the invariant manifold order reduction ap-

proaches in a more lucid and straightforward manner to facilitate our research objectives here. Back-transformation of our analyzed and controlled motion via inverse near identity transformation, inverse modal transformation and inverse L-F transformation will enable the closed-form dynamical solutions to be presented in the original coordinates. Next, we shall examine the theoretical backgrounds of the main approaches implemented in this dissertation In doing so, we shall highlight the inherent limitations of these methodologies and formulate techniques to overcome these limitations in a more straightforward and lucid manner with broad application. Illustrative examples will also be used to verify the accuracy of these proposed approaches.

2.1 Floquet Theory

Floquet theory enables stability and response analysis of linear systems with periodic coefficients. This section summarizes Floquet theory presented in [77]. Using the knowledge of characteristic exponents of STM; the theory infers that if the solution of a system is obtained over a full principle period, then the solution is known for all time [77], [78]. Consider the periodic nonlinear system subjected to an external periodic excitation as below,

$$\dot{\boldsymbol{x}}(t) = \boldsymbol{A}(t)\boldsymbol{x}(t) + \boldsymbol{f}(\mathbf{x}, t) + \tilde{\boldsymbol{F}}(t), \tag{2.1}$$

where $\boldsymbol{F}(\cdot)$ constitutes nonlinear terms of $\boldsymbol{f}_k$(**x**,t) representing homogeneous monomials in x_i of order k. $\tilde{\boldsymbol{F}}(t)$ is the periodic forcing term. **A**(t) is periodic with a principal period T. The linear part of equation (2.1) is given by

$$\dot{\boldsymbol{x}}(t) = \boldsymbol{A}(t)\boldsymbol{x}(t), \qquad \boldsymbol{A}(t) = \boldsymbol{A}(t+T). \tag{2.2}$$

Based on Floquet theorem [77], each fundamental matrix $\boldsymbol{\Phi}(t)$ of equation (2.2) can be represented as a product of two $n \times n$ matrices, i.e.

$$\boldsymbol{\Phi}(t) = \boldsymbol{Q}(t)e^{\boldsymbol{B}t}, \tag{2.3}$$

where $\boldsymbol{Q}(t) = \boldsymbol{Q}(t+T)$ is a T-periodic matrix and $\boldsymbol{B}$ is a constant matrix. In general $\boldsymbol{Q}(t)$ and $\boldsymbol{B}$ are complex. Moreover, a real $\boldsymbol{Q}(t)$ with a period 2T has a corresponding real $\boldsymbol{B}$ matrix in equation(2.3). $\boldsymbol{\Phi}(t)$ is the nonsingular STM whose columns are a solution to equation (2.2) such that $\boldsymbol{\Phi}(0) = \boldsymbol{I}$. Also,

$$\left.\begin{aligned} \dot{\boldsymbol{\Phi}}(t) &= \boldsymbol{A}(t)\boldsymbol{\Phi}(t), \\ \boldsymbol{\Phi}(t+T) &= \boldsymbol{\Phi}(t)\boldsymbol{C}, \\ \boldsymbol{\Phi}(T) &= \boldsymbol{\Phi}(0)\boldsymbol{C}. \end{aligned}\right\} \tag{2.4}$$

C is a nonsingular matrix. Then, it follows from the properties: $\boldsymbol{\Phi}(t)$ and $\boldsymbol{\Phi}(0) = \boldsymbol{I}$, that

$$\boldsymbol{\Phi}(T) = \boldsymbol{C}. \tag{2.5}$$

Hence, knowledge of the STM enables the solution of unforced equation (2.2) to be written as,

$$\boldsymbol{x}(t) = \boldsymbol{\Phi}(t)\boldsymbol{x}(0) = \boldsymbol{Q}(t)e^{\boldsymbol{B}t}\boldsymbol{x}(0), \tag{2.6}$$

where $\boldsymbol{x}(0)$ is the initial state vector. For time greater than one period $(t > T)$, we have

$$\boldsymbol{x}(t) = \boldsymbol{\Phi}(t+nT)\boldsymbol{x}(0) = \boldsymbol{\Phi}(t)[\boldsymbol{\Phi}(T)]^n\boldsymbol{x}(0), \tag{2.7}$$

where $t \in [0\,,\, T], \quad n = 1, 2, 3, \ldots$.

$\boldsymbol{\Phi}(T)$ is called the Floquet Transition Matrix (FTM) or the monodromy matrix. Equation (2.5) infers that if a solution is known throughout the principal period of time variations in the system, then the solution is known for all times. In order for the solution of $\boldsymbol{x}(t)$ to be bounded for all time t, we conclude from equation (2.7) that all the eigenvalues

of $\boldsymbol{\Phi}(T)$ $(= \boldsymbol{C})$ must have a magnitude, $|\rho_k| \leq 1$. The eigenvalues of FTM are called the Floquet or characteristic multipliers ρ_k and are generally complex ($\rho_k = \rho_{kk} + i\rho_{kI}$). Each ρ_k provides a measure of the local orbital divergence along a particular direction over one principal period of the closed orbit of equation (2.2). We can also define the Floquet or characteristic exponents; $\alpha_k \pm i\beta_k$ as,

$$\left.\begin{aligned} \alpha_k &= \frac{1}{T} ln|\rho_k|, \\ \beta_k &= \frac{1}{T} \arctan\left(\frac{\rho_{kI}}{\rho_{kk}}\right). \end{aligned}\right\} \tag{2.8}$$

A periodic solution to (2.2) is asymptotically stable if there are no Floquet multipliers outside the unit circle ($|\rho_k| < 1,\ \forall k$); and, it is unstable if one or more Floquet multipliers lie outside the unit circle ($k\ \exists$ s.t., $|\rho_k| > 1$) [79]. The knowledge of FTM at the end of one principal period is hence sufficient to determine the stability of the system.

Corollary: The Lyapunov-Floquet (L-F) transformation

$$\boldsymbol{x}(t) = \boldsymbol{Q}(t)\boldsymbol{z}(t), \tag{2.9}$$

reduces the original non-autonomous linear differential system given in equation (2.2) to an autonomous one with of the form,

$$\dot{\boldsymbol{z}}(t) = \boldsymbol{R}\boldsymbol{z}(t). \tag{2.10}$$

$\boldsymbol{R}$ is an $n \times n$ constant matrix. Further, by differentiating equation (2.9) and applying the properties of $\dot{\boldsymbol{\Phi}}(t)$ and $\dot{\boldsymbol{Q}}(t)$ it can be shown that,

$$\dot{\boldsymbol{z}}(t) = \boldsymbol{B}\boldsymbol{z}(t). \tag{2.11}$$

Therefore in our notation $\boldsymbol{B} = \boldsymbol{R}$. Recall, $\boldsymbol{B}$ is the Floquet constant matrix given in equation (2.3). The eigenvalues of $\boldsymbol{B}$ are the Floquet exponents.

2.2 Computation of Lyapunov-Floquet Transformation Matrix via Chebyshev Polynomials

In order to compute the LFT matrix, $\boldsymbol{Q}(t)$, the STM, $\boldsymbol{\Phi}(t)$ associated with the periodic linear system given in equation (2.2) has to be obtained first. To demonstrate the methodology of computing $\boldsymbol{Q}(t)$, we shall adapt the approach advanced by [75], [80]. In this approach, the STM of a linear periodic system is evaluated in terms of shifted Chebyshev polynomials of the first kind as an explicit function of time. Chebyshev polynomials are chosen because they produce better approximation and convergence than other special orthogonal polynomials [81]. The enticing feature of this technique is that the special polynomial functions decompose the original linear differential system into a system of linear algebraic equations. Standard techniques can then be employed to solve the resulting algebraic equations assuming that convergence is achieved in the polynomial representation of the solution.

This method expands both $\boldsymbol{A}(t)$ and the solution vector $\boldsymbol{x}(t)$ in terms of shifted Chebyshev polynomials in the interval $[0,\ T]$ as illustrated in the equations below,

$$\boldsymbol{x_i}(t) \approx \sum_{r=0}^{s-1} \boldsymbol{b}_r^i \boldsymbol{s}_r^*(t) \equiv \boldsymbol{s}^{*T}(t)\boldsymbol{b}^i \ , \qquad i = 1, 2, 3, ..., n, \tag{2.12}$$

$$\boldsymbol{A}(t) = \sum_{r=0}^{s-1} \boldsymbol{d}_r^{ij} \boldsymbol{s}_r^*(t) \equiv \boldsymbol{s}^{*T}(t)\boldsymbol{d}^{ij} \ , \quad i, j = 1, 2, 3, ..., \boldsymbol{n}, \tag{2.13}$$

where $\boldsymbol{b}^i = \{\boldsymbol{b}_0^i \ \boldsymbol{b}_1^i \ ... \ \boldsymbol{b}_{m-1}^i\}^T$: Unknown Chebyshev expansion coefficients of $\boldsymbol{x_i}(t)$.
$\boldsymbol{d}^{ij} = \{\boldsymbol{d}_0^{ij} \ \boldsymbol{d}_1^{ij} \ ... \ \boldsymbol{d}_{m-1}^{ij}\}^T$: Known Chebyshev expansion coefficients of $\boldsymbol{A}(t)$.
And,
$s_r^*(t) = \{s_0^*(t) \ s_1^*(t) \ s_{m-1}^*(t)\}$: Shifted Chebyshev polynomials of the first kind. After $\boldsymbol{x}(t)$ and $\boldsymbol{A}(t)$ have been expanded in shifted Chebyshev polynomials of the first kind, we can substitute them in the integral form of equation (2.2) to solve for the unknown Chebyshev

expansion coefficients $\boldsymbol{b}$. Finding the STM of the system requires a set of solutions with $\boldsymbol{n}$ initial conditions, i.e. $\boldsymbol{x}_i(0) = (1, 0, 0..., 0),\ (0, 1, 0..., 0),\ (0, 0, 1, 0..., 0),\ (0, 0, 0..., 1)$. Consequently, the STM valid for $0 \leq t \leq T$ (shifted Chebyshev polynomials are only valid over the interval [*0, T*] is given by,

$$\boldsymbol{\Phi}(t) = \hat{\boldsymbol{S}}(t)\bar{\boldsymbol{B}}, \tag{2.14}$$

where $\hat{\boldsymbol{S}}(t) = \boldsymbol{I} \otimes s^{*T}(t)$, $\bar{\boldsymbol{B}} = [\bar{\boldsymbol{b}}_{\boldsymbol{1}}\ \bar{\boldsymbol{b}}_{\boldsymbol{2}}\ \bar{\boldsymbol{b}}_{\boldsymbol{3}}\ \boldsymbol{...}\bar{\boldsymbol{b}}_{\boldsymbol{n}}]$, $\boldsymbol{\Phi}(0) = \boldsymbol{I}$ and $\otimes$ represents the Kronecker product. The STM for $t > T$ is evaluated using Floquet theory and property of $\boldsymbol{\Phi}(t)$ given in equation (2.7)——see [34], [75] for detailed computation. Once $\boldsymbol{\Phi}(t)$ is obtained, then from equation 16, the Lyapunov-Floquet transformation matrix is evaluated as $\boldsymbol{Q}(t) = \boldsymbol{\Phi}(t)e^{-\boldsymbol{B}t}$. The constant matrix $\boldsymbol{B}$ is computed via matrix logarithm as,

$$\boldsymbol{B} = \frac{log_m \Phi(T)}{T}. \tag{2.15}$$

To find $\boldsymbol{Q^{-1}}(t)$, first $\boldsymbol{\Phi^{-1}}(t)$ must be evaluated. Instead of pursuing a brute inversion of $\boldsymbol{\Phi}(t)$ via symbolic programming language; it is more feasible to consider the state transition matrix; $\boldsymbol{\Gamma}(t)$ of the adjoint system to equation (2.2) as shown below [27],

$$\dot{\boldsymbol{\nu}} = -\boldsymbol{A^T}(t)\boldsymbol{\nu}(t). \tag{2.16}$$

Then apply the relationship

$$\boldsymbol{\Phi^{-1}}(t) = \boldsymbol{\Gamma^T}(t). \tag{2.17}$$

From equation (2.3) $\boldsymbol{Q}(t) = \boldsymbol{\Phi}(t)e^{-\boldsymbol{B}t}$. Subsequently,

$$\boldsymbol{Q^{-1}}(t) = e^{\boldsymbol{B}t}\boldsymbol{\Phi^{-1}}(t) = e^{\boldsymbol{B}t}\boldsymbol{\Gamma^T}(t). \tag{2.18}$$

The above approximation of LFT matrix via Chebyshev polynomials contains elements $\boldsymbol{Q}_{ij}(t)$ with truncated Fourier representations as shown in equation below,

$$Q_{ij}(t) \approx \frac{a_0}{2} + \sum_{n=1}^{q} a_n \cos\left(\frac{\pi n t}{T}\right) + \sum_{n=1}^{q} b_n \sin\left(\frac{\pi n t}{T}\right). \tag{2.19}$$

$\boldsymbol{Q}_{ij}^{-1}(t)$ has similar Fourier representation. Readers are directed to references cited in the first paragraph of this section for complete details of this outlined approach to obtain $\boldsymbol{\Phi}(t)$ and $\boldsymbol{Q}(t)$ matrices.

2.3 Normal Forms

A significant segment of dynamical phenomena in engineering and physical sciences is modeled via a system of nonlinear ordinary differential equations (ODEs) which may possess constant or varying coefficients. Moreover, these analytical models may also include a periodic forcing term–further complicating the nonlinear system model structure. Examples of such dynamical systems are common in domains such as space systems dynamics, rotary craft dynamics, structural vibrations, etc. The complex make-up of analytical models of such nonlinear systems renders their analysis and feedback control via conventional methods a remarkably daunting endeavor. Consequently, appropriate techniques to simplify and reduce the complexity of such intricate nonlinear analytical models are a requisite to comprehensively investigate, understand and manipulate their respective engendering systems. Normal forms simplification facilitates construction of relatively lesser complex, but qualitatively equivalent models of the original nonlinear dynamical systems. This simplification is generally implemented on equations arising from Taylor series expansion via the successive application of nonlinear near-identity transformations. Such a transformation entails preservation of the original system's stability and bifurcation characteristics by the transformed models.

Origins of the normal form theory can be traced back to the work by [82]. Later, additional authors such as [83], [84], [85], [38], [86], [87], [88] (to mention a few) have conducted further investigations into the theory. Normal form is a local coordinate trans-

formation technique that spawns simplified models that are topologically equivalent to the original nonlinear system in the vicinity of a stable point. The stable point (which represents a known solution) could be a limit cycle; constant, stationary, or equilibrium solution, etc. [38]. Moreover, authors such as [89], [90], [80], etc. have extended the normal forms theory to nonlinear systems with periodic coefficients (i.e. parametrically excited). Therefore, multiple strategies to obtain normal forms for nonlinear systems with constant coefficients and parametrically excited nonlinear systems are hence easily found in literature. Normal forms simplification of nonlinear systems is also a very useful tool in nonlinear system dynamics and bifurcation analysis. It provides a means to investigate nonlinear systems represented by complex and unwieldy equation structures.

The conventional normal forms theory is generally applicable to nonlinear systems without any external periodic excitation. Presence of external periodic excitation renders the conventional near-identity transformation unsuitable. As a result, nonlinear systems with external periodic excitation have been traditionally analyzed using averaging and perturbations techniques. However, these techniques have a drawback of being restricted to minimally excited systems encompassing relatively small nonlinearity coefficients [75], and [36].

In the next section, we shall outline the conventional normal forms theory for simplifying nonlinear systems without a forcing term. We shall highlighting the requisite *resonance* conditions. Afterwards, we shall introduce intuitive system states augmentation and elucidate how this technique facilitates construction of normal forms for periodically forced nonlinear systems with constant and periodic coefficients.

2.3.1 Time Independent Normal Form (TINF)

The fundamental concept behind normal forms methodology is to simplify the system by eliminating as many nonlinear terms as possible. This is accomplished via application of successive series of near-identity transformations on the original system. The near-identity coordinate transformations are nonlinear and local (e.g. see [38], [82], [87] and [37]). Consider the nonlinear dynamical system given by,

$$\dot{\boldsymbol{x}} = \boldsymbol{A}\boldsymbol{x} + \boldsymbol{f}_2(\boldsymbol{x}) + \boldsymbol{f}_3(\boldsymbol{x}) + \cdots + \boldsymbol{f}_k(\boldsymbol{x}) + \boldsymbol{O}(|\boldsymbol{x}|^{k+1}). \tag{2.20}$$

A is an $n \times n$ matrix, $\boldsymbol{f}_r(\boldsymbol{x})$ are $n \times 1$ vectors of homogeneous monomials in $\boldsymbol{x}$ of order r; $(r = 2, 3, 4...k)$. After application of the modal transformation $\boldsymbol{x} = \boldsymbol{M}\boldsymbol{y}$, equation (2.20) is changed into its Jordan canonical form shown below

$$\begin{aligned} \dot{\boldsymbol{y}} =& \boldsymbol{J}\boldsymbol{y} + \boldsymbol{M}^{-1}\boldsymbol{f}_2(\boldsymbol{M}\boldsymbol{y}) + \boldsymbol{M}^{-1}\boldsymbol{f}_3(\boldsymbol{M}\boldsymbol{y}) + \cdots + \boldsymbol{M}^{-1}\boldsymbol{f}_k(\boldsymbol{M}\boldsymbol{y}) \\ &+ \boldsymbol{M}^{-1}\boldsymbol{O}(|\boldsymbol{M}\boldsymbol{y}|^{k+1}), \end{aligned} \tag{2.21}$$

where $\boldsymbol{M}$ is the modal transformation matrix and $\boldsymbol{J}$ is the Jordan canonical form of $\boldsymbol{A}$. $\boldsymbol{J}$, shown below, is a diagonal matrix containing the eigenvalues of the linear matrix A,

$$\boldsymbol{J} = \begin{bmatrix} \lambda_1 & & & \\ & \lambda_2 & & \\ & & \ddots & \\ & & & \lambda_n \end{bmatrix}. \tag{2.22}$$

Equation (2.21) is amenable to reduction to its simplest form via application of successive sequence of near-identity transformations of the form

$$\boldsymbol{y} = \boldsymbol{v} + \boldsymbol{h}_r(\boldsymbol{v}), \tag{2.23}$$

where $\boldsymbol{h}_r(\boldsymbol{v})$ is an $n \times 1$ homogeneous vector of monomials in $\boldsymbol{v}$ of degree r. It can hence be shown that elimination of higher order nonlinearities via successive application of the near-identity transformations spawns the general homological equation below,

$$\frac{\partial \boldsymbol{h}_r(\boldsymbol{v})}{\partial \boldsymbol{v}} \boldsymbol{J}\boldsymbol{v} - \boldsymbol{J}\boldsymbol{h}_r - \boldsymbol{f}_r(\boldsymbol{v}) = 0. \tag{2.24}$$

Note that, for $r > 3$, $\boldsymbol{f}_r(\boldsymbol{v})$ is expressed in terms of solutions of homological equation of order $r-1$.

Though is it not generally possible to evaluate the exact solution of the homological equation (2.24), an approximate solution in terms of series expansion can be obtained. Hence we express,

$$\left.\begin{aligned} \boldsymbol{h}_r(\boldsymbol{v}) &= \sum_{j=1}^{n} \sum_{\boldsymbol{m}_r} h_{r,j,\boldsymbol{m}_r} |\boldsymbol{v}|^{\boldsymbol{m}_r} \boldsymbol{e}_j, \\ \boldsymbol{f}_r(\boldsymbol{v}) &= \sum_{j=1}^{n} \sum_{\boldsymbol{m}_r} f_{r,j,\boldsymbol{m}_r} |\boldsymbol{v}|^{\boldsymbol{m}_r} \boldsymbol{e}_j, \end{aligned}\right\} \tag{2.25}$$

where $\boldsymbol{m}_r = (m_1, m_2, \ldots, m_n)$, $\sum_{i=1}^{n} m_i = r$, $(r = 2, 3, \ldots, k)$, $|\boldsymbol{v}|^{\boldsymbol{m}} = \boldsymbol{v}_1^{m_1} \boldsymbol{v}_2^{m_2} \cdots \boldsymbol{v}_n^{m_n}$ and $\boldsymbol{e}_j$ is the j^{th} member of the natural basis. After substituting equation (2.25) into equation (2.24) then equating coefficients of similar terms we obtain,

$$h_{r,j,\boldsymbol{m}_r} = \frac{f_{r,j,\boldsymbol{m}_r}}{\boldsymbol{m}_r \cdot \boldsymbol{\lambda} - \lambda_j}. \tag{2.26}$$

Here, $\boldsymbol{\lambda} = [\lambda_1, \lambda_2, \cdots \lambda_n]^T$ is a vector containing the eigenvalues of linear matrix $\boldsymbol{A}$, while Equation (2.26) represents the coefficients of r^{th} degree near-identity transformation. It hence is clear that coefficients of r^{th} order near-identity can only be obtained if the following solvability condition is satisfied,

$$\boldsymbol{m}_r \cdot \boldsymbol{\lambda} - \lambda_j \neq 0. \tag{2.27}$$

If the solvability condition is not satisfied, then it is referred to as a 'resonant' case and the corresponding resonant terms are retained in the transformed equation. Consequently

the transformed equation in its simplest nonlinear form is the normal form and can be written as,

$$\dot{\boldsymbol{v}} = \boldsymbol{J}\boldsymbol{v} - \sum_{r=2}^{k} \boldsymbol{f}_{\boldsymbol{r}}^{*}(\boldsymbol{v}) + \boldsymbol{O}(|\boldsymbol{v}|^{k+1}), \tag{2.28}$$

where $\boldsymbol{f}_r^*(\boldsymbol{v})$ constitute the resonant terms.

Usually, we can define a linear operator as below,

$$\mathscr{L}_A(\boldsymbol{h}_r) = \frac{\partial \boldsymbol{h}_r(\boldsymbol{v})}{\partial \boldsymbol{v}} \boldsymbol{J}\boldsymbol{v} - \boldsymbol{J}\boldsymbol{h}_r, \quad r = 2, 3, \ldots, k, \tag{2.29}$$

which carries homogeneous vector polynomials over to vector polynomials of the same degree. $\mathscr{L}_A(\boldsymbol{h}_r)$ is the Lie or Poisson bracket of the vector field $\boldsymbol{J}\boldsymbol{v}$ and $\boldsymbol{h}_r(\boldsymbol{v})$. If the set of eigenvalues of $\mathscr{L}_A$ does not contain any zeros, then $\mathscr{L}_A$ is invertible and equation (2.29) can be solved.

2.3.2 Time Dependent Normal Form (TDNF)

Here, we outline the theory behind construction of normal forms for nonlinear systems possessing periodic coefficients. Consider equation (2.30) of a nonlinear system with periodic coefficients,

$$\dot{\boldsymbol{x}} = \boldsymbol{A}(t)\boldsymbol{x} + \boldsymbol{f}_2(\boldsymbol{x}, t) + \boldsymbol{f}_3(\boldsymbol{x}, t) + \cdots + \boldsymbol{f}_k(\boldsymbol{x}, t) + \boldsymbol{O}(|\boldsymbol{x}|^{k+1}, t), \tag{2.30}$$

where $\boldsymbol{A}(t) = \boldsymbol{A}(t+T)$ i.e. an $n \times n$ T-periodic matrix; and, $\boldsymbol{f}_r(\boldsymbol{x}, t)$ are $n \times 1$ nonlinear monomials in $\boldsymbol{x}$ with T-periodic coefficients. The periodic coefficients in $\boldsymbol{A}(t)$ render the normal form methodology discussed in section 2.3 inapplicable. Therefore, requisite transformation of the of the time-variant elements of $\boldsymbol{A}(t)$ to time-invariant elements is accomplished via Lyapunov-Floquet (L-F) transformation matrix $\boldsymbol{Q}(t)$; whose elements have truncated Fourier series representation [75]. Applying the L-F transformation;

$$\boldsymbol{x} = \boldsymbol{Q}(t)\boldsymbol{z}, \tag{2.31}$$

to equation (2.30) results in the equation with a parameter-invariant linear part as below,

$$\begin{aligned}\dot{\boldsymbol{z}} =&\boldsymbol{R}\boldsymbol{z} + \boldsymbol{Q}^{-1}(t)\boldsymbol{f}_2(\boldsymbol{Q}(t)\boldsymbol{z},t) + \boldsymbol{Q}^{-1}(t)\boldsymbol{f}_3(\boldsymbol{Q}(t)\boldsymbol{z},t) + \cdots \\ &+ \boldsymbol{Q}^{-1}(t)\boldsymbol{f}_k(\boldsymbol{Q}(t)\boldsymbol{z},t) + \boldsymbol{Q}^{-1}(t)\boldsymbol{O}(|\boldsymbol{Q}(t)\boldsymbol{z}|^{k+1},t).\end{aligned} \tag{2.32}$$

$\boldsymbol{R}$ is a constant $n \times n$ matrix that generally tends to be complex. After this transformation, equation (2.32) can now be directly subjected to the method of Time-Dependent Normal Forms (TDNF). Subsequently, the Jordan canonical form of equation (2.32) is,

$$\dot{\boldsymbol{y}} = \boldsymbol{J}\boldsymbol{y} + \boldsymbol{M}^{-1}\boldsymbol{f}_2(\boldsymbol{y},t) + \ ... \ + \boldsymbol{M}^{-1}\boldsymbol{f}_k(\boldsymbol{y},t) + \boldsymbol{M}^{-1}\boldsymbol{O}(|\boldsymbol{y}|^{k+1},t), \tag{2.33}$$

where $\boldsymbol{J}$ is the Jordan form of $\boldsymbol{R}$ and $\boldsymbol{f}_k(\boldsymbol{y},t)$ are T-periodic functions containing homogeneous monomials of y_i of order *r*. The above equation is amenable to reduction to its simplest form via a successive application of near-identity transformations of the form,

$$\boldsymbol{y} = \boldsymbol{v} + \boldsymbol{h}_r(\boldsymbol{v},t), \tag{2.34}$$

where $\boldsymbol{h_r}(\boldsymbol{v},t)$ is a formal power series of in $\boldsymbol{v}$ of degree *r* with T-periodic coefficients. Application of above near-identity transformation to equation (2.33) yields,

$$\begin{aligned}\dot{\boldsymbol{v}} =&\boldsymbol{J}\boldsymbol{v} - \left[\frac{\partial \boldsymbol{h}_r(\boldsymbol{v},t)(\boldsymbol{v})}{\partial \boldsymbol{v}}\boldsymbol{J}\boldsymbol{v} - \boldsymbol{J}\boldsymbol{h}_r(\boldsymbol{v},t) + \frac{\partial \boldsymbol{h}_r(\boldsymbol{v},t)}{\partial t}\right] \\ &+ \boldsymbol{f}_r(\boldsymbol{v},t) + \boldsymbol{O}(|\boldsymbol{v}|^{r+1},t).\end{aligned} \tag{2.35}$$

To eliminate the nonlinear terms in equation (2.35), the near identity transformation has to satisfy the following homological equation

$$\frac{\partial \boldsymbol{h}_r(\boldsymbol{v},t)}{\partial \boldsymbol{v}}\boldsymbol{J}\boldsymbol{v} - \boldsymbol{J}\boldsymbol{h}_r(\boldsymbol{v},t) + \frac{\partial \boldsymbol{h}_r(\boldsymbol{v},t)}{\partial t} - \boldsymbol{f}_r(\boldsymbol{v},t) = 0. \tag{2.36}$$

Similar to TINF case, one can solve the time-periodic homological equation and obtain the following solvability condition for a given degree of nonlinearity as,

$$h_{r,j,\boldsymbol{m}_r,l} = \frac{f_{r,j,\boldsymbol{m}_r,l}}{il\omega + \boldsymbol{m}_r \cdot \boldsymbol{\lambda} - \lambda_j}, \tag{2.37}$$

where $\boldsymbol{\lambda} = [\lambda_1, \lambda_2, \cdots, \lambda_n]^T$ are the eigenvalues of $\mathbf{J}$ and are referred to as the Floquet exponents of the system. $i = \sqrt{-1}$, $\omega = \pi/T$ and $-k \leq l \leq k$. Clearly, the resonant condition that must be satisfied to determine the obtain all the coefficients of the near identity transformation is,

$$il\omega + \boldsymbol{m}_r \cdot \boldsymbol{\lambda} - \lambda_j \neq 0. \tag{2.38}$$

Otherwise the resonant terms will remain in the near-identity transformation which can be written in its simplest form as shown in equation below

$$\dot{\boldsymbol{v}} = \boldsymbol{J}\boldsymbol{v} - \sum_{r=2}^{k} \boldsymbol{f}_{\boldsymbol{r}}^{*}(\boldsymbol{v}, t) + \boldsymbol{O}(|\boldsymbol{v}, t|^{k+1}), \tag{2.39}$$

where $\boldsymbol{f}_r^*(\boldsymbol{v}, t)$ are the resonant nonlinear terms.

Moreover, averaging out the periodic terms and retaining only constant terms in $\boldsymbol{f}_{\boldsymbol{r}}^{*}(\boldsymbol{y})$ of equation (2.33), does not significantly jeopardize the quality of solutions. This results in autonomous equations which are amenable to Time-Independent Normal Form (TINF) theory. The resulting autonomous system with approximate states, $\tilde{\boldsymbol{y}}$ and nonlinear monomial functions, $\tilde{\boldsymbol{f}}_r^*(\tilde{\boldsymbol{y}}, t)$ is,

$$\dot{\tilde{\boldsymbol{y}}} = \boldsymbol{J}\tilde{\boldsymbol{y}} - \sum_{r=2}^{k} \tilde{\boldsymbol{f}}_r^*(\tilde{\boldsymbol{y}}, t) + \ \ldots \boldsymbol{O}(|\tilde{\boldsymbol{y}}|^{r+1}; t). \tag{2.40}$$

Application of time-independent near-identity transformation in equation (2.23) yields a simplified TINF as shown below,

$$\dot{\boldsymbol{v}} = \boldsymbol{J}\boldsymbol{v} - \sum_{r=2}^{k} \tilde{\boldsymbol{f}}_r^*(\tilde{\boldsymbol{v}}, t) + \ \ldots \boldsymbol{O}(|\tilde{\boldsymbol{v}}|^{r+1}; t). \tag{2.41}$$

Certainly the TINF case demands less computational effort than the TDNF one, however in both instances, normal form equations retain the stability characteristics of the original periodic nonlinear system. Solutions of the original periodic system in original coordinates are obtained through back transformation of the near-identity, modal and L-F transformations.

2.4 Center Manifold Reduction

A multitude of dynamical systems are modeled by a set of a large number of nonlinear ordinary differential equations (ODE) which may possess constant or periodic coefficients. Analytical models of space systems dynamics are often characterized by a large number of nonlinear ODEs. Consequently, the large dimensional nonlinear analytical models pose significant challenges in model characterization, analysis and control law synthesis. Analyzing such systems requires costly computational and manpower resources; is prone to convergence and numerical truncation errors; and, necessitates intricate treatment of the pertinent excitation parameters and the often coupled system states. Additionally, the system may be externally excited by a periodic forcing term–exacerbating the complexity of the analytical model structure. Therefore, research efforts in the Model Order Reduction (MOR) field continue to investigate propitious techniques of reducing the dimensions of analytical models representing nonlinear dynamical systems. Moreover, MOR techniques have the potential to directly impact related techniques in the field of mathematical modeling such as rapid development of fractional systems. Illustrative recent developments in fractional systems modeling that can be enhanced by MOR include [91], [92]

Order reduction can be defined as a procedure of constructing smaller dimensional systems from large-scale dynamical systems that retain the dominant features of the original system [93]. Order reduction is feasible in dynamical systems because dominant and non-dominant dynamics can be segregated. Consequently, the evolution and long-term dynamical behavior of the system can be exclusively captured and modeled by the reduced number of dominant states. In doing so, a relatively simpler model that is correspondingly

more amenable to system response analysis, optimization, control law development, etc. is achieved–[94], [95].

In general, reduced-order models that approximate the dynamics of the original high-dimension system can be accomplished via linear and nonlinear reduction techniques. There is an abundance of literature on linear order reduction–classical Guyan reduction [96].

On the other hand, nonlinear order reduction is based on a nonlinear projection of the full state-space onto low-dimensional sub-space via the construction of an invariant manifold. Nonlinear order reduction approaches can be broadly classified into the following three *i)* center manifold, *ii)* nonlinear normal modes (NNM), and *iii)* singular perturbation as further expounded by authors such as [51]–[53], [97] and [98]. The second and third techniques are comprehensively addressed in the literature and the reader is directed to the cited references further detailed discussion.

Center manifold is a nonlinear projection-based order reduction technique characterized by the construction of an invariant subspace (manifold) in the system phase-space such that any motion initiated on the subspace remains on the subspace for all time [99], [100]. The underlying premise behind center manifold reduction is the definition of a transformation such that the non-dominant states of the system are expressed as functions of the dominant states. This transformation is then substituted back in the original system to eliminate the non-dominant states. Center manifold reduction is applicable when the linear system matrix has some eigenvalues lying on the imaginary axis (critical modes) while the rest lie on the left-half (stable modes) of the complex plane. Consequently,the evolution of dynamics in such a system will be strictly governed by the critical modes and damped dynamics will passively follow the 'dominant dynamics' as well. Further, it is feasi-

ble to construct a qualitatively equivalent but minimally sized model which solely depends on the system critical modes.

As previously indicated, center manifold is a nonlinear subspace of the state space spanned by the solutions that correspond to marginally stable (critical) eigenvalues [101]. The basis of center manifold reduction is determining a nonlinear transformation that decouples the critical states from the stable states in the nonlinear system. Extension of the center manifold reduction was suggested by Malkin [102] and [51], [52], [75] extended the research further developing methodologies to compute the periodic center manifold with application to bifurcation analyses of nonlinear time periodic systems. Next we outline the time periodic center manifold reduction theory based on the works of [100] and [75]. This will be followed by center manifold reduction of nonlinear systems with constant coefficients.

2.4.1 Time Periodic Center Manifold Reduction

Consider the nonlinear dynamical system with time periodic coefficients below,

$$\dot{\boldsymbol{x}} = \boldsymbol{A}(t)\boldsymbol{x} + \boldsymbol{f}(\boldsymbol{x}, t). \tag{2.42}$$

$\mathbf{A}(t)$ is an $n \times n$ T-periodic matrix such that $\mathbf{A}(t) = \mathbf{A}(T + t)$, $\boldsymbol{x}$ is an $n \times 1$ state vector, $\boldsymbol{f}(\boldsymbol{x}, t)$ is an $n \times 1$ nonlinear T-periodic vector containing homogeneous monomials in $\mathbf{x}$ such that, $\mathbf{f}(0, t) = 0$. The periodic coefficients in $\boldsymbol{A}(t)$ render a direct procedure for center manifold reduction infeasible. The requisite transformation of the linear matrix to a nonautonomous one is first accomplished via via Lyapunov-Floquet (L-F) transformation, $\boldsymbol{x} = \boldsymbol{Q}(t)\boldsymbol{z}$. Elements of the LFT matrix $\boldsymbol{Q}(t)$ contain truncated Fourier series representation [75]. Applying the L-F transformation to equation (2.42) results in the

equation with a parameter-invariant linear part shown below,

$$\dot{\boldsymbol{z}} = \boldsymbol{R}\boldsymbol{z} + \boldsymbol{Q}^{-1}(t)\boldsymbol{f}(\boldsymbol{Q}(t)\boldsymbol{z}, t). \tag{2.43}$$

$\boldsymbol{R}$ is a constant $n \times n$ matrix that generally tends to be complex. After applying the modal transformation $\boldsymbol{z} = \boldsymbol{M}\boldsymbol{y}$ to equation (2.43) we obtain the Jordan canonical form as,

$$\dot{\boldsymbol{y}} = \boldsymbol{J}\boldsymbol{y} + \boldsymbol{M}^{-1}\boldsymbol{f}(\boldsymbol{y}, t) \equiv \boldsymbol{J}\boldsymbol{y} + \boldsymbol{w}(\boldsymbol{y}, t), \tag{2.44}$$

where $\boldsymbol{J}$ is the Jordan form of $\boldsymbol{R}$ and $\boldsymbol{w}(\boldsymbol{y}, t)$ represents T-periodic functions containing homogeneous monomials of y_i. Let matrix **J** in equation (2.44) be composed of *r* critical eigenvalues and $(n - r)$ stable eigenvalues. Hence, equation (2.44) can be partitioned as

$$\begin{bmatrix} \dot{\boldsymbol{y}}_c \\ \dot{\boldsymbol{y}}_s \end{bmatrix} = \begin{bmatrix} \boldsymbol{J}_c & 0 \\ 0 & \boldsymbol{J}_s \end{bmatrix} \begin{bmatrix} \boldsymbol{y}_c \\ \boldsymbol{y}_s \end{bmatrix} + \begin{bmatrix} \boldsymbol{w}_c(\boldsymbol{y}_c, \boldsymbol{y}_s, t) \\ \boldsymbol{w}_s(\boldsymbol{y}_c, \boldsymbol{y}_s, t) \end{bmatrix}, \tag{2.45}$$

where $\boldsymbol{y}_c$ is an $r \times 1$ vector of critical states $(r \ll n)$. $\boldsymbol{y}_s$ is an $(n - r) \times 1$ vector of stable states. $\boldsymbol{J}_c$ is an $r \times r$ Jordan block corresponding to critical states. $\boldsymbol{J}_s$ is the $(n-r) \times (n-r)$ Jordan block of dimension corresponding to the non-dominant states and $\boldsymbol{w}_c(\boldsymbol{y}_c, \boldsymbol{y}_s, t)$ and $\boldsymbol{w}_s(\boldsymbol{y}_c, \boldsymbol{y}_s, t)$ are monomials of $\boldsymbol{y}$ (of order *i*) with periodic coefficients. The *time periodic center manifold theorem* specifies existence of the following non-unique relation,

$$\boldsymbol{y}_s = \boldsymbol{H}(\boldsymbol{y}_c, t). \tag{2.46}$$

Substituting equation (2.46) into (2.45) decouples the critical states from the stables ones resulting in a system containing only critical states shown below,

$$\dot{\boldsymbol{y}}_c = \boldsymbol{J}_c\boldsymbol{y}_c + \boldsymbol{w}_c(\boldsymbol{y}_c, \boldsymbol{H}(\boldsymbol{y}_c, t), t). \tag{2.47}$$

The reduced equation (2.47) is dynamically equivalent to the original system in equation (2.42). We assume a nonlinear relationship between the dominant $\boldsymbol{y}_c$ and the non-dominant $\boldsymbol{y}_s$ states as,

$$\boldsymbol{y}_s = \sum_i \boldsymbol{h}_i(\boldsymbol{y}_c, t) \equiv \boldsymbol{H}(\boldsymbol{y}_c, t), \tag{2.48}$$

where,

$$\begin{aligned} \boldsymbol{h}_i &= \sum_{\bar{\boldsymbol{m}}} \bar{\boldsymbol{h}}_i(t) \boldsymbol{y}_i^{m_1} \dots \boldsymbol{y}_c^{m_r} \\ \bar{\boldsymbol{m}} &= [m_1, \dots, m_r]^T,\ m_1 + \dots + m_r = i,\ i = 1, 2, 3 \dots, k. \end{aligned} \tag{2.49}$$

$\bar{\boldsymbol{h}}_i(t)$ are the unknown periodic vector coefficients with period 2T. Substituting equation (2.48) into (2.45) yields,

$$\frac{\partial \boldsymbol{H}}{\partial t} + \frac{\partial \boldsymbol{H}}{\partial \boldsymbol{y}_c}(\boldsymbol{J}_c \boldsymbol{y}_c + \boldsymbol{w}_c) = \boldsymbol{J}_s \boldsymbol{H} + \boldsymbol{w}_s. \tag{2.50}$$

If the i^{th} order $\mathbf{H}$ in above equation is considered, then $\boldsymbol{w}_s$ has to be approximated to the i^{th} order as well, and we represent this by $\boldsymbol{w}_{si}$. However, all terms in $(\partial \boldsymbol{H}/\partial \boldsymbol{y}_c)\boldsymbol{w}_c$ are of the order *i*+1 or higher. Therefore, neglecting this product, we obtain,

$$\frac{\partial \boldsymbol{H}}{\partial t} + \frac{\partial \boldsymbol{H}}{\partial \boldsymbol{y}_c} \boldsymbol{J}_c \boldsymbol{y}_c - \boldsymbol{J}_s \boldsymbol{H} = \boldsymbol{w}_{si}. \tag{2.51}$$

This partial differentiation equation is approximately solved by expanding the known and the unknown periodic coefficient functions ($\bar{\boldsymbol{h}}_i(t)$) into finite Fourier series as,

$$\left.\begin{aligned} \boldsymbol{h}_i(\boldsymbol{y}_c, t) &= \sum_{j=1}^{s} \sum_{\bar{\boldsymbol{m}}} \sum_{\nu=-\infty}^{\infty} h_{j\bar{m}\nu} \boldsymbol{e}^{\bar{i}\nu\omega t} |\boldsymbol{y}_c|^{\boldsymbol{m}} \boldsymbol{e}_j \\ \boldsymbol{w}_{si}(\boldsymbol{y}_c, t) &= \sum_{j=1}^{s} \sum_{\bar{\boldsymbol{m}}} \sum_{\nu=-\infty}^{\infty} a_{j\bar{m}\nu} \boldsymbol{e}^{\bar{i}\nu\omega t} |\boldsymbol{y}_c|^{\boldsymbol{m}} \boldsymbol{e}_j, \end{aligned}\right\} \tag{2.52}$$

where $|\boldsymbol{y}_c|^{\boldsymbol{m}} = y_1^{m_1} y_2^{m_2} \cdots y_r^{m_r},\ \omega = \pi/T,\ \bar{i} = \sqrt{-1},\ m_1 + \ldots + m_r = i;\ i = 2, 3, \ldots, k.$ $a_{j\bar{m}\nu}$ are the unknown Fourier coefficients of the manifold and $\boldsymbol{e}_j$ is the j^{th} member of the natural basis. A term-by-term comparison of the Fourier coefficients yields,

$$h_{j\bar{m}\nu} = \frac{a_{j\bar{m}\nu}}{(\bar{i}\nu\omega) + \sum_{\ell=1}^{r}(m_\ell \lambda_\ell - \bar{\lambda}_p)}, \tag{2.53}$$

where $\lambda_1, \lambda_2, \ldots, \lambda_r$ are the eigenvalues of the Jordan matrix $\boldsymbol{J}_c$ and $\bar{\lambda}_p$; $p = 1, 2, \ldots, s$ are the eigenvalues of $\boldsymbol{J}_s$. Therefore, the *reducibility condition* is;

$$\begin{aligned} (\bar{i}\nu\omega) + \sum_{\ell=1}^{r} (m_\ell \lambda_\ell - \bar{\lambda}_p) \neq 0 \\ \forall \nu = 0, \pm 1, \pm 2, \ldots; \quad p = 1, 2, \ldots, s. \end{aligned} \tag{2.54}$$

Satisfying the *reducibility condition* evaluates vector $\boldsymbol{H}(\boldsymbol{y}_c)$ hence the stable states can be expressed in terms of the critical states.

For $\nu = 0$, a resonance occurs when some linear combination of λ_ℓ (Floquet exponents corresponding to the critical states) and $\lambda_{\bar{p}}$ (Floquet exponent of the stable states) add up to zero. This may be referred to as the *true internal resonance*. For the autonomous case, $\lambda_n = \pm i\omega_n$ (where ω_n are the natural frequencies corresponding to the original coordinates). Equation (2.54) provides conditions for the conventional *internal resonance* widely discussed in the literature.For $\nu \neq 0$ the denominator in equation (2.53) goes to zero when the parametric excitation frequency is a linear combination of λ_ℓ and λ_p. This situation is referred to as the *true combination resonance* case. If $\boldsymbol{J}_c$ matrix contains a pair of zeros, then the order reduction process necessarily boils down to finding a time-periodic center manifold relation between the stable and the critical states. Since Floquet multipliers are either -1 or +1; the system undergoes a 'flip' or a symmetry breaking (or transcritical) bifurcation, respectively. The reduced order model does not contain any linear terms; it is strictly a nonlinear model. Once $\boldsymbol{H}(\boldsymbol{w}_r, t)$ has been determined, we obtain the equation for the critical states $\boldsymbol{y}_c$ in the $\boldsymbol{y}$ domain as shown in equation (2.47). Results in the original coordinates are obtained through back transformation via inverse L-F and inverse modal transformations.

2.4.2 Constant Coefficients Center Manifold Reduction

The procedure for constructing center manifolds for nonlinear systems with constant coefficients is very similar to the preceding case of periodic coefficients. The major difference will be absence of time-dependent parameters and terms. Consider such a system with constant coefficients shown below

$$\dot{\boldsymbol{x}} = \boldsymbol{A}\boldsymbol{x} + \boldsymbol{f}(\boldsymbol{x}). \tag{2.55}$$

A is an $n \times n$ constant matrix. $\boldsymbol{f}(\boldsymbol{x})$ is an $n \times 1$ nonlinear vector containing homogeneous monomials in **x**. Then, it can be shown that following a similar procedure described in from equations (2.43) to (2.54), the reducability condition will be,

$$\sum_{\ell=1}^{r}(m_\ell \lambda_\ell - \bar{\lambda}_p) \neq 0 \qquad p = 1, 2, \ldots, s. \tag{2.56}$$

Parameters in equation (2.56) are as previously defined.

2.5 Analysis of Nonlinear Systems With External Periodic Excitation

The preceding two sections constitute crucial techniques that facilitate analysis of complex nonlinear motion. However, as noted previously, presence of periodic coefficients and/or external periodic excitations presents unique challenges to conventional normalization and model order reduction. The conventional normal forms methodology is applicable to nonlinear systems with constant coefficients and without a forcing term. Presence of variant coefficients and/or periodical external excitation renders the conventional near-identity transformation methodology inapplicable. Accordingly, forced nonlinear dynamical systems have been mostly analyzed using averaging and perturbations techniques. However, the main drawback to these two mentioned approaches is that they are

restricted to minimally excited systems with relatively small nonlinearity coefficients[36], [75]. Presence of external periodic excitation and/or periodic coefficients in the system dynamics introduces unique challenges that similarly render direct application of the conventional nonlinear order reduction methodologies infeasible. A number of authors have presented different approaches to address this type of problem. Some approaches incorporate a means to augment the state space by treating the forcing as an additional state while others construct invariant manifolds composed of temporal and dominant state variables. Consequently we introduce and apply the intuitive state augmentation technique to facilitate a lucid and plain analysis of periodically forced nonlinear system via normal forms and center manifold reduction.

2.5.1 Normal Forms of Nonlinear Systems with External Periodic Excitation

In addressing this problem, authors such as [37], [38], [36] and [39] have traditional applied special strategies that encompass 'book-keeping' parameters, detuning parameters *ad-hoc* unsolved equations, *ad-hoc* variables, etc. Principally, the foregoing expansion of system parameters hardly embraces a consistent and plain affiliation with the pertinent terms of the nonlinear equations under analysis. Consequently, such methodologies tend to appear daunting and convoluted stymieing their seamless broad application.

For instance, to construct the normal form of a 2-degree of freedom system with external periodic excitation, [36] propose an elaborate modification to the regular near-identity transformation shown in equation (2.57) to obtain the near-identity transformation shown below,

$$\begin{bmatrix} y_1 \\ y_2 \end{bmatrix} = \begin{bmatrix} v_1 \\ v_2 \end{bmatrix} + \begin{bmatrix} h_{1(0)} \\ h_{2(0)} \end{bmatrix} + \varepsilon \begin{bmatrix} h_{1(1,0)}v_1 + h_{1(0,1)}v_2 \\ h_{2(1,0)}v_1 + h_{2(0,1)}v_2 \end{bmatrix}$$

$$+\varepsilon \begin{bmatrix} h_{1(2,0)}v_1^2 + h_{1(1,1)}v_1v_2 + h_{1(0,2)}v_2^2 \\ h_{2(2,0)}v_1^2 + h_{2(1,1)}v_1v_2 + h_{2(0,2)}v_2^2 \end{bmatrix} \tag{2.57}$$

$$+\varepsilon \begin{bmatrix} \tilde{h}_{1(0)}v_1^3 + \tilde{h}_{1(2,1)}v_1^2v_2 + \tilde{h}_{1(1,2)}v_1v_2^2 + \tilde{h}_{1(0,3)}v_2^3 \\ \tilde{h}_{2(0)}v_1^3 + \tilde{h}_{2(2,1)}v_1^2v_2 + \tilde{h}_{2(1,2)}v_1v_2^2 + \tilde{h}_{2(0,3)}v_2^3 \end{bmatrix}.$$

ε is a *small* book-keeping parameter, $h_{r,i(m_1,m_2)}$ are time-periodic parameter and $\tilde{h}_{r,i(m_1,m_2)}$ are parameter independent (constant) coefficients. After application of the transformation, like powers of $\boldsymbol{v}$ are collected to evaluate the unknown constants $\boldsymbol{h_r}$. As shown by [36] this will lead to nonlinear differential and homological equations which are subsequently solved in the publication.

Therefore, we shall present a relatively more direct, plain and intuitive approach to obtain normal forms for nonlinear systems with external periodic excitation. Our approach does not require elaborate modifications to the conventional near-identity transformation, a detuning parameter or a 'book-keeping' parameter. Furthermore, this approach is empowered through augmenting the systems states by transforming the exciting frequency terms into system states. The augmented states directly emanate from the exciting frequency terms, hence they are neither *ad-hoc* nor arbitrary. As a result, the state aggrandizement is intuitive and consistently applicable over a broad range of nonlinear systems with external periodic excitation.

Because this state augmentation approach annihilates the original non-autonomous periodic forcing term, the conventional near-identity transformations presented in equa-

tion (2.23) can hence be innocuously applied to normalize the periodically forced nonlinear system. The intuitive state augmentation proposed here should be implemented immediately prior to normalization of forced nonlinear systems. Formulation of the intuitive state augmentation technique will be conducted separately for forced nonlinear systems with constant coefficients; and, forced nonlinear systems with periodic coefficients.

2.5.1.1 Systems with Constant Coefficients

We first consider external periodically excited nonlinear systems with constant coefficients. Therefore, the pertinent nonlinear system is of the form shown below,

$$\dot{\boldsymbol{x}} = \boldsymbol{A}\boldsymbol{x} + \breve{\boldsymbol{f}}(\boldsymbol{x}) + \boldsymbol{F}(t), \tag{2.58}$$

where $\breve{\boldsymbol{f}}(\boldsymbol{x})$ is an $n \times 1$ vector representing all the nonlinear monomial terms in $\boldsymbol{x}$ and $\boldsymbol{A}$ is as previously defined. $\boldsymbol{F}(t)$ is the $n \times 1$ periodic vector whose elements are periodic forcing terms as shown below,

$$\boldsymbol{F}(t) = \begin{bmatrix} B_1 g_1(t) \\ B_2 g_2(t) \\ \vdots \\ B_i g_i(t) \end{bmatrix}, \qquad i = 1, 2, 3, \ldots, n. \tag{2.59}$$

B_i is the amplitude of the forcing term and $g_i(t)$ represents a sine or cosine trigonometric function of i^{th}forcing angular frequency 'ω' i.e. $\sin(\omega_i t)$ or $\cos(\omega_i t)$. We augment the system states by delineating,

$$\left.\begin{array}{lll} p_1 = g_1(t) & \dot{p}_1 = \mp\omega_1\dot{g}_1(t) = \mp q_1 & \dot{q}_1 = \pm\omega_1^2 g_1(t) = \pm\omega_1^2 p_1, \\ p_2 = g_2(t) & \dot{p}_2 = \mp\omega_2\dot{g}_2(t) = \mp q_2 & \dot{q}_2 = \pm\omega_2^2 g_2(t) = \pm\omega_2^2 p_2, \\ \vdots & \vdots & \vdots \\ p_n = g_n(t) & \dot{p}_n = \mp\omega_n\dot{g}_n(t) = \mp q_n & \dot{q}_n = \pm\omega_n^2 g_n(t) = \pm\omega_n^2 p_n. \end{array}\right\} \tag{2.60}$$

Consequently, the augmented $\ell \times 1$ state vector is,

$$\tilde{\boldsymbol{x}} = [\boldsymbol{x},\ p_1,\ p_2,\ \ldots,\ p_n,\ q_1,\ q_2,\ \ldots,\ q_n\ ]^T. \tag{2.61}$$

Further, the augmented states nonlinear vector $\breve{\boldsymbol{F}}(\tilde{\boldsymbol{x}})$ containing augmented monomial terms will be as shown in the equation below,

$$\breve{\boldsymbol{F}}(\tilde{\boldsymbol{x}}) = \begin{bmatrix} B_1 f(\boldsymbol{x}, p_1, p_2, \ldots, p_n, q_1, q_2, \ldots, q_n) \\ B_2 f(\boldsymbol{x}, p_1, p_2, \ldots, p_n, q_1, q_2, \ldots, q_n) \\ \vdots \\ B_n f(\boldsymbol{x}, p_1, p_2, \ldots, p_n, q_1, q_2, \ldots, q_n) \\ 0 \\ 0 \\ 0 \\ 0 \\ \vdots \\ 0 \\ 0 \end{bmatrix},\ n = 3, 4, \ldots. \tag{2.62}$$

The state augmentation transforms (2.58) from nonautonomous to autonomous as shown below,

$$\dot{\tilde{\boldsymbol{x}}} = \tilde{\boldsymbol{A}}\tilde{\boldsymbol{x}} + \breve{\boldsymbol{F}}(\tilde{\boldsymbol{x}}). \tag{2.63}$$

Equation (2.63) is of the same form as equation (2.20) despite capturing the forced non-linear dynamics shown in equation (2.58). After applying the modal transformation $\tilde{\boldsymbol{x}} = \boldsymbol{M}\tilde{\boldsymbol{y}}$ to equation (2.63), we obtain,

$$\dot{\tilde{\boldsymbol{y}}} = \tilde{\boldsymbol{J}}\tilde{\boldsymbol{y}} + \boldsymbol{M}^{-1}\breve{\boldsymbol{F}}(\boldsymbol{M}\tilde{\boldsymbol{y}}). \tag{2.64}$$

$\tilde{\boldsymbol{J}}$ is the $\ell \times \ell$ Jordan canonical form of the augmented linear matrix $\tilde{\boldsymbol{A}}$. Let $s = {}^{(\ell\,-\,n)}/_{2}$ be the count of the number of forcing frequencies in the system. Then $\tilde{\boldsymbol{J}}$ will be structured as shown below,

$$\tilde{\boldsymbol{J}} = \left[\begin{array}{ccc|ccc} \lambda_1 & & & & & \\ & \lambda_2 & & & & \\ & & \ddots & & & \\ & & & \lambda_n & & \\ \hline & & & \lambda_{n+1} & & \\ & & & & \lambda_{n+2} & \\ & & & & & \ddots \\ & & & & & & \lambda_\ell \end{array}\right]. \tag{2.65}$$

To determine the resonant condition for the normal forms of the augmented system; let $\tilde{\boldsymbol{\lambda}}$ be the vector containing eigenvalues of linear matrix $\tilde{\boldsymbol{A}}$ as below,

$$\tilde{\boldsymbol{\lambda}} = [\lambda_1, \lambda_2, \ldots, \lambda_n, \lambda_{n+1}, \lambda_{n+2}, \ldots, \lambda_{\ell-1}, \lambda_\ell]^T, \tag{2.66}$$

where $\lambda_{n+1} = i\omega_1,\ \lambda_{n+2} = -i\omega_1,\ \lambda_{n+3} = i\omega_2,\ \lambda_{n+4} = -i\omega_2,\ \ldots,\ \lambda_{\ell-1} = i\omega_s,\ \lambda_\ell = -i\omega_s$.

and, $\tilde{\boldsymbol{m}}_r = (m_1, m_2, \ldots, m_\ell)$, then similar to equation (2.27), the resonant condition for the state augmented system will be,

$$\tilde{\boldsymbol{m}}_{\boldsymbol{r}} \cdot \tilde{\boldsymbol{\lambda}} - \lambda_k \neq 0, \tag{2.67}$$

where $k = 1, 2, 3, \ldots, n$.

If the above solvability condition is not satisfied, then the corresponding resonant terms will be retained in the simplified augmented system.

Consequently the conventional normalization principles outlined in section 2.3 are essentially applied to simplify the state augmented forced nonlinear system to its normal forms. Application of this state augmentation approach will be illustrated in section 2.5.2.1.

2.5.1.2 Systems with Periodic Coefficients

In order to analyze a periodically excited nonlinear system with periodic coefficients, consider the system below,

$$\dot{\boldsymbol{x}} = \boldsymbol{A}(t)\boldsymbol{x} + \breve{\boldsymbol{f}}(\boldsymbol{x}, t) + \boldsymbol{F}(t), \tag{2.68}$$

where $\breve{\boldsymbol{f}}(\boldsymbol{x}, t)$ is an $n \times 1$ vector representing all the nonlinear monomial terms in $\boldsymbol{x}$ with T-periodic coefficients. All the other terms are as previously defined. The L-F transformed equation (2.68) is given below,

$$\dot{\boldsymbol{z}} = \boldsymbol{R}\boldsymbol{z} + \boldsymbol{Q}^{-1}(t)\breve{\boldsymbol{f}}(\boldsymbol{Q}\boldsymbol{z}, t) + \boldsymbol{Q}^{-1}(t)\boldsymbol{F}(t). \tag{2.69}$$

We augment the system states as previously explained via equations (2.59), (2.60), (2.61) and (2.61) to obtain the system similar to equation (2.62) as shown below,

$$\dot{\tilde{\boldsymbol{z}}} = \tilde{\boldsymbol{R}}\tilde{\boldsymbol{z}} + \boldsymbol{Q}^{-1}(t)\breve{\tilde{\boldsymbol{F}}}(\tilde{\boldsymbol{z}}). \tag{2.70}$$

Here, state vector $\tilde{\boldsymbol{z}} = [\boldsymbol{z}, p_1, p_2, \ldots, p_n, q_1, q_2, \ldots, q_n]^T$ and $\breve{\tilde{\boldsymbol{F}}}(\tilde{\boldsymbol{z}})$ contains augmented nonlinear monomial terms in $\tilde{\boldsymbol{z}}$. $\tilde{\boldsymbol{R}}$ is the augmented states linear matrix. The Jordan canonical form of $\tilde{\boldsymbol{R}}$ is the matrix $\tilde{\boldsymbol{J}}$ whose structure is as previously shown in equation

(2.65). However, elements of vector $\tilde{\boldsymbol{\lambda}}$ in the range $\lambda_1, \ldots, \lambda_n$ as defined in equation (2.66) will be Floquet exponents. If fresh linear periodic coefficients emerge from the interaction of $\breve{\boldsymbol{F}}(t)$ with $\boldsymbol{Q}^{-1}(t)$; then an additional L-F transformation is necessary to render the linear terms parameter-invariant.

Subsequently, the non-resonance condition to be satisfied for corresponding terms to be annihilated from the simplified augmented normal form is,

$$il\omega + \boldsymbol{m}_r \cdot \tilde{\boldsymbol{\lambda}} - \lambda_k \neq 0, \tag{2.71}$$

where $k = 1, 2, 3, \ldots, n$. All the other terms remain as previously defined in section 2.5.1.1.

2.5.2 Illustrative Normal Forms Application

Here, we apply the intuitive system state augmentation technique to expeditiously obtain normal forms of forced nonlinear systems with both constant and periodic coefficients. We shall utilize forced nonlinear dynamics with parameter values similarly applied by [36] to facilitate comprehensive comparison of our approach with existing approaches.

2.5.2.1 Forced Nonlinear Systems With Constant Coefficients

We consider the forced Duffing's equation to illustrate application of the intuitive state augmentation methodology in analyzing forced nonlinear systems via normal forms as given below,

$$\begin{bmatrix} \dot{x}_1 \\ \dot{x}_2 \end{bmatrix} = \begin{bmatrix} 0 & 1 \\ -a & -d \end{bmatrix} \begin{bmatrix} x_1 \\ x_2 \end{bmatrix} - \varepsilon \begin{bmatrix} 0 \\ cx_1^3 \end{bmatrix} + B \begin{bmatrix} 0 \\ \cos(\omega t) \end{bmatrix}, \tag{2.72}$$

where $a, d, c,$ and ε are system parameters, while B is amplitude of the external periodic forcing term. To convert the forced nonlinear system from non-autonomous to autonomous via state augmentation, let

$$\left.\begin{aligned} p &= \cos(\omega t), \\ \dot{p} &= -\omega \sin(\omega t) = -q, \\ \dot{q} &= \omega^2 \cos(\omega t) = \omega^2 p. \end{aligned}\right\} \tag{2.73}$$

After substituting equations (2.73) into (2.72) we obtain the augmented system state space representation shown below

$$\begin{bmatrix} \dot{x}_1 \\ \dot{x}_2 \\ \dot{p} \\ \dot{q} \end{bmatrix} = \begin{bmatrix} 0 & 1 & 0 & 0 \\ -a & -d & B & 0 \\ 0 & 0 & 0 & -1 \\ 0 & 0 & \omega^2 & 0 \end{bmatrix} \begin{bmatrix} x_1 \\ x_2 \\ p \\ q \end{bmatrix} - \varepsilon \begin{bmatrix} 0 \\ cx_1^3 \\ 0 \\ 0 \end{bmatrix}. \tag{2.74}$$

Next we apply the modal transformation $\tilde{\boldsymbol{x}} = \boldsymbol{M}\tilde{\boldsymbol{y}}$, (where: $\tilde{\boldsymbol{x}} = [x_1\, x_2\, p\, q]^T$) to equation (2.74) and obtain the following equation,

$$\dot{\tilde{\boldsymbol{y}}} = \boldsymbol{\tilde{J}}\tilde{\boldsymbol{y}} - \boldsymbol{M}^{-1}\varepsilon \begin{bmatrix} 0 \\ c(M_{11}\tilde{y}_1 + M_{12}\tilde{y}_2)^3 \\ 0 \\ 0 \end{bmatrix}, \tag{2.75}$$

where $\boldsymbol{\tilde{J}}$ is in the Jordan canonical form. Equation (2.75) is hence of the form described in equation (2.21) as,

$$\dot{\tilde{\boldsymbol{y}}} = \boldsymbol{\tilde{J}}\tilde{\boldsymbol{y}} + \boldsymbol{M}^{-1}\boldsymbol{f}_3(\boldsymbol{M}\tilde{\boldsymbol{y}}). \tag{2.76}$$

The normal form is evaluated by successive application of the near identity transformation,

$$\tilde{\boldsymbol{y}} = \boldsymbol{v} + \boldsymbol{h_3}(\boldsymbol{v}). \tag{2.77}$$

To obtain the closed form analytical solution of the Duffing's equation via normal forms; we shall consider 3 cases delineated by different values of system parameters.

Case (i): Nonresonant excitation.

Here, $a = 3,\ d = 0.3,\ c = 1,\ B = 2,\ \omega = 4$ and $\varepsilon = 0.5$. The Time Independent Normal Form (TINF) subsequently realized after successive application of near-identity transformations is given below

$$\begin{bmatrix} \dot{v}_1 \\ \dot{v}_2 \\ \dot{v}_3 \\ \dot{v}_4 \end{bmatrix} = \begin{bmatrix} i4v_1 \\ -i4v_2 \\ (-0.15 + i1.72554)v_3 + i0.00117255v_1v_2v_3 \\ (-0.15 - i1.72554)v_4 - i0.00117255v_1v_2v_4 \end{bmatrix}. \tag{2.78}$$

When the external forcing term is augmented as a system state; the linear terms of the normal forms are made up of: *i)* magnitude of forcing frequency appearing as purely imaginary conjugate coefficients, i.e. 4, and *ii)* conjugate eigenvalues of the original linear matrix A, i.e. $(-0.15 \pm i1.72554)$. This is consistent with the structure of $\tilde{\boldsymbol{J}}$ presented in equation (2.65). Solving the normal form differential equation system (2.78) yields the closed form analytical solution as,

$$\left.\begin{aligned} v_1(t) &= C_1 e^{i4t}, \\ v_2(t) &= C_2 e^{-i4t}, \\ v_3(t) &= C_3 e^{[-0.15 + i(1.7255 + 0.00117255 C_1 C_2)]t}, \\ v_4(t) &= C_4 e^{[-0.15 - i(1.7255 + 0.00117255 C_1 C_2)]t}, \end{aligned}\right\} \tag{2.79}$$

$C_{1,2,3,4}$ are respective constants of integration. The closed form analytical solutions of $v_1(t),\ v_2(t),\ v_3(t)$, and $v_4(t)$, are then back transformed to the original coordinates and

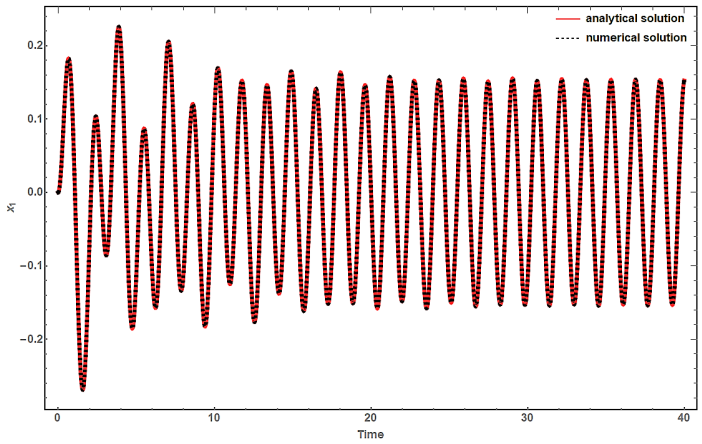

(a) $x_1(t)$

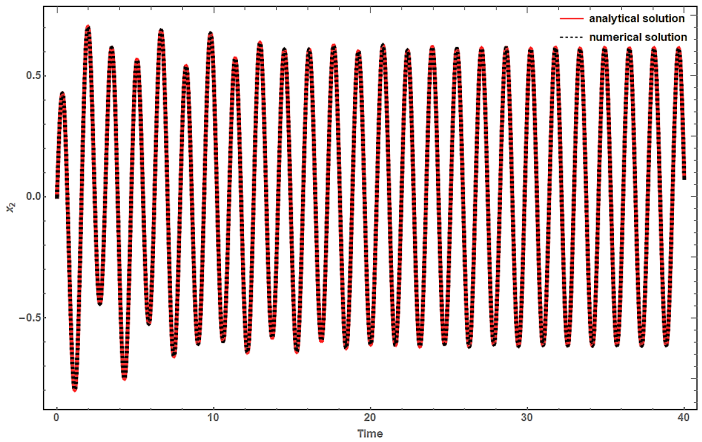

(b) $x_2(t)$

Figure 4: State Response Comparison for Nonresonant Excitation Case

the responses plotted. Figure 4 shows the closed form analytical solution compared to the numerically integrated solution for states $x_1(t)$ and $x_2(t)$ of the non-resonant forcing case.

Case (ii): Superharmonic resonance excitation.

Here, $a = 5,\ d = 0.3,\ c = 0.1,\ B = 4,\ \omega = 0.745$ and $\varepsilon = 0.5$. The TINF subsequently realized after successive near-identity transformations is given below

$$\begin{bmatrix} \dot{v}_1 \\ \dot{v}_2 \\ \dot{v}_3 \\ \dot{v}_4 \end{bmatrix} = \begin{bmatrix} (-0.15 + i2.23103)v_1 + i0.0193193v_1v_3v_4 \\ (-0.15 - i2.23103)v_2 - i0.0193193v_2v_3v_4 \\ i0.745v_3 \\ -i0.745v_4 \end{bmatrix}. \tag{2.80}$$

Consistent with the structure of $\tilde{\boldsymbol{J}}$ in equation (2.65); the linear terms of the normal forms are made up of: *i)* magnitude of forcing frequency appearing as purely imaginary conjugate coefficients, i.e. 0.745, and *ii)* conjugate eigenvalues of the original linear matrix A, i.e. $(-0.15 \pm i2.23103)$. Solving the normal form differential equation system (2.80) yields the closed form analytical solution as,

$$\left.\begin{aligned} v_1(t) &= C_1 e^{[-0.15+i(2.23103+0.0193193C_3C_4)]t}, \\ v_2(t) &= C_2 e^{[-0.15-i(2.23103+0.0193193C_3C_4)]t}, \\ v_3(t) &= C_3 e^{i0.745t}, \\ v_4(t) &= C_4 e^{-i0.745t}. \end{aligned}\right\} \tag{2.81}$$

The closed form analytical solutions of $v_1(t),\ v_2(t),\ v_3(t)$, and $v_4(t)$, are then back transformed to the original coordinates and the responses plotted. Figure 5 shows the closed form analytical solution compared to the numerically integrated solution for states $x_1(t)$ and $x_2(t)$.

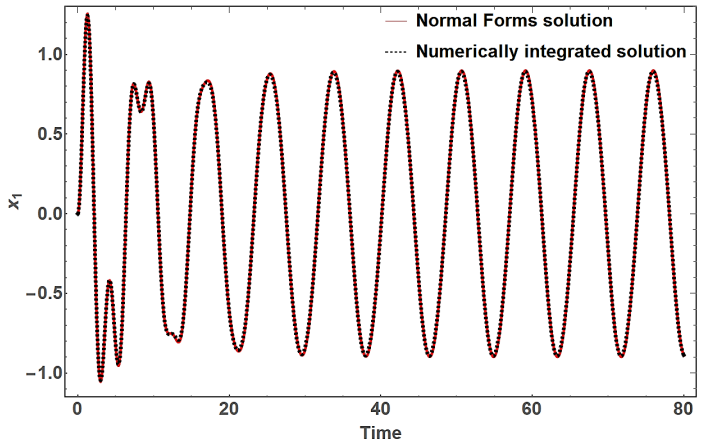

(a) $x_1(t)$

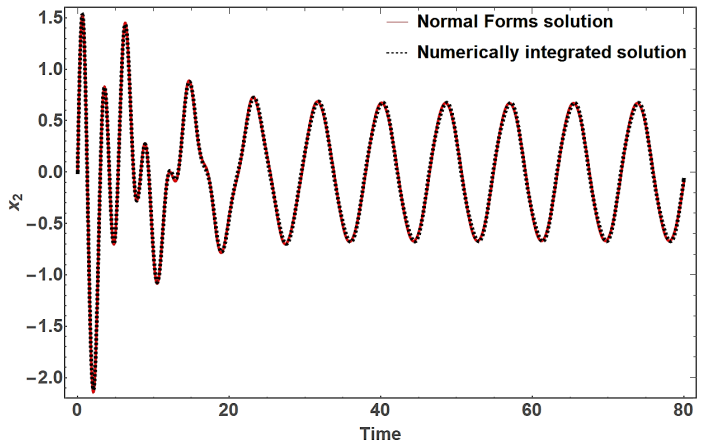

(b) $x_2(t)$

Figure 5: State Response Comparison for Superharmonic Excitation Case

Case (iii): Subharmonic resonance excitation.

Here, $a = 4,\ d = 0.1,\ c = 7.972,\ B = 10,\ \omega = 6.6$ and $\varepsilon = 0.5$. The TINF obtained after successive near-identity transformations is given below,

$$\begin{bmatrix} \dot{v}_1 \\ \dot{v}_2 \\ \dot{v}_3 \\ \dot{v}_4 \end{bmatrix} = \begin{bmatrix} i6.6v_1 \\ -i6.6v_2 \\ (-0.05 + i1.99937)v_3 + i0.00805922v_1v_2v_3 \\ (-0.05 - i1.99937)v_4 - i0.00805922v_1v_2v_4 \end{bmatrix}. \tag{2.82}$$

Similarly, the linear terms of the normal forms are made up of: *i)* magnitude of forcing frequency appearing as purely imaginary conjugate coefficients, i.e. 6.6, and *ii)* conjugate eigenvalues of the original linear matrix A, i.e. $(-0.05 \pm i1.99937)$. Solving the normal form differential equation system (2.82) yields,

$$\left.\begin{aligned} v_1(t) &= C_1 e^{i6.6t}, \\ v_2(t) &= C_2 e^{-i6.6t}, \\ v_3(t) &= C_3 e^{[-0.05+i(1.99937+0.00805922C_1C_2)]t}, \\ v_4(t) &= C_4 e^{[-0.05-i(1.99937+0.00805922C_1C_2)]t}. \end{aligned}\right\} \tag{2.83}$$

The closed form analytical solutions of $v_1(t),\ v_2(t),\ v_3(t),$ and $v_4(t)$, are then back transformed to the original coordinates and the responses plotted. Figure 6 shows the analytical solution compared to the numerically integrated solution for states $x_1(t)$ and $x_2(t)$.

We note that, all the foregoing closed-form analytical solutions of the periodically forced Duffing oscillator (with zero initial conditions) exactly match the transient and steady behaviors of the numerically integrated solutions.

2.5.2.2 Forced Nonlinear Systems With Periodic Coefficients

We employ the intuitive state augmentation methodology to analyze a Mathieu-Duffing equation whose linear and nonlinear terms possess periodic coefficients as shown below,

$$\begin{bmatrix} \dot{x}_1 \\ \dot{x}_2 \end{bmatrix} = \begin{bmatrix} 0 & 1 \\ -(a + b\cos(2\pi t)) & -d \end{bmatrix} \begin{bmatrix} x_1 \\ x_2 \end{bmatrix} - \varepsilon \cos(\pi t) \begin{bmatrix} 0 \\ x_1^3 \end{bmatrix} + \begin{bmatrix} 0 \\ B\cos(4\pi t) \end{bmatrix}, \tag{2.84}$$

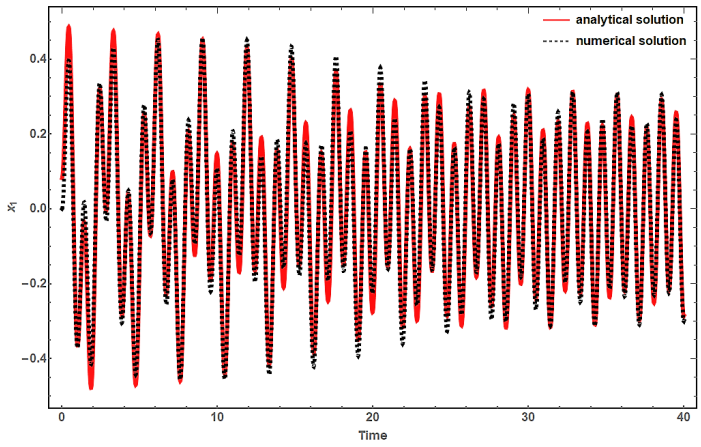

(a) $x_1(t)$

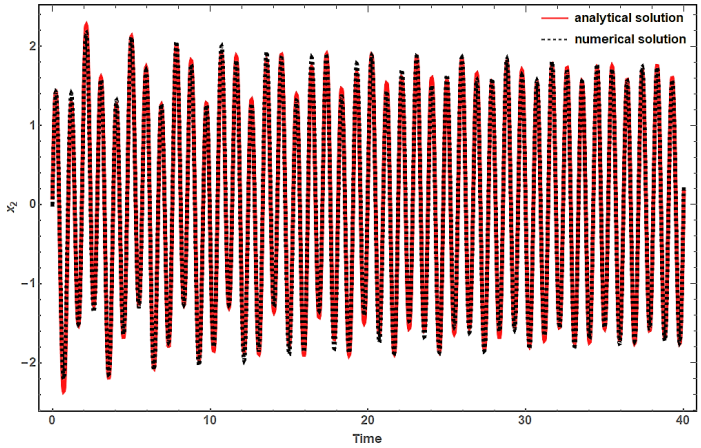

(b) $x_2(t)$

Figure 6: State Response Comparison for Subharmonic Excitation Case

where *a, b, c* and ε are system parameters. We consider a case with purely imaginary Floquet exponents which occurs when $a = 3,\ b = 1,\ d = 0,\ B = 1$ and $\varepsilon = 0.5$. To construct the normal forms of this system, we first transform the linear parameter-varying terms into parameter-invariant terms using LFT matrix $Q(t)$ obtained via the procedure outlined in section 2.2. The computed Floquet Transition Matrix (monodromy matrix), $\boldsymbol{\Phi}(T)$ and constant $\boldsymbol{R}$ matrix are given below,

$$\boldsymbol{\Phi}(T) = \begin{bmatrix} -0.16575 & 0.61105 \\ -1.59156 & -0.16574 \end{bmatrix}, \quad \boldsymbol{R} = \begin{bmatrix} 0 & 1.076478 \\ -2.8038 & 0 \end{bmatrix}. \tag{2.85}$$

The L-F transformation converts equation (2.84) into,

$$\dot{\boldsymbol{z}} = \boldsymbol{R}\boldsymbol{z} - \boldsymbol{Q}^{-1}\left\{\varepsilon\cos(\pi t)\begin{bmatrix}0\\(Q_{11}z_1 + Q_{12}z_2)^3\end{bmatrix}\right\} + \boldsymbol{Q}^{-1}\begin{bmatrix}0\\B\cos(4\pi t)\end{bmatrix}. \tag{2.86}$$

The above system is hence amenable to system states augmentation. Consequently, we let,

$$\left.\begin{aligned}
p_1 &= \cos(\pi t),\\
\dot{p}_1 &= -\pi\sin(\pi t) = -q_1,\\
\dot{q}_1 &= \pi^2\cos(\pi t) = \pi^2 p_1,\\
p_2 &= \cos(4\pi t)\\
\dot{p}_2 &= -4\pi\sin(4\pi t) = -q_2,\\
\dot{q}_2 &= 16\pi^2\cos(4\pi t) = 16\pi^2 p_2.
\end{aligned}\right\} \tag{2.87}$$

Substituting equation (2.87) into equation (2.86) yields the following augmented system whose highest nonlinearity is of degree 4,

$$\begin{bmatrix} \dot{z}_1 \\ \dot{z}_2 \\ \dot{p}_1 \\ \dot{q}_1 \\ \dot{p}_2 \\ \dot{q}_2 \end{bmatrix} = \begin{bmatrix} 0 & 1.07647 & 0 & 0 & 0 & 0 \\ -2.8038 & 0 & 0 & 0 & 0 & 0 \\ 0 & 0 & 0 & -1 & 0 & 0 \\ 0 & 0 & \pi^2 & 0 & 0 & 0 \\ 0 & 0 & 0 & 0 & 0 & -1 \\ 0 & 0 & 0 & 0 & 16\pi^2 & 0 \end{bmatrix} \begin{bmatrix} z_1 \\ z_2 \\ p_1 \\ q_1 \\ p_2 \\ q_2 \end{bmatrix} \tag{2.88}$$

$$- \begin{bmatrix} Q_{12}^{-1}\{\varepsilon p_1 (Q_{11}z_1 + Q_{12}z_2)^3 - Bp_2\} \\ Q_{22}^{-1}\{\varepsilon p_1 (Q_{11}z_1 + Q_{12}z_2)^3 - Bp_2\} \\ 0 \\ 0 \\ 0 \\ 0 \end{bmatrix}.$$

After applying the modal matrix followed by application of successive near-identity transformation given in equation (2.34), we obtain the following linear normal form in equation (2.89). As outlined in section 2.3.2, the resulting TDNF is characterized by a large set of nonlinear monomial terms as shown in Appendix A.1. Consequently, by averaging out the periodic terms and discarding the infinitesimal terms, we obtain the TINF below,

$$\begin{bmatrix} \dot{v}_1 \\ \dot{v}_2 \\ \dot{v}_3 \\ \dot{v}_4 \\ \dot{v}_5 \\ \dot{v}_6 \end{bmatrix} = \begin{bmatrix} -i1.7373v_1 \\ i1.7373v_2 \\ -i\pi v_3 \\ i\pi v_4 \\ -i4\pi v_5 \\ i4\pi v_6 \end{bmatrix}. \tag{2.89}$$

Consistent with the previously established structure of $\tilde{\boldsymbol{J}}$, the linear normal forms are composed of conjugate Floquet exponents i.e. $\pm i1.7373$; conjugate magnitude of first forcing frequency i.e. $\omega_1 = \pi$, and; conjugate magnitude of second forcing frequency i.e. $\omega_2 = 4\pi$.

The solutions of the normal forms ODEs are straightforward. These analytical closed form solutions are then back-transformed via inverse near-identity and inverse modal transformation into the original coordinates. The corresponding solutions are then plotted and compared to the numerical solution of the original forced periodic system as shown in figure 7. The initial conditions considered are $x_1(0) = x_2(0) = 0.1$.

The numerical and analytical results for forced nonlinear system with periodic coefficients similarly match as was the case for constant coefficients cases in section 2.5.2.1. Therefore, the relatively simpler, more straightforward and intuitive state augmentation approach for analysis of forced nonlinear systems via normal forms is demonstrated to be accurate.

2.5.3 Center Manifold Reduction of Nonlinear Systems with External Periodic Excitation

In this section we demonstrate how to intuitively augment system states in order to facilitate lucid center manifold reduction of nonlinear systems subjected to external periodic excitation.

The conventional center manifold reduction approach presented in the section 2.4 is inapplicable on nonlinear systems subjected to external periodic excitation. Consequently, externally forced nonlinear systems require a valid alternative approach to decouple the

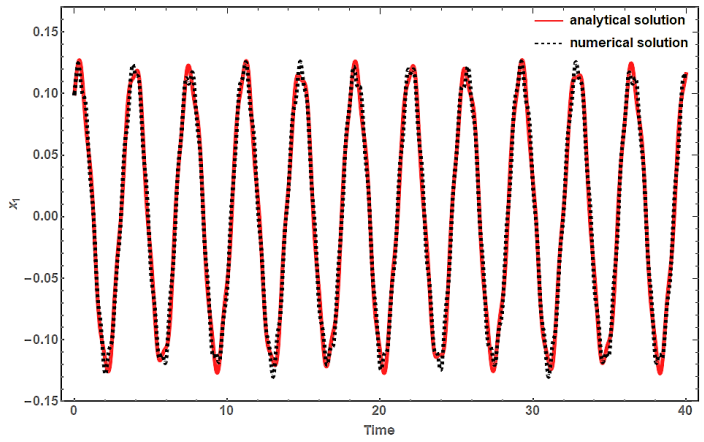

(a) $x_1(t)$

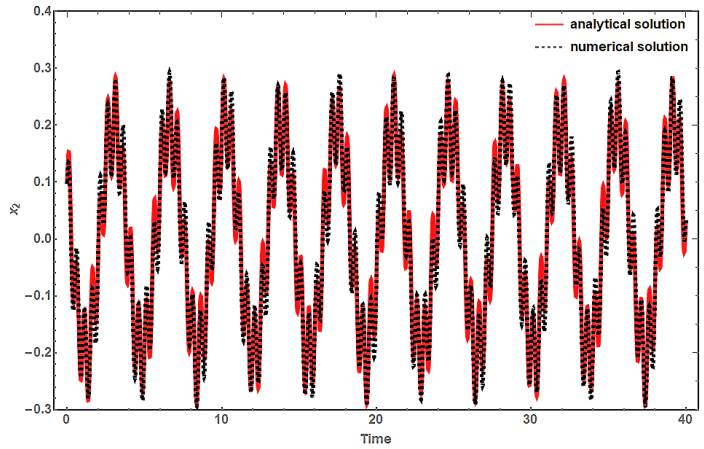

(b) $x_2(t)$

Figure 7: State Response Comparison for Mathieu-Duffing System

critical states from the stable ones as described in equation (2.46) and subsequently reduce the system model order on the invariant manifold.

To address this problem, a number of leading authors have proposed several approaches. For instance, [47] apply a form of state augmentation in NNM using perturbation techniques to realize a formulation applicable only to minimally excited systems. Further, NNM-based approaches are similarly suggested by [48] who involve PDEs, polynomial expansions and numerical techniques. [51], [53] and [52] employ an extended invariant manifold methodology that treats the center manifold as time modulated non-

linear functions with a special structure in temporal and spatial terms. This approach requires a 'book-keeping' parameter designated as 'ε' to be associated with the nonlinearity.

Formulation of prevailing methodologies to realize center manifold MOR, therefore, require special *ad-hoc* strategies. These strategies include the need for 'book-keeping' parameters, detuning parameters, minimal excitation, etc. The foregoing aggrandized parameters lack consistent, direct and plain affiliations with the pertinent terms of the analytical model. Consequently, implementation of these techniques becomes convoluted and increasingly arduous–stifling their seamless broad application.

Therefore, to address this matter, we demonstrate a relatively plain, direct and intuitive approach to accomplish center manifold reduction of nonlinear systems subjected to external periodic excitation. Our formulation is based on augmenting the system states by transforming the excitation frequency terms into system states. The state augmentation approach here is intuitive because the augmented states directly emanate from the excitation frequency terms –hence they are neither *ad-hoc* nor arbitrary. Moreover, this approach is liberated from the need for special treatment such as a 'book-keeping' parameter, detuning parameter, minimal excitation and so on. Therefore, this approach is broadly applicable in a seamless manner over a wide range of nonlinear systems.

The introduced state augmentation annihilates the original non-autonomous periodic forcing terms making it possible to innocuously apply the conventional center manifold reduction theory (see 2.4) on nonlinear systems with external periodic excitation.

2.5.3.1 Systems with Periodic Coefficients

When the nonlinear system in equation (2.42) is subjected to periodic external excitation, we obtain the system in equation below,

$$\dot{\boldsymbol{x}} = \boldsymbol{A}(t)\boldsymbol{x} + \boldsymbol{f}(\boldsymbol{x}, t) + \boldsymbol{F}(t), \tag{2.90}$$

where $\boldsymbol{F}(t)$ is the $n \times 1$ vector of periodic forcing terms as shown in equation (2.59). All the terms are as previously defined.

Prior to system state augmentation, a requisite L-F transformation is undertaken to transform the periodic linear matrix into an invariant one. The L-F transformed equation (2.90) is given below,

$$\dot{\boldsymbol{z}} = \boldsymbol{R}\boldsymbol{z} + \boldsymbol{Q}^{-1}(t)\boldsymbol{f}(\boldsymbol{Q}(\boldsymbol{t})\boldsymbol{z}, t) + \boldsymbol{Q}^{-1}(t)\boldsymbol{F}(t). \tag{2.91}$$

We augment the system states as delineated in equation (2.60). Consequently, the augmented $\mathbb{k} \times 1$ state vector is,

$$\tilde{\boldsymbol{z}} = [\boldsymbol{z}, p_1,\ p_2,\ \ldots,\ p_n,\ q_1,\ q_2,\ \ldots,\ q_n\ ]^T. \tag{2.92}$$

Further, the augmented states nonlinear vector $\breve{\boldsymbol{F}}(\tilde{\boldsymbol{z}})$ containing augmented monomial terms will be as shown below,

$$\breve{\boldsymbol{F}}(\tilde{\boldsymbol{z}}) = \begin{bmatrix} B_1 f(\boldsymbol{z}, p_1, p_2, \ldots, p_n, q_1, q_2, \ldots, q_n) \\ B_2 f(\boldsymbol{z}, p_1, p_2, \ldots, p_n, q_1, q_2, \ldots, q_n) \\ \vdots \\ B_n f(\boldsymbol{z}, p_1, p_2, \ldots, p_n, q_1, q_2, \ldots, q_n) \\ 0 \\ 0 \\ 0 \\ 0 \\ \vdots \\ 0 \\ 0 \end{bmatrix}, \; n = 3, 4, \ldots. \tag{2.93}$$

The state augmentation transforms (2.91) from nonautonomous to autonomous as shown in equation below,

$$\dot{\tilde{\boldsymbol{z}}} = \tilde{\boldsymbol{R}}\tilde{\boldsymbol{z}} + \boldsymbol{Q}^{-1}(t)\breve{\boldsymbol{F}}(\tilde{\boldsymbol{z}}). \tag{2.94}$$

Here, state vector $\tilde{\boldsymbol{z}} = [\boldsymbol{z}, p_1, p_2, \ldots, p_n, q_1, q_2, \ldots, q_n]^T$ and $\breve{\boldsymbol{F}}(\tilde{\boldsymbol{z}})$ contains augmented nonlinear monomial terms in $\tilde{\boldsymbol{z}}$. $\tilde{\boldsymbol{R}}$ is the augmented states constant linear matrix. Equation (2.94) is generally of the same form as equation (2.42) despite capturing the forced nonlinear dynamics introduced in equation (2.90). If fresh linear periodic coefficients emerge from the interaction of $\breve{\boldsymbol{F}}(t)$ with $\boldsymbol{Q}^{-1}(t)$; then an additional L-F transformation is necessary to render the linear terms parameter-invariant.

After applying the modal transformation $\tilde{\boldsymbol{z}} = \boldsymbol{M}\tilde{\boldsymbol{y}}$ to equation (2.94), we obtain,

$$\dot{\tilde{\boldsymbol{y}}} = \tilde{\boldsymbol{J}}\tilde{\boldsymbol{y}} + \boldsymbol{M}^{-1}\boldsymbol{Q}^{-1}(t)\breve{\boldsymbol{F}}(\boldsymbol{M}\tilde{\boldsymbol{y}}), \tag{2.95}$$

where $\tilde{\boldsymbol{J}}$ is the $\mathbb{k} \times \mathbb{k}$ Jordan canonical form of the augmented linear matrix $\tilde{\boldsymbol{R}}$. The diagonal elements in $\tilde{\boldsymbol{J}}$ are Floquet exponents of the system. Clearly, equation (2.95) is of

the same form as equation (2.44) i.e $\boldsymbol{J}\boldsymbol{y}+\boldsymbol{w}(\boldsymbol{y},t),$ hence amenable to the center manifold reduction criteria described in section 2.4.1. However, the structure of $\tilde{\boldsymbol{J}}$ will include additional critical eigenvalues due to the augmented periodic dynamics. Let $d = {}^{(\mathbb{k}-n)}/_{2}$ be the count of the number of considered forcing frequencies in the system. Then $\tilde{\boldsymbol{J}}$ will be structured as shown below,

$$\tilde{\boldsymbol{J}} = \left[\begin{array}{cc|ccccc} \boldsymbol{J}_c & 0 & & & & & \\ 0 & \boldsymbol{J}_s & & & & & \\ \hline & & i\omega_1 & & & & \\ & & & i\omega_2 & & & \\ & & & & \ddots & & \cdot \\ & & & & & & \\ & & & & & & i\omega_{2d} \end{array}\right] \tag{2.96}$$

Let $\boldsymbol{J}_c^* = [\boldsymbol{J}_c, i\omega_1, i\omega_2 \ldots i\omega_{2d}]^T$ be the diagonal of the $(r+2d)\times(r+2d)$ augmented critical eigenvalues matrix. Therefore by re-arranging the modal matrix columns, equation (2.95) can be expressed in the form given in equation (2.45) as,

$$\begin{bmatrix} \dot{\boldsymbol{y}}_c \\ \dot{\boldsymbol{y}}_s \end{bmatrix} = \begin{bmatrix} \boldsymbol{J}_c^* & 0 \\ 0 & \boldsymbol{J}_s \end{bmatrix} \begin{bmatrix} \boldsymbol{y}_c \\ \boldsymbol{y}_s \end{bmatrix} + \begin{bmatrix} \boldsymbol{w}_c(\boldsymbol{y}_c, \boldsymbol{y}_s, t) \\ \boldsymbol{w}_s(\boldsymbol{y}_c, \boldsymbol{y}_s, t) \end{bmatrix}. \tag{2.97}$$

To determine the reducibility condition of the augmented system, we follow the conventional procedure outlined in equations (2.46) to (2.53). The reducibility condition for nonlinear systems subjected to periodic external excitation will hence be,

$$\begin{gathered} (\bar{i}\nu\omega) + \sum_{\ell=1}^{r+2d} (m_\ell \lambda_\ell^* - \bar{\lambda}_p) \neq 0, \\ \forall \nu = 0, \pm 1, \pm 2, \ldots; \quad p = 1, 2, \ldots, s, \end{gathered} \tag{2.98}$$

where $\lambda_1^*, \lambda_2^*, \ldots, \lambda_{r+2d}^*$ are the eigenvalues of the Jordan matrix $\boldsymbol{J}_c^*$ and $\bar{\lambda}_p; p = 1, 2, \ldots, s$ are the eigenvalues of $\boldsymbol{J}_s$.

2.5.3.2 Systems with Constant Coefficients

Consider the system with constant coefficients subjected to a periodic external excitation given below,

$$\dot{\boldsymbol{x}} = \boldsymbol{A}\boldsymbol{x} + \boldsymbol{f}(\boldsymbol{x}) + \boldsymbol{F}(t). \tag{2.99}$$

The parameters are as previously defined. Next, the system states are augmented using the procedure described in equations (2.60), (2.92), (2.93) and (2.94). The resulting nonautonomous system is,

$$\dot{\tilde{\boldsymbol{x}}} = \tilde{\boldsymbol{A}}\tilde{\boldsymbol{x}} + \breve{\boldsymbol{F}}(\tilde{\boldsymbol{x}}). \tag{2.100}$$

Here, state vector $\tilde{\boldsymbol{x}} = [\boldsymbol{x}, p_1, p_2, \ldots, p_n, q_1, q_2, \ldots, q_n]^T$ and $\breve{\boldsymbol{F}}(\tilde{\boldsymbol{x}})$ contains augmented nonlinear monomial terms in $\tilde{\boldsymbol{x}}$. After applying the modal transformation $\tilde{\boldsymbol{x}} = \boldsymbol{M}\tilde{\boldsymbol{y}}$ to equation (2.100), we obtain the Jordan canonical of the system as,

$$\dot{\tilde{\boldsymbol{y}}} = \tilde{\boldsymbol{J}}\tilde{\boldsymbol{y}} + \boldsymbol{M}^{-1}\breve{\boldsymbol{F}}(\boldsymbol{M}\tilde{\boldsymbol{y}}), \tag{2.101}$$

where $\tilde{\boldsymbol{J}}$ is the $n \times n$ Jordan canonical form of the augmented linear matrix $\tilde{\boldsymbol{A}}$. At this point, equation (2.101) is of the form shown (2.95); the only difference being the time-invariant nonlinear term. Consequently, a similar subsequent procedure described in equations (2.96) to (2.98) is followed to obtain the following reducibility condition,

$$\sum_{\ell=1}^{r}(m_\ell\lambda_\ell - \bar{\lambda}_p) \neq 0 \quad p = 1, 2, \ldots, s, \tag{2.102}$$

where $\lambda_1, \lambda_2, \ldots, \lambda_r$ are the eigenvalues of the Jordan matrix $\boldsymbol{J}_c$ and $\bar{\lambda}_p$ are the eigenvalues of $\boldsymbol{J}_s$.

2.5.4 Illustrative Center Manifold Reduction Application Cases

In this section we consider two types of illustrative cases to demonstrate application of the intuitive system state augmentation technique in center manifold reduction of nonlinear systems with periodic external excitation. A periodically forced nonlinear system with periodic coefficients will be considered first. In the second case a nonlinear system with periodic external excitation and constant coefficients is analyzed.

2.5.4.1 Systems With Periodic Coefficients

We consider a coupled periodic-quasiperiodic nonlinear system subjected to periodic external excitation given in equation below,

$$\begin{bmatrix} \dot{x}_1 \\ \dot{x}_2 \end{bmatrix} = \begin{bmatrix} 1+\alpha\cos^2 t & 1-\alpha\sin t\cos t \\ -1-\alpha\sin t\cos t & -1+\alpha\sin^2 t \end{bmatrix} \begin{bmatrix} x_1 \\ x_2 \end{bmatrix} + \beta \begin{bmatrix} x_1^3 \\ x_2^3 \end{bmatrix} + \begin{bmatrix} 0 \\ B\sin\omega t \end{bmatrix}. \tag{2.103}$$

This equation is of the form given in equation (2.90); it is special system with known L-F transformation in closed form and stable for $\beta < 0$. Here, α and β are system parameters while B is amplitude of the external periodic forcing. The L-F transformed system will be as shown in equation (2.91) where:

$$\boldsymbol{R} = \begin{bmatrix} \alpha-1 & 0 \\ 0 & -1 \end{bmatrix}, \quad \boldsymbol{Q} = \begin{bmatrix} \cos t & \sin t \\ -\sin t & \cos t \end{bmatrix}, \quad \boldsymbol{Q}^{-1} = \begin{bmatrix} \cos t & -\sin t \\ \sin t & \cos t \end{bmatrix}. \tag{2.104}$$

In applying the intuitive state augmentation, we first apply the trigonometric identity; [$\sin\omega t = 2\sin(\frac{\omega}{2}t)\cos(\frac{\omega}{2}t)$] to the external periodic excitation term. The let,

$$\left.\begin{aligned} p &= \sin(\frac{\omega}{2}t), \\ \dot{p} &= \frac{\omega}{2}\cos(\frac{\omega}{2}t) = q, \\ \dot{q} &= -\frac{\omega^2}{4}\sin(\frac{\omega}{2}t) = -\frac{\omega^2}{4}p. \end{aligned}\right\} \tag{2.105}$$

Therefore, substituting equation (2.105) into the L-F transformed system we obtain the state augmented system as,

$$\begin{aligned} \begin{bmatrix} \dot{z}_1 \\ \dot{z}_2 \\ \dot{p} \\ \dot{q} \end{bmatrix} &= \begin{bmatrix} \alpha - 1 & 0 & 0 & 0 \\ 0 & -1 & 0 & 0 \\ 0 & 0 & 0 & 1 \\ 0 & 0 & -\omega^2/4 & 0 \end{bmatrix} \begin{bmatrix} z_1 \\ z_2 \\ p \\ q \end{bmatrix} \\ &+\beta \begin{bmatrix} Q_{11}^{-1}x_1^3 + Q_{12}^{-1}\left(x_2^3 + \frac{4}{\omega}pq\right) \\ Q_{21}^{-1}x_1^3 + Q_{22}^{-1}\left(x_2^3 + \frac{4}{\omega}pq\right) \\ 0 \\ 0 \end{bmatrix}, \end{aligned} \tag{2.106}$$

where $x_1 = Q_{11}z_1 + Q_{12}z_2$ and $x_2 = Q_{21}z_1 + Q_{22}z_2$.

After setting $\alpha = 1,\ \beta = -0.75,\ B = 1$ and $\omega = 1$ we apply the modal transformation to obtain the system represented by equation (2.95) and subsequently obtain:

- Eigenvalues of the augmented states linear matrix are,

Critical: $\lambda_1^* = 0,\ \lambda_3^* = i0.5$ and $\lambda_4^* = -i0.5$.

Stable: $\lambda_2^* = -1$.

- Parametric equation of the center manifold is,

$$z_2 = \cos t(0.5p^2 + 2pq - 2q^2). \tag{2.107}$$

- Reduced system is,

$$\begin{aligned}
\dot{z}_1 =& -\sin t(4pq - 0.75(-z_1 \sin t + \cos t(2pq\cos t - 2q^2\cos t \\
&+ 0.25p^2(\cos t - i\sin t)(1 + \cos 2t + i\sin 2t)))^3) \\
&- 0.75\cos t(z_1\cos t + \sin t(2pq\cos t - 2q^2\cos t \\
&+ 0.25p^2(\cos t - i\sin t)(1 + \cos 2t + i\sin 2t)))^3, \\
\dot{p} =& q, \\
\dot{q} =& -\frac{p}{4}.
\end{aligned} \tag{2.108}$$

It should be noted that $z_2 = h(z_1, p, q, t)$. In equation (2.107) the coefficient of the z_1 nonlinearity is zero. Though $z_1(0) = 0$ for the original and reduced systems; $z_2(0) = 0.5$ for the reduced system and zero for the original system. Consequently, $x_2(0) = 0.5$ as well due the structure of the system's LFT matrix $\mathbf{Q}$ shown in equation (2.104).

Equation (2.105) completely model the dynamics $p(t)$ and $q(t)$ which are hence substituted in the reduced system to yield a system represented by $\dot{z}_1 = h(z_1, t)$ in equation below,

$$\begin{aligned}
\dot{z}_1 =& -0.4956 + 0.5073\cos 2t - 0.011\cos 6t - 0.00073\cos 10t \\
&- 0.0146\cos t\sin t - 0.0117\sin 4t - 0.0066\sin 6t \\
&+ 0.0007\sin 10t + (\cos t)^4(\sin t)^2(-1.125 + 2.25\cos t\sin t)z_1 \\
&+ (-0.0703\cos 2t + 0.0703\cos 6t + 0.1406\cos t\sin t \\
&+ 0.1406\sin 4t + 0.0703\sin 6t)z_1^2 \\
&+ (-0.5625 - 0.1875\cos 4t)z_1^3.
\end{aligned} \tag{2.109}$$

The long term behavior of the reduced system in the original coordinates is obtained by numerically solving for $z_1(t)$ then applying the inverse L-F transformation, $\boldsymbol{z} = \boldsymbol{Q}^{-1}\boldsymbol{x}$. Figure 8 shows the comparison of long term states response evolution between the original system (equation (2.103)) and the reduced system (equation (2.108)). Further, a comparison of the original and reduced system's phase portrait is shown in figure 9.

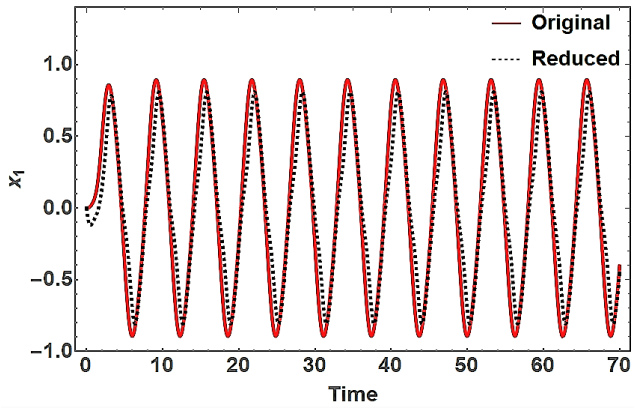

(a) $x_1(t)$

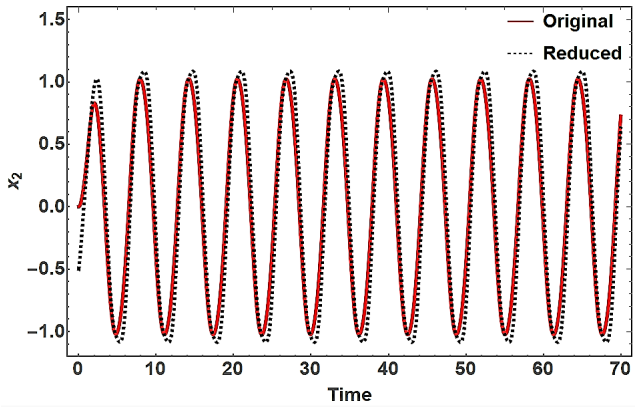

(b) $x_2(t)$

Figure 8: Periodic System State Response Comparison

The above analyses show that the transient and long term behaviors (with zero initial conditions) of the original system are reasonably comparable to those of the reduced system.

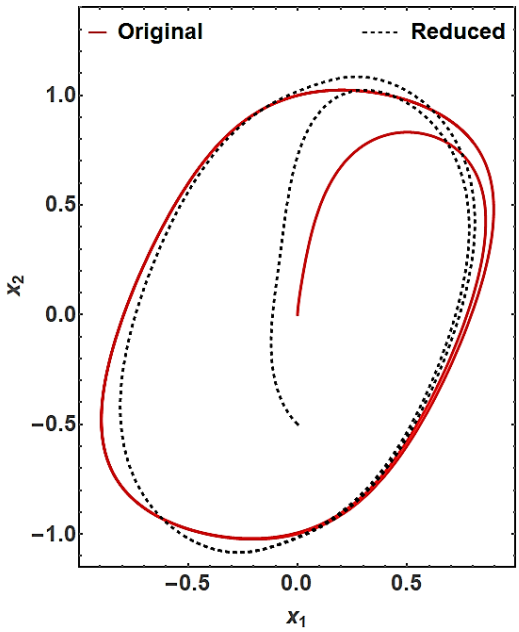

Figure 9: Periodic System Phase Portrait

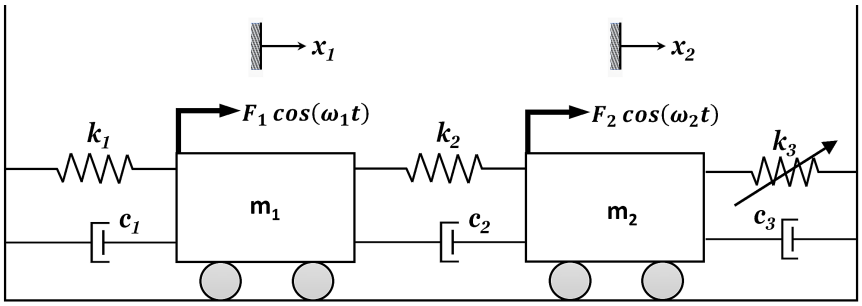

Figure 10: 2-dof Spring-Mass-Damper System

2.5.4.2 Systems With Constant Coefficients

In this case we shall demonstrate center manifold order reduction of a 2-dof mass-spring-damper system consisting of linear springs and dampers. An additional nonlinear spring is connected between mass m_2 and the wall as shown in figure 10.

The masses can vibrate in $x-$direction with no friction and are individually subjected to disparate external excitation frequencies, i.e. $(F_1 \cos(\omega_1 t))$ and $(F_2 \cos(\omega_2 t))$ acting on

m_1 and m_2 respectively. The dynamical system is described by the following full state-space equations of motion with spring nonlinearities assumed to be of the cubic form,

$$\begin{bmatrix} \dot{x}_1 \\ \dot{x}_2 \\ \dot{x}_3 \\ \dot{x}_4 \end{bmatrix} = \begin{bmatrix} 0 & 0 & 1 & 0 \\ 0 & 0 & 0 & 1 \\ A_{31} & {}^{k_2}/_{m_1} & A_{33} & {}^{c_2}/_{m_1} \\ {}^{k_2}/_{m_2} & A_{42} & {}^{c_2}/_{m_2} & A_{44} \end{bmatrix} \begin{bmatrix} x_1 \\ x_2 \\ x_3 \\ x_4 \end{bmatrix} + \begin{bmatrix} 0 \\ 0 \\ -\alpha x_1^3 \\ -\alpha x_2^3 \end{bmatrix} + \begin{bmatrix} 0 \\ 0 \\ F_1 \cos(\omega_1 t) \\ F_2 \cos(\omega_2 t) \end{bmatrix}, \tag{2.110}$$

where:

- $A_{31} = -{}^{(k_1 + k_2)}/_{m_1}$, $A_{33} = -{}^{(c_1 + c_2)}/_{m_1}$.
- $A_{42} = -{}^{(k_2 + k_3)}/_{m_2}$, $A_{44} = -{}^{(c_2 + c_3)}/_{m_2}$.

Intuitive state augmentation is implemented by first designating;

$$\left.\begin{aligned} p_1 &= \cos(\omega_1 t), \\ \dot{p}_1 &= \omega_1 \sin(\omega_1 t) = -q_1, \\ \dot{q}_1 &= \omega_1^2 \cos(\omega_1 t) = \omega_1^2 p_1, \\ p_2 &= \cos(\omega_2 t), \\ \dot{p}_2 &= \omega_2 \sin(\omega_2 t) = -q_2, \\ \dot{q}_2 &= \omega_2^2 \cos(\omega_2 t) = \omega_2^2 p_2. \end{aligned}\right\} \tag{2.111}$$

Substituting equation (2.111) into (2.110) yields the augmented 8×8 state space system as represented in equation (2.100). This system is shown below,

$$\begin{bmatrix} \dot{x}_1 \\ \dot{x}_2 \\ \dot{x}_3 \\ \dot{x}_4 \\ \dot{p}_1 \\ \dot{p}_2 \\ \dot{q}_1 \\ \dot{q}_2 \end{bmatrix} = \begin{bmatrix} 0 & 0 & 1 & 0 & 0 & 0 & 0 & 0 \\ 0 & 0 & 0 & 1 & 0 & 0 & 0 & 0 \\ A_{31} & {}^{k_2}/_{m_1} & A_{33} & {}^{c_2}/_{m_1} & F_1 & 0 & 0 & 0 \\ {}^{k_2}/_{m_2} & A_{42} & {}^{c_2}/_{m_2} & A_{44} & 0 & F_2 & 0 & 0 \\ 0 & 0 & 0 & 0 & 0 & 0 & -1 & 0 \\ 0 & 0 & 0 & 0 & 0 & 0 & 0 & -1 \\ 0 & 0 & 0 & 0 & \omega_1^2 & 0 & 0 & 0 \\ 0 & 0 & 0 & 0 & 0 & \omega_2^2 & 0 & 0 \end{bmatrix} \begin{bmatrix} x_1 \\ x_2 \\ x_3 \\ x_4 \\ p_1 \\ p_2 \\ q_1 \\ q_2 \end{bmatrix} + \begin{bmatrix} 0 \\ 0 \\ -\alpha x_1^3 \\ -\alpha x_2^3 \\ 0 \\ 0 \\ 0 \\ 0 \end{bmatrix}. \quad (2.112)$$

We set $m_1 = m_2 = 1,\ k_1 = 1,\ k_2 = 1,\ k_3 = 1,\ c_1 = 0,\ c_2 = 1,\ c_3 = 0,\ F_1 = 1,\ F_2 = 2,\ \omega_1 = 4,\ \omega_2 = 8$ and $\alpha = 1$. Then, after applying the modal transformation $\tilde{\boldsymbol{x}} = \boldsymbol{M}\tilde{\boldsymbol{y}}$, we obtain the system equivalent to the one described by equation (2.101). Computation of the center manifold via the reducability condition outlined in the section titled Constant Coefficients Center Manifold Reduction is undertaken on the Jordan form system of equations resulting in:

Eigenvalues of the augmented states linear matrix are,

Critical: $\lambda_1^* = i8,\ \lambda_2^* = -i8,\ \lambda_3^* = i4,\ \lambda_4^* = -i4,\ \lambda_5^* = i$ and $\lambda_6^* = -i$

Stable: $\lambda_7^* = -1 + i\sqrt{2}$ and $\lambda_8^* = -1 - i\sqrt{2}$

We considered a cubic order of expansion for the center manifold hence the parametric equations and the reduced system contain equations with very many terms (> 1800 for $\dot{y}_1$ and $\dot{y}_2$). We shall hence only show the few first and last terms of such equations here. Moreover, the full y_7 and y_8 equations are shown in Appendix A.2. Parametric equations

of the center manifold are;

$$\begin{aligned} y_7 =&(8.41688 - i44.0124)y_1^2 y_3 - (5.25571 - i151.631)y_1 y_2 y_3 \\ &- (107.972 + i145.859)y_2^2 y_3 + \cdots + (4.41791 \times 10^{10} \\ &- i1.76106 \times 10^{10})y_5 y_6^2 - (5.79082 \times 10^9 - i1.13602 \times 10^9)y_6^3, \\ y_8 =&(28.043 - i1.97305)y_1^2 y_3 - (75.8602 - i9.05606)y_1 y_2 y_3 \\ &+ \cdots + (4.22011 \times 10^{10} + i5.28005 \times 10^{10}) - (3.34833 \times 10^9 \\ &+ i5.73262 \times 10^9)y_6^3. \end{aligned} \tag{2.113}$$

The reduced system is,

$$\begin{aligned} \dot{y}_1 =&\frac{1}{12}\left\{i6y_1^3 - i9y_1^2(2y_2 - 233y_3 + 233y_4 - 7954y_5) - i12y_1 + i18y_2^2 \right. \\ &+ i12y_1(17550. + i29217.8)y_3^2 + \cdots + (4.41791 \times 10^{10} - i1.76106 \times 10^{10})y_5 y_6^2 \\ &\left. - (5.79082 \times 10^9 - i1.13602 \times 10^9)y_6^3\right\}, \\ \dot{y}_2 =&\frac{1}{12}\left\{i6y_1^3 - i6y_2^3 + i9y_2^2\left[233y_3 - 233y_4 + 7954(y_5 - y_6)\right] - i9y_1^2(2y_2 - 233y_3 \right. \\ &+ 233y_4 - 7954y_5 + 7954y_6) + i18y_1 y_2^2 + (210600 + i350613)y_1 y_3^2 \\ &- (210600 - i350613)y_1 y_4^2 + \cdots + (4.41791 \times 10^{10} - i1.76106 \times 10^{10})y_5 y_6^2 \\ &\left. - (5.79082 \times 10^9 - i1.13602 \times 10^9)y_6^3\right\}, \\ \dot{y}_3 =& -i4y_3, \\ \dot{y}_4 =& i4y_4, \\ \dot{y}_5 =& -i8y_5, \\ \dot{y}_6 =& i8y_6. \end{aligned} \tag{2.114}$$

Initial conditions for all the states were set to zero. It should be noted that this will trans-

late to $p_1(0) = p_2(0) = 1$ as per the delineation in equation (2.111). Dynamics in the original coordinates are obtained via the modal matrix back-transformation. Figures 11 and 12 show the comparison of transient and long-term state behaviors of the original and reduced systems.

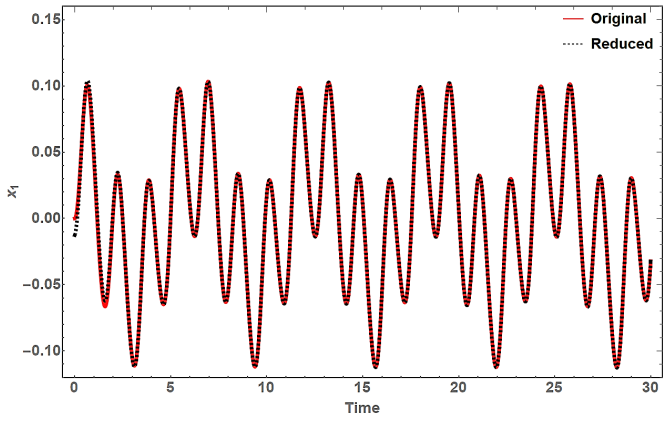

(a) $x_1(t)$

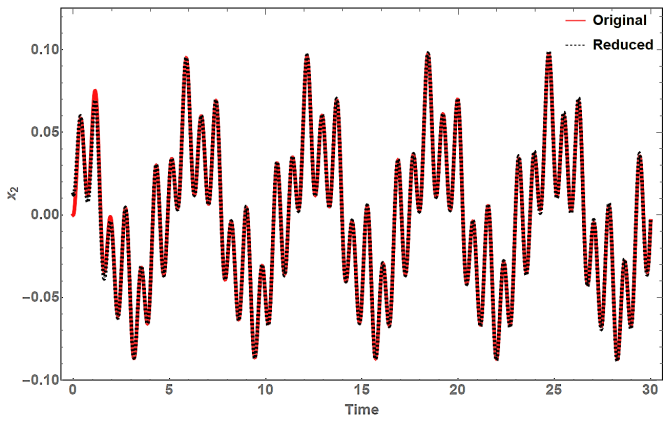

(b) $x_2(t)$

Figure 11: Spring-Mass-Damper System State Response Comparison

Moreover, comparison of the original and reduced system's phase portraits are shown in figure 13.

Once again, results of the constant coefficients system analysis show that; *i)* the tran-

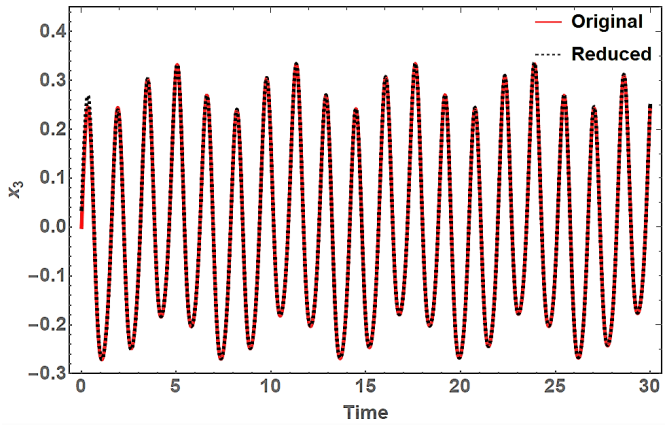

(a) $x_3(t)$

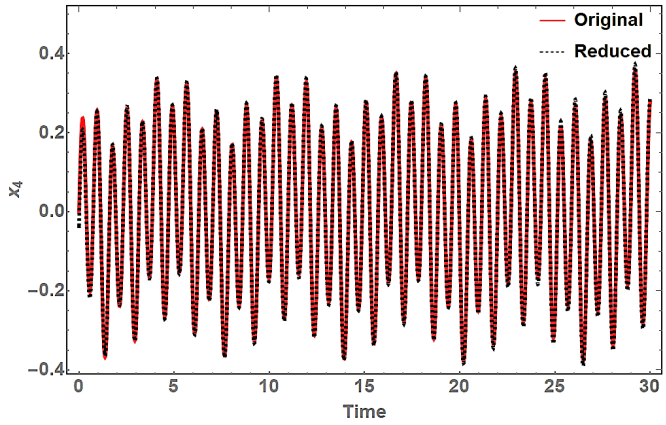

(b) $x_4(t)$

Figure 12: Spring-Mass-Damper System State Response Comparison

sient behavior of the original system is reasonably comparable to that of the reduced system, and *ii)* the long-term steady-state behavior of the reduced system is exactly the same as that of the original system. This agreement is observed in all the states. Further, though not shown here, the sinusoidal augmented states behaviors are globally preserved in the reduced order system.

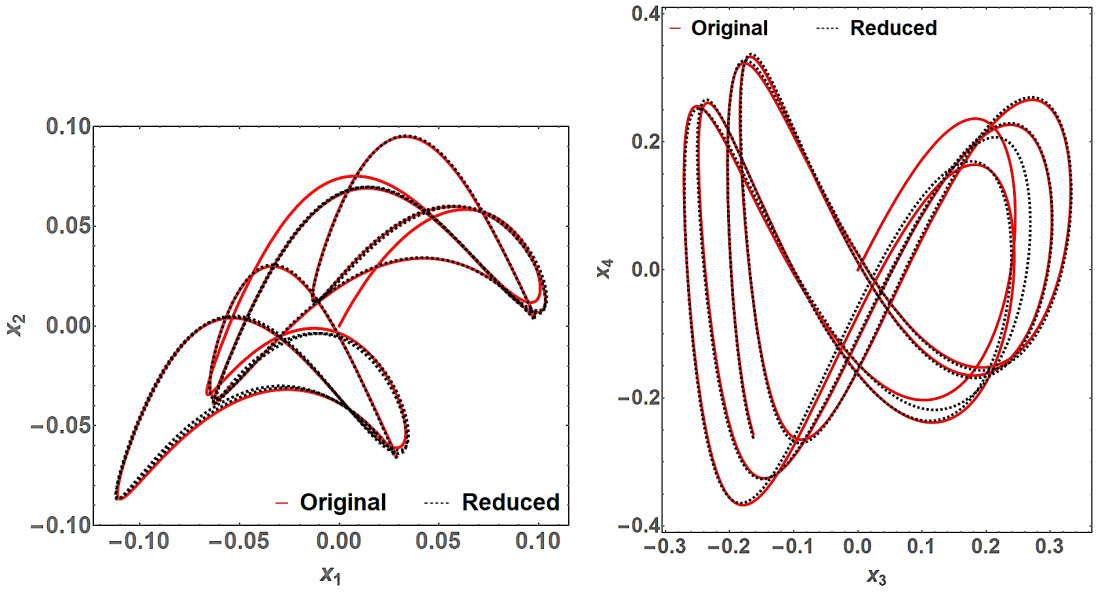

(a) $x_1(t) - x_2(t)$ (b) $x_3(t) - x_4(t)$

Figure 13: Spring-Mass-Damper System State Response Comparison

2.6 Summary and Discussion

Analysis and control law synthesis of nonlinear systems with external periodic excitation that describe the motion of our space system is not a trivial task. Therefore, we proposed to employ system state augmentation, Normal Forms theory and MOR techniques in our methodology. A summary of the theoretical framework behind these techniques is described in this section. In doing so, we demonstrated how parametrically excited and constant coefficient nonlinear systems subjected to external periodic excitation can be transformed into more amenable forms via normalization and model order reduction.

We demonstrated a relatively more lucid and straightforward approach to obtain the normal forms of nonlinear systems with external periodic excitation. We further demonstrated analysis of the nonlinear systems via the computed normal forms and compared

the results with numerically integrated solutions. Nonlinear systems with either constant coefficients or parametric excitation that were externally excited periodically were considered in this methodology.

Unlike the prevailing comparable approaches in literature, our unifying approach is based on intuitive system state augmentation and does not involve detuning parameters, 'book-keeping' parameters, *ad-hoc* unsolved equations, mandatory minimal excitation. The augmented states have a plain and direct affiliation with the existing excitation frequency terms. This attribute enables a consistent and broad application of this methodology over a wide range of nonlinear systems with external periodic excitation.

By augmenting the states accordingly, periodic coefficients associated with nonlinear terms can be similarly converted from non-autonomous to autonomous in the same manner as elements of the periodic forcing vector, $\boldsymbol{F}(t)$. Therefore, the intuitive state augmentation technique innocuously facilitates construction of normal forms for a previously non-autonomous system. This was illustrated in the alternative approach to obtain normal forms of the Mathieu-Duffing equation in section 2.5.2.2.

Four cases of the forced Duffing's equation and two cases Mathieu-Duffing equation case were considered to validate the accuracy of our methodology. Results of all the time-history analyses demonstrated compliance between numerically integrated and analytically obtained normal forms time-history analysis.

Frequency response analysis of the Duffing oscillator similarly validated the accuracy of the normal form approach here. Our future work will improve the normal forms back-transformation strategy to obtain multiple amplitude values corresponding to the same frequency on overlapping paths of frequency response curves.

Therefore, our relatively direct and simpler approach to obtain normal forms facilitates a relatively lucid analysis of forced nonlinear system via normal forms.

The demonstrated center manifold methodology methodology for obtaining reduced-order nonlinear dynamical system models–characterized by a lesser number of state variables and equations compared to the original system model. This is realized by via the center manifold reduction approach which constructs an invariant subspace on which a lesser number of equations represent the dynamics of a given system. In doing so, we formulated a unified approach that extends the conventional center manifold reduction to nonlinear systems subjected to external periodic excitation.

Our approach presented is based on intuitive state augmentation and does not require special treatment such as the inclusion of 'book-keeping' parameters, detuning parameters, minimal excitation, etc. Further, *ad-hoc* variables and equations are avoided since the augmented states have plain direct affiliations with the exciting frequency terms. Our methodology was validated as accurate by the agreements in the time-history and phase space behaviors of the derived reduced-order models and corresponding numerically integrated original system.

Though it may appear as if the demonstrated methodology increases the dimension of the system model instead of reducing it; judicious scrutiny exposes the deficiency of such a misleading perception. Firstly, the augmented states are fictitious states whose simple, sinusoidal dynamics are comprehensively understood. Secondly, the model dimension described by ODEs of the actual states was reduced by half in all the illustrative applications considered. Finally, the simplified order reduction methodology that captures the unwieldy external periodic excitations far outweighs the addition of innocuous dynamics due to simple virtual states.

The chapter concluded by demonstrating application of state augmentation in normalization and center manifold order reduction analysis of nonlinear systems with exter-

nal periodic excitation. The relatively direct and unified approach was verified to be accurate by comparing the obtained results with numerical integration outcomes.

Part I

ATTITUDE MOTION OF A GRAVITY GRADIENT STABILIZED SPACECRAFT IN ECCENTRIC ORBIT

(This page is intentionally left blank.)

Chapter 3

GRAVITY GRADIENT ATTITUDE STABILIZATION IN ECCENTRIC ORBIT

In this section, we shall describe and analytically characterize the attitude motion of a gravity gradient stabilized spacecraft in an eccentric orbit. This will be followed by a comprehensive motion analysis using the methodologies presented in Chapter 2. We shall investigate the motion time trace, stability, chaos, periodicity, bifurcation, resonance etc.

3.1 Dynamical Model Development

A gravity gradient stabilized spacecraft attains a state of stable relative equilibrium when its I_z points along the radius vector, I_y points along the normal to the orbit plane, and I_x is along the tangent to the orbit in the LVLH frame (Hill frame) as shown in figure 14(a). In addition, the condition, $I_y > I_x > I_z$ must similarly be satisfied.

If the work done by external perturbing torques is greater than the rotational kinetic energy of the spacecraft about its COM, motion of the spacecraft in an elliptical orbit will be libratory as illustrated in figure 14(b). Equations representing the spacecraft orbital motion are identical with those of a point mass in an inverse square-law force field. To analyze the attitude dynamics, the spacecraft orbital motion (motion of COM) can be reasonably assumed to be independent of the spacecraft attitude motion (motion about COM). This assumption is justifiable because the satellite is small compared to the dimensions of the orbit. Under this assumption, the spacecraft's orbital motion can hence transfer energy to the attitude motion, but the converse is assumed not to be possible. Thus, orbital param-

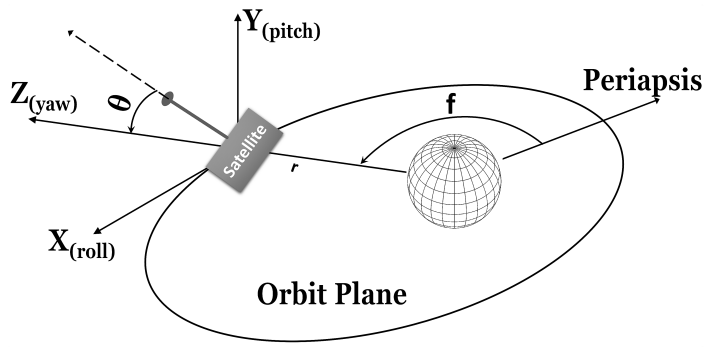

(a) Geometry of Orbit and Attitude Parameters

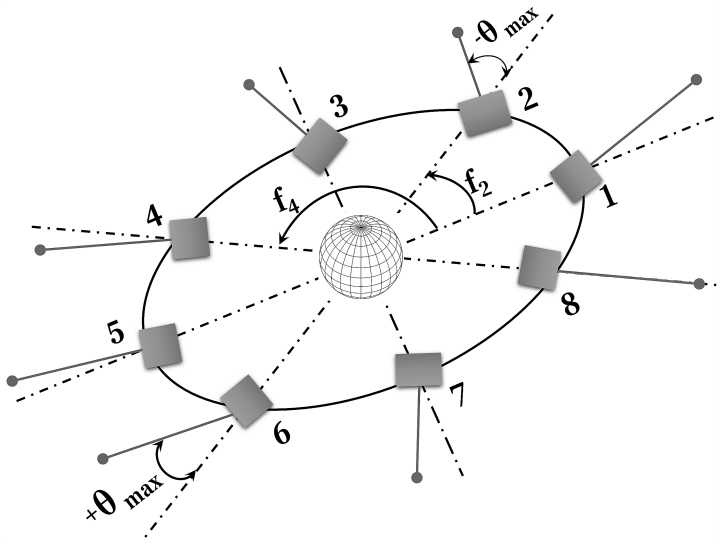

(b) Pitch Angle Librations

Figure 14: Gravity Gradient Stabilization

eters as determined functions of time are considered in analyzing attitude motion [15], [103].

When the spacecraft is considered as a rigid body in an inverse-square force field along an elliptical orbit a complete formulation of equations of motion can be derived [13], [15], [57]. The resulting six second-order differential equations of motion are nonlinear and coupled. These equations of motion cannot be solved analytically in this exact form.

Ignoring other torques such as aerodynamic, magnetic, thermal bending and solar radiation pressure we can derive the equations of spacecraft attitude motion under the in-

fluence of inverse-square force field in an elliptical orbit. Additional assumptions are; an ideal, perfect sphere earth without oblateness; largest spacecraft dimensions are extremely small compared to the orbit radius, and the spacecraft mass is negligible compared to the mass of the central body [103].

We further assume that the exact equations of motion can be linearized in small-angle motion characterization. Subsequently, the attitude dynamics models maybe considered to consist of two equations with coupled roll-yaw angles and a third uncoupled equation describing the pitch angle dynamics. The pitch motion equation is hence independent of roll-yaw motion. The coupled roll-yaw equations are homogeneous and can be solved for $\Psi = \dot{\Psi} = \Omega = \dot{\Omega} = 0$. [13], [15], [57], [103].

Consequently, the exact problem is reduced to the equation of pitch motion with orbital parameters as functions of time and spacecraft mass parameters as shown below,

$$\ddot{\Theta} + 3\frac{\mu}{r^3}\sigma \sin\Theta \cos\Theta = -\dot{\omega}, \tag{3.1}$$

Here, $0 \leq \sigma \leq 1$ is a dimensionless ratio of the spacecraft's principal moments of inertia given by,

$$\sigma = \frac{I_x - I_z}{I_y} = \frac{I_{roll} - I_{yaw}}{I_{pitch}}. \tag{3.2}$$

To analyze attitude motion in eccentric orbit, we substitute time with true anomaly, f as the independent variable. Moreover, the COM will obey the following Keplerian orbit relations,

$$r = \frac{P}{1 + e\cos f}, \tag{3.3}$$

$$\omega = \frac{df}{dt} = \frac{\sqrt{\mu P}}{r^2} = \frac{\sqrt{\mu P}}{P^2}(1 + e\cos f)^2. \tag{3.4}$$

Thus,

$$\dot{\omega} = -2\frac{\mu}{r^3}e \sin f, \tag{3.5}$$

$$\ddot{\Theta} = (1 + e\cos f)\frac{\mu}{r^3}\left(\frac{d^2\Theta}{df^2}\right) - 2\frac{\mu}{r^3}e\sin f\left(\frac{d\Theta}{df}\right). \tag{3.6}$$

Substituting equations (3.5) and (3.6) into (3.1) yields,

$$(1 + e\cos f)\Theta'' - 2e\sin f\Theta' + 3\sigma\sin\Theta\cos\Theta = 2e\sin f. \tag{3.7}$$

This is the well-known equation of plane pitch angle libratory motion in elliptical orbit [13], [15], [57], [103]. The primes indicate differentiation with respect to f. The planar pitch attitude motion equation is hence nonlinear with periodic coefficients in f. Analysis of this motion and subsequent synthesis of a fitting controller is not a trivial task. We hence intend to analyze this motion and synthesize suitable controllers to stabilize the system.

3.2 Implicit Time History Analysis

Strictly speaking the behavior of the motion is characterized in terms variation in true anomaly, f as shown in equation (3.7). However, the true anomaly similarly varies with time hence the implicit time history is preferred. To demonstrate implicit time history behavior, we initially select $e = 0.2$ and $\sigma = 0.3$. Later on in section 3.3 we shall analyze the impact of different $e - \sigma$ pair values on the motion. Both the motion in original coordinates, equation (3.7) and the corresponding state augmented system will be scrutinized. Figure 15 shows the implicit time history behavior of the motion in original coordinates.

Similarly, we scrutinize the history behavior of the state augmented system as outlined in section 2.5.1 on the motion represented in equation (3.7). In accordance with binomial expansion theorem [104], since $|e\cos f| < 1$ and $|(-1)e\cos f| \ll 1$, then the magnitude of the terms in the binomial series progressively become smaller. Therefore, the binomial expansion of the term $(1 + e\cos f)^{-1}$ can be approximated as $(1 - e\cos f)$. Equation (3.7)

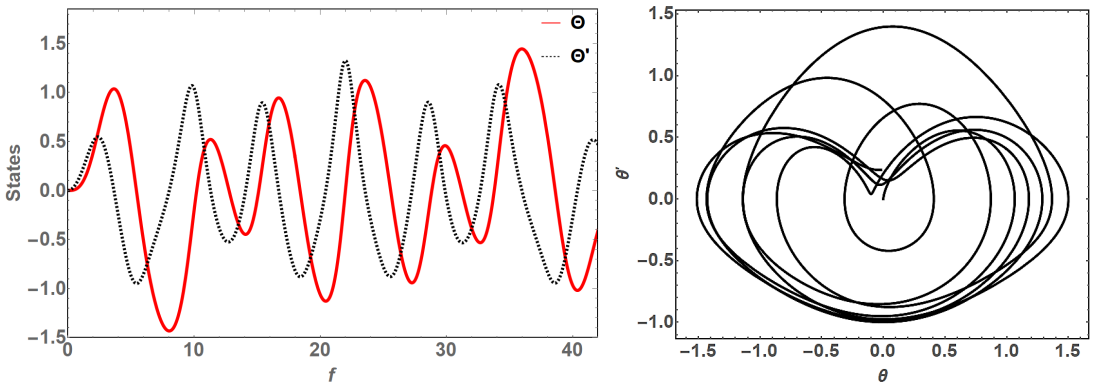

(a) Θ and Θ' (b) Phase Portrait

Figure 15: State Response of the Motion in Original Coordinates

becomes,

$$\Theta'' = (1 - e\cos f)(2e\sin f\Theta' - 3\sigma\sin\Theta\cos\Theta + 2e\sin f). \tag{3.8}$$

Let

$$\left.\begin{aligned} p &= \cos(f), \\ p' &= -\sin(f) = -q, \\ q' &= \cos(f) = p. \end{aligned}\right\} \tag{3.9}$$

After further substituting the trigonometric product term with its series approximation given in equation (3.12) to the 7^{th} order, the motion in equation (3.8) can be expressed as,

$$\Theta'' = (1 - ep)\left[2eq\Theta' - 3\sigma\left(\Theta - \frac{2}{3}\Theta^3 + \frac{2}{15}\Theta^5 - \frac{4}{315}\Theta^7\right) + 2eq\right]. \tag{3.10}$$

Therefore, the augmented system state space representation with $(\Theta_1' = \Theta_2, \Theta_2' = \Theta_1'')$ is shown in the equation below,

$$\begin{bmatrix} \Theta_1' \\ \Theta_2' \\ q' \\ p' \end{bmatrix} = \begin{bmatrix} 0 & 1 & 0 & 0 \\ -3\sigma & 0 & 2e & 0 \\ 0 & 0 & 0 & 1 \\ 0 & 0 & -1 & 0 \end{bmatrix} \begin{bmatrix} \Theta_1 \\ \Theta_2 \\ q \\ p \end{bmatrix}$$

$$+ \begin{bmatrix} 0 \\ 2eq\left[ep(1-\Theta_2)+\Theta_2\right] - 3\sigma ep\Theta_1 - 3\sigma(1+ep)\left(-\frac{2}{3}\Theta_1^3 + \frac{2}{15}\Theta_1^5 - \frac{4}{315}\Theta_1^7\right) \\ 0 \\ 0 \end{bmatrix}. \tag{3.11}$$

Figure 16 shows the augmented state system history behavior. Allowing for the expected minor discrepancies due to series and binomial expansion approximations; the system state response is comparable to that of the system in original coordinates shown in figure 15.

From figures 15 and 16(a,b) the attitude motion is quasiperiodic as characterized by absence of closed trajectory attractors in the phase space. The pitch angle librates roughly between $-1.5 < \Theta < +1.5\ radians$ while the pitch angle rate of change varies between $-1.0 < \Theta' < +1.5$. The orbits generally appear to follow a 'heart-shaped' path starting at the origin with two non-closing lobes on either side. Conversely, the augmented states are periodic as characterized by the closed circular limit cycle attractor centered at the origin in figure 16(d). The motion behavior discussed here indicates that Θ and Θ' are susceptible to instability, unpredictability and chaos. Consequently, these aspects of the motion flow will be investigated next. Neither the eigenvalues of the linear periodic term of equation 3.7 nor of the state augmented system (3.11) can be used to determine stability. Conse-

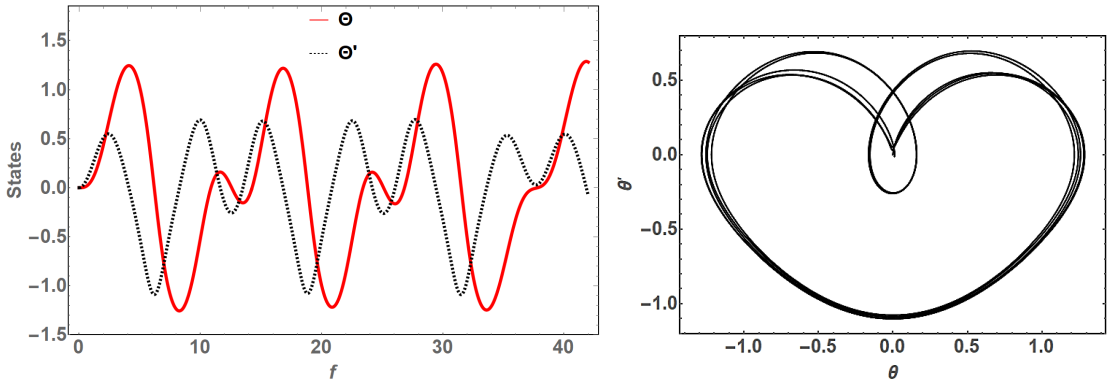

(a) Θ and Θ′ Response (b) Θ and Θ′ Phase Portrait

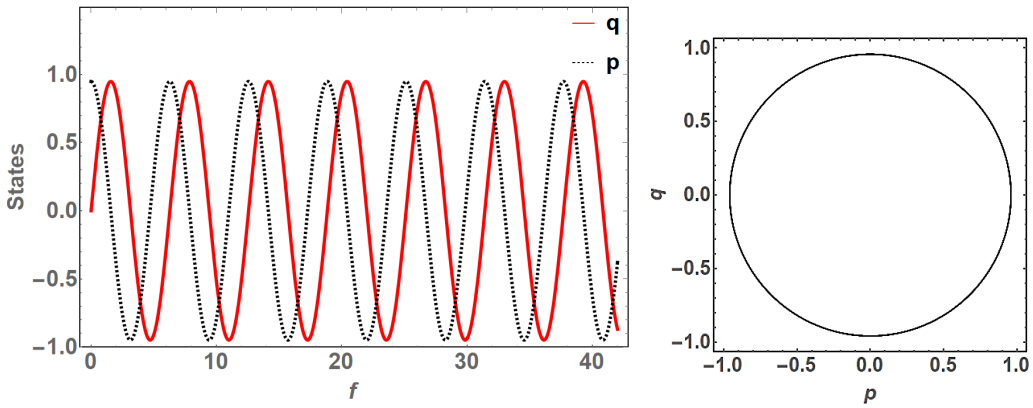

(c) $q(f)$ and $p(f)$ Response (d) $q(f)$ and $p(f)$ Phase Portrait

Figure 16: State Response of Augmented States System

quently, we'll have to construct the Floquet Transformation Matrix (FTM) to analyze the dynamical system's stability.

3.3 Stability and Chaos

Stability analysis is preceded by computation of the state transition matrix as outlined in section 2.1. We first prepare the motion in equation (3.7) for expansion via shifted Chebyshev polynomials of the first kind by normalizing the principal period. This is because shifted Chebyshev polynomials are only valid for the period interval $[0\,,\,1]$

The pitch angle trigonometric product term in equation (3.7) can be represented as a product of the respective Taylor series expansion of sine and cosine as,

$$\sin\Theta\cos\Theta = \Theta - \frac{2}{3}\Theta^3 + \frac{2}{15}\Theta^5 - \frac{4}{315}\Theta^7 + \ldots + a_k\Theta^{2k-1} \tag{3.12}$$

where $k = 1, 2, 3, 4\ldots$, Also, series coefficient: $a_k \longrightarrow 0$, as $k \longrightarrow \infty$.

We can ignore the terms of order greater than 7 in equation (3.12) without significant loss of accuracy because the follow-on terms have relatively small successive coefficients that rapidly approach zero. For instance, the 9^{th} order term has the coefficient $a_5 = 6.7791 \times 10^{-4}$ while the 11^{th} order term's coefficient is $a_6 = 1.98412 \times 10^{-5}$. Substituting the expanded trigonometric product in equation (3.7), we obtain,

$$\Theta'' = \frac{1}{(1 + e\cos f)}\left(2e\sin f\Theta' - 3\sigma\left(\Theta - \frac{2}{3}\Theta^3 + \frac{2}{15}\Theta^5 - \frac{4}{315}\Theta^7\right) + 2e\sin f\right). \tag{3.13}$$

To normalize the principal period, let $f = 2\pi\zeta$. Equivalently, $\zeta \in [0\,, 1]$ represents duration within the principal period. Let Z represent the principal period, then this implies that for a periodic term; $\boldsymbol{A}(\zeta) = \boldsymbol{A}(\zeta + Z)$. It follows,

$$\Theta' = \frac{d\Theta}{d\zeta}\cdot\frac{1}{2\pi}, \qquad \Theta'' = \frac{1}{4\pi^2}\frac{d^2\Theta}{d\zeta^2}. \tag{3.14}$$

After substituting Θ' and Θ'' from equation (3.14) into (3.13), the obtained state space representation of the normalized attitude motion is given below,

$$\begin{aligned}\begin{bmatrix}\mathring{x}_1\\ \\ \mathring{x}_2\end{bmatrix} &= \begin{bmatrix}0 & 1\\ \\ \dfrac{-12\pi^2\sigma}{(1+e\cos 2\pi\zeta)} & \dfrac{4\pi e\sin 2\pi\zeta}{(1+e\cos 2\pi\zeta)}\end{bmatrix}\begin{bmatrix}x_1\\ \\ x_2\end{bmatrix}\\ &+ \frac{12\pi^2\sigma}{(1+e\cos 2\pi\zeta)}\begin{bmatrix}0\\ \\ \dfrac{2}{3}x_1^3 - \dfrac{2}{15}x_1^5 + \dfrac{4}{315}x_1^7\end{bmatrix} + \begin{bmatrix}0\\ \\ \dfrac{8\pi^2 e\sin 2\pi\zeta}{(1+e\cos 2\pi\zeta)}\end{bmatrix},\end{aligned} \tag{3.15}$$

where, ${}^{d\Theta}/_{d\zeta} = \mathring{x_1}$ and ${}^{d^2\Theta}/_{d\zeta^2} = \mathring{x_2}$. Further, $\{\Theta(0) = 0,\ \mathring{\Theta}(0) = 0\}$ constitute the initial conditions of the represented motion which correspond to pitch librations at position 1 of figure 14(b).

It is clear that equation (3.15) is of the form,

$$\mathring{\boldsymbol{x}}(\zeta) = \boldsymbol{A}(\zeta)\boldsymbol{x}(\zeta) + \boldsymbol{f}(\zeta, \boldsymbol{x}) + \boldsymbol{F}(\zeta). \tag{3.16}$$

3.3.1 Floquet Multipliers and Exponents

To facilitate computation of STM, FTM and LFT matrices using Chebyshev polynomials, we utilized the Chebfun software package on MATLAB™[105]. Summarily, Chebfun applies piece-wise Chebyshev polynomial interpolation to construct smooth functions over the interval $[-1\,, +1]$. Recall that $\zeta = \frac{f}{2\pi}$ and Z is the normalized principal period, hence the computed $FTM = \boldsymbol{\Phi}(Z)$ is,

$$\boldsymbol{\Phi}(Z) = \begin{bmatrix} 0.9462 & -0.0529 \\ 1.9796 & 0.9462 \end{bmatrix}. \tag{3.17}$$

The computed Floquet multipliers are critical since they lie on the unit circle with values of $(0.9462 \pm 0.3236i)$ as shown in figure 17. Consequently, this reveals a marginally stable system for the chosen e-σ pair. It follows that the corresponding Floquet exponents, $(0 \pm 0.3295i)$ are purely imaginary. This is consistent with the quasi-periodic system phase portraits that illustrate a librational motion.

The motion is hence stable in the sense of Lyapunov but the inherent oscillations are disruptively significant to jeopardize nominal execution of the spacecraft mission.

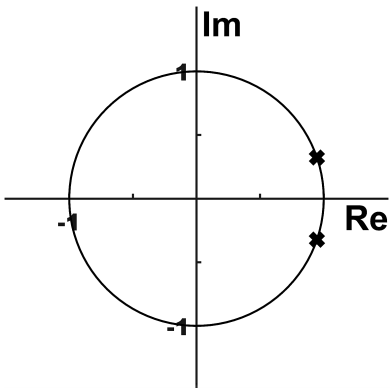

Figure 17: Floquet Multipliers Location

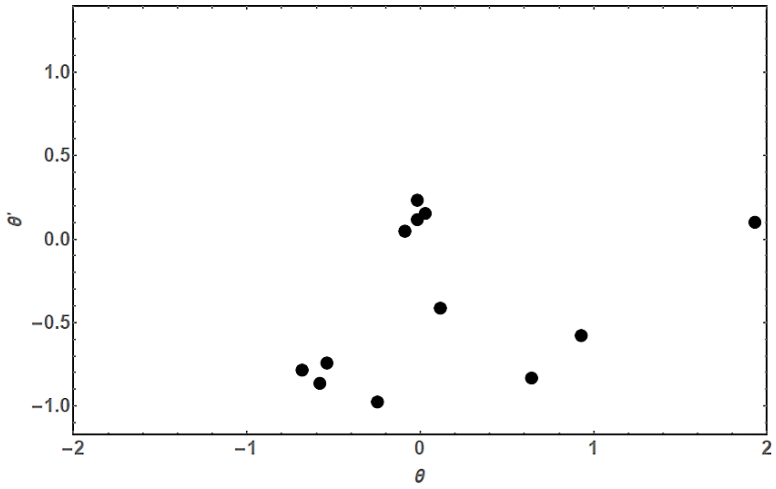

Figure 18: Poincaré Section of the Attitude Motion

3.3.2 Poincaré Map

Figure 18 shows the constructed Poincaré section of the flow. There is a discernible main cluster of points in close proximity to the origin but restricted to the positive side of Θ'. Relatively scanty, isolated discrete points occupy the lower bottom half of the plot bound by $-1 < \Theta < 2$.

The Poincaré section composition suggests two possible flow behaviors. The group-

ings suggests a quasi-periodic trajectory. On the other hand, the scanty random points devoid of clustering could be due to transient behavior or chaos. A chaotic motion can briefly dwell on a near periodic trajectory before changing to a disparate trajectory with a period that is a multiple of the preceding motion. Consequently, it is needed to further investigate the presence of chaos in the attitude motion dynamics.

3.3.3 Chaos

We define chaos as a bounded aperiodic steady-state motion behavior that is not in equilibrium and is sensitive to initial conditions. A minuscule divergence in the input rapidly grows to spawn an overwhelming difference in the system response. We begin investigating chaos in the attitude motion by plotting the system implicit time history with a minute divergence to the initial condition of the state, Θ. We set the first initial condition to zero; the divergent second initial condition is obtained by adding $\epsilon = 10^{-12}$ to the zero initial condition. The obtained implicit time history of the two curves reveal the onset and progression of an overwhelming difference in the system response as illustrated in figure 19. The slightly divergent initial condition results in an overwhelming difference in response that begins in the second half of the 4^{th} orbit then rapidly grows in the subsequent orbits. The attitude motion in hence chaotic.

3.3.4 Lyapunov Exponents

To determine the average rate of divergence between the initially neighboring trajectories defined locally in the state space; we shall scrutinize the dynamic behavior of the motion's Lyapunov exponents. Lyapunov exponent stability analysis afford a means of

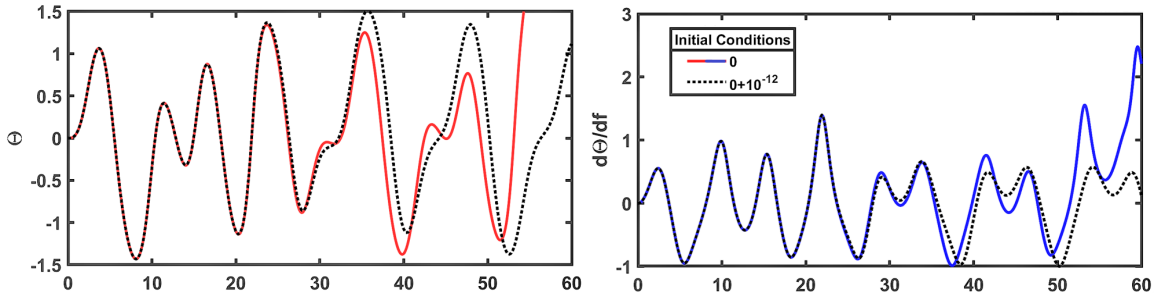

Figure 19: Chaos: Attitude Motion Sensitivity to Initial Conditions

quantifiable expression for initial conditions sensitivity-dependence (i.e. chaos), by describing the exponential rate of growth or decay of a perturbation to a trajectory as time progresses [79]. Lyapunov exponent, λ is numerically expressed as,

$$\lambda = \lim_{t\to\infty} \frac{1}{t} ln \left(\left\| \frac{\boldsymbol{\delta y}(t)}{\boldsymbol{\delta y}(0)} \right\| \right) , \tag{3.18}$$

where $\boldsymbol{\delta y}(t)$ is the tiny separating perturbation vector between the trajectories. The value of Lyapunov exponent will distinguish the nature of the trajectory according to the following criteria: *i)* $\lambda < 0$: Trajectory is stable and the motion is asymptotically stable. *ii)* $\lambda = 0$: Trajectory is neutral and the motion is characterized by some sort of steady-state. *iii)* $\lambda > 0$: Trajectory is unstable and chaotic. The Lyapunov exponents behavior for the motion given equation (3.15) is illustrated in Figure 20.

The computed Lyapunov exponents are equal in magnitude but opposite in sign with increasing periods because the flow in equation (3.15) is non-autonomous Hamiltonian. Hamiltonian systems are conservative. Therefore the magnitude of λ_1 which measures expansion in one direction; is equal to the magnitude of λ_2 which measures contraction in another direction. Since $\lambda_1 > 0$ always, then as prescribed by the above distinction for λ, the attitude motion is chaotic. This outcome is consistent with the preceding chaos analyzes that scrutinized motion sensitivity to initial conditions.

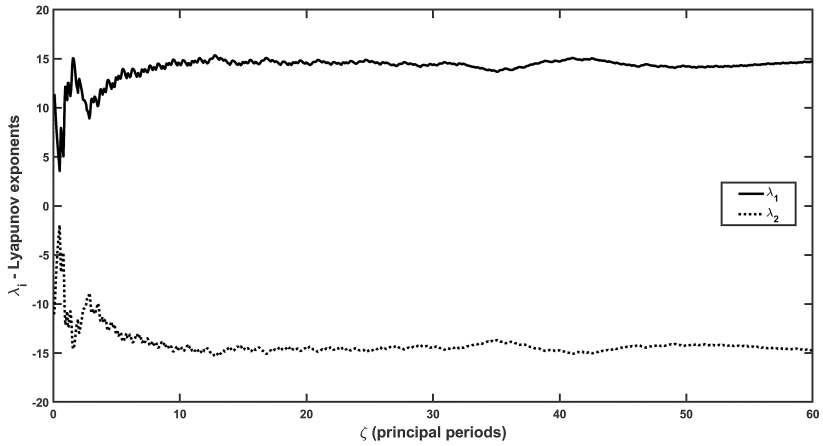

Figure 20: Dynamics of Lyapunov Exponents for the Attitude Motion

3.3.5 Stability Charts

The orbit eccentricity and spacecraft's ratio of principal moments of inertia are respectively defined as $e \in \{0\,,1\}$ and $\sigma \in \{0\,,1\}$. On the other hand, our stability analysis so far has been illustrated courtesy of arbitrarily set values of $(e = 0.2\ , \sigma = 0.3)$. Consequently is it essential to holistically scrutinize the motion behavior for all possible values of e and σ. Constructing stability charts which partition the e-σ plane into stable and unstable regions enable scrutiny of motion stability as e and σ vary simultaneously. Transition curves in stability charts constitute frontiers that separate stable regions from unstable regions. We can derive transition curves in closed form via the FTM. Floquet theory requires a stable system to have a Floquet multiplier of magnitude, $|\rho_k| \leq 1$. It can hence be proved that the transition from stability to instability occurs when both Floquet multipliers are equal to 1 or both are equal to -1 (See figure 17). Therefore, the transition curves in the e-σ plane where the solution to the linear periodic term of equation (3.16) changes from stable to unstable (or vice versa) are determined by the conditions, $Trace[FTM] = \pm 2$, or $|\rho_k| = 1$.

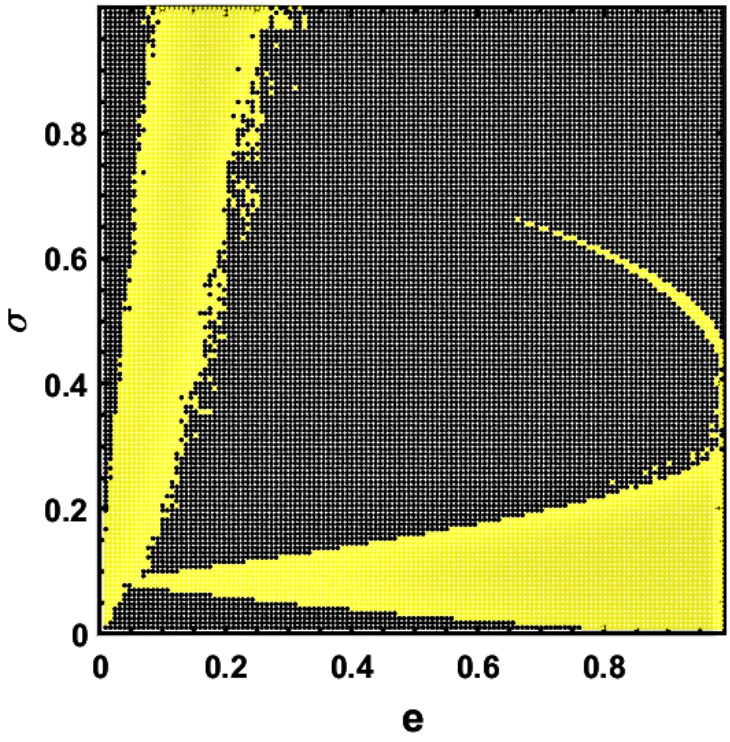

Figure 21: Stability Chart of the Attitude Motion

Even though we can only construct transition curves associated with the linear term of the attitude motion equation; the outcome provides insightful perusal into the behavior of the whole equilibrium solution. The complete solution behavior can be arrived at by augmenting the evaluated linear periodic stability behavior with the combined effect of the nonlinear term $\boldsymbol{f}(x, \zeta)$ and forcing term $\boldsymbol{F}(\zeta)$ in equation (2.1). For instance, if a given $\{e, \sigma\}$ pair is initially located in the unstable region of the FTM-dependent stability chart; then, the nonlinear and forcing terms will tend to exacerbate this instability rendering the complete solution unstable for that particular $\{e, \sigma\}$ combination. A similar argument can be made for an $\{e, \sigma\}$ pair located in a stable region. The constructed stability chart of the attitude motion is shown in figure 21.

The darker regions constitute stable points while the lighter regions are unstable. The

Table 1: Stability of Representative $e - \sigma$ Pairs

Stability Region	***e***	***σ***	**Floquet Multipliers,** (ρ_1, ρ_2)	$\lvert\rho_1\rvert$	$\lvert\rho_2\rvert$
Unstable	0.82	0.6	-1.06522 , -0.93877	1.06	0.94
	0.6	0.1	-0.20126 , -4.96854	0.20	4.96
	0.8	0.14	-0.10212 , -9.79244	0.10	9.79
Marginal	0.2	0.5	$0.1346 \pm 0.99099i$	1	1
Stable	0.4	0.4	$0.7971 \pm 0.60382i$	1	1
	0.6	0.5	$-0.1117 \pm 0.9937i$	1	1
	0.8	0.9	$0.7156 \pm 0.6984i$	1	1

stability chart has a slightly larger stable region than the unstable region. Unstable solutions appear to be dominated by two regions approximately defined by *i)* $\sigma \in \{0\,,\,0.2\}$ and increasing values of e plus *ii)* $e \in \{0\,,\,0.3\}$ and increasing values of σ. Essentially, a spacecraft with mass distribution such that $\sigma > 0.2$ is amenable to a wider range of eccentricity values above 0.2 to achieve an intended stable pitch angle motion.

For instance, we have previously considered the pair $\{e = 0.2, \sigma = 0.3\}$; this pair is located in the stable region corresponding to critical Floquet multipliers confirmed in figure 17. The motion at this location is stable in the sense of Lyapunov. The stability chart further accords a means of scrutinizing generalized stability behavior trends or commonalities between disparate $e - \sigma$ pairs. By picking representative $e - \sigma$ pairs from different regions, we tabulate the resultant illustrative Floquet multipliers as shown in Table 1.

From the table, we note that both selected marginal and stable regions are associated with critical Floquet multipliers. This implies that the pertinent *e-σ* pair characterizes a motion stable in the sense of Lyapunov; i.e. the pitch angle librations are bound by $\Theta \in \{-\pi\,,+\pi\}$. This is consistent with the dynamics presented in figures 17 and 15. However, in the unstable regions, Floquet multipliers have magnitudes $|\rho_k| > 1$, implying that the pitch angle wanders beyond $\pm\pi$.

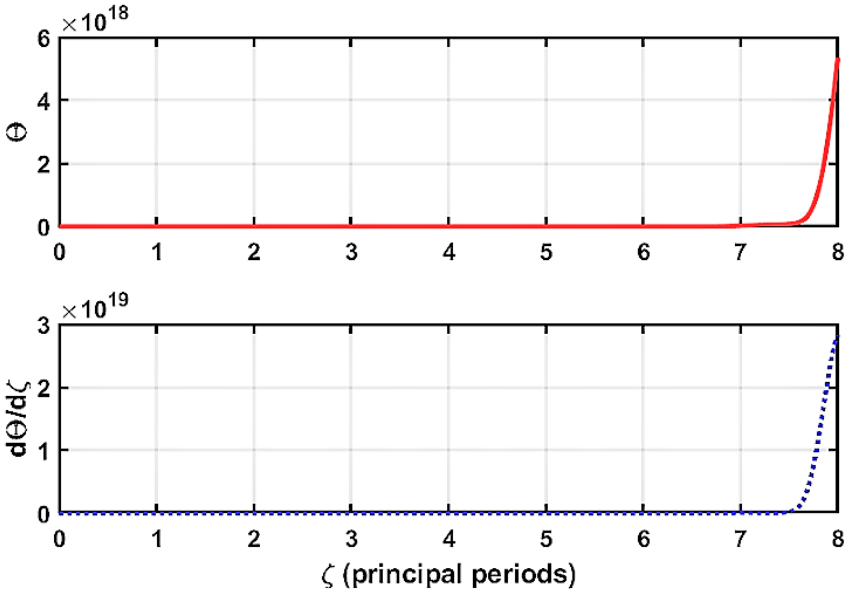

Figure 22: Resonance in Linear and Forcing Terms

3.4 Resonance

The attitude dynamics are dominated by the linear and forcing terms delineated in equation (3.16). This is because if we consider the motion composed of only the linear and forcing terms i.e $\mathring{\boldsymbol{x}}(\zeta) = \boldsymbol{A}(\zeta)\boldsymbol{x}(\zeta) + \boldsymbol{F}(\zeta)$,the numerical solution is unbounded as shown in figure 22. This is not the case if we consider motion composed of any of the following term combinations; $\mathring{\boldsymbol{x}}(\zeta) = \boldsymbol{A}(\zeta)\boldsymbol{x}(\zeta)$, $\mathring{\boldsymbol{x}}(\zeta) = \boldsymbol{A}(\zeta)\boldsymbol{x}(\zeta) + \boldsymbol{f}(x,\zeta)$, or $\mathring{\boldsymbol{x}}(\zeta) = \boldsymbol{f}(x,\zeta) + \boldsymbol{F}(\zeta)$.

Moreover, if we consider the L-F transformed motion in equation (2.58), Floquet exponents (eigenvalues of $\boldsymbol{R}$) represent frequencies associated with the linear term. Periodic elements of the nonlinear matrix are a product of the truncated Fourier series matrices $\boldsymbol{Q}(\zeta)$ and $\boldsymbol{Q}^{-1}(\zeta)$. On the other hand, periodic elements of the forcing matrix are likewise multiplied by $\boldsymbol{Q}^{-1}(\zeta)$. Subsequently, resonance between the Floquet exponents and any

of the periodic terms in the forcing matrix elements will trigger instability in the motion as well.

Bifurcation triggers the system's equilibrium solutions to transition between the disparate regions of the stability chart. The orbit eccentricity, e is the bifurcation parameter for the attitude motion (see equation (3.15)). This is because the general on-orbit spacecraft mass properties represented by σ, typically tend to be constant for a gravity gradient stabilized spacecraft. Therefore, it is essential to analyze the equilibrium solution dynamics as small increments are applied on the bifurcation parameter. We develop the normal form of our dynamics in the next section to facilitate bifurcation behavior analysis. Normal forms are not unique, consequently near identity transformation for the state augmented system and the L-F transformed system will be undertaken separately.

3.5 Versal Deformation of the Normal Form and Bifurcation Analysis

Versal deformation refers to embedding the system in a parameterized family of systems containing all possible dynamics that can occur near the bifurcation point. Moreover, the family of systems should be transverse to the bifurcation surface with the number of parameters equal to the codimension of the bifurcation [106]. The attitude motion undergoes a codimension one bifurcation because only one parameter, e is responsible for the loss of stability (for gravity gradient stabilization to be maintained, σ has to remain fixed). Because our critical Floquet multipliers are complex and lie on the unit circle; this system will experience a Hopf bifurcation. Further, it is "well-known" that Hopf Bifurcation is a codimension one bifurcation. Firstly, we shall formulate the normal forms of nonlinearities up to the cubic order in equations (3.15) and (3.11) to demonstrate the

intended approach. Normalization of dynamics with higher order nonlinearities can be accomplished via the same techniques.

3.5.1 State Augmented System

To normalize the augmented states system, we first apply the modal transformation $\boldsymbol{\Theta} = \boldsymbol{M}\boldsymbol{y}$ (here, $\boldsymbol{\Theta} = [\Theta_1 \ \ \Theta_2 \ \ q \ \ p]^T$) to equation (3.11) and obtain the equation below,

$$\boldsymbol{y'} = \boldsymbol{J}\boldsymbol{y} + \boldsymbol{M}^{-1} \begin{bmatrix} 0 \\ 2eq\left[ep(1-\Theta_2)+\Theta_2\right] - 3\sigma ep\Theta_1 - 3\sigma(1+ep)\left(-\frac{2}{3}\Theta_1^3\right) \\ 0 \\ 0 \end{bmatrix}. \tag{3.19}$$

This system now possesses 4^{th} order nonlinearity. $\boldsymbol{J}$ is in the Jordan canonical form. Equation (3.19) is hence of the form described in equation (2.33). The normal form is evaluated by successive application of the near identity transformation,

$$\boldsymbol{y} = \boldsymbol{v} + \boldsymbol{h_4}(\boldsymbol{v}, f). \tag{3.20}$$

The state augmented system is independent of periodic coefficients hence we solely obtain the TINF as,

$$\begin{bmatrix} v_1' \\ v_2' \\ v_3' \\ v_4' \end{bmatrix} = \begin{bmatrix} -iv_1 \\ iv_2 \\ -i0.948683v_3 + i30.4002v_1v_2v_3 + i1.05409v_3^2v_4 \\ i0.948683v_4 - i30.4002v_1v_2v_4 - i1.05409v_3v_4^2 \end{bmatrix}. \tag{3.21}$$

When the external forcing term is augmented as a system state, the magnitude of the external forcing frequency appears as solitary, linear, imaginary conjugate coefficients in the

normal form, i.e. 1 (see equation (3.8)). Eigenvalues of the linear matrix in equation (3.11) constitute the conjugate coefficients in the linear terms of the reduced nonlinearity normal forms, (i.e. $\pm i0.948683$).

Moreover, after obtaining the straightforward solutions of $v_1(f)$ and $v_2(f)$ then substituting these values in the equations for $v_3'(f)$ and $v_4'(f)$; the last two equations of the normal form can be expressed as,

$$v_3' = i(-0.948683 + 30.4002C_1C_2)v_3 + i1.05409v_3^2v_4,$$
$$v_4' = i(0.948683 - 30.4002C_1C_2)v_4 - i1.05409v_3v_4^2.$$

Here, C_1 and C_2 are the integration constants originating from the analytical solutions of $v_1(f)$ and $v_2(f)$ respectively.

We shall investigate the bifurcation of equation (3.11) via its normal form given above. Because the periodic system maintains the same general structure, we may treat the respective limit cycles as equilibria and study their bifurcations. We utilize the versal deformation of the normal form to investigate the change in the stability structure of the dynamics in the neighborhood of the critical point of the bifurcation parameter. Essentially, construction of versal deformation of the normal form facilitates characterization of system dynamics at the critical point and its small neighborhood. Therefore, we handily gain complete understanding of the qualitative phase space dynamics of the dynamical system in the neighborhood of the critical point.

We define the normal form versal deformation parameter as μ_1. The parameter μ_1 represents a small change in the eigenvalues of the normal form corresponding to a small change in the bifurcation parameter in the original system coordinates. It is a prerequisite condition to obtain a relationship between the the versal deformation parameter, μ_1 and the original system bifurcation parameter e. Incorporating μ_1 in equation (3.21) we

obtain,

$$\begin{bmatrix} v_1' \\ v_2' \\ v_3' \\ v_4' \end{bmatrix} = \begin{bmatrix} \mu_1 - i & 0 & 0 & 0 \\ 0 & \mu_1 + i & 0 & 0 \\ 0 & 0 & \mu_1 - \varpi & 0 \\ 0 & 0 & 0 & \mu_1 + \varpi \end{bmatrix} \begin{bmatrix} v_1 \\ v_2 \\ v_3 \\ v_4 \end{bmatrix} + \begin{bmatrix} 0 \\ 0 \\ i1.05409 v_3^2 v_4 \\ -i1.05409 v_3 v_4^2 \end{bmatrix}, \tag{3.22}$$

where $\varpi = i(0.948683 - 30.4002 C_1 C_2)$.

By defining small increments on the bifurcation parameter as η, we can write $e_k = e_c + \eta_k$ to represent the k disparate sets of bifurcation parameter in the neighborhood of the critical parameter $e_c = 0.2$. We employ the least squares, curve-fitting technique proposed by [107] to obtain the relationship between μ_1 and η as, $\mu_1 = (1.47476 + i0.301628)\eta - (1.82052 + i0.414608)\eta^2$. N.B. Values of C_1 and C_2 in equation (3.22) were evaluated by forward action transformations of initial conditions in the original coordinates i.e $\Theta_1 = \Theta_2 = 0, p = 1, q = 0$.

The closed form analytical solutions for $v_1(f)$ and $v_2(f)$ in the versal deformation equation (3.22) is straightforward. To obtain $v_3(f)$ and $v_4(f)$ we introduce the complex changes of variable; $v_3(f) = u_1 - iu_2$ and $v_4(f) = u_1 + iu_2$ followed by the polar coordinates $u_1 = R\cos\theta$ and $u_2 = Rsin(\theta)$. The last two equations in (3.22) become,

$$\left.\begin{aligned} R' &= Re(\mu_1)R, \\ \theta' &= 0.948683 - 30.4002 C_1 C_2 - 1.05409 R^2. \end{aligned}\right\} \tag{3.23}$$

After solving equation (3.23), we utilize the results to complete the closed form analytical solution of equation (3.22) as,

$$v_1(f) = e^{\mu_1 f} C_1 \exp(-if),$$
$$v_2(f) = e^{\mu_1 f} C_2 \exp(if),$$
$$v_3(f) = e^{\mu_1 f} C_3 \exp - \left((0.948683 - 30.4 C_1 C_2) f - \frac{0.52705 e^{2\mu_1 t} C_3^2}{\mu_1} + C_4 \right) i, \quad (3.24)$$

$$v_4(f) = e^{\mu_1 f} C_3 \exp \left((0.948683 - 30.4 C_1 C_2) f - \frac{0.52705 e^{2\mu_1 f} C_3^2}{\mu_1} + C_4 \right) i.$$

Similarly, C_3 and C_4 are the integration constants originating from the analytical solutions of $v_3(f)$ and $v_4(f)$ respectively. The values of these integration constants is evaluated from the initial conditions specified in the original coordinates. After back transformation of the normal form closed form analytical solutions above, we obtain the motion in the original coordinates.

The back transformed $v1(f)$ and $v_2(f)$ constitute the augmented states given in figure 16(c). Moreover, $\mu_1 \neq 0$; but is generally small in the order of magnitude 10^{-4}. The integration constants on evaluation are imaginary whose magnitudes are close to identity. Consequently, from equation (3.24), back transformation of the sinusoidal $v1(f)$ and $v_2(f)$ will result in the trigonometric augmented states whose amplitude is determined by the magnitude of the integration constants. From equation (3.23), we can express the transient solution of R as $R = e^{i(\mp i\mu_1 \pm |C|)}$. Since $\mu_1 \neq 0$, the motion is characterized by a locally stable limit cycle in the neighborhood of the bifurcation point. The limit cycle is stable in the sense of Lyapunov but not asymptotically stable. Post bifurcation attractors that transform into quasi-periodic attractors portraying a limit cycle in the original coordinates are obtained via back transformation and subsequently shown in figure 23 ($\eta = 0.00001$).

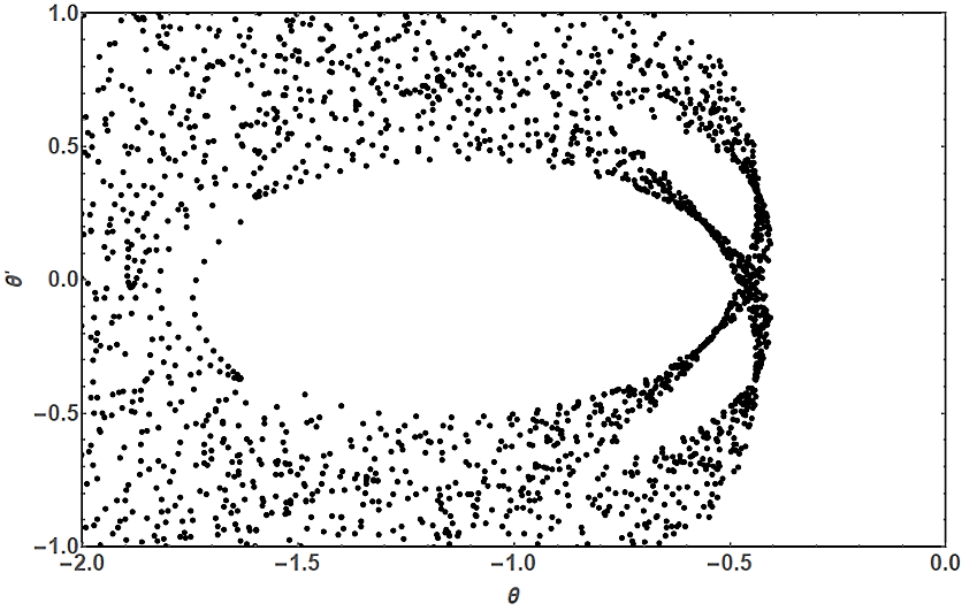

Figure 23: Poincaré Map of State Augmented Motion Post-Bifurcation Behavior

3.5.2 L-F Transformed System

Here, we also demonstrate analysis of bifurcation behavior subject to different values of e-σ pair. Consequently, by utilizing the developed stability chart (figure 21) we select $\{e = 0.1\,, \sigma = 0.2\}$. This e-σ pair lies on a transition curve hence the system is guaranteed to be bifurcating. Again, by considering up to the cubic nonlinearity, the history behavior from equation 3.15 is shown in figure 24.

The system likewise possesses critical Floquet multipliers that lie on the unit circle of values ($0.1435 \pm 0.9896i$) and purely imaginary Floquet exponents, $0 \pm 1.4268i$. The computed FTM and $\boldsymbol{R}$ matrices are;

$$\boldsymbol{\Phi}(Z) = \begin{bmatrix} 0.1435 & -0.1914 \\ 5.1161 & 0.1435 \end{bmatrix}, \qquad \boldsymbol{R} = \begin{bmatrix} 0 & -0.276 \\ 7.376 & 0 \end{bmatrix}. \tag{3.25}$$

The computed periodic LFT matrix, $\boldsymbol{Q}(\zeta)$ and $\boldsymbol{Q}^{-1}(\zeta)$ are plotted in figure 25.

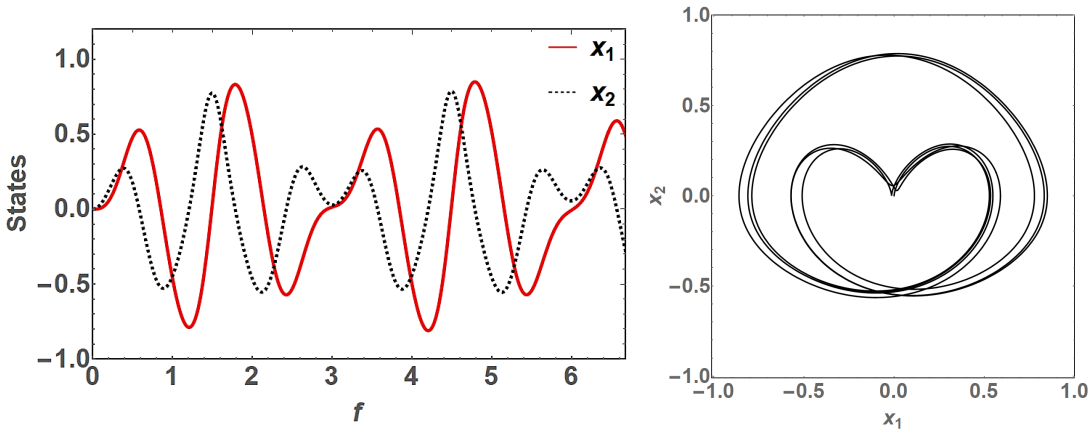

(a) x_1 and x_2 (b) Phase Plot

Figure 24: L-F Transformed System Implicit Time History Response

We consider the L-F transformed dynamics in equation (3.26) up to the cubic nonlinearity. After applying the LFT matrix given in equation (3.18) on the attitude motion in equation (3.15), we obtain the system,

$$\mathring{\boldsymbol{z}} = \boldsymbol{R}\boldsymbol{z} + \boldsymbol{Q}^{-1}\begin{bmatrix} 0 \\ \dfrac{12\pi^2\sigma}{(1+e\cos 2\pi\zeta)}\left\{\dfrac{2}{3}(Q_{11}z_1 + Q_{12}z_2)^3\right\} \end{bmatrix} + \boldsymbol{Q}^{-1}\begin{bmatrix} 0 \\ \dfrac{8\pi^2 e\sin 2\pi\zeta}{(1+e\cos 2\pi\zeta)} \end{bmatrix}. \tag{3.26}$$

To normalize this externally excited motion the system states are augmented to convert the system from non-autonomous to autonomous. We define additional states as

$$\left.\begin{aligned} p(\zeta) &= \cos(2\pi\zeta), \\ \mathring{p}(\zeta) &= -2\pi sin(2\pi\zeta) = -q(\zeta), \\ \mathring{q}(\zeta) &= 4\pi^2\cos(2\pi\zeta) = 4\pi^2 p(\zeta), \end{aligned}\right\} \tag{3.27}$$

which are further plotted in figure 26.

After substituting the above augmented states into equation (3.26), we obtain the system shown in equation (3.28)–whose order of nonlinearity increases to four. The trans-

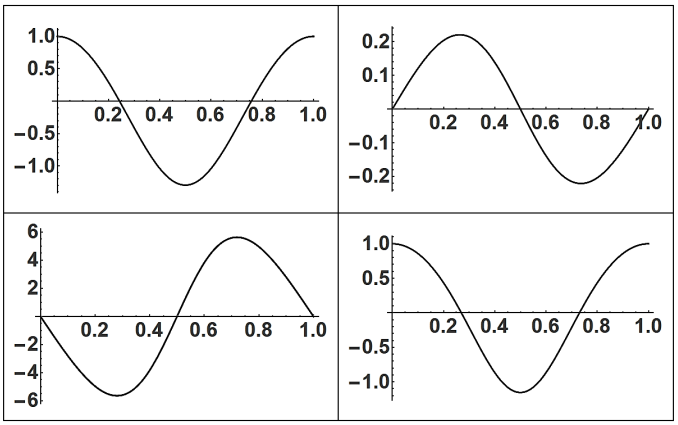

(a) $Q_{ij}(\zeta)$

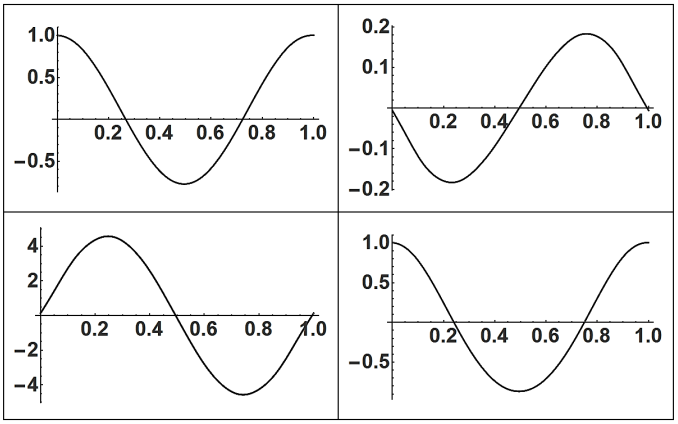

(b) $Q_{ij}^{-1}(\zeta)$

Figure 25: Plot of Elements of the LFT Matrix and its Inverse

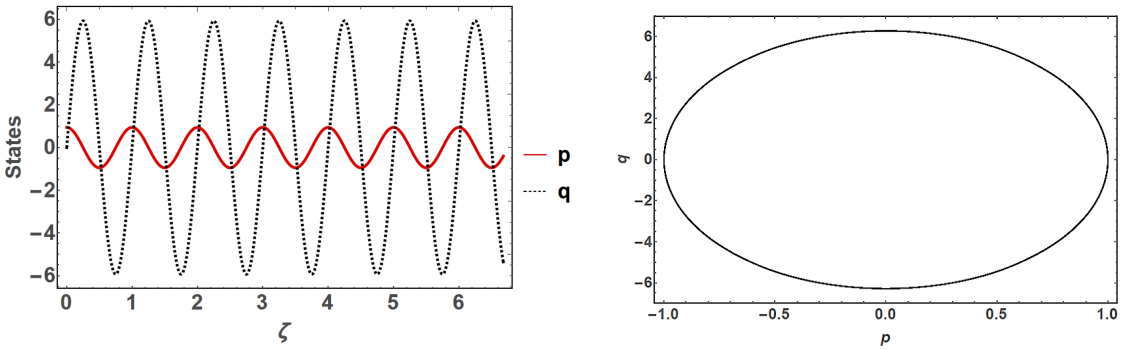

(a) $p(\zeta)$ and $q(\zeta)$ (b) Phase Portrait

Figure 26: Augmented System States

formed denominator term $(1 + e\cos(2\pi\zeta))^{-1}$ has been approximated by the binomial expansion equivalent i.e. $(1 + ep)^{-1} \approx (1 - ep)$.

Apart from raising the order of nonlinearity, state augmentation further introduces periodic linear terms, $4\pi e Q_{12}^{-1} q$ and $4\pi e Q_{22}^{-1} q$ as shown below,

$$\begin{bmatrix} \mathring{z}_1 \\ \mathring{z}_2 \\ \mathring{p} \\ \mathring{q} \end{bmatrix} = \begin{bmatrix} 0 & -0.276 & 0 & 0 \\ 7.376 & 0 & 0 & 0 \\ 0 & 0 & 0 & -1 \\ 0 & 0 & 4\pi^2 & 0 \end{bmatrix} \begin{bmatrix} z_1 \\ z_2 \\ p \\ q \end{bmatrix} + 8\pi^2\sigma \begin{bmatrix} (1-ep)(Q_{11}z_1 + Q_{12}z_2)^3 Q_{12}^{-1} \\ (1-ep)(Q_{11}z_1 + Q_{12}z_2)^3 Q_{22}^{-1} \\ 0 \\ 0 \end{bmatrix} + 4\pi e \begin{bmatrix} q(1-ep)Q_{12}^{-1} \\ q(1-ep)Q_{22}^{-1} \\ 0 \\ 0 \end{bmatrix}. \tag{3.28}$$

Consequently, the augmented dynamics with linear parameter variant coefficients necessitate a second LFT to convert the linear term to parameter invariant. The computed parameters corresponding to the second LFT are as follows; critical Floquet multipliers $0.1435 \pm 0.9897i$, and purely imaginary Floquet exponents, $0 \pm 1.4268i$. The computed second FTM and constant $\boldsymbol{R}$ matrices are given in equation (3.29) and (3.30) respectively;

$$\mathbf{\Phi}^*(Z) = \begin{bmatrix} 0.1435 & -0.1914 & -0.4343 & -0.054 \\ 5.1161 & 0.1435 & -2.0844 & 0.307 \\ 0 & 0 & 1 & 1 \\ 0 & 0 & 0 & 1 \end{bmatrix}, \tag{3.29}$$

$$\boldsymbol{R}^* = \begin{bmatrix} 0 & -0.276 & -0.6456 & -0.0022 \\ 7.376 & 0 & -0.1165 & 0.4524 \\ 0 & 0 & 0 & 0 \\ 0 & 0 & 0 & 0 \end{bmatrix}. \tag{3.30}$$

The computed second periodic LFT matrix, $\boldsymbol{Q}^*(\zeta)$ and its inverse, $\boldsymbol{Q}^{*-1}(\zeta)$ are similarly presented as plots in figure 27.

We designate the second L-F transformation as $\boldsymbol{z} = \boldsymbol{Q}^*\boldsymbol{w}$. Here, $\boldsymbol{z} = [z_1 \;\; z_2 \;\; p \;\; q]^T$. After applying the second L-F transformation to the state augmented periodic system we obtain,

$$\mathring{\boldsymbol{w}} = \boldsymbol{R}^*\boldsymbol{w} + \boldsymbol{Q}^{*-1}(8\pi^2\sigma) \begin{bmatrix} (1-ep)(Q_{11}z_1 + Q_{12}z_2)^3 Q_{12}^{-1} \\ (1-ep)(Q_{11}z_1 + Q_{12}z_2)^3 Q_{22}^{-1} \\ 0 \\ 0 \end{bmatrix} - \boldsymbol{Q}^{*-1}(4\pi e^2) \begin{bmatrix} qpQ_{12}^{-1} \\ qpQ_{22}^{-1} \\ 0 \\ 0 \end{bmatrix}. \tag{3.31}$$

Applying the modal transformation $\boldsymbol{w} = \boldsymbol{M}\boldsymbol{y}$ to equation (3.31) transmutes this system into,

$$\mathring{\boldsymbol{y}} = \boldsymbol{J}\boldsymbol{y} + \boldsymbol{M}^{-1}\boldsymbol{Q}^{*-1} \left((8\pi^2\sigma) \begin{bmatrix} (1-ep)(Q_{11}z_1 + Q_{12}z_2)^3 Q_{12}^{-1} \\ (1-ep)(Q_{11}z_1 + Q_{12}z_2)^3 Q_{22}^{-1} \\ 0 \\ 0 \end{bmatrix} - (4\pi e^2) \begin{bmatrix} qpQ_{12}^{-1} \\ qpQ_{22}^{-1} \\ 0 \\ 0 \end{bmatrix} \right), \tag{3.32}$$

where

$$z_1 = \sum_{i=1}^{4} Q_{1i}^* w_i, \;\; z_2 = \sum_{i=1}^{4} Q_{2i}^* w_i, \;\; p = \sum_{i=1}^{4} Q_{3i}^* w_i, \;\; q = \sum_{i=1}^{4} Q_{4i}^* w_i.$$

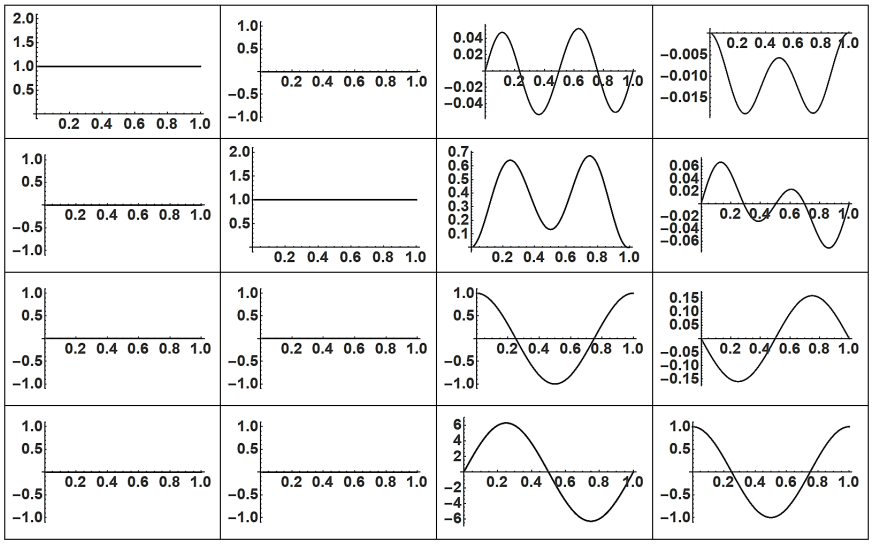

(a) $Q^{*}_{ij}(\zeta)$

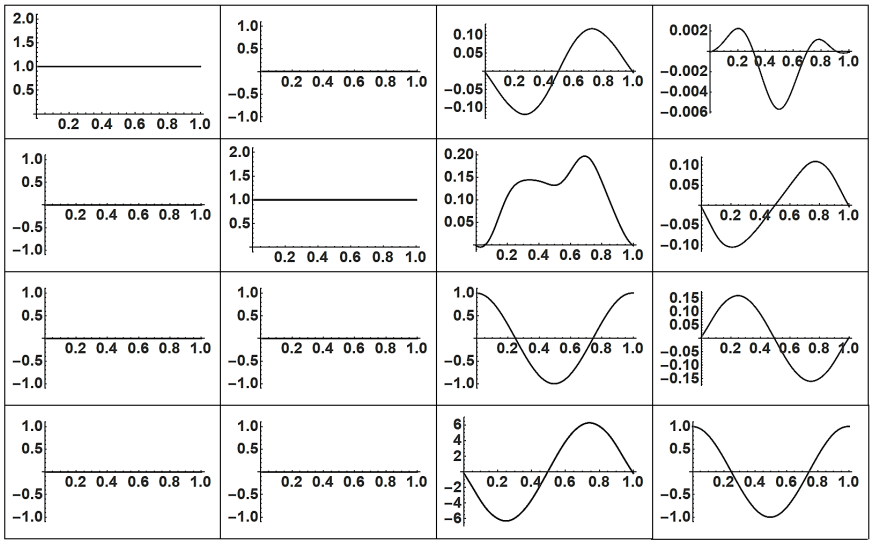

(b) $Q^{*-1}_{ij}(\zeta)$

Figure 27: Plot of Elements of the Second LFT Matrix and its Inverse

And

$$w_1 = \sum_{i=1}^{4} M_{1i} y_i, \;\; w_2 = \sum_{i=1}^{4} M_{2i} y_i, \;\; w_3 = \sum_{i=1}^{4} M_{3i} y_i, \;\; w_4 = \sum_{i=1}^{4} M_{4i} y_i.$$

$\boldsymbol{J}$, $\boldsymbol{y}$ and $\mathring{\boldsymbol{y}}$ take the form previously described in equations (3.19) and (3.20).

We first evaluate the TDNF as stipulated in equation (2.39) then as stated in equation (2.41), average out the periodic terms to obtain the simplified TINF as,

$$\begin{bmatrix} \mathring{v}_1 \\ \mathring{v}_2 \\ \mathring{v}_3 \\ \mathring{v}_4 \end{bmatrix} = \begin{bmatrix} 0 \\ 0 \\ -(0.0106945 - i2.12186)v_3 + i0.0005599 v_3^2 v_4 \\ -(0.0106945 + i2.12186)v_4 - i0.0005599 v_3 v_4^2 \end{bmatrix}. \tag{3.33}$$

The closed form analytical solutions for $v_1(\zeta)$ and $v_2(\zeta)$ are constants. Variables $v_1(\zeta)$ and $v_2(\zeta)$ in the $\mathring{v}_3$ and $\mathring{v}_4$ differential equations are substituted by their respective computed constants. This computation is carried out through the forward action transform of the L-F, modal and near-identity transformations of the initial conditions declared in the original coordinates. The Floquet exponents are conjugate coefficients in the linear terms of the normal forms before being multiplied by the substituted constant values equal to v_1 and v_2.

Similarly, we define the normal form versal deformation parameter as μ_2 and incorporate it into equation (3.33) to obtain,

$$\begin{bmatrix} \mathring{v}_1 \\ \mathring{v}_2 \\ \mathring{v}_3 \\ \mathring{v}_4 \end{bmatrix} = \begin{bmatrix} 0 & 0 & 0 & 0 \\ 0 & 0 & 0 & 0 \\ 0 & 0 & \mu_2 - \lambda_3 & 0 \\ 0 & 0 & 0 & \mu_2 - \lambda_4 \end{bmatrix} \begin{bmatrix} v_1 \\ v_2 \\ v_3 \\ v_4 \end{bmatrix} + \begin{bmatrix} 0 \\ 0 \\ -i0.0005599 v_3^2 v_4 \\ i0.0005599 v_3 v_4^2 \end{bmatrix}, \tag{3.34}$$

where $\lambda_3 = (0.0106945 + i2.12186)$, and $\lambda_4 = (0.0106945 - i2.12186)$.

After defining small increments on the bifurcation parameter again as η, we express the k disparate sets of bifurcation parameter in the neighborhood of the critical parameter $e_c = 0.1$ as, $e_k = e_c + \eta$. The relationship between μ_2 and η is evaluated via the procedure previously stated in section 3.5.1 to yield; $\mu_2 = (0.132784 - i0.842528)\eta - (3.04196 - i7.13545)\eta^2$.

The closed form analytical solutions for $v_1(\zeta)$ and $v_2(\zeta)$ of the versal deformation normal form are straightforward. To obtain $v_3(\zeta)$ and $v_4(\zeta)$ we introduce the complex changes of variable; $v_3(\zeta) = u_1 - iu_2$ and $v_4(\zeta) = u_1 + iu_2$ followed by the polar coordinates $u_1 = R\cos\theta$ and $u_2 = Rsin(\theta)$. The last two equations in (3.34) become,

$$\left.\begin{aligned} \mathring{R} &= [Re(\mu_2) - 0.0106945]\, R, \\ \mathring{\theta} &= 2.12187 + 0.0005599R^2. \end{aligned}\right\} \tag{3.35}$$

We solve equation (3.35) and use the results to obtain the remaining analytical solutions of equations (3.34) as shown in equation (3.36)

$$\begin{aligned} v_1(\zeta) &= \mu_2\zeta + C_1, \\ v_2(\zeta) &= \mu_2\zeta + C_2, \\ v_3(\zeta) &= e^{(-0.01069+\mu_2)\zeta}C_3e^{-\Gamma i}, \\ v_4(\zeta) &= e^{(-0.01069+\mu_2)\zeta}C_3e^{\Gamma i}, \end{aligned} \tag{3.36}$$

where $\Gamma = \left(2.1219\zeta + \dfrac{0.00028e^{(-0.02138+2\mu_2)\zeta}Re(C_3^2)}{\mu_2 - 0.01069} + Re(C_4)\right)$.

C_i ($i = 1, 2, 3, 4$), are the respective constants of integration whose value is evaluated from the initial conditions specified in the original coordinates. C_1 and C_2 are real whereas C_3 and C_4 are complex. μ_2 is similarly small in the order of magnitude 10^{-4}. $v_1(\zeta)$ and $v_2(\zeta)$ back transformation via inverse near-identity, modal and single L-F transformations forms the augmented states given in equation (3.27) and plotted in figure 26. Equation

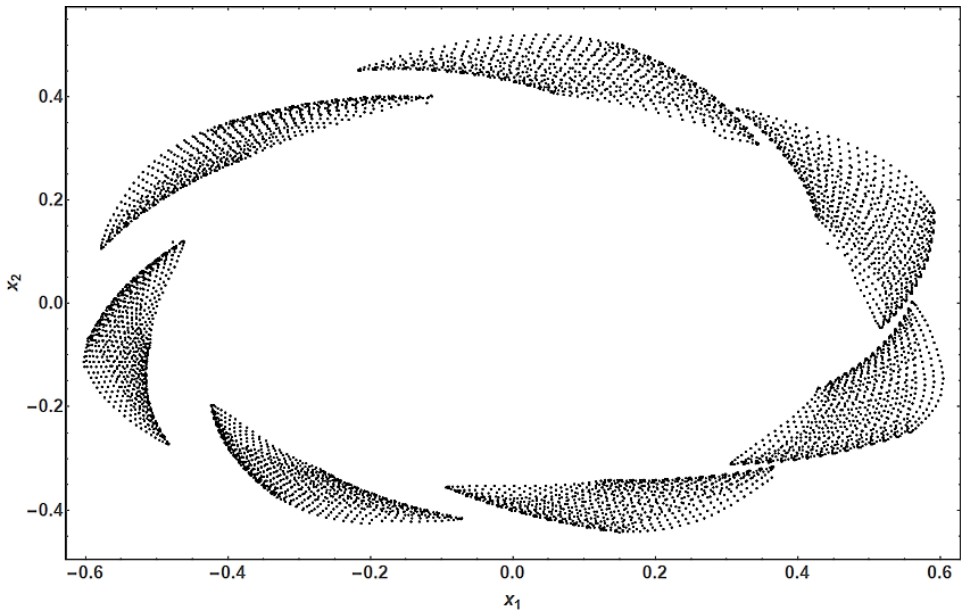

Figure 28: Poincaré Map of L-F Transformed Motion Post-Bifurcation Behavior

(3.35) yields a steady state solution of the limit cycle amplitude as $R = \frac{Re(\mu_2)}{0.0106945}$. When $\mu_2 \neq 0$ the solution of $v_3(\zeta)$ and $v_4(\zeta)$ results in locally stable limit cycle with amplitude corresponding to $R = \frac{Re(\mu_2)}{0.0106945}$. Consequently, the quasi-periodic attractors in the original coordinates delineating a limit cycle are obtained after back transformation as shown in figure 28 ($\eta = 0.0001$).

Solutions of the versal deformation equations enable investigation of the post-bifurcation steady-state behavior in the small neighborhood of the bifurcation point. However, as observed by [107], this method is only useful for local analysis. This is because minor errors introduced by back transformation close to the bifurcation points significantly grow as you move further away

3.6 Summary and Discussion

In this chapter we presented and characterized the attitude motion of a gravity gradient stabilized spacecraft in eccentric orbit. Ambient torques in the perturbing space environment engendered attitude motion modeled by nonlinear dynamics coupled in the roll-yaw axes; and, uncoupled planar dynamics in the pitch axis. The non-planar dynamics equations are homogeneous and analytically solvable. However, the pitch attitude motion is nonlinear, possesses parameter-varying coefficients and periodically excited.

We demonstrated a technique for analyzing the parameter-varying and periodically excited nonlinear attitude motion for a gravity gradient stabilized spacecraft. This approach is based on system states augmentation, Lyapunov-Floquet transformation and versal deformation of the normal forms. The preceding transformations transmute and reduce the original system dynamics to schemes that are more amenable to analyzes of stability, chaos, periodicity and bifurcation behavior.

Analysis showed that the attitude motion is quasi-periodic, chaotic and stable in the sense of Lyapunov for particular e-σ pairs. Subsequently the motion stability chart constructed facilitated prediction of e-σ combination leading to stable or unstable dynamics. The stable regions of the stability curve were found to predict marginal and not asymptotically stable dynamics. However, the emanating librations need to be stabilized for nominal mission operations to be realized. Conversely, the e-σ combinations located in the unstable regions resulted in aperiodic unstable dynamics. The computed Lyapunov exponents indicate that the chaotic dynamics also depend on initial values of $\{\Theta,\ \Theta'\}$ pair not just on the magnitudes of e-σ pairs.

Both outcomes of the two-fold versal deformation analyzes (disparate values of e-σ pairs considered); indicate establishment of locally stable limit cycles by the quasi-periodic

flow post bifurcation. Since the eccentricity varies as $0 < e < 1$, relatively small deviations from the critical point, e_c of the order $10^{-4} < \eta < 10^{-3}$ trigger a significant topological change in the structure of the motion flow.

Chapter 4

CONTROL OF GRAVITY GRADIENT STABILIZED ATTITUDE MOTION

After setting $e = 0.2$ and $\sigma = 0.3$ then numerically integrate the motion in equation (3.8) and equation (3.15) to obtain the uncontrolled responses shown in figure 29 (a) and (b) respectively. (N.B figure 29 (a) is the same as figure 15(a)). The slight difference in the long-term motion behavior in figure 29(b) may be attributed to the approximation of the trigonometric product term by a truncated series in equation (3.12) and possibly fidelity of the numerical integrator used in the computation. As established in section 3.3, the attitude motion for the considered $(e - \sigma)$ pair is quasiperiodic, marginally stable and chaotic. Despite the system being stable in the sense of Lyapunov, the inherent oscillations are disruptively significant and require stabilization if the spacecraft is expected to successfully conduct its mission.

In conformity with our outlined methodology in figure 3, motion controller design is undertaken on augmented states, L-F transformed or near identity transformed coordi-

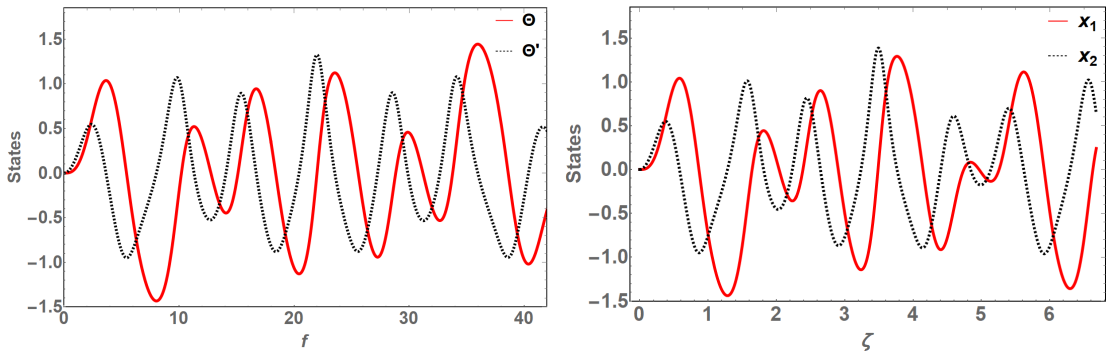

(a) Original Coordinates ($T = 2\pi$) (b) Normalized Principal Period ($T = 1$)

Figure 29: Uncontrolled Attitude Motion

nates. We shall hence first transform the system dynamics into these more amenable but topologically equivalent dynamical structures that retain the Lyapunov stability and bifurcation properties of the original system. Augmentation of the attitude dynamics states has been conducted in section 4.3.2. Control law development will be first considered in L-F transformed coordinates then followed by near-identity transformed coordinates of equation (3.15).

4.1 Lyapunov-Floquet Transformation

Prior to computing the LFT matrix $\boldsymbol{Q}(\zeta)$ and its inverse, $\boldsymbol{Q}^{-1}(\zeta)$ matrices (for the $e = 0.2,\ \sigma = 0.3$ case), we computed the FTM and $\boldsymbol{R}$ matrices over the interval $\zeta \in [0\,,1]$ via shifted Chebyshev polynomials of the first kind for the system in equation (3.15). The evaluated aforementioned matrices are shown below,

$$\boldsymbol{\Phi}(Z) = \begin{bmatrix} 0.9462 & -0.0529 \\ 1.9796 & 0.9462 \end{bmatrix}, \qquad \boldsymbol{R} = \begin{bmatrix} 0 & -0.0539 \\ 2.0159 & 0 \end{bmatrix}, \tag{4.1}$$

$$\boldsymbol{Q}(\zeta) = \begin{bmatrix} Q_{11} & Q_{12} \\ Q_{21} & Q_{22} \end{bmatrix}, \qquad \boldsymbol{Q}^{-1}(\zeta) = \begin{bmatrix} Q_{11}^{-1} & Q_{12}^{-1} \\ Q_{21}^{-1} & Q_{22}^{-1} \end{bmatrix}, \tag{4.2}$$

where

$$\begin{aligned} Q_{11} = {} & -0.138896 + 1.24968\cos(2\pi\zeta) - 0.121824\cos(4\pi\zeta) + 0.0121464\cos(4\pi\zeta) \\ & -0.00121854\cos(8\pi\zeta) + 0.000122567\cos(10\pi\zeta), \\ Q_{12} = {} & 0.201902\sin(2\pi\zeta) - 0.0196812\sin(4\pi\zeta) + 0.00196227\sin(6\pi t) \\ & -0.000196857\sin(8\pi\zeta), \end{aligned}$$

$$
\begin{aligned}
Q_{21} &= -7.44496\sin(2\pi\zeta) + 1.49121\sin(4\pi\zeta) - 0.224998\sin(6\pi\zeta) \\
&\quad +0.0302284\sin(8\pi\zeta), \\
Q_{22} &= 0.0074811 + 1.20128\cos(2\pi\zeta) - 0.24076\cos(4\pi\zeta) + 0.0363337\cos(6\pi\zeta), \\
&\quad -0.00488192\cos(8\pi\zeta) + 0.000615458\cos(10\pi\zeta),
\end{aligned}
$$

$$
\begin{aligned}
Q_{11}^{-1} &= 0.178684 + 0.831759\cos(2\pi\zeta) - 0.00416167\cos(4\pi\zeta) \\
&\quad -0.00201274\cos(6\pi\zeta) - 0.001088\cos(8\pi\zeta) - 0.000706808\cos(10\pi\zeta) \\
&\quad -0.000523275\cos(12\pi\zeta) - 0.000466034\cos(14\pi\zeta) \\
&\quad -0.0258801\sin(2\pi\zeta) + 0.000259231\sin(4\pi\zeta) + 0.000188365\sin(6\pi\zeta) \\
&\quad +0.000136072\sin(8\pi\zeta) + 0.000110821\sin(10\pi\zeta) + 0.000103106\sin(14\pi\zeta),
\end{aligned}
$$

$$
\begin{aligned}
Q_{12}^{-1} &= -0.0043031\cos(2\pi\zeta) - 0.000772303\cos(4\pi\zeta) + 0.00012908\cos(6\pi\zeta) \\
&\quad +0.000115479\cos(8\pi\zeta) + 0.000107006\cos(10\pi\zeta) + 0.000110097\cos(12\pi\zeta) \\
&\quad +0.000112704\cos(14\pi\zeta) - 0.138297\sin(2\pi\zeta) - 0.0123985\sin(4\pi\zeta) \\
&\quad +0.00137926\sin(6\pi\zeta) + 0.000923347\sin(8\pi\zeta) + 0.00068248\sin(10\pi\zeta) \\
&\quad +0.000583058\sin(12\pi\zeta) + 0.000509416\sin(14\pi\zeta),
\end{aligned}
$$

$$
\begin{aligned}
Q_{21}^{-1} &= 0.155206\cos(2\pi\zeta) - 0.00365144\cos(4\pi\zeta) - 0.00363534\cos(6\pi\zeta) \\
&\quad -0.00338305\cos(8\pi\zeta) - 0.00343186\cos(10\pi\zeta) - 0.00327608\cos(12\pi\zeta) \\
&\quad -0.00335147\cos(14\pi\zeta) + 4.98815\sin(2\pi\zeta) - 0.0586199\sin(4\pi\zeta) \\
&\quad -0.0388447\sin(6\pi\zeta) - 0.0270502\sin(8\pi\zeta) - 0.0218882\sin(10\pi\zeta) \\
&\quad -0.0173497\sin(12\pi\zeta) - 0.0151485\sin(14\pi\zeta),
\end{aligned}
$$

$$
\begin{aligned}
Q_{22}^{-1} = {} & 0.0835005 + 0.844365\cos(2\pi\zeta) + 0.0815938\cos(4\pi\zeta) - 0.00321618\cos(6\pi\zeta) \\
& -0.00173261\cos(8\pi\zeta) - 0.0010434\cos(10\pi\zeta) - 0.000742632\cos(12\pi\zeta) \\
& -0.00062635\cos(14\pi\zeta) - 0.0262723\sin(2\pi\zeta) - 0.00508249\sin(4\pi\zeta) \\
& +0.000300991\sin(6\pi\zeta) + 0.00021669\sin(8\pi\zeta) + 0.000163595\sin(10\pi\zeta) \\
& +0.000140229\sin(12\pi\zeta) + 0.000138575\sin(14\pi\zeta).
\end{aligned}
$$

Here, we alternatively present elements of $\boldsymbol{Q}(\zeta)$ and $\boldsymbol{Q}^{-1}(\zeta)$ as truncated Fourier series as described in equation (2.19). Previously in figures 25 and 27, we have presented the periodic plots of these series. Further, recall that $\zeta = \frac{f}{2\pi}$ and Z is the normalized principal period, hence $FTM = \boldsymbol{\Phi}(Z)$. After applying the L-F transformation, $\boldsymbol{x}(\zeta) = \boldsymbol{Q}(\zeta)\boldsymbol{z}(\zeta)$ to the attitude motion in equation (3.15), it becomes,

$$
\mathring{\boldsymbol{z}} = \boldsymbol{R}\boldsymbol{z} + \boldsymbol{Q}^{-1}\begin{bmatrix} 0 \\ \dfrac{12\pi^2\sigma}{(1+e\cos 2\pi\zeta)}\left\{\dfrac{2}{3}k^3 - \dfrac{2}{15}k^5 + \dfrac{4}{315}k^7\right\} \end{bmatrix} + \boldsymbol{Q}^{-1}\begin{bmatrix} 0 \\ \dfrac{8\pi^2 e\sin 2\pi\zeta}{(1+e\cos 2\pi\zeta)} \end{bmatrix}, \tag{4.3}
$$

where $k = (Q_{11}z_1 + Q_{12}z_2)$.

The Lyapunov stability properties are preserved in the new coordinates after the system is transformed by the LFT matrix. The L-F transformation theory guarantees that a suitable controller realized in the L-F transformed coordinates will be correspondingly efficacious after back transformation into the original system coordinates. Consequently, we shall endeavor to systematically synthesize suitable controllers to stabilize the motion in the transformed coordinates. Our control synthesis strategy will first consider linear control laws before exploring nonlinear control strategies.

In order to formulate appropriate control laws that would stabilize the quasi-periodic motion analyzed in chapter 3; we introduce a control input $u(t)$ in equation (3.1) as shown below,

$$
\ddot{\Theta} = -3\frac{\mu}{r^3}\sigma\sin\Theta\cos\Theta - \dot{\omega} + u(t). \tag{4.4}
$$

Using equations (3.5) and (3.6), we perform a change of independent variable from time (t) to true anomaly (f). The closed loop attitude dynamics hence will be,

$$\Theta'' = \frac{1}{(1 + e\cos f)} \left(2e \sin f \Theta' - 3\sigma \sin\Theta\cos\Theta + 2e\sin f \right) + u(f). \tag{4.5}$$

The control action $u(f)$ will generally represent torque per unit moment of inertia as a function of true anomaly. Equation (4.5) is first used to synthesize linear control laws followed by nonlinear control laws development.

4.2 Linear Control

Though linear control law principles are conventionally intended for controlling linear parameter invariant systems [108]; we initially consider them to control our nonlinear dynamics as an initial analysis step. Since most linear control methods tend to be relatively simpler to analyze and implement compared to nonlinear control methods, it is prudent to ascertain the suitability of linear control prior to embarking on relatively more complicated techniques. To implement linear control, we shall consider pole-placement approach to determine the negative feedback gain required to stabilize the system.

4.2.1 State Augmented System

The autonomous state augmented system in equation (3.11) can be represented in abbreviated form as,

$$\boldsymbol{\Theta}' = \boldsymbol{A}\boldsymbol{\Theta}(f) + \boldsymbol{f}(\boldsymbol{\Theta}, f), \tag{4.6}$$

where $\boldsymbol{f}(\boldsymbol{\Theta}, f)$ constitutes the nonlinear terms. $\boldsymbol{A}$ is the linear matrix and $\boldsymbol{\Theta} = [\Theta_1\ \Theta_2\ q\ p]^T$–the state vector.To synthesize the parameter-invariant linear state feedback

controller, equation (4.5) becomes,

$$\boldsymbol{\Theta}' = \boldsymbol{A\Theta}(f) + \boldsymbol{f}(\boldsymbol{\Theta}, f) + \boldsymbol{G_1}u(f). \tag{4.7}$$

The linear state feedback controller is of the form $u = -\boldsymbol{K\Theta}(f)$ and the control input scaling vector is $\boldsymbol{G_1} = [0\ 1\ 0\ 0]^T$. Though $\boldsymbol{A}$ is full rank, the linear pair $\{\boldsymbol{A}\ , \boldsymbol{G_1}\}$ is not controllable. This is because the system controllability matrix, **CM**, shown below has a rank of 2, instead of rank 4,

$$\boldsymbol{CM} = \begin{bmatrix} 0 & 1 & 0 & -0.9 \\ 1 & 0 & -0.9 & 0 \\ 0 & 0 & 0 & 0 \\ 0 & 0 & 0 & 0 \end{bmatrix}. \tag{4.8}$$

Consequently, a linear state feedback controller cannot stabilize the system dynamics associated with the $e - \sigma$ pair considered. It is to be noted that the two states, (p, q) in equation (4.7) are virtual states serving to simplify the system but are not accessible in the actual system dynamics. This is illustrated by the fact that controllability matrix does not have full rank.

4.2.2 L-F transformed System

In this case, the parameter-invariant linear state feedback controller is similarly of the form $u(\zeta) = -\boldsymbol{Kz}(\zeta)$. The control input is scaled by the matrix $\boldsymbol{G_2} = [1\ 1]^T$ in L-F transformed coordinates. Back transformation of the $\boldsymbol{G_2}u(\zeta)$ product via inverse LFT matrix will guarantee a single control input in the system original coordinates as will be demonstrated in equations (4.17) and (4.18). $\boldsymbol{R}$ is full rank and the linear pair $\{\boldsymbol{R}\ , \boldsymbol{G_2}\}$ is controllable. The L-F transformed equation (4.5) will be,

$$\mathring{\boldsymbol{z}} = \boldsymbol{Rz}(\zeta) + \boldsymbol{Q^{-1}f}(\boldsymbol{z}, \zeta) + \boldsymbol{Q^{-1}F}(\zeta) + \boldsymbol{G_2}u(\zeta). \tag{4.9}$$

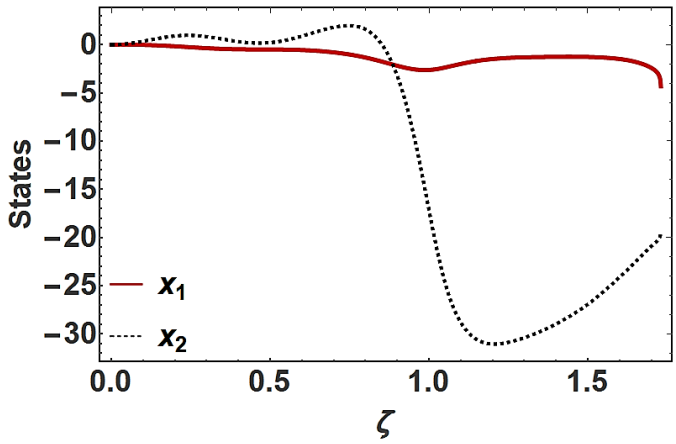

Figure 30: Linear Control of L-F Transformed State

Therefore, the system closed-loop dynamics subjected to a linear control law will be of the form,

$$\mathring{\boldsymbol{z}} = [\boldsymbol{R} - \boldsymbol{G_2 K}]\boldsymbol{z}(\zeta) + \boldsymbol{Q^{-1}} \boldsymbol{f}(\boldsymbol{z}, \zeta) + \boldsymbol{Q^{-1}} \boldsymbol{F}(\zeta). \tag{4.10}$$

We initially place poles at $(-1\ , 0)$. Then we evaluate the corresponding matrix $\boldsymbol{K} = [K_1\ K_2]$ to realize this pole-placement. Several stable double pole locations with a decreasing factor of 10 (i.e. -1, -10, -100, -1000...) were considered. None of these pole-placement locations demonstrated notable success in stabilizing the system. For instance, poles placed at $\{p_1 = -0.1\ ,\ p_2 = -0.2\}$ produces a response for a duration of slightly beyond 1.5 cycles before the states abruptly become indeterminate at about $\zeta \approx 1.74$ as shown in figure 30.

In this analysis, the system response in the original coordinates is realized via the back-transformation $\boldsymbol{z}(\zeta) = \boldsymbol{Q}^{-1}(\zeta)\boldsymbol{x}(\zeta)$. Therefore, similar to the state augmentation case, the L-F transformed nonlinear system demonstrates inability to be stabilized by a linear control law. The presence of periodic coefficients (elements of $\boldsymbol{Q^{-1}}(\zeta)$) associated with the nonlinear and forcing terms render the system untenable to be controlled via LTI sys-

tems control approaches. In general, the 'region of application' of linear control for nonlinear systems is dependent on magnitude of nonlinearity and initial conditions. Many times, linear control may stabilize nonlinear systems locally, but this is not guaranteed.

4.3 Nonlinear Control

Nonlinear control appears more suitable than linear control to stabilize the attitude motion. However, conventional nonlinear techniques are not readily amenable to dynamics with periodic coefficients and periodic external excitation. Hence, as illustrated in figure 3, requisite system state augmentation, L-F or near-identity transformations will be undertaken prior to controller design. We shall first consider Sliding Mode Control (SMC), then, bifurcation control will be implemented on the marginally stable system to stabilize post bifurcation response.

4.3.1 Sliding Mode Control

Sliding mode control is a robust nonlinear feedback control methodology that is suitable for achieving accurate tracking for a class of nonlinear systems. SMC methodology is based on variable structure control law that results in the state trajectory "sliding" along a discontinuity surface in the state space [109], [110]. Though SMC is deterministic, nonlinear and robust , its implementation is prone to undesirable "chattering" along the sliding surface [111]. Design of SMC involves *i)* selection of the switching function (stable hyperplane in the state space on which the dynamics will be restricted), *ii)* control law synthesis.

4.3.1.1 State Augmented System

Here, we implement a SMC that tracks a desired null pitch angle via a negative rate of growth. Dynamics in the original coordinates possess periodic coefficients rendering the dynamics unwieldy and unfavorable to synthesize a SMC. Therefore we develop the SMC law based on the augmented states dynamics–which are liberated from periodic coefficients. To design a sliding mode controller for the state augmented systems, we designate the switching function as,

$$s_1 = (\beta\Theta_1 + \Theta_2)^2. \tag{4.11}$$

The switching function represents the actual system state (i.e attitude pitch angle) reference error (difference between desired and actual pitch angle) that the controller desires to maintain at zero. Therefore, when $s_1 = 0$, $\Theta_1 \longrightarrow 0$ as $\Theta_2 \longrightarrow 0$.

Subsequently, the closed-loop dynamics of the controlled system are similar to equation (4.5) as shown below,

$$\left.\begin{aligned}
\Theta_1' &= \Theta_2, \\
\Theta_2' &= 2eq + 2e^2pq(1-\Theta_2) + 2eq\Theta_2 - 3\Theta_1\sigma - 3ep\Theta_1\sigma \\
&\quad - 3(1+ep)\left\{-\frac{2}{3}\Theta_1^3 + \frac{2}{15}\Theta_1^5 - \frac{4}{315}\Theta_1^7\right\}\sigma + u(f), \\
q' &= p, \\
p' &= -q,
\end{aligned}\right\} \tag{4.12}$$

where $u(f)$ represents the control input. Derivative of the switching function with Θ_1' and Θ_2' substituted from equation (4.12) is,

$$\begin{aligned}
s_1' =& \frac{2}{105}(\beta\Theta_1 + \Theta_2)\Big(\big(1+ep\big)\big(210eq + \sigma\Theta_1[-315 + 210\Theta_1^2 - 42\Theta_1^4 + 4\Theta_1^6]\big) \\
&+ 105(\beta - 2e(-1+ep)q)\Theta_2\Big) + u(f).
\end{aligned} \tag{4.13}$$

Setting $\beta = 1$, we derive the following control input,

$$u(f) = -\frac{2}{105}(\Theta_1 + \Theta_2)\ \Big((1+ep)\left(210eq + \sigma\Theta_1[-315 + 210\Theta_1^2 - 42\Theta_1^4 + 4\Theta_1^6]\right) - 105(1 - 2e(-1+ep)q)\Theta_2 \Big)\ - \varrho\, sgn(s_1), \tag{4.14}$$

where

$$\varrho(\mathbf{\Theta}) > \Big| -\frac{2}{105}(\beta\Theta_1 + \Theta_2)\ \Big((1+ep)\left(210eq + \sigma\Theta_1[-315 + 210\Theta_1^2 - 42\Theta_1^4 + 4\Theta_1^6]\right) - 105(\beta - 2e(-1+ep)q)\Theta_2 \Big)\ \Big|, \tag{4.15}$$

A sigmoid function, $\frac{s_1}{|s_1|+\varepsilon}$ is preferred instead of the signum function to reduce chattering around the sliding surface typical of sliding mode controllers. ε is generally small. Employing a direct Lyapunov approach, stability of the sliding mode controller applied here is ascertained by setting $V = \frac{1}{2}s_1^2$ to be the Lyapunov function. Hence, $V' = s_1 s_1'$. The guaranteed negative definiteness of the Lyapunov function derivative demonstrated by the equation below,

$$V' = -2\, s_1^{\frac{3}{2}} \left[\varrho\, \frac{s_1}{|s_1| + \epsilon} \right] < 0 \quad \forall s_1 \neq 0, \tag{4.16}$$

points to a stable controller. This equation is obtained after subsequent substitution for s_1' and $u(f)$ in the equation of V'. Figure 31 shows the sliding mode controlled system response.

It is observable that the sliding mode controller in the state augmented system achieves stabilization the motion throughout any number of orbits. Both Θ_1 and Θ_2 are adequately confined to zero. The augmented states p and q remain unaffected.

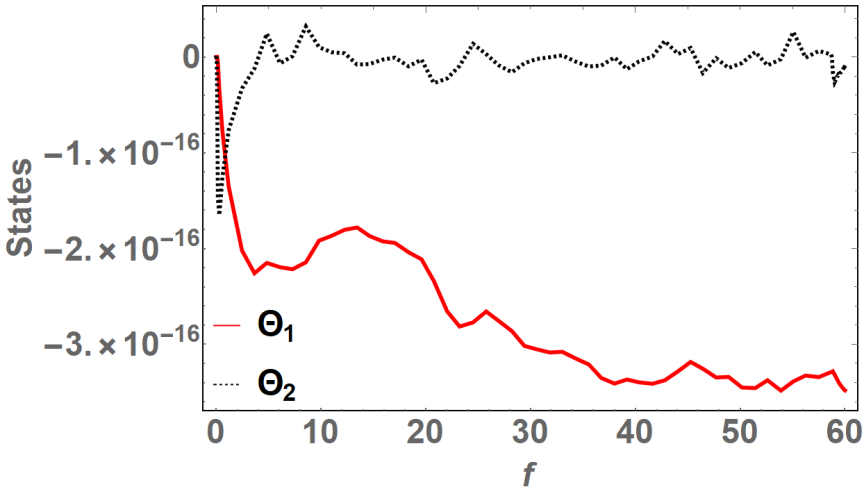

(a) Θ_1 and Θ_2

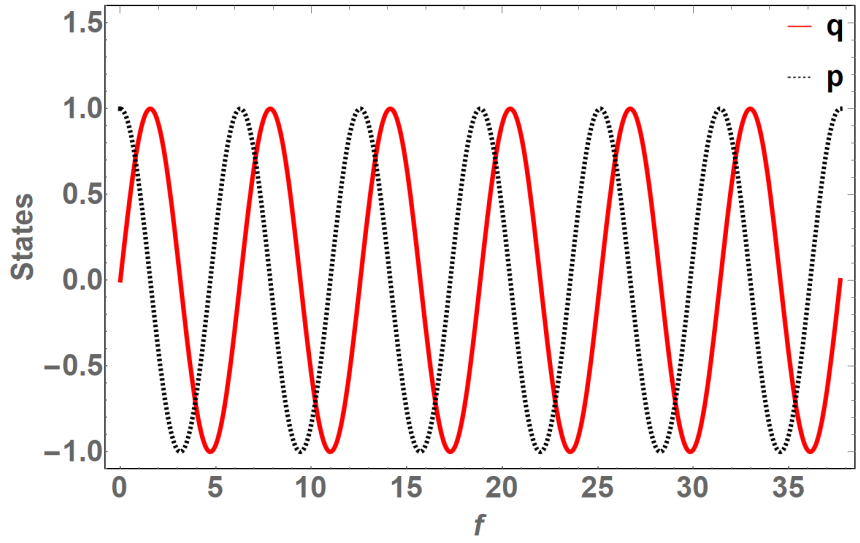

(b) q and p

Figure 31: Sliding Mode Controlled Actual and Augmented States

4.3.1.2 L-F Transformed System

In this case, we similarly assume a control input $u(\zeta)$ first applied to equation (3.15)– prior to L-F transformation as shown below,

$$\begin{bmatrix} \mathring{x}_1 \\ \mathring{x}_2 \end{bmatrix} = \begin{bmatrix} 0 & 1 \\ \dfrac{-12\pi^2\sigma}{(1+e\cos 2\pi\zeta)} & \dfrac{4\pi e \sin 2\pi\zeta}{(1+e\cos 2\pi\zeta)} \end{bmatrix} \begin{bmatrix} x_1 \\ x_2 \end{bmatrix} + \frac{12\pi^2\sigma}{(1+e\cos 2\pi\zeta)} \begin{bmatrix} 0 \\ \dfrac{2}{3}x_1^3 - \dfrac{2}{15}x_1^5 + \dfrac{4}{315}x_1^7 \end{bmatrix} + \begin{bmatrix} 0 \\ \dfrac{8\pi^2 e \sin 2\pi\zeta}{(1+e\cos 2\pi\zeta)} \end{bmatrix} + \boldsymbol{G_3} u(\zeta). \tag{4.17}$$

$\boldsymbol{G_3} = [0 \;\; 1]^T$ is the control input scaling vector. It then follows from equation (4.3) that the controlled L-F transformed system is,

$$\left.\begin{aligned} \mathring{z}_1 =& R_{11}z_1 + R_{12}z_2 + Q_{12}^{-1}\left(\frac{12\pi^2\sigma}{(1+e\cos 2\pi\zeta)} \left[\frac{2}{3}k^3 - \frac{2}{15}k^5 + \frac{4}{315}k^7\right] + \left[\frac{8\pi^2 e \sin 2\pi\zeta}{(1+e\cos 2\pi\zeta)}\right] + u(\zeta)\right), \\ \mathring{z}_2 =& R_{21}z_1 + R_{22}z_2 + Q_{22}^{-1}\left(\frac{12\pi^2\sigma}{(1+e\cos 2\pi\zeta)} \left[\frac{2}{3}k^3 - \frac{2}{15}k^5 + \frac{4}{315}k^7\right] + \left[\frac{8\pi^2 e \sin 2\pi\zeta}{(1+e\cos 2\pi\zeta)}\right] + u(\zeta)\right), \end{aligned}\right\} \tag{4.18}$$

where $k = Q_{11}z_1 + Q_{12}z_2$. We define the sliding function according to the equation,

$$s_2 = \alpha z_1 + z_2, \tag{4.19}$$

to ensure that; when $s_2 = 0$, $z_1 \longrightarrow 0$ as $z_2 \longrightarrow 0$. The sliding surface represents the reference pitch angle error. The controller attempts to maintain a zero error throughout, i.e. $s_2 = 0,\ \forall f > 0$.

After obtaining the derivative of the sliding function, we substitute for $\mathring{z}_1$ and $\mathring{z}_2$ from equation (4.18) to obtain,

$$\begin{aligned}\mathring{s}_2 =& R_{21}z_1 + \alpha R_{12}z_2 + (\alpha Q_{12}^{-1} + Q_{22}^{-1}) \left(\frac{12\pi^2\sigma}{(1+e\cos 2\pi\zeta)} \left[\frac{2}{3}k^3 - \frac{2}{15}k^5 + \frac{4}{315}k^7\right] \right. \\ &\left. + \left[\frac{8\pi^2 e \sin 2\pi\zeta}{(1+e\cos 2\pi\zeta)}\right] + u(\zeta) \right).\end{aligned} \tag{4.20}$$

Moreover, from equation (4.1), $R_{11} = R_{22} = 0$. From equation (4.20), we set $\alpha = 1$ and derive the following sliding mode control law,

$$\begin{aligned}u(\zeta) = & \left(-R_{21}z_1 - R_{12}z_2 - (Q_{12}^{-1} + Q_{22}^{-1}) \left\{ \frac{12\pi^2\sigma}{(1+e\cos 2\pi\zeta)} \left[\frac{2}{3}k^3 - \frac{2}{15}k^5 + \frac{4}{315}k^7\right] \right. \right. \\ & \left. \left. - \left[\frac{8\pi^2 e \sin 2\pi\zeta}{(1+e\cos 2\pi\zeta)}\right] \right\} \right) \frac{1}{(Q_{12}^{-1} + Q_{22}^{-1})} - \rho\,\mathrm{sgn}(s_2),\end{aligned} \tag{4.21}$$

where

$$\begin{aligned}\rho(\boldsymbol{z}) > & \left| \left(-R_{21}z_1 - R_{12}z_2 - (Q_{12}^{-1} + Q_{22}^{-1}) \left\{ \frac{12\pi^2\sigma}{(1+e\cos 2\pi\zeta)} \left[\frac{2}{3}k^3 - \frac{2}{15}k^5 + \frac{4}{315}k^7\right] \right. \right. \right. \\ & \left. \left. \left. - \left[\frac{8\pi^2 e \sin 2\pi\zeta}{(1+e\cos 2\pi\zeta)}\right] \right\} \right) \frac{1}{(Q_{12}^{-1} + Q_{22}^{-1})} - \rho\,\mathrm{sgn}(s_2) \right|.\end{aligned} \tag{4.22}$$

To reduce chattering around the sliding surface typical of sliding mode controllers due to fast switching of the signum function, a sigmoid function is similarly preferred. We again apply the direct Lyapunov approach to analyze the sliding mode controller stability by selecting $V = \frac{1}{2}s_2^2$ as the Lyapunov function. Asymptotic stability will be guaranteed if the sliding function derivative is negative-definite. Hence, the switching function derivative is $\mathring{V} = s_2\mathring{s}_2$. Substituting for $\mathring{s}_2$ above with the control input like-wise substituted we obtain the stability-criteria satisfying relationship below,

$$\mathring{V} = -s_2 \left[\rho \frac{s_2}{|s_2| + \epsilon}\right] < 0 \quad , \quad \forall s_2 \neq 0. \tag{4.23}$$

Figure 32 shows the sliding mode controlled system in L-F transformed coordinates.

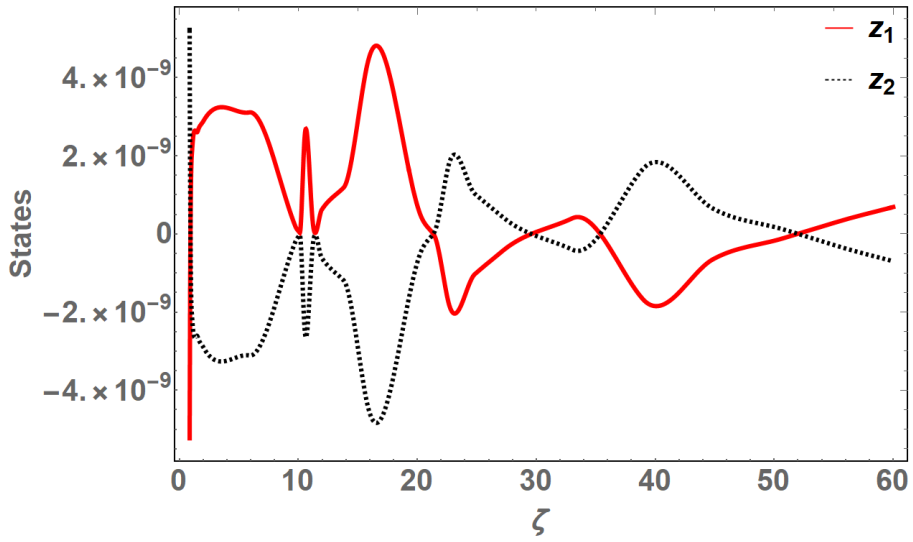

Figure 32: Sliding Mode Controlled States in L-F Transformed Coordinates

The response in figure 32 is back transformed via the inverse LFT resulting in controlled states in the original coordinates shown in figure 33.

We observe that, similar to the state augmented case, the sliding mode controller stabilizes the the L-F transformed motion as well by invariably confining the states to zero as desired. Though specific values for the $e - \sigma$ were used to demonstrate this technique, stabilization of the planar pitch motion by SMC approach is independent of the assigned $e - \sigma$ values. However, the possibility of a synthesized sliding mode controller being impractical to implement exists if the required control effort is colossally prohibitive.

4.3.2 Bifurcation Control

The critical Floquet multipliers corresponding to purely imaginary Floquet exponents (section) indicate that the system is in the stability boundary. Consequently, it is essential to stabilize the system post bifurcation apart from modifying other motion characteristics

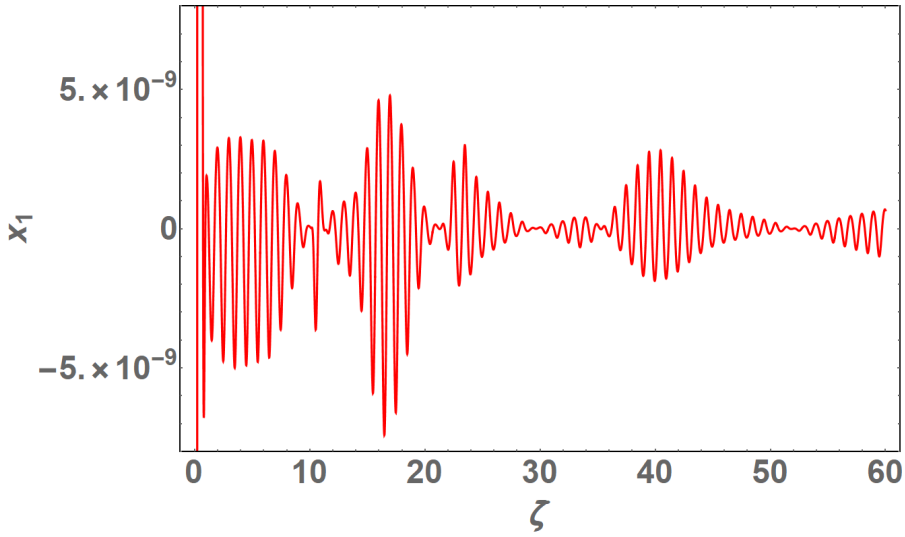

(a) x_1 State

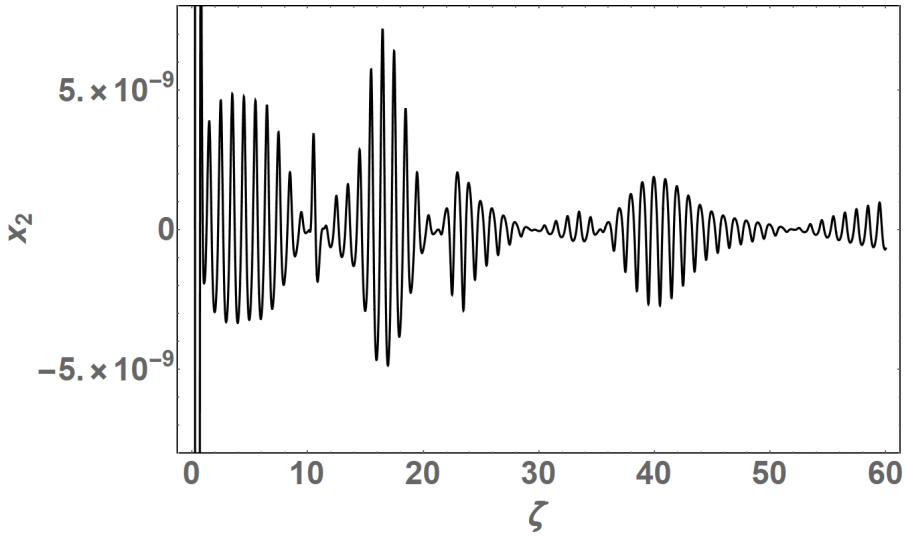

(b) x_2 State

Figure 33: Sliding Mode Controlled States in Original Coordinates

such as rate of growth. To achieve these objectives, we engage nonlinear bifurcation control with full state feedback. Synthesis of such a controller is facilitated by the normalized dynamics which are relatively more tractable compared to the dynamics as represented in the original coordinates. Periodic coefficients and complexity in structure of the dynamics equations in the original coordinates drastically convolute synthesis of bifurcation control law. Dynamics of the states in the original coordinates will eventually be obtained via back transformation of the normal form, modal and L-F transformations. Location of the complex Floquet multipliers on the unit circle (figure 17) indicates that the pitch attitude motion is undergoing a Hopf bifurcation with a limit cycle attractor of controllable radius. Therefore, the structure of the normal form will also verify a Hopf bifurcation occurring in the neighborhood of the critical point of the bifurcation parameter (i.e. orbit eccentricity).

To illustrate the intended approach, we shall formulate the normal forms of nonlinearities up to the cubic order in equations (3.11) and (3.15). Normalization of dynamics with higher order nonlinearities can be accomplished through the same techniques. Similar to the preceding cases, we'll consider the augmented states and L-F transformed systems separately.

4.3.2.1 State Augmented System

In section 3.5.1, we demonstrated how to obtain the TINF of the state augmented system–shown in equation (3.22). Obtaining the closed form analytical solutions for $v_1(f)$ and $v_2(f)$ in equation (3.22) is straight forward. On the other hand to evaluate $v_3(f)$ and $v_4(f)$ we introduce the complex changes of variable; $v_3 = u_1 - iu_2$ and $v_4 = u_1 + iu_2$ followed by the polar coordinates $u_1 = R\cos(\theta)$ and $u_2 = R\sin(\theta)$. The last two

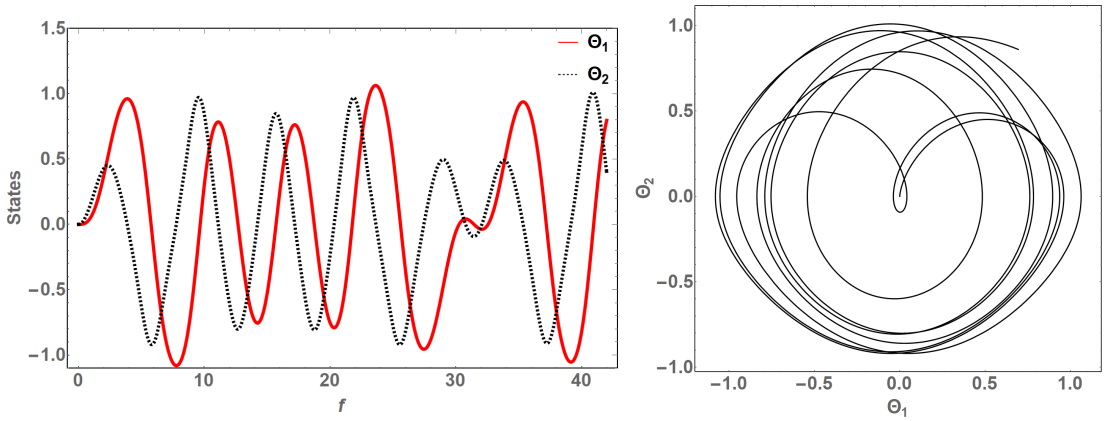

(a) Θ and Θ′ Response (b) Phase Portrait

Figure 34: Uncontrolled Dynamics of the Normalized State Augmented System

equations in (3.22) become,

$$\left.\begin{aligned} R' &= 0, \\ \theta' &= 0.948683 - 30.4002 C_1 C_2 - 1.05409 R^2. \end{aligned}\right\} \tag{4.24}$$

Here, C_1 and C_2 are the integration constants obtained when solving for $v_1(f)$ and $v_2(f)$ respectively.

We solve equation (4.24) then utilize the results to complete the closed form analytical solution of equation (3.22). The closed form solutions of $v_1(f)$, $v_2(f)$, $v_3(f)$, and $v_4(f)$ are then back-transformed to the original coordinates producing the uncontrolled motion behavior shown in figure 34. The system response in figure 34 is a cognate approximation of the originally obtained numerical solution in figures 29 and 16(a). Again, a quasi-periodic motion is characterized by non-closed curves is observed in the corresponding phase portrait. Moreover, a codimension one Hopf Bifurcation is verified by the normal form structure.

To synthesize a bifurcation control law of the normal form, we introduce a control

input as shown below,

$$\begin{bmatrix} v_1' \\ v_2' \\ v_3' \\ v_4' \end{bmatrix} = \begin{bmatrix} -i & 0 & 0 & 0 \\ 0 & i & 0 & 0 \\ 0 & 0 & i0.948683 & 0 \\ 0 & 0 & 0 & -i0.948683 \end{bmatrix} \begin{bmatrix} v_1 \\ v_2 \\ v_3 \\ v_4 \end{bmatrix} + \begin{bmatrix} 0 \\ 0 \\ i30.4002v_1v_2v_3 + i1.05409v_3^2v_4 \\ -i30.4002v_1v_2v_4 - i1.05409v_3v_4^2 \end{bmatrix} + \boldsymbol{G_4 u}. \tag{4.25}$$

Let the scaling matrix and control input respectively be of the form,

$$\boldsymbol{G_4} = \begin{bmatrix} 0 & 0 & 0 & 0 \\ 0 & 0 & 0 & 0 \\ 0 & 0 & 1 & 0 \\ 0 & 0 & 0 & 1 \end{bmatrix}, \qquad \boldsymbol{u} = \gamma_1 \begin{bmatrix} 0 \\ 0 \\ K_1 v_1 v_2 v_3 + K_2 v_3^2 v_4 \\ K_1 v_1 v_2 v_3 + K_2 v_3 v_2^4 \end{bmatrix}. \tag{4.26}$$

Back transformation of the $\boldsymbol{G_4 u}$ product via inverse normal form and modal transformations will guarantee a single control input in the system original coordinates as demonstrated in equations (4.17) and (4.18). The proportional gains are custom tuned to $K_1 = -5$ and $K_2 = -10$. $\gamma_1 = 1$ is a scalable parameter meant to suppress strange trajectory behavior according to Poincaré-Bendixson theorem in the system phase space. The resulting response of the bifurcation controlled augmented states system is shown in figure 35. The augmented states remain unaffected as previously shown in figure 31(b).

The libratory amplitude of the quasi-periodic pitch angle motion is tremendously stabilized and confined to a significantly diminished limit cycle attractor as illustrated in figure 34.

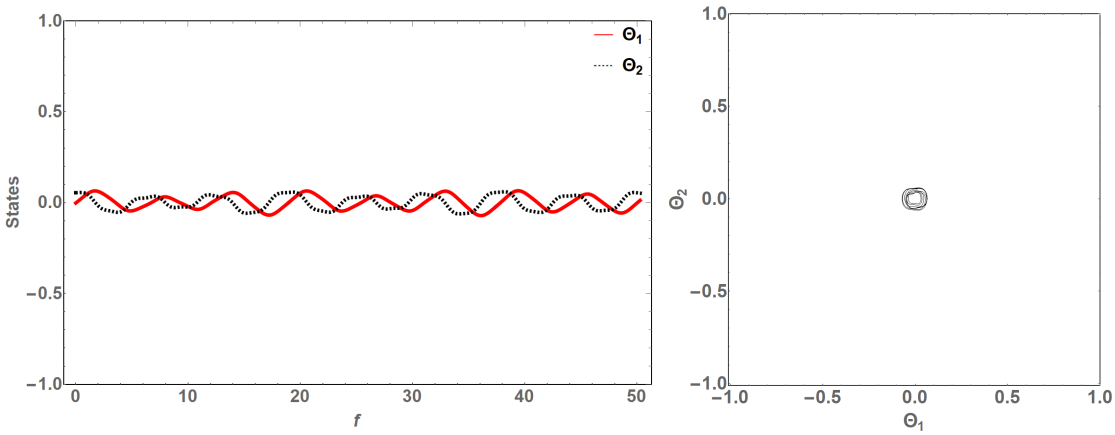

(a) Θ and Θ′ Response (b) Phase Plot

Figure 35: Dynamics of the Bifurcation Controlled State Augmented System

4.3.2.2 L-F Transformed System

As already indicated in section 3.5.2; in addition to synthesizing bifurcation control law via L-F transformed dynamics, we shall also demonstrate analysis of the spacecraft attitude dynamics due to different values of e and σ. Therefore, $e = 0.1$ and $\sigma = 0.2$ is once again considered in this section. L-F transformation analysis of the attitude dynamics associated with these values of e and σ has been comprehensively conducted in section 3.5.2. Subsequently, the normalized TINF system was obtained in equation (3.33).

In equation (3.33), the closed form analytical solutions for $v_1(\zeta)$ and $v_2(\zeta)$ are constants. Variables v_1 and v_2 in the $\mathring{v}_3$ and $\mathring{v}_4$ differential equations are substituted by their respective computed constants. This computation is carried out through the forward action transform of the L-F, modal and near-identity transformations of the initial conditions declared in the original coordinates.

The Floquet exponents are conjugate coefficients in the linear terms of the normal forms before being multiplied by the substituted constant values equal to v_1 and v_2.

To obtain $v_3(\zeta)$ and $v_4(\zeta)$ we introduce the complex changes of variable; $v_3 = u_1 - iu_2$

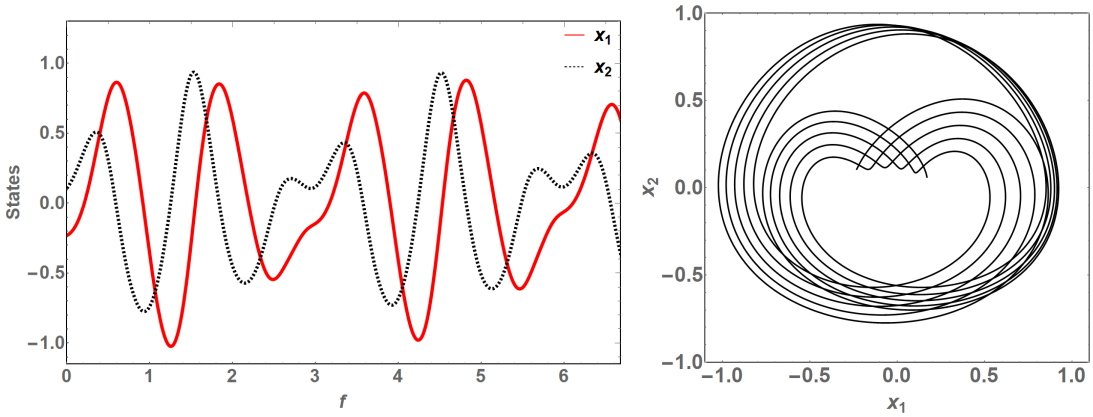

(a) Orignial Back Transformed Normalized States (b) Phase Plot

Figure 36: Dynamics of the Normalized L-F Transformed System

and $v_4 = u_1 + iu_2$ followed by the polar coordinates $u_1 = R\cos(\theta)$ and $u_2 = Rsin(\theta)$. The last two equations in (3.33) becomes,

$$\left.\begin{aligned} \mathring{R} &= -0.0106945R, \\ \mathring{\theta} &= 2.12186 + 0.0005599R^2. \end{aligned}\right\} \tag{4.27}$$

Results from the easier to solve equation (4.27) are then used to obtain the closed form analytical solutions to equation (3.33). Then, $[v_1(\zeta)\ \ v_2(\zeta)\ \ v_3(\zeta)\ \ v_4(\zeta)]^T$ are then back-transformed to the original coordinates producing the uncontrolled motion shown in figure 36. The system response in figure 36 (with nonzero initial conditions) is a cognate approximation of the originally obtained numerical integration solution in figure 24. The back transformed augmented states are similarly shown in figure 37 corresponding to equation (3.27) where the amplitude of $q(\zeta)$ is 2π times that of p.

The normal form in equation (3.33) verifies that this is a system undergoing a codimension one Hopf Bifurcation. To synthesize a bifurcation control law, a control input

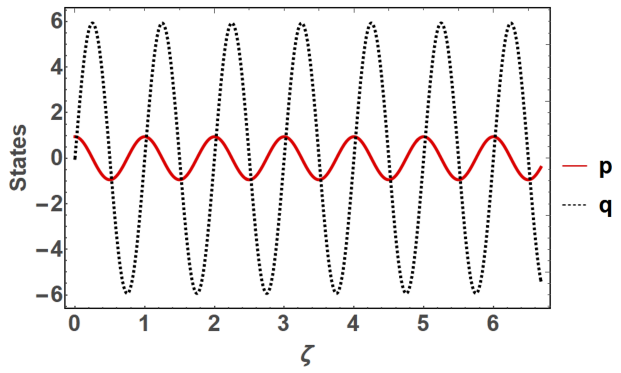

Figure 37: Back Transformed Normalized Augmented States

is added to equation (3.33) as below,

$$\begin{bmatrix} \mathring{v}_1 \\ \mathring{v}_2 \\ \mathring{v}_3 \\ \mathring{v}_4 \end{bmatrix} = \begin{bmatrix} 0 & 0 & 0 & 0 \\ 0 & 0 & 0 & 0 \\ 0 & 0 & -0.0106945 - i2.12186 & 0 \\ 0 & 0 & 0 & -0.0106945 + i2.12186 \end{bmatrix} \begin{bmatrix} v_1 \\ v_2 \\ v_3 \\ v_4 \end{bmatrix} + \begin{bmatrix} 0 \\ 0 \\ -i0.0005599 v_3^2 v_4 \\ i0.0005599 v_3 v_4^2 \end{bmatrix} + \boldsymbol{G_5 u}. \tag{4.28}$$

Let the scaling matrix and control input be of the form,

$$\boldsymbol{G_5} = \begin{bmatrix} 0 & 0 & 0 & 0 \\ 0 & 0 & 0 & 0 \\ 0 & 0 & 1 & 0 \\ 0 & 0 & 0 & 1 \end{bmatrix}, \quad \boldsymbol{u} = \gamma_2 \begin{bmatrix} 0 \\ 0 \\ K_1 v_3^2 v_4 \\ K_2 v_3 v_4^2 \end{bmatrix}. \tag{4.29}$$

The proportional gains are custom-tuned to $K_1 = K_2 = -2$ and $\gamma_2 = 1$. Figure 38 shows dynamic behavior of the implemented bifurcation control in original coordinates with nonzero initial conditions.

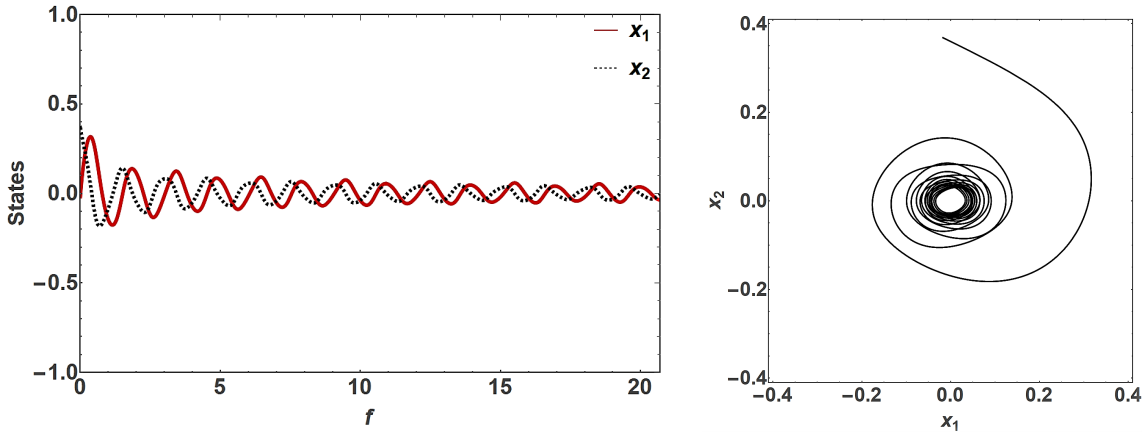

(a) x_1 and x_2 Response (b) Phase Plot

Figure 38: State Response of the Bifurcation Controlled L-F Transformed System

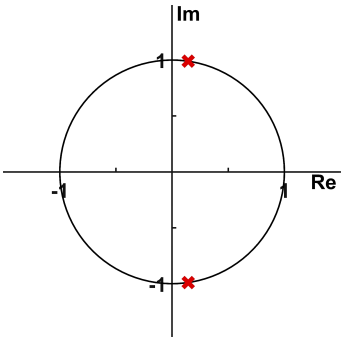

Figure 39: Preserved Locations of Floquet Multipliers After Bifurcation Control

The oscillating amplitude of the quasi-periodic pitch angle motion is tremendously stabilized relative to the initial behavior illustrated in figure 36. This hence demonstrates successful control of the post bifurcation attitude dynamics about the spacecraft center of mass.

Bifurcation control is a nonlinear control technique that affects the behavior of the closed loop system by modifying nonlinearity and post bifurcation behavior. Therefore, the location of Floquet multipliers (exponents) is generally preserved post bifurcation control. Figure 39 shows the preserved locations of the Floquet multipliers before and after

bifurcation control ($e = 0.1$ and $\sigma = 0.2$). This location of Floquet multipliers is consistent with the limit cycle shown in figure 38(b) corresponding to a simply stable system with relatively subdued librations.

4.4 Summary and Discussion

In this chapter we demonstrated that the quasi-periodic, nonlinear planar pitch attitude motion is challenging to control.

The synthesized linear controller served as starting point for developing more adept control laws. Not surprisingly, the linear controller failed to stabilize the nonlinear motion with periodic coefficients and external periodic excitation. As stated, in general the 'region of application' of linear control for nonlinear systems is dependent on magnitude of nonlinearity and initial conditions. Many times, linear control may stabilize nonlinear systems locally, but this is not guaranteed.

On-orbit perturbations cause disturbing torques that bifurcate the attitude motion, it is hence imperative to stabilize the system attitude dynamics in the small neighborhood of the bifurcation parameter's critical-point. Local nonlinear bifurcation control law implemented on the attitude motion undergoing a Hopf bifurcation was shown to stabilize the attitude motion. The bifurcation controller which modifies the nonlinearity and post bifurcation behavior–further prevents the attitude motion from becoming chaotic because bifurcation is the path to chaos. Implemented in the TINF, the bifurcation control law would subsequently stabilize the secular and periodic attitude perturbations experienced by a spacecraft in elliptical orbit about its nominal operating point.

Sliding mode control law was based on driving both system states to zero on the sliding

surface when the sliding surface reference error is equal to zero. The SMC law was similarly shown to be successful by invariably restricting the pitch angle to zero.

The numerical and symbolic computation techniques employed in this investigation are resource intensive. For instance, despite utilizing computer workstations possessing 8^{th} generation Intel™ CPU and up to $48GB$ RAM; extensively protracted code running times were frequently observed.

Part II

SPACECRAFT DYNAMICS IN THE VICINITY OF IRREGULARLY SHAPED SMALL BODIES

(This page is intentionally left blank.)

Chapter 5

MOTION IN THE VICINITY OF IRREGULARLY SHAPED SMALL BODIES

In this investigation, irregularly shaped small bodies (ISSB) refers to celestial objects that cannot be classified as planets (or moons) due to their relatively diminished size and are asymmetrically formed. Examples of such objects include asteroids, comets, and other relatively small objects in space. Correspondingly, ISSB often pose an incomparable challenge to seamlessly model and analyze motion in their vicinity using point mass Keplerian and Newtonian principles that are traditionally applied in the vicinity of large objects e.g. planets. This is because, due to their irregular shape, ISSB are characterized by uncertainty in mass and orbital parameters, weak gravitational forces, strong susceptibility to 3^{rd}-body and solar radiation pressure perturbations, etc [18], [63], [112], [113]. Therefore, to accurately describe the dynamical environment in the vicinity of ISSB, we require the development of adaptable analytical models that accurately portray the irregularities of the body's total mass distributions in terms of the corresponding gravitational potential. Then, we may characterize the motion in the vicinity of ISSB as Newtonian between a larger arbitrarily shaped body (with distributed mass) and a massless particle (i.e. spacecraft) interacting with the former's irregular gravity field.

Therefore, it is essential to develop accurate models that represent the gravitational attraction of a larger body with an arbitrarily distributed mass on a single point mass object. To this end, three common classifications of approaches to model gravitational potential of irregularly shaped bodies are i) spherical harmonics models, ii) closed-form gravitational potentials, and iii) other gravity field representations [63]. The closed-form models encompass gravitational potential models based on ellipsoidal and polyhedron shapes.

The third category brings together techniques that employ methods such as point mass-concentrations and logarithmic potential. These different approaches have varying merits and drawbacks that depend on the intended application context. Some offer a good initial model for analysis but have a low fidelity; while others may be more accurate but are computationally intensive and so on. In the next section, we shall briefly examine the various common techniques for modeling gravitational potential.

5.1 Gravitational Potential Models

Briefly, according to the theory of potential [114], [115], the potential function V is a scalar function of position whose derivatives are components of a vector i.e. attraction of the body. The potential function V for the effect of several particles conglomerated to form a continuous body of variable density ρ can be integrated over the body as,

$$V = G \int_B \frac{1}{\rho} dm, \tag{5.1}$$

where G is the gravitational constant and dm is the differential mass. The potential can further be expressed in terms of components of attractions along the three Cartesian axes. These components of attraction can be obtained by differentiating V with respect to x,y,z and hence can similarly be defined by triple integrals. The significance of the potential function is outlined in the following expression;

Amount of work done in moving from one point to another against an attracting force = Difference in the value of potential function at these two points.

A key property of the potential function is satisfaction of the Laplacian property at all exterior points, i.e.,

$$\nabla^2 V = 0. \tag{5.2}$$

Further, the main characteristics properties of a potential functional are;

- V is continuous throughout all space.
- The first derivatives of V exist and are continuous everywhere except on a given surface S on which there maybe a surface distribution of matter.
- On the exterior of S, $\nabla^2 V = 0$.
- On the exterior of S, $\nabla^2 V$ is arbitrary.
- V vanishes at infinity.

Having described and outlined the main properties of the potential function in general, we can now examine how the gravitational potential of an irregularly shaped bodies can be modeled using various techniques to facilitate investigation of dynamics in the vicinity of such objects.

5.1.1 Spherical Harmonics Models

To model the gravity field of an arbitrary body, the classical approach considers the body as a collection of particles (differential elements). Consequently the gravitational force acting on a point mass located external to the body due to a particular differential mass element in the body can be derived using inverse square law between the two particles. To obtain the net force due to all the mass elements is then evaluated by integrating over the body's total mass distribution. However, due to uncertainties in the knowledge of the irregularly shaped body parameters including the total mass, it is hence reasonable to expand the gravitational potential into harmonic series. The derivation of gravitational potential model based on spherical harmonics expansion is well documented in literature e.g. [63], [114]–[118]. Therefore, here we shall briefly outline the main aspects of this derivation.

The solution to Laplace's equation corresponding to the total mass distribution of a

body is essentially the gravitational potential. Solving the Laplace's equation using separation of variables in terms of spherical coordinates gives the general form of spherical harmonic gravitational potential as shown below,

$$U(r,\delta,\lambda) = \frac{\mu}{r}\sum_{l=0}^{\infty}\sum_{m=0}^{l}\left(\frac{r_o}{r}\right)P_{lm}(\sin\delta)[C_{lm}\cos m\lambda + S_{lm}\sin m\lambda], \tag{5.3}$$

where the spherical coordinates corresponding to a positional vector $\boldsymbol{r} = x\hat{\boldsymbol{x}} + y\hat{\boldsymbol{y}} + z\hat{\boldsymbol{z}}$ are given by $\sin\delta = {}^{z}/_{r}$ and $\tan\lambda = {}^{y}/_{x}$. Here, $\mu = GM$, δ is the latitude and λ is the longitude, μ is the body's gravitational parameter, r_o is the normalizing radius (normally selected as mean radius or maximum radius of the object), P_{lm} are the Associated Legendre Functions, and C_{lm} and S_{lm} are called the gravity field harmonic coefficients (or Stokes coefficients). These coefficients encode information about the mass distribution of the extended body. Further, the Associated Legendre Functions can be defined by the closed form relationship below,

$$P_{lm}(\sin\delta) = \cos^{m}\delta \sum_{i=0}^{\text{int}[(l-m)/2]} T_{lmi}\sin^{l-m-2i}\delta. \tag{5.4}$$

$$T_{lmi} = \frac{(-1)^{i}(2l-2i)!}{2^{l}i!(l-i)!(l-m-2i)!}, \tag{5.5}$$

where the int$[x]$ function returns the integer part of x. Spherical harmonic expansion functions are orthogonal, therefore, the gravity coefficients C_{lm} and S_{lm} can be computed if a mass distribution is given. If the density of the body is specified at each point as $\sigma(\boldsymbol{\rho})$, then the we find the gravity coefficients from the integrals below,

$$(C,S)_{lm} = \frac{(2-\delta_{m}^{0})}{M}\frac{(l-m)!}{(n+m)!}\int_{B}\left(\frac{r}{r_o}\right)P_{lm}(\sin\delta)\text{cs}(m\lambda)\sigma dv. \tag{5.6}$$

$$\sigma dv = \sigma(r,\delta,\lambda)r^{2}\cos\delta dr d\delta d\lambda, \tag{5.7}$$

where cs denotes the cosine or sine function for computation of the C_{lm} or S_{lm} gravity coefficient, respectively. If the body has a constant density, then one integration can be

performed over the radius and the above formula reduces to,

$$(C,S)_{lm} = \frac{\sigma(2-\delta_m^0)}{M}\frac{(l-m)!}{(n+m)!}\int_S \frac{R^3(\delta,\lambda)}{l+3}\left(\frac{R(\delta,\lambda)}{r_o}\right)^l P_{lm}(\sin\delta)\mathrm{cs}(m\lambda)\cos\delta d\delta d\lambda, \tag{5.8}$$

where the radius $R(\delta,\lambda)$ becomes a function of the latitude and longitude and defines the shape of the body.

5.1.1.1 Types of Spherical Harmonics

The spherical harmonic model in equation (5.3) describes the gravity field of a body via a potential function consisting of spherical harmonics functions of various degrees and order. The individual terms in the summation uniquely contribute to the gravity representation of the body and correspond to a spherical harmonic of a given degree, l and order, m. Consequently, the effect of a given harmonic is directly dependent on the degree and order of the harmonic term. Spherical harmonics can be visualized and classified by associating zeros to each spherical harmonics and corresponding Legendre polynomials i.e. $P_{l,m} = 0$. Solutions of this equation define lines that divide the reference spherical shape into different regions depending on the degree and order of the harmonic. Ultimately, the regions contribute to the total gravitational potential depending on their mass properties and location. Three types of spherical harmonics are then obtained as follows;

a. $l,\ m = 0$ (zonal harmonics)
b. $l \neq m$ (tesseral harmonics)
c. $l = m$ (sectoral harmonics)

Illustrative examples of different types of spherical harmonics are shown in the figure 40.

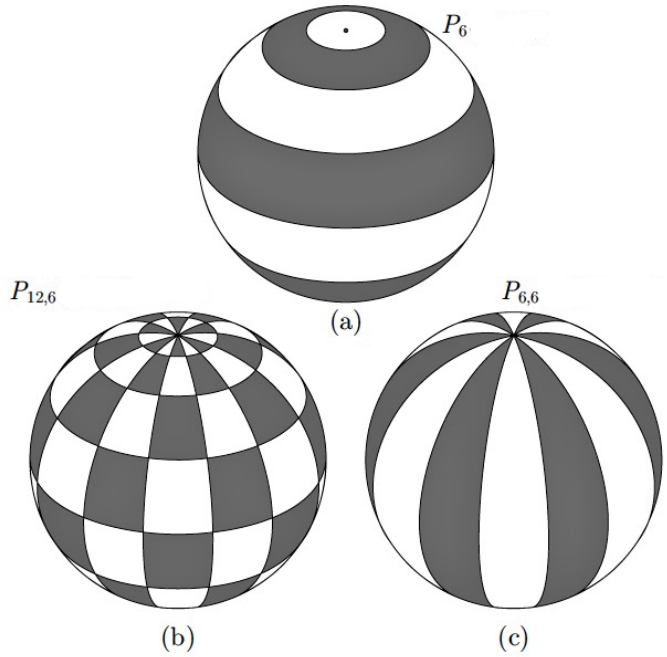

Figure 40: Types of Spherical Harmonics: (a) Zonal, (b) Tesseral, and (c) Sectorial (Courtesy MathWorks ®)

5.1.1.2 A Simple Harmonic Model

Understood relationships exist between gravity coefficients of all degrees and orders and the high order mass distribution moments of arbitrary bodies. Out of these relationships, those of up to degree and order two are of most interest. The first degree and order gravity coefficients are related to the body center of mass. When the origin of the body-fixed reference frame of a body is defined to coincide with the COM of the body; the first degree and order terms are rendered identically zero, $C_{11} = S_{11} = C_{10} = 0$. Therefore this implies that the first term beyond the spherical attraction of the body emanate at the second degree and order. We note that if a body has constant density distribution, then the COM and center of figure of a body will coincide. The second degree and order gravity

coefficients are related to the moments of inertia of the body as shown below, [63];

$$I_{xx} - I_{yy} = -4Mr_o^2 C_{22}, \tag{5.9}$$

$$I_{yy} - I_{zz} = Mr_o^2(C_{20} + C_{22}), \tag{5.10}$$

$$I_{zz} - I_{xx} = -Mr_o^2(C_{20} - C_{22}), \tag{5.11}$$

$$I_{xy} = -2Mr_o^2 S_{22}, \tag{5.12}$$

$$I_{yz} = -Mr_o^2 S_{21}, \tag{5.13}$$

$$I_{zx} = -Mr_o^2 C_{21}. \tag{5.14}$$

The above results are independent of internal density heterogeneity. The moments of inertia can thus be only defined as differences between the second degree and order gravity coefficients. However, the data obtained by observing small bodies cannot reveal the full moments of inertia exposing a main drawback in application of this gravitational potential model. Further, it is always possible to define a set of coordinates such that the products of inertia ($I_{xy},\ I_{yz},\ I_{zx}$) equal zero. Therefore, it is also possible to define a coordinate frame where the following second degree and order gravity coefficients $S_{22} = S_{21} = C_{21} = 0$ as well. Hence, the second degree and order gravity field can be reduced to the two gravity coefficients C_{20} and C_{22}. Consequently, in space missions to small irregularly shaped bodies, the gravity field is estimated by initially choosing the small body-fixed coordinate reference frame to be nominally aligned with the constant density principal axis.

Therefore, the simplest form of gravitational potential starts at the second degree and order with only the coefficients C_{20} and C_{22}, (N.B. In literature, C_{20} is the often referred to as " $-J_2$"). Finally, the simplest, non-trivial gravity field for studying dynamics in the vicinity of a body is hence,

$$U = \frac{\mu}{r}\left[1 + \left(\frac{r_o}{r}\right)^2 \left\{C_{20}\left(1 - \frac{3}{2}\cos^2\delta\right) + 3C_{22}\cos^2\delta\cos(2\lambda)\right\}\right]. \tag{5.15}$$

Further, previous studies have established second degree and order gravity accounts for the most disturbances on the dynamical system further highlighting the significance of this model.

The spherical harmonic approach is however susceptible to a number of drawbacks. Key among them include;

- Many small irregularly shaped bodies are characterized by elongated, non-spherical and extensively cratered shapes. Consequently, representation of the corresponding gravity field for such bodies by conventional spherical harmonic expansion techniques requires high degree and order expansions which are very difficult to obtain [119]. Moreover, the quantities in spherical harmonic models have a global and not a local scope–incorporating a unique surface feature will generally affect every coefficient.
- Lack of explicit expression of the mass distribution inside a small body makes it very difficult to directly derive by integration the C_{lm} or S_{lm} gravity coefficients. Consequently, since these coefficients are central to gravity field modeling, they are normally estimated via inversion from flight data and approximation involving the body's shape and density.
- The spherical harmonic approach assumes that series converge to the true gravity field. Consequently, when considering the gravitational potential close to a small irregularly shaped body, then the spherical harmonics are not accurate. Specifically, the spherical series is divergence is severe within the circumscribing sphere of the body (Brillouin sphere) rendering the gravitational potential unsuitable for dynamical analysis.

Despite the foregoing limitations, the simple second degree and order spherical harmonic gravity model converges beyond the circumscribing sphere, reasonably approxi-

mates the gravity field around ISSB. Nevertheless spherical harmonics gravitational models are very useful in undertaking preliminary low fidelity dynamical analysis in the vicinity of ISSB.

5.1.2 Ellipsoidal Harmonics Models

The ellipsoidal harmonics approach aims to improve the spherical harmonics model in approximating the irregular gravitational field by considering a constant density ellipsoid which yields exact closed form solutions up to and on the surface of the body. Equation (5.16) shows the ellipsoidal harmonic expansion of the potential at a massless point [117], [120],

$$U = \mu \sum_{l=0}^{\infty} \sum_{m=1}^{2n+l} \alpha_{lm} \frac{F_{lm}(\lambda_1)}{F_{lm}(\lambda_e)} F_{lm}(\lambda_2) F_{lm}(\lambda_3), \tag{5.16}$$

where $\lambda_1, \lambda_2, \lambda_3$ are orthogonal ellipsoidal coordinates, λ_e indicates the reference ellipsoid (or Brillouin ellipsoid), which defines the convergence domain of equation (5.16). F_{lm} are the canonical solutions to Lamé equation, which are continuous functions when $\lambda_1 \geq \lambda_e$. α_{lm} indicates ellipsoidal coefficients. The illustrative the improvements of the ellipsoidal harmonics method over the spherical harmonics method are shown in figure 41. It compares the convergence domains of these two methods about the asteroid Castalia. The reference sphere due to spherical harmonics approach in figure 41(a) excludes a large area traversed by orbits. The reference ellipsoid in figure 41(b) on the other hand envelopes Castalia's overall shape better and widens the convergence domain of the gravitational formulas.

As noted by [63], the gravitational coefficients of the ellipsoid's shape spherical harmonics expansion taken about its COM have relatively simple forms. The only non-zero

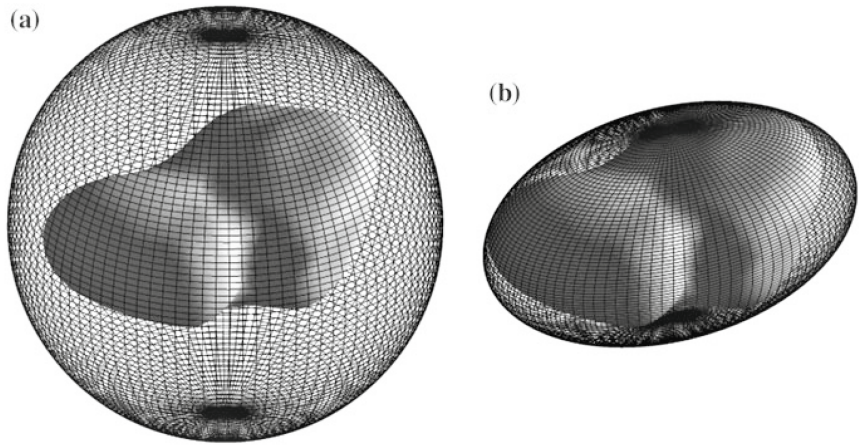

Figure 41: The Reference Sphere and Ellipsoid About Asteroid 4769 Castalia. *(a)* Reference Sphere of Spherical Harmonics. *(b)* Reference Ellipsoid of Ellipsoidal Harmonics (Courtesy: [117])

gravity coefficients are those of the form $C_{2l,2m},\ l,m = 0,1,2,\ldots$. The first few terms of the explicit formula for the ellipsoids gravity field coefficients are;

$$\left.\begin{aligned} C_{20} &= \frac{1}{5r_o^2}\left(\gamma^2 - \frac{\alpha^2+\beta^2}{2}\right), \\ C_{22} &= \frac{1}{20r_o^2}\left(\alpha^2-\beta^2\right), \\ C_{40} &= \frac{15}{7}\left(C_{20}^2 + 2C_{22}^2\right), \\ C_{42} &= \frac{5}{7}C_{20}C_{22}, \\ C_{44} &= \frac{5}{28}C_{22}, \end{aligned}\right\} \tag{5.17}$$

where $\gamma \leq \beta \leq \alpha$ are the constant density ellipsoid axes.

5.1.3 Polyhedron Models

The polyhedral method has its roots in geological modeling, its application in modeling the shape and describing the gravity potential of ISSB was mostly developed in a series

of works by Werner et al. [119], [121]. The authors derived the expressions of the gravitational potential, attraction and gradient matrix of a homogeneous (constant density) polyhedron based on dyads of the second order to describe the irregular gravitational field of a small body.

The formulation begins by assuming an arbitrary polyhedron with triangular faces, then from Euler-Descartes formula for a polyhedron with triangular faces specified by v vectors there must be $f = 2v - 4$ faces and $e = 3(v-2)$ edges. Each face is associated with a set of three vertex vectors $\boldsymbol{r}_i^f,\ i = 1, 2, 3$, s.t the three vertices taken in order are counter -clockwise about a normal to the face, $\hat{\boldsymbol{n}}_f$. Two vertices $\boldsymbol{r}_i^e,\ i = 1, 2$, and two faces, f and f' which join at the edge are associated with each edge. A unit vector $\hat{\boldsymbol{n}}_e^f$ denotes the edge normal corresponding to face f and perpendicular to the edge and to $\hat{\boldsymbol{n}}_f$ while pointing away from the center as shown in figure 42. Subsequently, the general formula for the homogeneous polyhedron is as shown below, [119].

$$U(\boldsymbol{r}) = \frac{G\sigma}{2}\left[\sum_{e\in edges} \boldsymbol{r}_e \cdot \boldsymbol{E}_e \cdot \boldsymbol{r}_e L_e - \sum_{f\in faces} \boldsymbol{r}_f \cdot \boldsymbol{F}_f \cdot \boldsymbol{r}_f \omega_f\right], \tag{5.18}$$

$$\nabla U = -G\sigma\left[\sum_{e\in edges} \boldsymbol{E}_e \cdot \boldsymbol{r}_e L_e - \sum_{f\in faces} \boldsymbol{F}_f \cdot \boldsymbol{r}_f \omega_f\right], \tag{5.19}$$

$$\nabla(\nabla U) = G\sigma\left[\sum_{e\in edges} \boldsymbol{E}_e L_e - \sum_{f\in faces} \boldsymbol{F}_f \omega_f\right], \tag{5.20}$$

where $\boldsymbol{r}_e$ is the vector from any point on the edge e to $\boldsymbol{r}$ and $\boldsymbol{r}_f$ is the vector from any point on the face f to $\boldsymbol{r}$. Also;

$$\left.\begin{aligned} \boldsymbol{E}_e &= \hat{\boldsymbol{n}}_f \hat{\boldsymbol{n}}_e^f + \hat{\boldsymbol{n}}_{f'} \hat{\boldsymbol{n}}_e^{f'}, \\ \boldsymbol{F}_f &= \hat{\boldsymbol{n}}_f \hat{\boldsymbol{n}}_f, \\ L_e &= \ln \frac{r_1^e + r_2^2 + e_e}{r_1^e + r_2^2 - e_e}, \\ \omega_f &= 2\arctan\left(\frac{\boldsymbol{r}_1^f \cdot \tilde{\boldsymbol{r}}_2^f \cdot \boldsymbol{r}_3^f}{r_1^f r_2^f r_3^f + r_1^f \boldsymbol{r}_2^f \cdot \boldsymbol{r}_3^f + r_2^f \boldsymbol{r}_3^f \cdot \boldsymbol{r}_1^f + r_3^f \boldsymbol{r}_1^f \cdot \boldsymbol{r}_2^f}\right), \end{aligned}\right\} \tag{5.21}$$

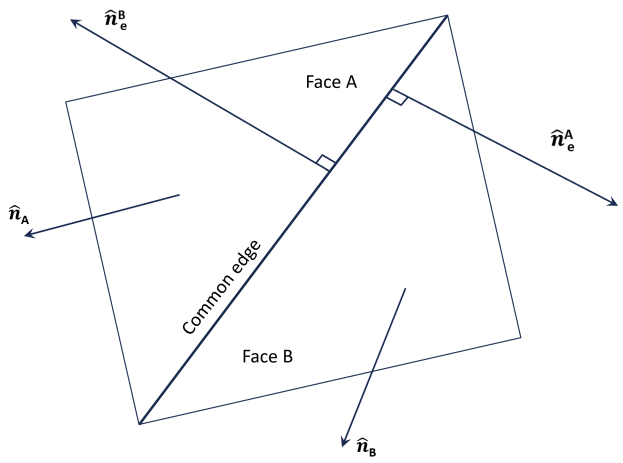

Figure 42: Polyhedron Faces Denoting the Edges, Vertices and Normal Vectors

where $e = |\boldsymbol{r}_1^e - \boldsymbol{r}_2^e|$ is the actual length of edge. The Laplacian is similarly shown to be

$$\nabla^2 U = -G\sigma \sum_{f \in faces} \omega_f, \tag{5.22}$$

where ω_f denotes the signed area of the face f projected onto the unit sphere centered at the point $\boldsymbol{r}$. Thus, the total signed projection equals 0 when the point is outside of the body and it equals 4π when inside the body satisfying the Laplace and Poisson equations. Consequently, the potential and partials can be used to compute the gravitational field down to and on the surface.

There are several advantages of the polyhedral method. Firstly, the closed forms of the polyhedral method avoid truncation errors during computation and gives exact gravitational potential for a given shape and density. This gravitational potential is valid from infinity to the surface of the body meaning that there is no region of divergence. The resolution of the calculated field however depends on the level of discretization chosen for a given shape. This method enables a quick and convenient judgment of whether a point has entered the interior of a polyhedron. The quantities that parameterize the potential expression (and acceleration) are local in scope. Consequently, incorporating a surface

feature only affects faces in the vicinity unlike harmonic expansion methods whose quantities have a global in scope. Notably, the polyhedron model is still an approximation of the actual shape of the body and the gravity field accuracy is consistent with the shape determination.

5.1.4 Other Gravity Field Representations

As described by [63], numerous other methods of approximating the gravitational potential of an arbitrary body employ a collection of simple closed-form potential solutions that collectively mimic the gravity field of an actual body. One such approach fills the the irregularly shaped body with point masses ('mascons'–mass concentrations) on an evenly spaced grid. The total mass of the body is realized by the collective combination of the individually assigned masses. Similar to the harmonics approach, the mascon approach does not provide information whether the point is inside or outside the body. Though the mascon approach does not diverge, the number of individual mascons become arbitrarily large and there are force computation is prone to significant errors. The mascon approach is also less accurate than the harmonic approach for a given computational effort in its region of convergence [121]. Also because this approach models the gravitational field of "cube" of material as a "sphere", systematic errors are hence introduced because the two shapes have demonstratively different gravity fields when in close proximity.

The use of logarithmic potential is also another approach to model the gravitational potential of ISSB. The logarithmic potential is the gravitational potential of a line element with with linear density [122]. Natural logarithms are used to obtain a simple closed-form of these potentials that collectively mimic the gravitational potential of ISSB when point

masses are incorporated. Since this methodology is yet to fully mature, its use in practical scenarios is limited.

5.2 Dynamical Model Development

To effectively study the general motion of a spacecraft about a small body, we require at least the specification of the body's gravitational field, U, its rotational dynamics and the perturbing environment regime. We first consider the spacecraft motion in close proximity to the body where other perturbations (i.e. solar gravity and radiation) are small compared to the gravitational attraction of the central body. Dynamics of such a system are then analyzed by transforming them to a body-fixed coordinate frame which introduces the angular velocity of the small body, $\boldsymbol{\omega}_T$ relative to the inertial reference frame. Making the assumption that the small body experiences torque-free motion, then, the fundamental classical equation of motion near a rotating small body expressed in 3-dimensional Euclidean space as,

$$\ddot{\boldsymbol{r}} + 2\boldsymbol{\omega}_T \times \dot{\boldsymbol{r}} + \boldsymbol{\omega}_T \times (\boldsymbol{\omega}_T \times \boldsymbol{r}) + \dot{\boldsymbol{\omega}}_T \times \boldsymbol{r} + \frac{\partial U(\boldsymbol{r})}{\partial \boldsymbol{r}} = 0, \tag{5.23}$$

where $\boldsymbol{r}$ is the radius vector from the small body's COM to the spacecraft's position in the rotating body-fixed frame. The time derivatives are taken with respect to the rotating frame leading to the inclusion of Coriolis and centripetal accelerations. $U(\boldsymbol{r})$ is the gravitational potential of the small body. Two general cases normally occur for these systems, *i)* The angular velocity is vector is time-periodic in the body-frame and hence the term, $\dot{\boldsymbol{\omega}}_T \neq 0$. In this case, the small body is in an arbitrary rotation state, tumbling in inertial space and following the torque-free solution. *ii)* The angular velocity vector is consonant, $\dot{\boldsymbol{\omega}}_T = 0$ and the equations of motion in the body-frame become time-invariant. This is

the common case where the small body is uniformly rotating about its maximum moment of inertia [63], [66], [71], [117], [123], [124].

When the body is rotating at a uniform angular velocity (i.e. $\dot{\boldsymbol{\omega}}_T = 0$), the dynamical system has a conserved Jacobi integral given by, [63], [112], [125] expressed as,

$$J = \frac{1}{2}\ddot{\boldsymbol{r}} \cdot \ddot{\boldsymbol{r}} - \frac{1}{2}(\boldsymbol{\omega}_T \times \boldsymbol{r}) \cdot \boldsymbol{\omega}_T \times \boldsymbol{r} + \boldsymbol{U}(r). \tag{5.24}$$

Existence of the Jacobi integral allows zero-velocity regions to be defined and applied to establish stability of the motion. Also, it implies the existence of equilibrium points and dense periodic orbits in the phase space.

In the special body-fixed frame, the dynamical equation (5.23) in component form is expressed as,

$$\left.\begin{aligned} &\ddot{x} - \dot{\omega}_T y - 2\omega_T \dot{y} - \omega_T^2 x + \frac{\partial U}{\partial x} = 0, \\ &\ddot{y} + \dot{\omega}_T x + 2\omega_T \dot{x} - \omega_T^2 y + \frac{\partial U}{\partial y} = 0, \\ &\ddot{z} + \frac{\partial U}{\partial z} = 0. \end{aligned}\right\} \tag{5.25}$$

The effective potential is independent of z and is related only to the position of the spacecraft in the body-fixed frame as shown in the equation below.

$$V = U - \frac{\omega_T^2}{2}(x^2 + y^2). \tag{5.26}$$

Similarly, the Jacobi integral reduces to,

$$J = U + \frac{1}{2}(\dot{x}^2 + \dot{y}^2 + \dot{z}^2) - \frac{\omega_T^2}{2}(x^2 + y^2). \tag{5.27}$$

Using the effective potential, the component form of the dynamical equation (5.25) becomes

$$\left.\begin{aligned} &\ddot{x} - \dot{\omega}_T y - 2\omega_T \dot{y} + \frac{\partial V}{\partial x} = 0, \\ &\ddot{y} + \dot{\omega}_T x + 2\omega_T \dot{x} + \frac{\partial V}{\partial y} = 0, \\ &\ddot{z} + \frac{\partial V}{\partial z} = 0. \end{aligned}\right\} \tag{5.28}$$

As discussed in section 5.1.1, the second degree and order gravitational potential is employed as the simplest non-trivial gravity field for studying dynamics in the vicinity of ISSB. To facilitate this formulation, the initial analysis and design of space missions to small bodies usually assumes that the COM and center of figure will coincide since the body is assumed to have a constant mass distribution. Subsequently, close proximity observation data will verify any existence of the first degree and order gravity coefficients.

The second degree and order gravitational potential given in in equation (5.15) can be expressed in Cartesian coordinates using the following transformations,

$$\left.\begin{aligned} x &= r\cos\lambda\cos\delta, \\ y &= r\sin\lambda\cos\delta, \\ z &= r\sin\delta. \end{aligned}\right\} \tag{5.29}$$

Therefore, in Cartesian coordinates, the second degree order gravitational potential becomes,

$$U = -\frac{\mu C_{20}(x^2+y^2-2z^2)}{2r^5} + \frac{3\mu C_{22}(x^2-y^2)}{r^5}, \tag{5.30}$$

where $r = \sqrt{x^2+y^2+z^2}$ i.e $\|r\|$. For definiteness, we shall specify the a body-fixed reference frame such that $I_{xx} \leq I_{yy} \leq I_{zz}$ with axes x, y and z. The second degree order gravitational coefficients will are directly related to the principal moments of inertia of the body (normalized by the body mass) [124], i.e.,

$$\left.\begin{aligned} C_{20} &= -\frac{1}{2}(2I_{zz} - I_{xx} - I_{yy}), \\ C_{22} &= \frac{1}{4}(I_{yy} - I_{xx}). \end{aligned}\right\} \tag{5.31}$$

The gravity coefficients as given here have units of distance squared. If we define a mass-distribution parameter as,

$$\hat{\sigma} = \frac{I_{yy} - I_{xx}}{I_{zz} - I_{xx}} = -\frac{4C_{22}}{C_{20} - 2C_{22}}, \tag{5.32}$$

where $0 \leq \hat{\sigma} \leq 1$ for any mass distribution. When $\hat{\sigma} = 0$, the body has a rotational symmetry about the z-axis ($I_{yy} = I_{xx}$). A value of $\hat{\sigma} = 1$ denotes a body with rotational symmetry about the x-axis ($I_{yy} = I_{zz}$). We can express the gravitational coefficients in terms of this parameter as,

$$\left.\begin{aligned} C_{20} &= -\frac{1}{2}(I_{zz} - I_{xx})(2 - \hat{\sigma}), \\ C_{22} &= \frac{1}{4}(I_{zz} - I_{xx})\hat{\sigma}. \end{aligned}\right\} \tag{5.33}$$

5.3 Motion Analysis: A case for Asteroid 4179 Toutatis

To comprehensively investigate dynamics in the vicinity of ISSB, we shall consider a more challenging case of equation (5.23) where the angular velocity is vector is time-periodic in the body-frame i.e. $\dot{\boldsymbol{\omega}}_T \neq 0$. In this case, the small body is in an arbitrary rotation state, tumbling in inertial space and following the torque-free solution. As previously stated, the Jacobi integral is not preserved in this case and hence zero-velocity regions cannot be defined and applied to establish stability of the motion. Further, the existence of equilibrium points and dense periodic orbits in the phase space are difficult to predict. The dynamical nonlinear system describing this motion will hence be parametrically excited and further subjected to external periodic excitation in the form of perturbing accelerations. The variable angular velocity in the body-fixed coordinate frame can generally be modeled as a periodic quantity with a period $\tilde{T} = \dfrac{2\pi}{\omega_T}$, and with a mean value lying between the maximum and minimum amplitude peaks as illustrated in the figure below.

Let

$$\left.\begin{aligned} \omega_T &= \omega_o + \omega_\delta \sin(\omega_o t), \\ \dot{\omega}_T &= \omega_o \omega_\delta \cos(\omega_o t), \end{aligned}\right\} \tag{5.34}$$

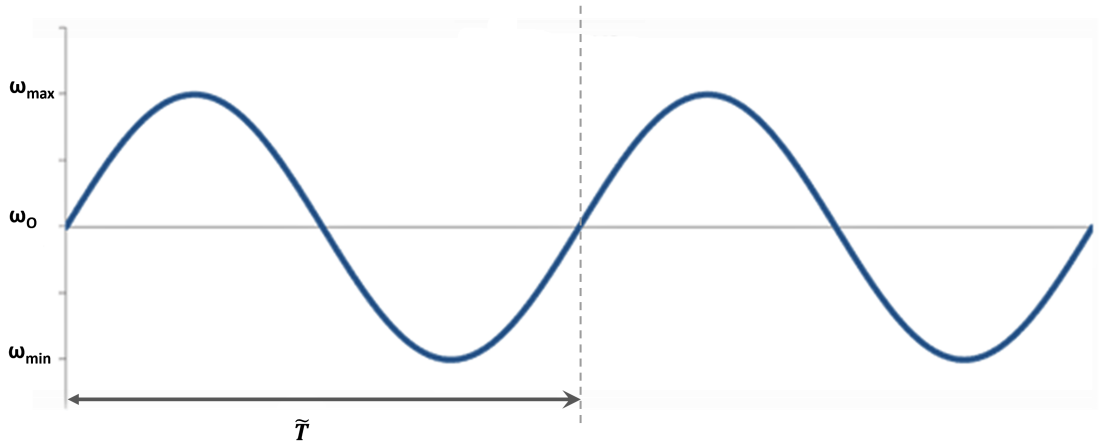

Figure 43: Periodic Variation of the Small Body Angular Velocity

where ω_o is the mean value of ω_T, and

$$\left.\begin{aligned} \omega_o &= \frac{\omega_{max} + \omega_{min}}{2}, \\ \omega_\delta &= \frac{\omega_{max} - \omega_{min}}{2}, \\ \omega_T &= \frac{2\pi}{\tilde{T}}. \end{aligned}\right\} \tag{5.35}$$

We can similarly represent the periodic perturbations as,

$$\boldsymbol{F}(t) = \boldsymbol{B} \sin \boldsymbol{\omega_\rho} t, \tag{5.36}$$

where $\boldsymbol{B}$ the vector of the amplitude of the perturbing accelerations and $\boldsymbol{\omega}_p$ is the perturbation frequency vector.

Because the actual motion analysis involves very small values of frequency and time compared to the other quantities like gravitational parameters, mass etc., we introduce a time scaling in our analysis as shown below,

$$\tau = \omega_s t. \tag{5.37}$$

Therefore, $\dfrac{d\tau}{dt} = \omega_s,$ and if we denote $(\cdot)' = \dfrac{d(\cdot)}{d\tau},$ then,

$$\dot{x} = \frac{dx}{dt} = \frac{dx}{d\tau}\frac{d\tau}{dt} = x'\omega_s, \tag{5.38}$$

and the second derivative will be

$$\ddot{x} = x''\omega_s^2. \tag{5.39}$$

We can similarly represent the second derivatives of y and z with respect to the scaled time as $\ddot{y} = y''\omega_s^2$ and $\ddot{z} = z''\omega_s^2$ receptively.

The small body angular velocity and its derivative given in equation (5.34) can be represented with respect to the scaled time, $\tau = \omega_s t$ as,

$$\left.\begin{aligned} \omega_\tau &= \omega_o + \omega_\delta \sin(\omega_o/\omega_s \tau), \\ \omega'_\tau &= (\omega_o/\omega_s)\, \omega_\delta \cos(\omega_o/\omega_s \tau). \end{aligned}\right\} \tag{5.40}$$

Subsequently, to describe the motion about the ISSB in the most complete sense, we substitute equations (5.39) and (5.40) into equation (5.28) then include the periodic perturbing accelerations given in equation (5.36). We then denote $x = x_1,\ x'_1 = x_2,$ and so forth to obtain the state space system below,

$$\begin{bmatrix} x'_1 \\ x'_2 \\ y'_1 \\ y'_2 \\ z'_1 \\ z'_2 \end{bmatrix} = \frac{1}{\omega_s^2} \begin{bmatrix} 0 & 1 & 0 & 0 & 0 & 0 \\ 0 & 0 & \omega'_\tau & 2\omega_\tau\omega_s & 0 & 0 \\ 0 & 0 & 1 & 0 & 0 & 0 \\ \omega'_\tau & -2\omega_\tau\omega_s & 0 & 0 & 0 & 0 \\ 0 & 0 & 0 & 0 & 0 & 0 \\ 0 & 0 & 0 & 0 & 0 & 0 \end{bmatrix} \begin{bmatrix} x_1 \\ x_2 \\ y_1 \\ y_2 \\ z_1 \\ z_2 \end{bmatrix} - \begin{bmatrix} 0 \\ \partial V/\partial x \\ 0 \\ \partial V/\partial y \\ 0 \\ \partial V/\partial z \end{bmatrix} + \begin{bmatrix} 0 \\ B_x \sin(\omega_\rho t) \\ 0 \\ B_y \sin(\omega_\rho t) \\ 0 \\ B_z \sin(\omega_\rho t) \end{bmatrix}, \tag{5.41}$$

where $B_{x,y,z}$ are the disturbance amplitude components along the x, y and z axes respectively. ω_τ and ω'_τ are as shown in equation (5.40). The effective potential components are evaluated as shown in equation (5.26) to obtain,

$$\left.\begin{aligned} \frac{\partial V}{\partial x} &= \omega_\tau^2 x + \frac{\partial U}{\partial x}, \\ \frac{\partial V}{\partial y} &= \omega_\tau^2 y + \frac{\partial U}{\partial x}, \\ \frac{\partial V}{\partial z} &= \frac{\partial U}{\partial z}, \end{aligned}\right\} \tag{5.42}$$

where the first-order partial derivatives of the second degree and order gravitational potential (equation (5.30)) are;

$$\frac{\partial U}{\partial x} = -\frac{C_{20}x}{r^5} - \frac{5C_{20}x(x^2+y^2-2z^2)}{2r^7} + \frac{6C_{22}x}{r^5} - \frac{15C_{22}x(x^2-y^2)}{r^7}, \tag{5.43}$$

$$\frac{\partial U}{\partial y} = -\frac{C_{20}y}{r^5} + \frac{5C_{20}y(x^2+y^2-2z^2)}{2r^7} + \frac{6C_{22}y}{r^5} - \frac{15C_{22}y(x^2-y^2)}{r^7}, \tag{5.44}$$

$$\frac{\partial U}{\partial z} = \frac{C_{20}z}{r^5} + \frac{5C_{20}z(x^2+y^2-2z^2)}{2r^7} - \frac{15C_{22}z(x^2-y^2)}{r^7}. \tag{5.45}$$

Note that C_{20} and C_{22} will generally be small with respect to unity.

To demonstrate motion analysis in the vicinity of a small body with a variable spin rate about a given principle axis, we shall consider dynamics in the vicinity of the asteroid 4179 Toutatis. Toutatis is complex rotator with non-uniform angular velocity hence it is a suitable application case for the equations we have developed above. The asteroid is in a tumbling long-axis mode and hence we assume that body will follow torque free rigid body dynamics. Toutatis physical model and orbital parameters have been studied and presented in several publications such as [65], [126]–[128].

Toutatis is a near-earth asteroid about 4.5 km long and close to a 4:1 orbital resonance with earth. Since its discovery in 1989, it has made six close earth flybys [128]. Table 2 summarizes Toutatis orbital parameters while Toutatis orbit around the sun is shown in figure 44.

According to [65], the composition of Toutatis is either homogeneous or its inhomogeneities mimic the inertia tensor of a homogeneous body. Hence we shall likewise assume that Toutatis is homogeneous with a density of $2.5\, g/cc$. Our body fixed coordinate frame will originate at the Toutatis model centroid. The axes (x, y, z) will correspond to the principal axes of smallest, intermediate and largest moment of inertia respectively as shown in figure 45. Toutatis fits into a bounding cuboid of dimensions $-2.516 \leq x \leq 2.086$,

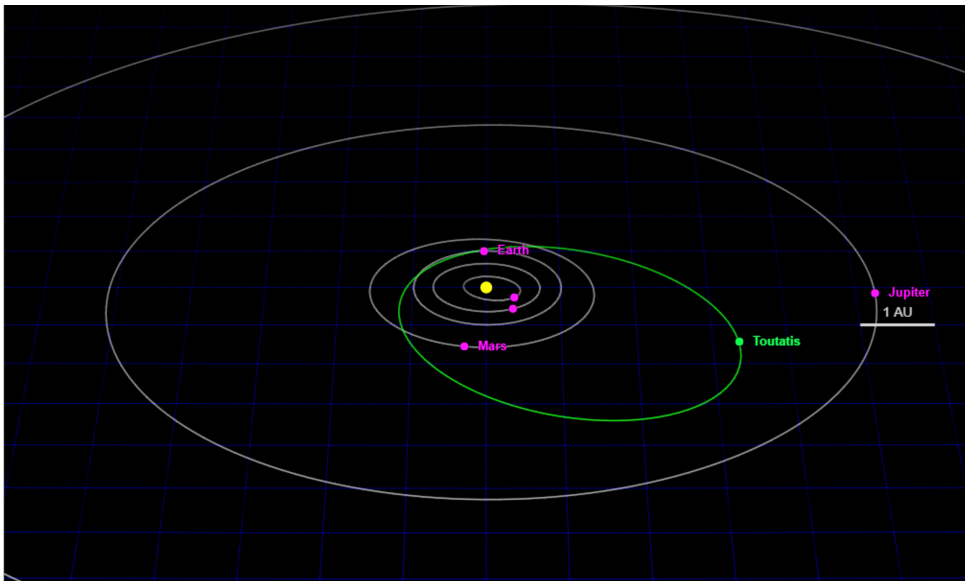

Figure 44: Toutatis Orbit Around the Sun (Courtesy Dominic Ford)

Table 2: Toutatis Orbital Parameters (Courtesy NASA-JPL)

	Epoch 26-Apr-2019
Apoapsis	4.1355 AU
Periapsis	0.9509 AU
Semi-major axis	2.5432 AU
Eccentricity	0.6260903
Inclination	0.4478^o
Longitude of asc. node	125.19^o
Argument of periapsis	278.08^o
Orbital period	4.056 years
Avg. orbital speed	16.69 $^{km}/_{s}$

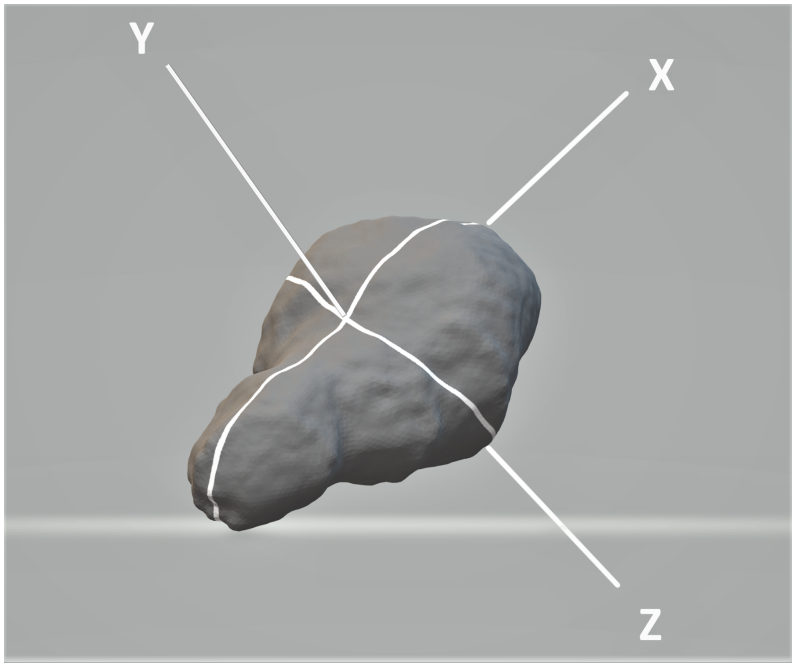

Figure 45: Toutatis Shape and Coordinate Axes

$-1.174 \leq y \leq 1.116,\ -0.950 \leq z \leq 0.980$, it has a volume of $7.670\ km^3$, and a mean radius of $1.223\ km$.

Other parameters used in this analysis are; total mass $M = 1.917 \times 10^{13}\ kg$, gravitational parameter, $\mu = 1.279 \times 10^{-6}\ {km^3}/{s^2}$. The ratios of the moments of inertia given as,

$$\left.\begin{aligned} \frac{I_{xx}}{I_{zz}} &= 0.31335, \\ \frac{I_{yy}}{I_{zz}} &= 0.94471, \end{aligned}\right\} \tag{5.46}$$

and the gravitational harmonic expansion coefficients are

$$\left.\begin{aligned} C_{20} &= 0.77768, \\ C_{22} &= -0.01634. \end{aligned}\right\} \tag{5.47}$$

Toutatis is in unforced (torque-free) non-principal axis spin rate [65]. The angular

Table 3: Periodic Variation of Toutatis Angular velocity Amplitude.

Description	**Value**
ω_{max}	$2.1287 \times 10^{-5}\ {}^{rad}/_{s}$
ω_{min}	$2.1122 \times 10^{-5}\ {}^{rad}/_{s}$
ω_{δ}	$8.25 \times 10^{-8}\ {}^{rad}/_{s}$
ω_{o}	$2.12045 \times 10^{-5}\ {}^{rad}/_{s}$

velocity vector of Toutatis varies periodically with time. Within one orbit magnitude of the angular velocity vector varies as shown in the table 3 below.

The period of the rotational velocity in the body-fixed frame is $\tilde{T} = 5.42\ days$. The angle between the rotational velocity vector and the x-axis also varies between 21.904^{oo} and 20.162^{0o} while the angular momentum vector varies between $50.456°$ and $49.55°$ with the x-axis.

Because the magnitudes of angular velocity considered are to the order of 10^{-5}, set the scaling time as $\tau = \sqrt{10^{-6}}t$ (i.e. $\omega_s = \sqrt{10^{-6}}$). Further, let $B_x = B_y = 0.1$, $B_z = 1$, and the perturbing frequency $\omega_\rho = 2.1 \times 10^{-5}\ {}^{rad}/_{s}$. We then substitute these values and the gravitational coefficients values from equation (5.47) into the system in equation (5.41) to obtain our dynamical model as shown below,

$$
\begin{bmatrix} x_1' \\ x_2' \\ y_1' \\ y_2' \\ z_1' \\ z_2' \end{bmatrix} = \begin{bmatrix} 0 & 0 & 1 & 0 & 0 & 0 \\ A_{21} & 0 & A_{23} & A_{24} & 0 & 0 \\ 0 & 0 & 0 & 1 & 0 & 0 \\ A_{41} & A_{42} & A_{43} & 0 & 0 & 0 \\ 0 & 0 & 0 & 0 & 0 & 1 \\ 0 & 0 & 0 & 0 & 1.9893 & 0 \end{bmatrix} \begin{bmatrix} x_1 \\ x_2 \\ y_1 \\ y_2 \\ z_1 \\ z_2 \end{bmatrix}
$$

$$
+ \begin{bmatrix} 0 \\ -2.80011x_1^3 - 2.17315x_1y_1^2 + 4.97326x_1z_1^2 \\ 0 \\ -2.80011x_1^2y_1 - 2.17315y_1^3 + 4.97326y_1z_1^2 \\ 0 \\ -2.80011x_1^2z_1 - 2.17315y_1^2z_1 + 4.97326z_1^3 \end{bmatrix} + \begin{bmatrix} 0 \\ 0.1\sin(0.021\tau) \\ 0 \\ 0.1\sin(0.021\tau) \\ 0 \\ \sin(0.021\tau) \end{bmatrix}, \tag{5.48}
$$

where

$$
\begin{aligned}
A_{21} =& (1.1205 + 3.49874 \times 10^{-6}\sin(0.0212045\tau) + 6.80625 \times 10^{-9}\sin(0.0212045\tau)^2), \\
A_{23} =& 0.00174937\cos(0.0212045\tau), \\
A_{24} =& (42.409 + 0.165\sin(0.0212045\tau)), \\
A_{41} =& -0.00174937\cos(0.0212045\tau), \\
A_{42} =& -(42.409 + 0.165\sin(0.0212045\tau)), \\
A_{43} =& (0.869709 - 3.49874 \times 10^{-6}\sin(0.0212045\tau) \\
& + 6.80625 \times 10^{-9}\sin(0.0212045\tau)^2).
\end{aligned} \tag{5.49}
$$

Notably, the above periodic nonlinear system with external periodic forcing is of the form,

$$
\boldsymbol{x}'(\tau) = \boldsymbol{A}(\tau)\boldsymbol{x}(\tau) + \boldsymbol{f}(\boldsymbol{x}, \tau) + \boldsymbol{F}(\tau), \tag{5.50}
$$

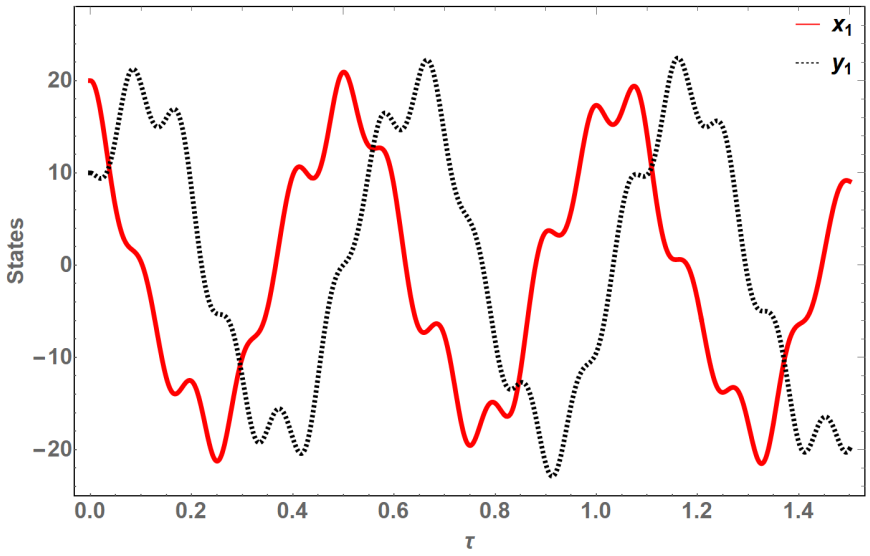

Figure 46: States Time-History Responses in the Vicinity of Toutatis

and is similar to the one previously given in equation (2.1)

5.3.1 Time History Analysis

We numerically integrate the dynamical model in the original coordinates in equation (5.48) to gain insight into the time-history behavior of the dynamics in the vicinity of Toutatis. In this analysis we considered a rather conservative case of initial conditions by setting $x_1(0) = 20,\ y_1(0) = z_1(0) = 10$, while $x_2(0) = y_2(0) = z_2(0) = 0$. These initial conditions imply an orbit starting at the prescribed location with zero initial velocity. The time-history behaviors of the positional states ($x_1(\tau), y_1(\tau), z_1(\tau)$) are shown in figures 46 and 47.

The numerical integration outcome show a very similar behavior between ($x_1(\tau)$) and $y_1(\tau)$. The two states attain roughly similar amplitudes in the positive and negative directions, are quasi-periodic and their main trajectory-paths are frequently punctuated by mi-

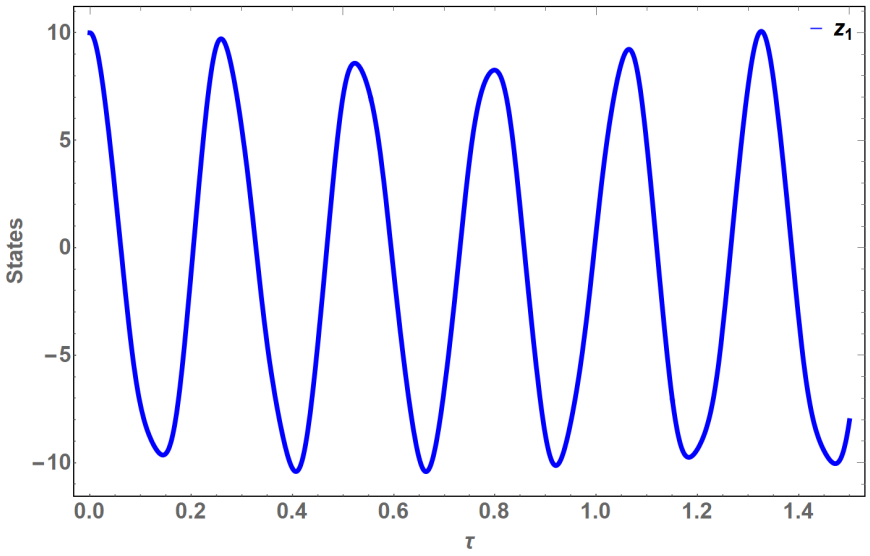

Figure 47: States Time-History Responses in the Vicinity of Toutatis

nor deflections. However, these two exhibit a time-shift (and phase-shift) in their progression. This erratic, 'wobbly' behavior in position of a spacecraft is definitely not conducive to effectively conduct science missions in the vicinity of small irregularly-shaped bodies. The third positional state, $z_1(\tau))$ appears to be more periodically stable with relatively no significant interruptions on the smooth flow of its trajectory. The response of this state is generally periodic, out of phase with the other two states and has amplitude peaks that are about half the magnitude of the other states.

The time-history behaviors of the motion position derivative states ($x_2(\tau), y_2(\tau), z_2(\tau)$) are shown in figures 48 and 49. The time-history behavior of the velocity states show an almost similar behavior to the cases above.

Though ($x_2(\tau)$) and $y_2(\tau)$ have roughly the same general quasi-periodicity and peak magnitudes, they have a significantly larger time-shift and higher frequency compared to $x_1(\tau)$ and $y_1(\tau)$. Moreover, these two state responses do not contain any frequent deflections in their main trajectory-curves. On the other hand, $z_2(\tau))$ has a larger frequency

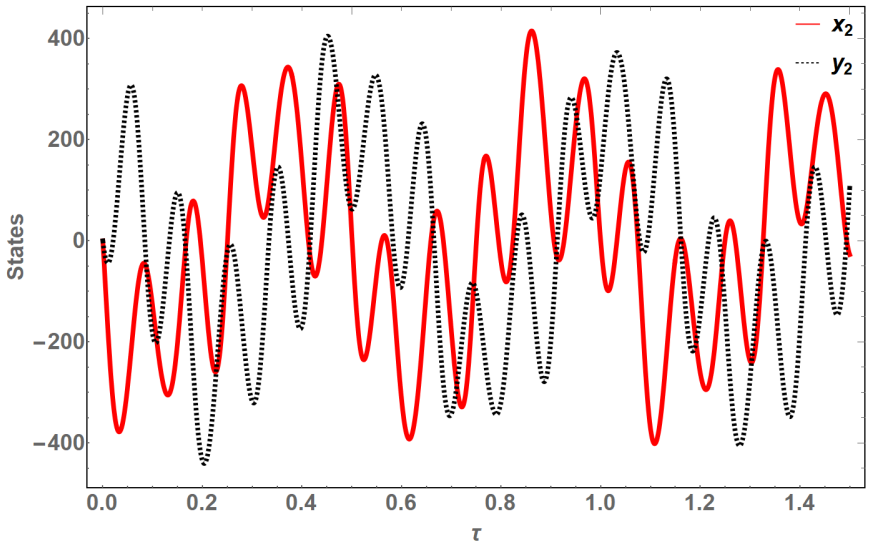

Figure 48: States Time-History Responses in the Vicinity of Toutatis

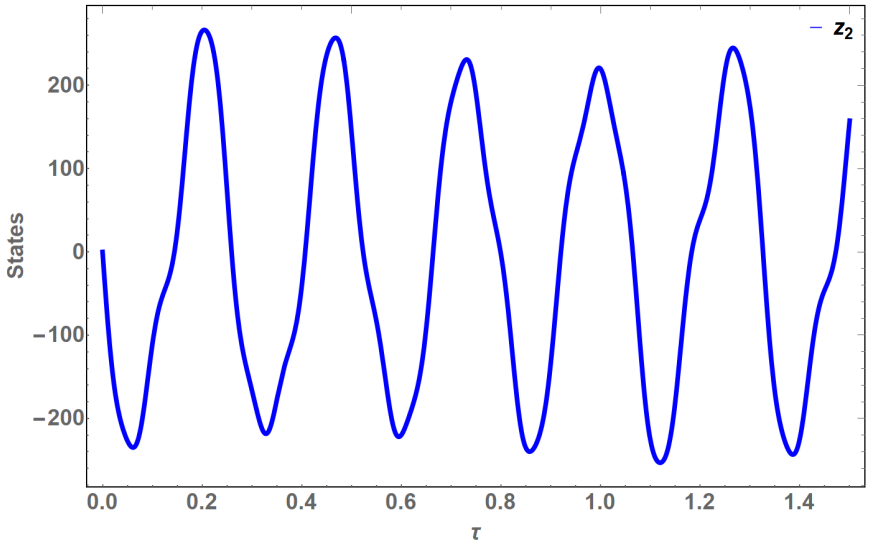

Figure 49: States Time-History Responses in the Vicinity of Toutatis

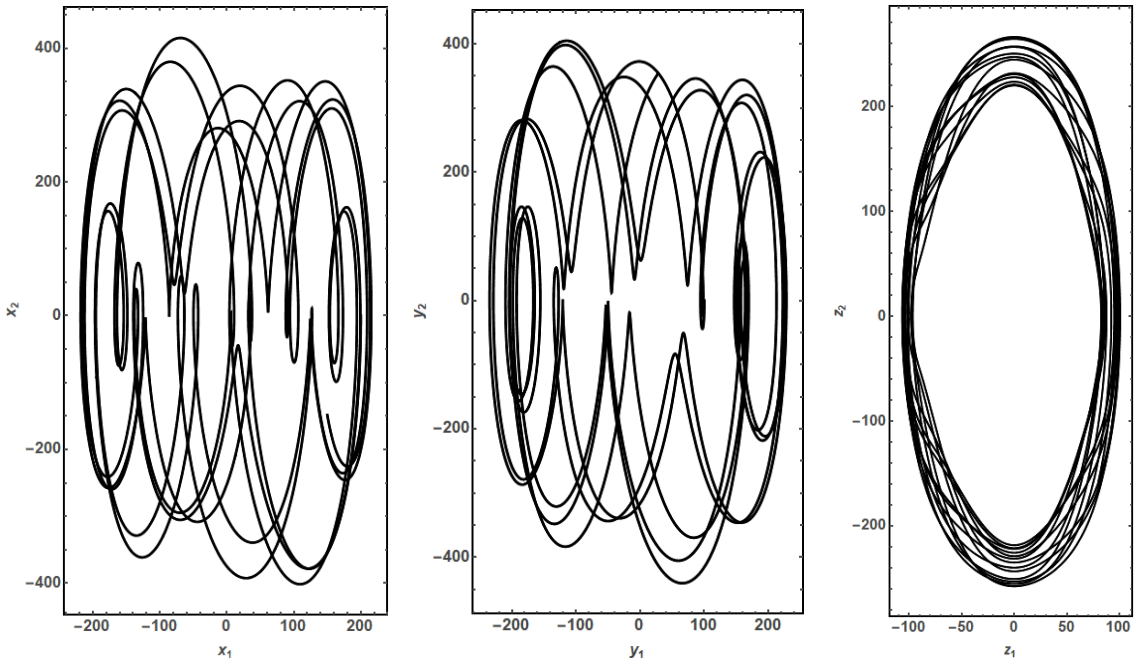

(a) $x_1(\tau)$ and $x_2(\tau)$ (b) $y_1(\tau)$ and $y_2(\tau)$ (c) $z_1(\tau)$ and $z_2(\tau)$

Figure 50: Phase Portraits of the Motion in the Vicinity of Toutatis

comparable to that of $z_1(\tau)$ with amplitude peaks that are slightly smaller in magnitude relative to those of ($x_2(\tau)$ and $y_2(\tau)$.

The corresponding phase portraits of this motion are shown in figure 50. The phase portraits in figure 50(a) and (b) lack an enclosed attractor though the trajectories display a shifting phenomenon of the dominant attracting shape. Therefore, we can conclude that this is a quasi-periodic behavior. Similarly, the dominant attractor in 50(c) exhibits a common attractor with a slight shift indicating a generally periodic motion.

By propagating the numerically integrated solutions of $x_1(\tau)$, $y_1(\tau)$ and $z_1(\tau)$ in time within the small-body centered 3-D coordinate reference frame, we can obtain the geometric structure of the corresponding orbit. Consequently, our dynamical system prescribes the orbit shown in figure 51 given the earlier stated initial conditions. These orbits and

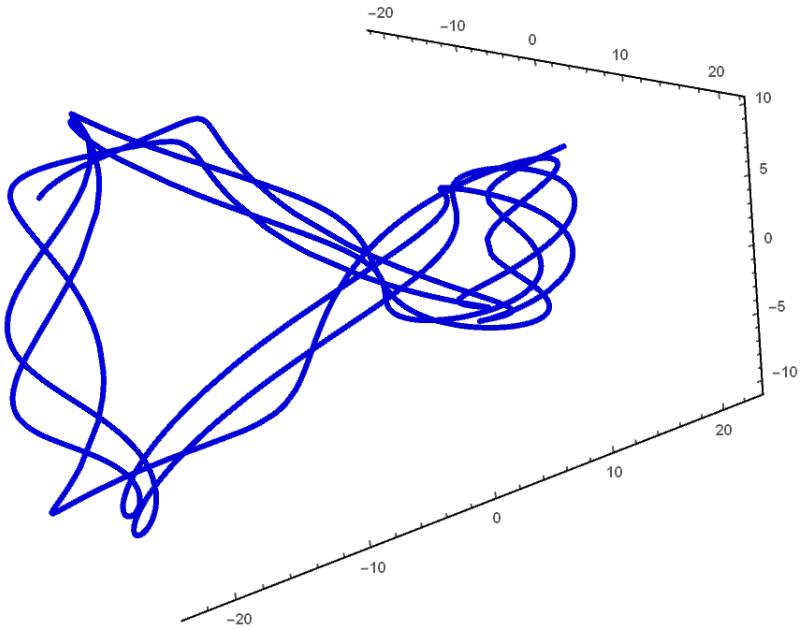

Figure 51: 3-Dimension View of Orbital Motion in the Vicinity of the Small Irregularly Shaped Body

the ISSB share a common centroid in the illustration. Additional elevations of the orbit shown in figures 52. Figure 52(a) shows the $x-y$ 'top' elevation while figure 52(b) shows the $y-z$ 'side' elevation.

As inferred from the state time-history response, figures 51 and 52 show an orbital configuration with very erratic and complex motion in the vicinity of ISSB. The orbital motion is characterized by frequent abrupt changes in direction with a constantly shifting phase. Consequently, such an orbit is not conducive to effectively conduct scientific missions targeting the small irregularly shaped body. As a result, a means to control the orbital dynamics with the aim of realizing relatively more regular and periodic behavior which enables a more conducive environment to conduct science missions aimed at the small irregularly shaped body.

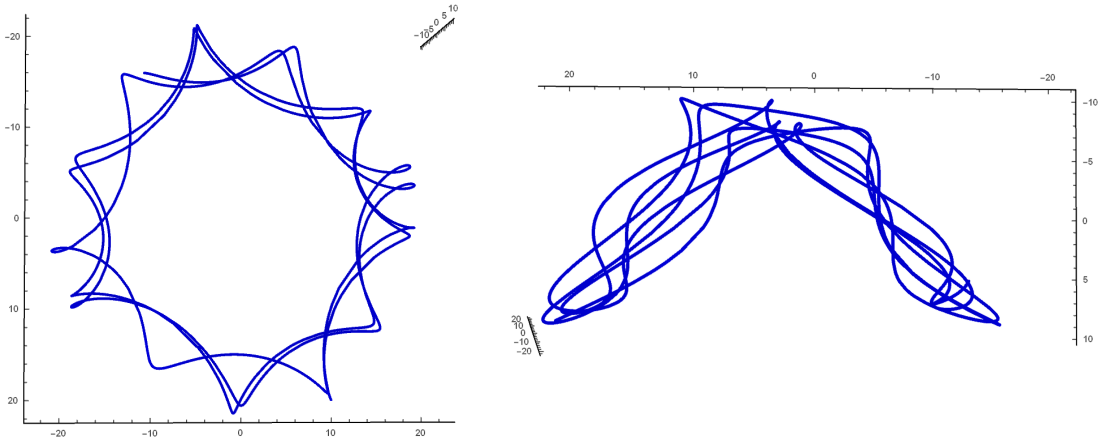

(a) $x - y$ 'Top' (b) $y - z$ 'Side'

Figure 52: Additional Elevations of the Orbit Configuration in the Vicinity of the Small Irregularly Shaped Body–Toutatis

5.3.2 Stability

In addition to the implied quasi-periodicity nature of the motion as deduced above from the time-history analysis, we further scrutinize the stability of our time-periodic nonlinear motion using Floquet theory as outlined in section 2.1. Further, scrutinizing the sensitivity of our motion to initial conditions will provide insights into its chaotic behavior.

5.3.2.1 Floquet Multipliers and Exponents

As part of the procedure, we evaluated the motion's STM to obtain the Floquet Transition Matrix (FTM), Floquet multipliers and exponents. The computed FTM is,

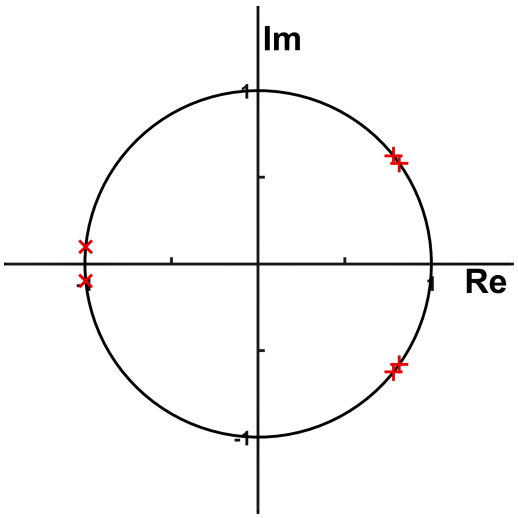

Figure 53: Floquet Multipliers Location for the Uncontrolled Dynamics in the Vicinity of Toutatis

$$FTM = \begin{bmatrix} 0.815 & -0.0268 & 0.5111 & 0.0008 & 0 & 0 \\ -0.03 & 0.7816 & 0.0006 & -0.6244 & 0 & 0 \\ -0.6585 & -0.0008 & 0.815 & -0.0303 & 0 & 0 \\ -0.0008 & 0.6244 & -0.0263 & 0.7816 & 0 & 0 \\ 0 & 0 & 0 & 0 & -0.9952 & -0.0692 \\ 0 & 0 & 0 & 0 & 0.1376 & -0.9952 \end{bmatrix}. \quad (5.51)$$

The values of the computed Floquet multipliers are;

$$\begin{aligned} &0.8150 \pm i0.5795, \\ &0.7816 \pm i0.6238, \\ &-0.9952 \pm i0.0976, \end{aligned} \quad (5.52)$$

and the corresponding locations are illustrated in figure 53.

The computed Floquet exponents are;

$$\begin{aligned} &\pm i0.0021, \\ &\pm i0.0023, \\ &\pm i0.0103. \end{aligned} \tag{5.53}$$

Location of the Floquet multipliers on the unit circle (and the corresponding purely imaginary Floquet exponents) indicate that the motion is marginally stable in the sense of Lyapunov. This is consistent with the quasi-periodic behavior of the motion's time-history and phase portraits analyzed in section 5.3.1. Though the motion is stable in the sense of Lyapunov, the erratic trajectories with abrupt deflections are significantly disruptive to jeopardize nominal execution space missions in the vicinity of the small irregular shaped body.

5.3.3 Chaos

The motion in the vicinity of the small irregular shaped body was found not to be chaotic. After subjecting the states initial conditions (individually and collectively) to a minuscule divergence by adding $\epsilon = 10^{-6}$ to the original initial condition; no difference in the system response occurred. This outcome is illustrated in figure 54.

5.3.4 Poincaré Map

The constructed Poincaré sections in figures 55(a) and (b) do not contain any isolated discernible clusters of points or a single point which would indicate transient behavior, chaos, quasi-periodic or periodic flows. Consequently, in combination with the corre-

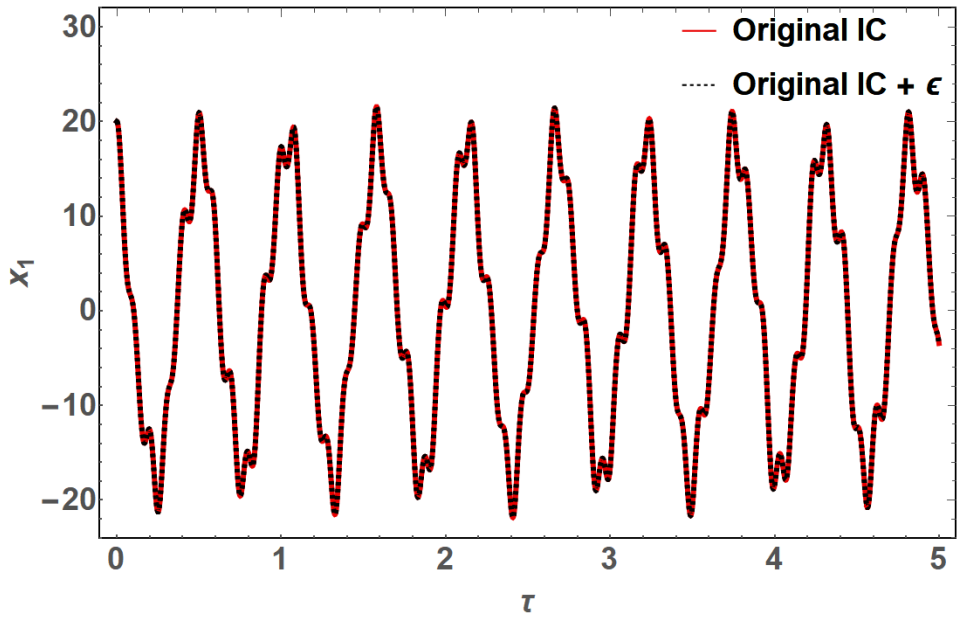

Figure 54: Chaos: Motion Insensitivity to Initial Conditions

sponding time-history results, we can infer that this motion is mostly aperiodic though we cannot rule out quasi-periodicity as well. Figures 55(c) contains points that are dominantly clustered in to form a main ring. Therefore, this motion is quasi-periodic.

A general conclusion from the constructed Poincaré maps is that the motion in the vicinity of the small irregularly shaped body is quasi-periodic. This is consistent with the time-history analyses in section 5.3.1.

5.4 Summary and Discussion

This chapter constitutes the beginning of the second part of this dissertation. Here, we introduced the parametrically excited nonlinear motion of spacecraft which occurs in the vicinity of small irregularly shaped bodies. The ensuing dynamics in the vicinity of small irregularly shaped bodies possess inimitable challenges that necessitate an alternative

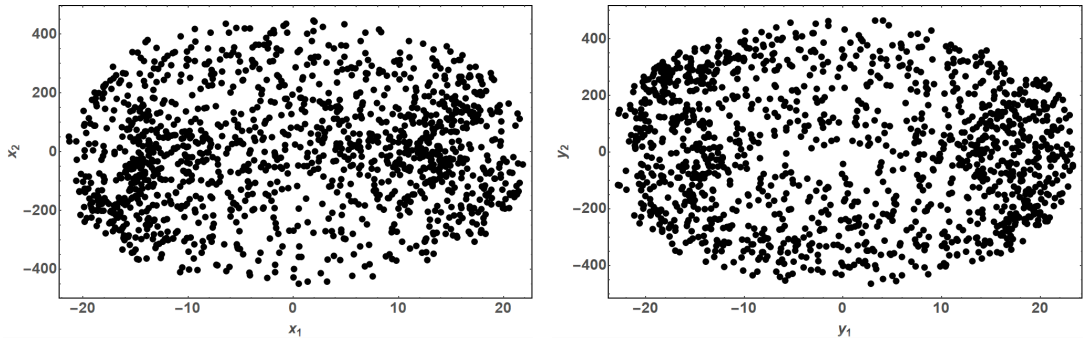

(a) $x_1(\tau)$ and $x_2(\tau)$ (b) $y_1(\tau)$ and $y_2(\tau)$

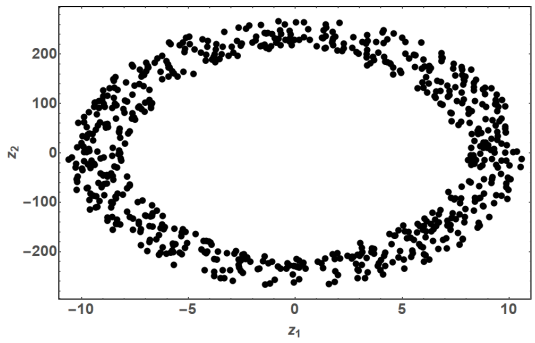

(c) $z_1(\tau)$ and $z_2(\tau)$

Figure 55: Poincaré Sections of the Motion in the Vicinity of ISSB

approach to motion analysis than that traditionally applied to large bodies e.g. planets. This is due to their irregular shape, weak gravitation forces, strong susceptibility to 3^{rd}-body perturbation, uncertainty in mass and orbital parameters, etc. Consequently, we have developed adaptable analytical models that accurately describe the irregularities of the body's total mass distributions in terms of the corresponding gravitational potential. To do so, we summarized the main gravitational potential modeling approaches that are commonly used in studying dynamics around small irregularity shaped bodies. We examined four main approaches i.e spherical harmonic models, ellipsoidal models, polyhedron models and other approaches (mascons and logarithmic potential). Despite having specific advantages and drawbacks, the different gravitational potential modeling approaches are generally useful as determined by their intended application context. We proceeded

with the simplest non-trivial second degree and order spherical harmonic model of the gravitational potential.

We considered the dynamical case of a variable angular velocity vector of the small body and proceeded to analyze the dynamics around asteroid 4179 Toutatis. The time history and phase portrait analysis indicated a generally quasi-periodic motion. By conducting a progression in time of the positional states numerical solutions in 3-D reference frame centered in the ISSB, we were able to construct the geometric configuration of the orbital motion around the small body. The orbit shape is defined by erratic trajectories with abrupt deflections which would significantly impinge on the ability of a spacecraft to conduct an effective scientific investigation. This is because special requirements that complicate the mission architecture design and increasing the mission cost would emanate. Such special considerations include prohibitively re-pointing and frequent swiveling of instrument configurations; prohibitively attitude control and stabilization of the spacecraft; excessive sloshing of propellant the tanks leading to frequent changes in the spacecraft mass properties, etc. Therefore, it is important for the orbit to be controlled in order to attain a regular smoother trajectory free of undue erratic behavior.

Stability analysis via the Floquet multipliers and exponents indicated a marginally stable system because the former were located on the unit circle while the latter were purely imaginary. This is consistent with the time-history analyses results. The Poincaré maps, however, indicated possible presence of chaotic, aperiodic or quasi-periodic dynamics. Because the dynamics were insensitive to minuscule variation in the input of prescribed initial conditions, we concluded that the motion is not chaotic for the considered initial conditions. However, it should be noted that this result is likely confined to this specific case and a different set of initial conditions could spawn a chaotic motion. The response of

nonlinear dynamics is largely dependent on the magnitude of the initial conditions and the strength of nonlinearity.

Since we have now gained knowledge of the uncontrolled motion behavior in the vicinity of Toutatis, in the next chapter, we shall explore ways to synthesize appropriate dynamics control strategies so that we may achieve orbital motion that is more conducive to nominal scientific space mission architectures targeting small irregularly shaped bodies.

Chapter 6

CONTROL OF MOTION IN THE VICINITY OF SMALL IRREGULARLY SHAPED BODIES

Analysis of the dynamics in the vicinity of Toutatis that were undertaken in section 5.3 outlined the need to control the motion about the its equilibrium in order to realize orbital motion that is more conducive to space mission design. Consequently, we shall develop the appropriate control laws in this chapter so that realize space-mission favorable dynamics around Toutatis. A nonlinear control law is most likely to succeed in controlling the unfavorable motion around Toutatis. Unfortunately, in general, control law development techniques are extremely challenging to implement on the parametrically excited nonlinear dynamics with external periodic excitation that model the dynamics around Toutatis as shown in equation (5.48). Consequently, as summarized in chapter 2, we shall;

a. Apply Lyapunov-Floquet (L-F) transformation to convert the periodic linear coefficients to invariant parameters.
b. Intuitively augment the system states by transforming the excitation frequency terms into system states.
c. Reduce the dimension of our dynamical model via center manifold reduction approach.
d. Construct the normal from simplification of our reduced order system.
e. Develop appropriate nonlinear control law on our reduced-order and simplified model (but, qualitatively equivalent to the original system).
f. Solve the controlled system and back-transformed the solutions to the original coordinates.

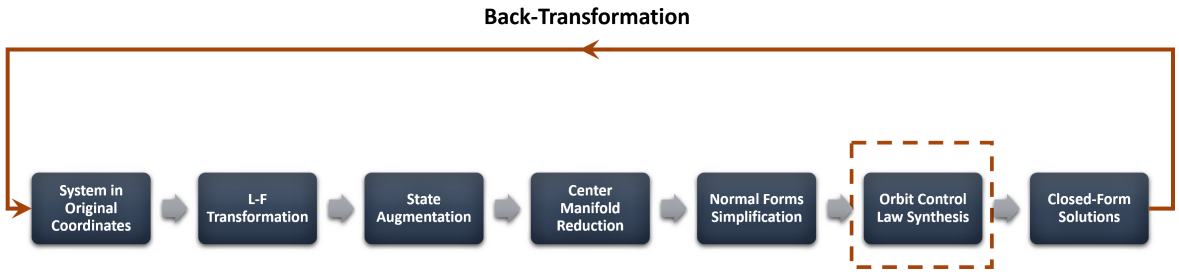

Figure 56: Motion Analysis and Control Law Development Sequence

The procedure above is illustrated in the schematic shown in figure 56.

6.1 Lyapunov-Floquet Transformation

To begin the Lyapunov-Floquet transformation (LFT) process, we designate the the L-F transformation here as,

$$\boldsymbol{x}(\tau) = \boldsymbol{Q}(\tau)\boldsymbol{s}(\tau), \tag{6.1}$$

where $\boldsymbol{x}(\tau)$ is the state in vector original coordinates , $\boldsymbol{Q}(\tau)$ is the LFT matrix and $\boldsymbol{s}(\tau)$ is the state vector in L-F transformed coordinates (see equation (2.9)). Note that we shall subsequently drop the (τ) from our $\boldsymbol{Q}$ and $\boldsymbol{s}$ notations to shorten the typed length of equations.

As described in section 2.5.3, equation (5.50) is the same as equation (2.90). Therefore, the L-F transformed system of equation (5.50) will similarly be as that shown in equation (2.91) , i.e.,

$$\dot{\boldsymbol{s}} = \boldsymbol{R}\boldsymbol{s} + \boldsymbol{Q}^{-1}\boldsymbol{f}(\boldsymbol{Q}\boldsymbol{s}, \tau) + \boldsymbol{Q}^{-1}\boldsymbol{F}(\tau). \tag{6.2}$$

The computed Floquet constant matrix, $\boldsymbol{R}$ and the periodic LFT matrix, $\boldsymbol{Q}$ and its in-

verse, $\boldsymbol{Q}^{-1}$ are;

$$\boldsymbol{R} = \begin{bmatrix} 0 & -0.0001 & 0.0018 & 0 & 0 & 0 \\ -0.0001 & 0 & 0 & -0.0023 & 0 & 0 \\ -0.0024 & 0 & 0 & -0.0001 & 0 & 0 \\ 0 & 0.0023 & -0.0001 & 0 & 0 & 0 \\ 0 & 0 & 0 & 0 & 0 & -0.0073 \\ 0 & 0 & 0 & 0 & 0.0145 & 0 \end{bmatrix}, \tag{6.3}$$

$$\boldsymbol{Q} = \begin{bmatrix} Q_{11} & Q_{12} & Q_{13} & Q_{14} & Q_{15} & Q_{16} \\ Q_{21} & Q_{22} & Q_{23} & Q_{24} & Q_{25} & Q_{26} \\ Q_{31} & Q_{32} & Q_{33} & Q_{34} & Q_{35} & Q_{36} \\ Q_{41} & Q_{42} & Q_{43} & Q_{44} & Q_{45} & Q_{46} \\ Q_{51} & Q_{52} & Q_{53} & Q_{54} & Q_{55} & Q_{56} \\ Q_{61} & Q_{62} & Q_{63} & Q_{64} & Q_{65} & Q_{66} \end{bmatrix}, \boldsymbol{Q}^{-1} = \begin{bmatrix} Q_{11}^{-1} & Q_{12}^{-1} & Q_{13}^{-1} & Q_{14}^{-1} & Q_{15}^{-1} & Q_{16}^{-1} \\ Q_{21}^{-1} & Q_{22}^{-1} & Q_{23}^{-1} & Q_{24}^{-1} & Q_{25}^{-1} & Q_{26}^{-1} \\ Q_{31}^{-1} & Q_{32}^{-1} & Q_{33}^{-1} & Q_{34}^{-1} & Q_{35}^{-1} & Q_{36}^{-1} \\ Q_{41}^{-1} & Q_{42}^{-1} & Q_{43}^{-1} & Q_{44}^{-1} & Q_{45}^{-1} & Q_{46}^{-1} \\ Q_{51}^{-1} & Q_{52}^{-1} & Q_{53}^{-1} & Q_{54}^{-1} & Q_{55}^{-1} & Q_{56}^{-1} \\ Q_{61}^{-1} & Q_{62}^{-1} & Q_{63}^{-1} & Q_{64}^{-1} & Q_{65}^{-1} & Q_{66}^{-1} \end{bmatrix}, \tag{6.4}$$

where

$$\begin{aligned} Q_{11} =& 1.0006\cos(0.0212045\tau) + 0.0043\sin(0.0212045\tau), \\ Q_{12} =& (-0.2419 + 0.8899\cos(0.0212045\tau) - 0.6480\cos(2 \times 0.0212045\tau))10^{-4} \\ & - 0.0208\sin(0.0212045\tau), \\ Q_{13} =& 0.0010 - 0.0038\cos(0.0212045\tau) + 0.0027\cos(2 \times 0.0212045\tau) \\ & + 0.8815\sin(0.0212045\tau), \\ Q_{14} =& 0.0236\cos(0.0212045\tau) + 10^{-3}(0.1010\sin(0.0212045\tau) \\ & - 0.0735\sin(2 \times 0.0212045\tau)), \\ Q_{15} =& Q_{16} = 0, \end{aligned}$$

$$
\begin{aligned}
Q_{21} =&(-0.0024 + 0.0997\cos(0.0212045\tau) - 0.1387\cos(0.0212045\tau))10^{-3} \\
&- 0.0233\sin(0.0212045\tau),\ \ Q_{22} = \cos(0.0212045\tau), \\
Q_{23} =&0.0205\cos(0.0212045\tau) + (0.0878\sin(0.0212045\tau) \\
&- 0.1222\sin(2 \times 0.0212045\tau))10^{-3}, \\
Q_{24} =&\sin(0.0212045\tau),\ \ Q_{25} = Q_{26} = 0, \\
Q_{31} =&-0.0013 + 0.0049\cos(0.0212045\tau) - 0.0035\cos(2 \times 0.0212045\tau) \\
&- 1.1357\sin(0.0212045\tau), \\
Q_{32} =&-0.0236\cos(0.0212045\tau) + (-0.1010\sin(0.0212045\tau) \\
&+ 0.0735\sin(2 \times 0.0212045\tau))10^{-3}, \\
Q_{33} =&1.0006\cos(0.0212045\tau) + 0.0043\sin(0.0212045\tau), \\
Q_{34} =&(-0.0313 + 0.1147 * Cos(0.0212045\tau) - 0.0834 * Cos(2 \times 0.0212045\tau))10^{-3} \\
&- 0.0268\sin(0.0212045\tau), \\
Q_{35} =&Q_{36} = 0, \\
Q_{41} =&-0.0265\cos(0.0212045\tau) + (-0.1132\sin(0.0212045\tau) \\
&+ 0.1573\sin(2 \times 0.0212045\tau))10^{-3}, \\
Q_{41} =&\sin(0.0212045\tau), \\
Q_{43} =&(-0.0024 + 0.0997 * Cos(0.0212045\tau) - 0.1386\cos(2 \times 0.0212045\tau))10^{-3} \\
&- 0.0233\sin(0.0212045\tau), \\
Q_{44} =&\cos(0.0212045\tau),\ \ Q_{45} = Q_{46} = 0,
\end{aligned}
$$

$$
Q_{51} = Q_{52} = Q_{53} = Q_{54} = 0,\ \ Q_{55} = \cos(0.0212045\tau),\ \ Q56 = 0.7090\sin(0.0212045\tau),
$$

$$
Q_{61} = Q_{62} = Q_{63} = Q_{64} = 0,\ \ Q_{65} = -1.4104\sin(0.0212045\tau),\ \ Q_{66} = \cos(0.0212045\tau).
$$

We alternatively choose to plot the periodic elements of the inverse LFT matrix, $\boldsymbol{Q}^{-1}$ as shown in the following figures. Figure 57 plots 18 of the elements of $\boldsymbol{Q}^{-1}$, s.t. $\forall\, Q_{ij}^{-1},\ i =$

$1, 2, \ldots, 6, j = 1, 2, 3$. On the other hand, figure 58 plots the other 18 of the elements of $\boldsymbol{Q}^{-1}$, s.t. $\forall\, Q_{ij}^{-1},\ i = 1, 2, \ldots, 6, j = 4, 5, 6$.

By substituting equations (6.3) and (6.4) into equation (6.2) obtain the L-F transformed system that now has invariant linear coefficients. Here, $\boldsymbol{s} = [s_1\ s_2\ s_3\ s_4\ s_5\ s_6]^T$, and $\boldsymbol{F}(\tau)$ is as shown in equation (5.50).

6.2 Center Manifold Reduction

After obtaining the L-F transformed system, next, we convert the system from a non-autonomous to an autonomous one. This is achieved via the intuitive state augmentation methodology described in sections 2.5.3.1.

Consider the $x-$element of the external periodic excitation vector defined in scaled time variable as,

$$F_x(\tau) = B_x \sin\left(\frac{\omega_\rho}{\omega_s}\tau\right). \tag{6.5}$$

We can rewrite equation (6.5) using the double-angle trigonometric identity formula as,

$$F_x(\tau) = 2B_x \sin\left(\frac{\omega_\rho}{2\omega_s}\tau\right)\cos\left(\frac{\omega_\rho}{2\omega_s}\tau\right). \tag{6.6}$$

We then augment the states by designating;

$$\left.\begin{aligned} p &= \sin\left(\frac{\omega_\rho}{2\omega_s}\tau\right), \\ p' &= \left(\frac{\omega_\rho}{2\omega_s}\right)\cos\left(\frac{\omega_\rho}{2\omega_s}\tau\right) = q, \\ q' &= -\left(\frac{\omega_\rho^2}{4\omega_s^2}\right)\sin\left(\frac{\omega_\rho}{2\omega_s}\tau\right) = -\left(\frac{\omega_\rho^2}{4\omega_s^2}\right)p. \end{aligned}\right\} \tag{6.7}$$

Substituting equation (6.7) into (6.6) we obtain the autonomous forcing term as,

$$F_x(\tau) = 4B_x pq\left(\frac{\omega_s}{\omega_\rho}\right). \tag{6.8}$$

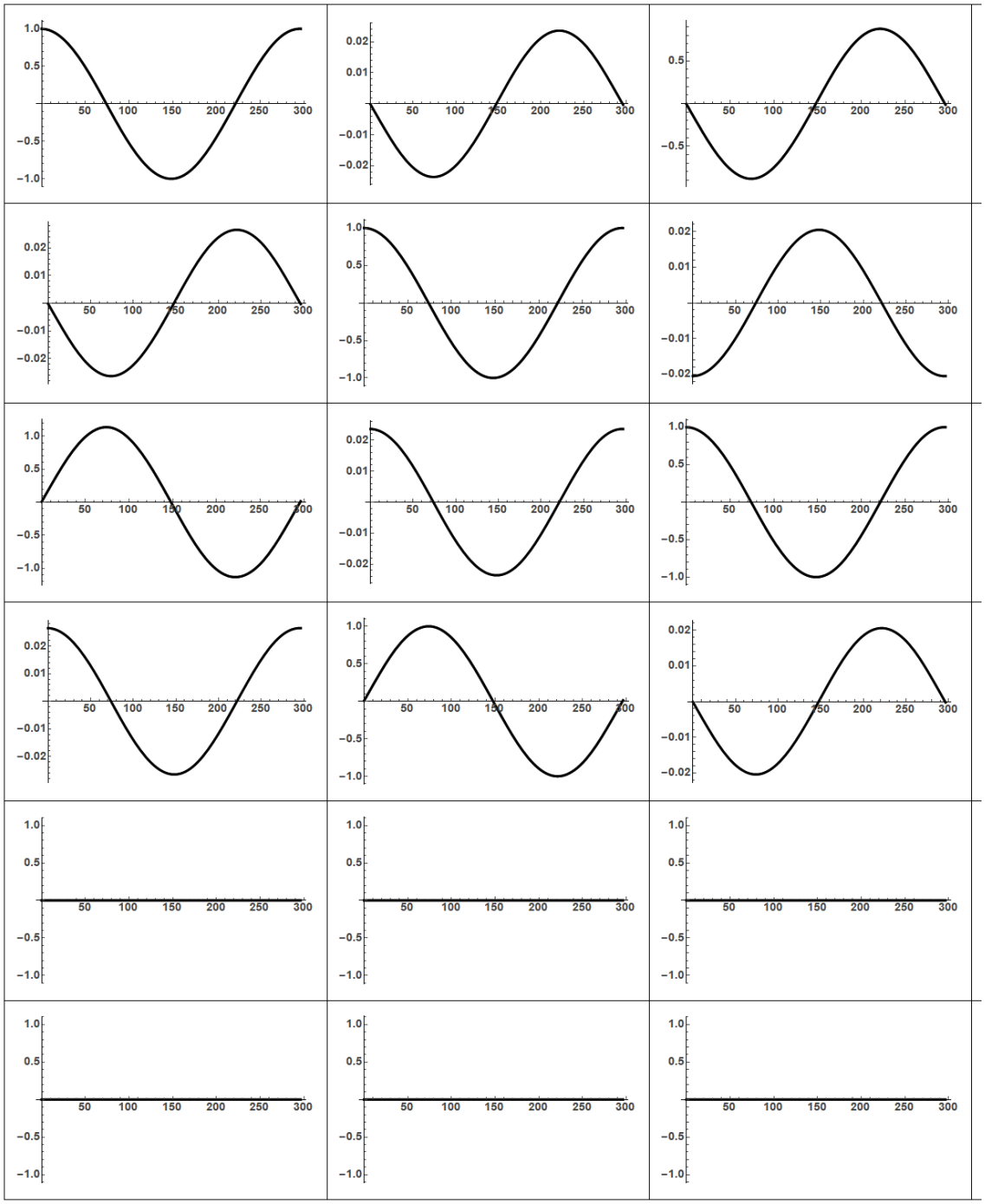

Figure 57: Plot of Half of the Elements of LFT Matrix

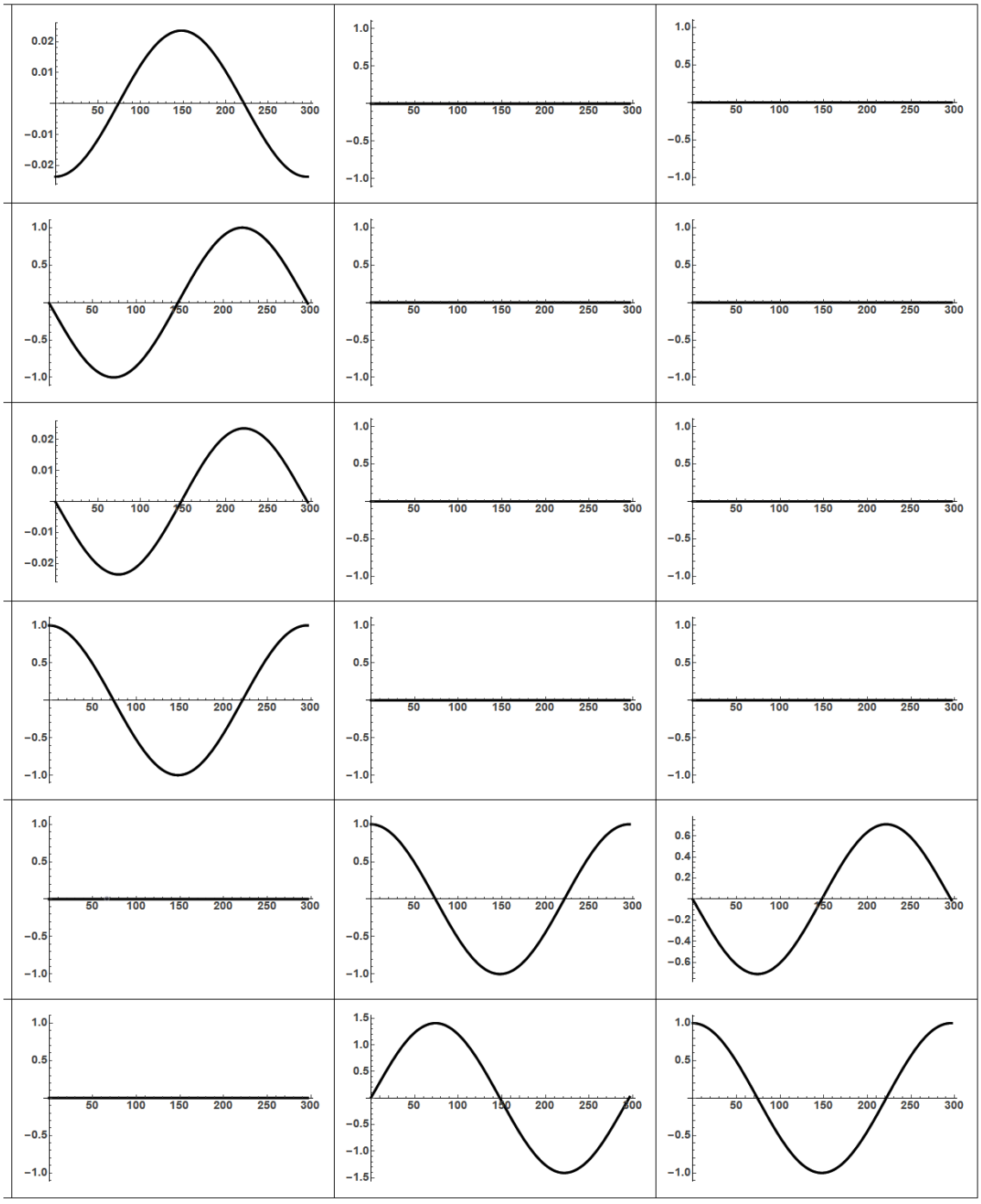

Figure 58: Plot of the Remaining Half of the Elements of LFT Matrix

We can derive similar expressions for the other two forcing vector elements, $F_y(\tau)$ and $F_z(\tau)$.

By converting the non-autonomous system to an autonomous one, the dimension of the nonlinear system increases from six to eight, i.e.,

$$\begin{bmatrix} s_1' \\ s_2' \\ s_3' \\ s_4' \\ s_5' \\ s_6' \\ p' \\ q' \end{bmatrix} = \begin{bmatrix} f(s_1(\tau)) \\ f(s_2(\tau)) \\ f(s_3(\tau)) \\ f(s_4(\tau)) \\ f(s_5(\tau)) \\ f(s_6(\tau)) \\ q \\ -\dfrac{(441p)}{4000000} \end{bmatrix}. \tag{6.9}$$

The full expressions for $f(s_{1,2,3,4,5,6}(\tau))$ contain too many monomial terms to present them here and are given in Appendix B.1. We then obtain the Jordan form of this system via the modal transformation and compute the center manifold reduction using the procedure outlined in section 2.5.3.1.

Eigenvalues of the augmented states linear matrix are,

Critical: $\lambda_1^* = i0.0105,\ \lambda_2^* = -i0.0105,\ \lambda_3^* = i0.0102884,$ and $\lambda_4^* = -i0.0102884,$

Stable: $\lambda_5^* = -1 \times 10^{-7} + i0.00229784,\ \lambda_6^* = -1 \times 10^{-7} - i0.00229784,\ \lambda_7^* = -1 \times 10^{-7} + i0.0020759,$ and $\lambda_8^* = -1 \times 10^{-7} - i0.0020759.$

The reduced order system on the invariant center manifold is:

Parametric equations of the center manifold are;

$$\begin{aligned} s_1(\tau) =& P_1(\tau), \\ s_2(\tau) =& P_2(\tau), \\ s_3(\tau) =& P_3(\tau), \\ s_4(\tau) =& P_4(\tau). \end{aligned} \tag{6.10}$$

The reduced system is

$$\begin{aligned} s_5' =& P_5'(\tau), \\ s_6' =& P_6'(\tau), \\ p' =& q(\tau), \\ q' =& -\frac{(441p(\tau))}{4000000}. \end{aligned} \tag{6.11}$$

The full expressions for $P_{1,2,3,4}(\tau)$ and $P_{5,6}'(\tau)$ similarly contain too many monomial terms to present them here and are given in Appendix B.2.

6.3 Normal Forms Simplification

Even though the dimension of our system's analytical model has been reduced from eight to two, the model is still very complex with thousands of nonlinear monomial terms. We should also note that, despite dealing with a four dimensional reduced system, there are only two unsolved variables, s_5 and s_6. This is becasue the dynamics of the other two variables, $p(\tau)$ and $q(\tau)$ are fully known as shown in equation (6.7). Consequently, we shall utilize normal forms simplification as outlined in section 2.3 to obtain a simpler but qualitatively equivalent nonlinear system with conserved bifurcation and Lyapunov properties.

We first compute the TDNF, then by averaging out the periodic terms, we shall obtain the simpler TINF of our system. The normal form shown in equation (6.12) is sub-

sequently obtained after computation as outlined in section 2.3,

$$\begin{bmatrix} v_5' \\ v_6' \\ v_7' \\ v_8' \end{bmatrix} = \begin{bmatrix} -i0.0105v_5 \\ +i0.0105v_6 \\ -i0.010288v_7 + (0.02111598 - i0.0007817)v_5^2 v_6^2 v_7 + i745.4783 v_7^3 v_8^2 \\ +i0.010288v_8 + (0.02111598 + i0.0007817)v_5^2 v_6^2 v_8 - i745.4783 v_7^2 v_8^3 \end{bmatrix}. \tag{6.12}$$

Note that we can further simplify this normal form by substituting the straightforward solutions of $v_5(\tau)$ and $v_6(\tau)$ into the third and fourth ODEs of equation (6.12). Then, by solving this system and obtaining $v_7(\tau)$ and $v_8(\tau)$, we can then back transform these solutions to the original coordinates to obtain the uncontrolled system as previously shown in sections 3.5.1 and 3.5.2. Because our reason for undertaking the normal from simplification here is to facilitate development of appropriate control laws for our system, we shall focus on back-transforming the controlled dynamics.

6.4 Nonlinear Control and Periodic Orbit Realization

To determine the nonlinear controller, we first add a control input to the normal form in equation (6.12) as shown below,

$$\begin{bmatrix} v_5' \\ v_6' \\ v_7' \\ v_8' \end{bmatrix} = \begin{bmatrix} -i0.0105 & 0 & 0 & 0 \\ 0 & +i0.0105 & 0 & 0 \\ 0 & 0 & -i0.010288 & 0 \\ 0 & 0 & 0 & +i0.010288 \end{bmatrix} \begin{bmatrix} v_5 \\ v_6 \\ v_7 \\ v_8 \end{bmatrix} + \begin{bmatrix} 0 \\ 0 \\ (0.02111598 - i0.0007817)v_5^2 v_6^2 v_7 + i745.4783 v_7^3 v_8^2 \\ (0.02111598 + i0.0007817)v_5^2 v_6^2 v_8 - i745.4783 v_7^2 v_8^3 \end{bmatrix} + \boldsymbol{G_6 u}. \tag{6.13}$$

Let the scaling matrix and control input be of the form,

$$\boldsymbol{G_6} = \begin{bmatrix} 0 & 0 & 0 & 0 \\ 0 & 0 & 0 & 0 \\ 0 & 0 & 1 & 0 \\ 0 & 0 & 0 & 1 \end{bmatrix}, \qquad \boldsymbol{u} = \gamma_3 \begin{bmatrix} 0 \\ 0 \\ K_1 v_5^2 v_6^2 v_7 + K_2 v_7^3 v_8^2 \\ K_1 v_5^2 v_6^2 v_8 + K_2 v_7^2 v_8^3 \end{bmatrix}. \tag{6.14}$$

Therefore, the simplified controlled system becomes,

$$\begin{bmatrix} v_5' \\ v_6' \\ v_7' \\ v_8' \end{bmatrix} = \begin{bmatrix} -i0.0105 v_5 \\ +i0.0105 v_6 \\ V_{31} \\ V_{41} \end{bmatrix}, \tag{6.15}$$

where

$$\begin{aligned} V_{31} =& \{-i0.010288 + (0.02111598 - i0.0007817)C_5^2 C_6^2 + C_5^2 C_6^2 K_1\} v_7 \\ & + (K_2 + i745.4783) v_7^3 v_8^2, \\ V_{41} =& \{+i0.010288 + (0.02111598 + i0.0007817)C_5^2 C_6^2 + C_5^2 C_6^2 K_1\} v_8 \\ & + (K_2 - i745.4783) v_7^2 v_8^3. \end{aligned}$$

C_5 and C_6 are the integration constants from the solutions of $v_5(\tau)$ and $v_6(\tau)$.

The proportional gains are custom-tuned to $K_1 = -20$ and $K_2 = -20$ while $\gamma_3 = 1$. The closed form solutions for $v_5(\tau)$ and $v_6(\tau)$ are straight forward. To solve for $v_7(\tau)$ and $v_8(\tau)$ we introduce the complex changes of variable; $v_7 = u_1 - iu_2$ and $v_8 = u_1 + iu_2$ followed by the polar coordinates $u_1 = R\cos(\theta)$ and $u_2 = R\sin(\theta)$. The last two unsolved equations in the system shown in equation (6.15) become,

$$\left.\begin{aligned} R' =& C_5^2 C_6^2 (0.021116 + K_1)R + K_2 R^5, \\ \theta' =& 0.0102883 + 0.000781747 C_5^2 C_6^2 - 745.478 R^4. \end{aligned}\right\} \tag{6.16}$$

After solving equation (6.16), R and θ are use to find $v_7(\tau)$ and $v_8(\tau)$. The evaluated solutions of the normal form shown in equation (6.15) are as shown below,

$$\begin{aligned} v_5(\tau) =& C_5 \exp(i0.0105\tau), \\ v_6(\tau) =& C_6 \exp(-i0.0105\tau), \\ v_7(\tau) =& \frac{[\text{NUM}(1.30564 \times 10^7 + 6.1832 \times 10^8 K_1)^{\frac{1}{4}}\{\cos(\Gamma) - i\sin(\Gamma)\}]}{\text{DEN}}, \\ v_8(\tau) =& \frac{[\text{NUM}(1.30564 \times 10^7 + 6.1832 \times 10^8 K_1)^{\frac{1}{4}}\{\cos(\Gamma) + i\sin(\Gamma)\}]}{\text{DEN}}, \end{aligned} \tag{6.17}$$

where

$$\left.\begin{aligned} \text{NUM} = & (0.707107 - i0.707107)\sqrt{C_5 C_6} \times \\ & \exp\{C_5^2 C_6^2 (C_7(1.30564 \times 10^7 + 6.1832 \times 10^8 K_1) + (0.021116 + K_1)\tau)\}, \end{aligned}\right\}$$

$$\left.\begin{aligned} \text{DEN} = & (-1 + 6.1832 \times 10^8 K_2 \\ & \exp\{(C_5 C_6)^2 (C_7(5.22258 \times 10^7 + 2.47328 \times 10^9 K_1) + (0.0844639 + 4K_1)t)\})^{\frac{1}{4}}, \end{aligned}\right\}$$

$$\left.\begin{aligned} \Gamma = & 0.000781747 C_5^2 C_6^2 \tau + C_8 + 0.0102883\tau + \\ & \frac{186.37\,(C_5^2 C_5^2 (C_7(2.47328 \times 10^9 K_1 + 5.22258 \times 10^7) + (4K_1 + 0.0844639)\tau))}{K_2} \\ & + \frac{\log - K_2)}{K_2}. \end{aligned}\right\}$$

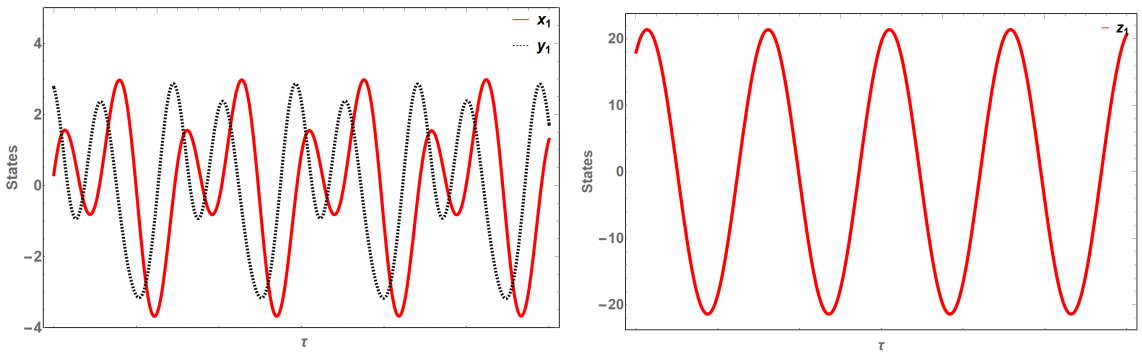

(a) x_1 and y_1 (b) z_1

Figure 59: Controlled States Responses in the Vicinity of Toutatis

C_7 and C_8 are the integration constants from the solutions of $v_7(\tau)$ and $v_8(\tau)$.

We then back transform these obtained closed form solutions $v_5(\tau)$, $v_6(\tau)$, $v_7(\tau)$ and $v_8(\tau)$ via inverse near identity transformation to the center manifold reduced order coordinates s. Then, we combine these solutions with the already obtained ones, $s_1(\tau)$, $s_2(\tau)$, $s_3(\tau)$ and $s_4(\tau)$ and beck transform the combined closed from solutions to the original coordinates via inverse modal and inverse L-F transformation. The obtained the controlled states responses are as shown in figure 59. Similarly, the responses of the derivative states are shown in figure 60.

By propagating the controlled then back-transformed closed-form solutions of $x_1(\tau)$, $y_1(\tau)$ and $z_1(\tau)$ in time, we can obtain the geometric configuration of the controlled orbit within Toutatis centered 3-D coordinate frame. This outcome prescribes the orbit shown shown in figure 61 under the same initial conditions as previously given in figure 51.

Additional elevations and view angles of the orbit are shown in figures 62 and 63.

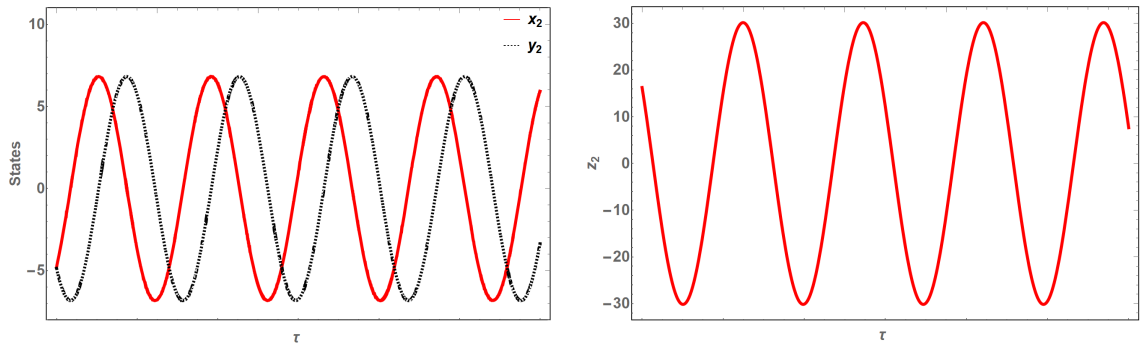

(a) x_2 and y_2 (b) z_2

Figure 60: Controlled States Responses in the Vicinity of Toutatis

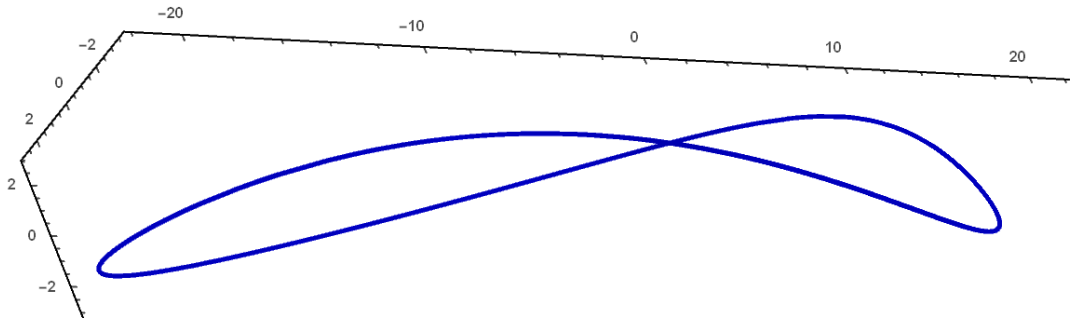

Figure 61: 3-Dimension View of Orbital Motion in the Vicinity of the Small Irregularly Shaped Body

Unlike the previous case, the resulting orbit after the implementation of the nonlinear controller is smoother and regular in the general trajectory path. There are no frequent abrupt deflections and it is periodic. Consequently, such an orbit is ideal and conducive to effectively conduct scientific missions targeting the small irregularly shaped body. The nonlinear control law which acts about the stable points of the solutions has hence been shown to enable a regular periodic orbits to be achieved around the small irregularly shaped body.

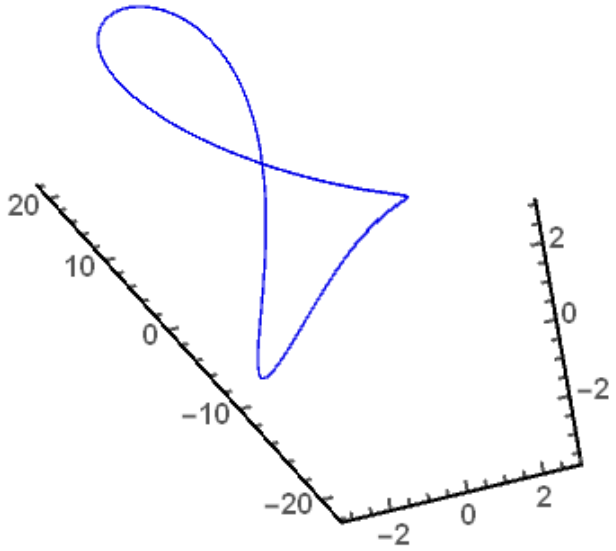

Figure 62: Additional View Angle of the Orbit Shape in the Vicinity of Toutatis

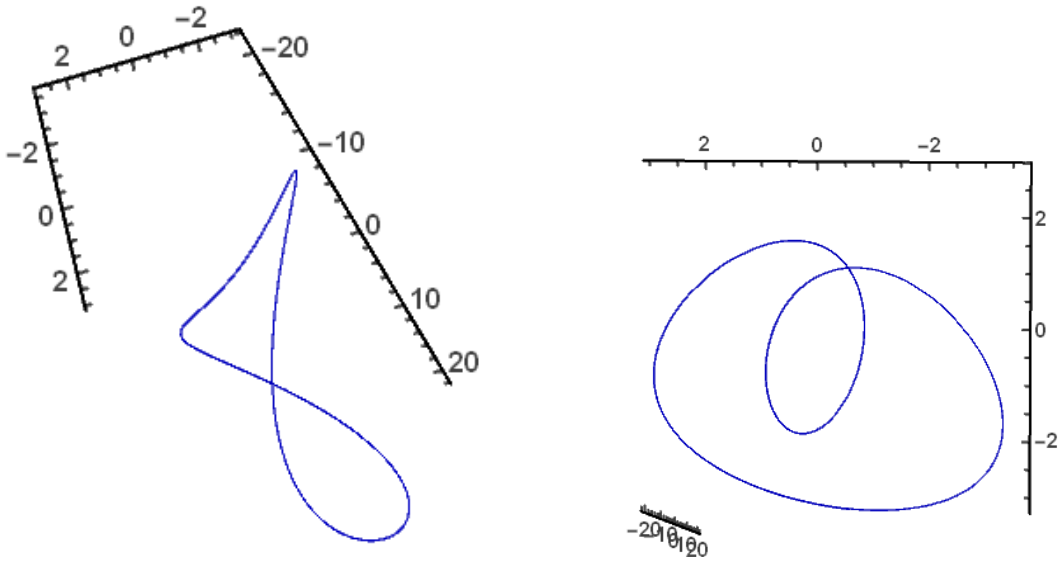

(a) (b)

Figure 63: Additional View Angle and Elevation of the Orbit Shape in the Vicinity of Toutatis

6.5 Summary and Discussion

This chapter demonstrated how to control the dynamics in the vicinity of small irregularly shaped bodies in order to transform the prevailing erratic, quasi-periodic motion into a regular periodic motion that will facilitate effective scientific space missions targeting such bodies.

As we indicated earlier, the ISSB are characterized by inimitable challenges such as uncertainty in orbital parameters and total mass, irregular shape and gravitational potential, etc. Consequently, the dynamical models need to be adaptable to model the ensuing dynamical behavior of a spacecraft in close proximity to such a body. Since the nonlinear controller that we developed in this chapter is based on a full state feedback control law, the controller dynamics are adaptable to control the dynamics in the vicinity of our case application–Toutatis.

By applying the L-F transformation, we were able to transform the periodic linear coefficients in the dynamical model to invariant parameters. Consequently, the system was amenable to the transformation from non-autonomous to autonomous via intuitive state augmentation that targeted excitation frequency terms in the external periodic forcing vector and coefficients of nonlinear monomial terms. When the time is set to zero, the LFT matrix reduces to a simple identity matrix.

We chose to transform the trigonometric functions to their equivalent product functions prior to state augmentation because this will eliminate the possibility of new linear periodic terms emanating after state augmentation. Such a case is unfavorable because the procedure will require a second L-F transformation and possibly another state augmentation. The center manifold reduction reduced the dimension of our analytical model enabling the normal forms to be obtained. By solving the normal forms, we were able to

realize a closed-form solution to a dynamical system that was not analytically solvable into closed-form solutions, to begin with. Without performing a MOR on our system, the model would be too complex and cumbersome to work with making it extremely challenging to synthesize a control law. Therefore, all these steps need to be taken in the order enumerated at the beginning of this chapter. We chose to implement a full-state feedback nonlinear control law. However, this is not the only control approach possible. Other nonlinear control approaches e.g. sliding mode control, or even feasible linear control laws can be implemented.

Though the corresponding phase portraits were plotted for the numerically solved uncontrolled system in the original coordinates, we should note that for a system with a dimension greater than two (as is our case), phase portraits constructed by the parametric behavior of only two states at a time only portray a partial dynamical picture of our system. This is because only the isolated contribution of the two considered dynamics are analyzed; while in actuality, their coupling and dynamical interaction with the other states is what completes the system's dynamical portrait in the phase-space.

Finally, the chapter achieved the overall objective of realizing suitable dynamics in the vicinity of a small irregularly shaped body despite the prevailing intricate and volatile dynamical environment

Chapter 7

CONCLUSIONS AND FUTURE DIRECTIONS

In this final chapter, we shall holistically summarize the methodologies, findings and contributions of this research. Afterwards, we shall discuss future areas to extend this and related research.

7.1 Summary and Contributions

The research presented in this dissertation focused on analyzing and controlling intricate and complexly structured nonlinear dynamical models that describe motion of space systems. In doing so, we pursued approaches that are not commonly applied compared to other approaches to investigate space system dynamics. Consequently, we had to initially develop the analytical strategies that would facilitate this investigation by extending the fundamental theories in periodic dynamics, model order reduction and normal forms simplification to be applicable on the considered intricate motion in a lucid, straightforward and broad manner.

Our reliance on space-based technologies as an essential component of our modern lifestyles is indisputable. Unfortunately, space is a harsh, unwelcoming and uncooperative environment to operate it. In addition to the inimical physical encounters, space systems have to endure a perturbing dynamical environment that persistently disorients spacecraft attitude, dislodges spacecraft from their designated orbital positions and compels spacecraft to follow undesirable orbital trajectories. As a result, accurate modeling, analysis and

control of spacecraft dynamics is a fundamental aspect of space mission analysis and design that continues to receive zealous research attention in the field of astronautics.

Inopportunely, space systems dynamics tend to be commonly represented by large, coupled, nonlinear analytical models that are parametrically excited and are further subjected to external periodic excitation. It is hence not feasible to obtain closed form analytical solutions of such systems. The conventional analytical approaches to analyzing and solving such systems relies on linearization, perturbation and averaging approaches. However, as we have seen, these methodologies possess inherently limiting drawbacks such as restriction to minimally excited systems or constrains to small domains about the operating point. These drawbacks serve to counter the desire to accurately model and analyze space systems dynamics for effective mission formulation. Consequently, it is the objective of this dissertation to contribute towards tackling this problem.

In doing so, we chose to rely on a series of fundamental techniques encompassing Floquet theory, center manifold order reduction and normal forms simplification. We then introduced an intuitive state augmentation methodology that enabled the preceding techniques to be seamlessly extended to our analysis in a plain and straightforward manner– hence making the analysis and control of our intricate dynamics possible. This plan of approach was described in chapter 2 and two schematics used to summarize our dissertation strategy. Chapter 2 further outlined the fundamental theoretical concepts of Floquet theory, normal forms and center manifold reduction. Floquet theory enables representation of periodic dynamical models by a product of a periodic matrix and an exponential matrix. Moreover, the periodic Lyapunov-Floquet transformation matrix transforms linear varying coefficients into invariant parameters. Floquet theory simplifies nonlinear systems while center manifold reduction reduces the dynamical model dimension on the invariant

manifold. In outlining the preceding methods, we segregated nonlinear systems with constant coefficients from those with periodic coefficients.

After, highlighting the limitations of these techniques when applied to parametrically excited nonlinear systems with external periodic excitation, we introduced intuitive state augmentation as a means to address this limitation. The intuitive state augmentation targeted the excitation frequency terms to aggrandize the states hence converting the system from non-autonomous to autonomous. As a result, steps analogous to the fundamental theories of normalization and order reduction could be innocuously applied to our augmented system even though the excitation was inherently accounted for. We were able to verify the accuracy of the developed approaches in normal forms and center manifold reduction via illustrative examples involving multiple cases that were separated according to periodic and constant coefficients. Only after verifying the efficacy of these methods did we feel confident enough to apply them on our actual space system dynamics.

To address a fair representation of complex space systems dynamics, we considered two different types of motions. The first type addressed the problem of motion about the center of mass of a spacecraft as it orbited a large mass in an eccentric orbit. The second type addressed the problem of motion of the spacecraft center of mass around a small irregularly shaped body. Consequently, the dissertation problem is divided into two parts.

The first part part of dissertation investigated the attitude motion of a gravity gradient stabilized spacecraft about it center of mass as it orbited the earth in an eccentric orbit. It was shown that the attitude motion culminates into a libratory planar motion about the pitch axis that is determined in part by the orbital parameters such as eccentricity and true anomaly. The motion analysis showed a quasi-periodic, chaotic motion that was marginally stable. Further, the post bifurcation behavior indicated the establishment of locally stable limit cycles through the constructed versal deformations of the normal

forms intended to scrutinize the attitude dynamics bifurcation behavior. The oscillatory nature of the pitch attitude necessitated a control regime in order to stabilize the spacecraft's attitude. As a result we demonstrated how linear and nonlinear control laws can be developed to control the oscillations. The control laws were developed in the transformed coordinates of either L-F transformation or normal forms. Only the nonlinear controllers (i.e. sliding mode and bifurcation control) were shown to be capable of controlling the attitude dynamics. Consequently, our methodology showed how to analyze and control the parametrically excited nonlinear attitude dynamics with external periodic excitation in a more accurate manner using Floquet theory, center manifold reduction and normal forms.

In the second part of the dissertation, we investigated the motion of spacecraft in the vicinity of small irregularly shaped bodies. The unique challenges associated with dynamics in the vicinity of such bodies necessitated the construction of adaptable analytical dynamics models that accounted for the irregularities in the mass properties and gravitational potential. Consequently, we briefly outlined the main approaches in developing gravitational gradient models highlighting their fundamental concepts, advantages, drawbacks and applications. Using the simplest non-trivial second degree and order spherical harmonic model, we formulated the dynamical model for motion in the vicinity of a small irregular shaped body and considered a more complex scenario involving the small body's periodic angular velocity vector about its COM in the local coordinate frame. We applied this formulation to asteroid 4179 Toutatis and numerically showed how unfavorable quasi-periodic, erratic orbits characterized motion in the vicinity of this small body. Subsequently, using our methodology that involved L-F transformation, center manifold reduction and normal forms, we were able to analyze and control the dynamics in the vicinity of Toutatis and realize a regular periodic trajectory that is more conducive to space mis-

sion design. Once again our approach enabled analysis of the dynamics and formulation of viable control laws that were implemented in closed-form solutions.

This dissertation extended normal forms simplification and center manifold reduction to parametrically excited nonlinear systems with external periodic excitation in a lucid, straightforward and broadly applicable manner. This accomplishment was definitively facilitated by the intuitive system states augmentation process we introduced. In doing so, we made the following contributions as the novelty of our research to these two fields. Our methodologies,

i) unify analysis of parametrically excited nonlinear systems and nonlinear systems with constant coefficients.
ii) are liberated from the need for special strategies such as detuning parameters, 'book-keeping' parameters, *ad-hoc* unsolved ODEs etc., normally included in finding the normal forms or center manifold reduction of parametrically excited nonlinear c=systems with external forcing.
iii) do not mandate the system to be minimally excited.
iv) are based on intuitively augmented system states that are neither *ad-hoc* nor arbitrarily introduced, hence the approaches are applicable in a consistent manner.
v) utilize augmented states that have a consistent, plain and direct affiliation with the excitation frequency terms.
vi) are seamlessly applicable over a broad range of nonlinear systems subjected to external periodic excitation in order to obtain either the normal forms or center manifold reduction (or both).

Additional contributions in the specific dynamical problems studies are described below

7.1.1 Part I: Gravity Gradient Attitude Motion

We demonstrated an analytical methodology for analyzing the parametrically excited nonlinear dynamics with external periodic excitation of the attitude motion for a gravity gradient stabilized spacecraft that investigates stability, chaos and periodicity. Importantly, this methodology solves the dynamics to yield closed-form analytical solutions.

This dissertation showed that the attitude motion is quasi-periodic and chaotic. Further, we constructed a stability chart that facilitated the prediction of $(e-\sigma)$ combinations that cause stable or unstable dynamics. The stable regions of the stability chart were found to predict marginal and not asymptotically stable dynamics.

Our bifurcation analysis established that the attitude motion undergoes a Hopf bifurcation in the neighborhood of the critical point, e_c.

Our versal deformation analysis showed that the attitude motion's post bifurcation behavior establish locally stable limit cycles and relatively small deviations from the critical point, e_c of the order $10^{-4} < \eta < 10^{-3}$ trigger a significant topological change in the structure of the attitude motion flow.

We showed how the parametrically excited motion with external periodic excitation can be transformed into topologically equivalent domains that are amenable to conventional control law synthesis techniques.

Using representative $e - \sigma$ pairs, we showed that linear control strategies were unable to control the planar nonlinear attitude motion.

On the other hand, we demonstrated how the robust control sliding mode control law stabilized the attitude motion and eliminated oscillations of the pitch angle.

To check the chaotic post-bifurcation behavior with undesired librations, we demonstrated how to design a bifurcation controller via the normal form and showed that this

nonlinear control strategy stabilizes the motion by significantly diminishing emanating pitch angle oscillations.

7.1.2 Part II: Motion in the Vicinity of Small Irregularly Shaped Bodies

We demonstrated how to model the periodic perturbing accelerations in the vicinity of small irregularly shaped bodies using a generalized periodic function that facilitates analysis of motion in the vicinity of such bodies. The function can be extended to represent constant perturbations as well.

We have developed an adaptable analytical model that accurately described the irregularities of the body's dynamical environment including the periodic external perturbations.

We demonstrated an analytical methodology for analyzing the parametrically excited nonlinear dynamics with external periodic excitation of the motion in the vicinity of small irregularly shaped bodies. With application to Toutatis, we showed how this methodology investigates stability, chaos and periodicity. Importantly, this methodology solves the dynamics to yield closed-form analytical solutions.

Our analysis showed that the dynamics in the vicinity of Toutatis spawn erratic trajectories with abrupt deflections which would significantly impinge on the ability of spacecraft to conduct effective scientific mission.

We showed how the parametrically excited dynamics with external periodic excitation that describes motion in the vicinity of ISSB can be transformed into topologically equivalent but simplified normal forms that are amenable to conventional control law synthesis techniques.

We demonstrated how the nonlinear control law developed in the normal forms do-

main stabilized the motion in close proximity of Toutatis by eliminating erratic behavior to yield regular periodic trajectories that are conducive to mission design.

By solving the system equations in their normal forms, we were able to realize a closed-form analytical solutions to dynamical systems that were not analytically solvable into closed-form solutions, to begin with.

7.2 Future Research Directions

The demonstrated plain order reduction methodology can be extended to general MOR of forced nonlinear systems despite being applied here to strictly obtain center manifold reduction. This is because the external periodic excitation is comprehensively retained in the augmented system facilitating general model order reduction approaches. Consequently, retention of the forcing term(s) is similarly achieved in the reduced-order system model irrespective of the MOR technique followed. Therefore, future work will include the application of the intuitive state augmentation in other MOR techniques for nonlinear systems with external periodic excitation. Another area of future investigation by this technique includes the application of this methodology in general MOR techniques to be employed in the rapid development of fractional systems.

In future, the normal forms simplification technique should be extended to the frequency response analysis of parametrically excited nonlinear systems with periodic external excitation. Specifically, how to back-transform the normal forms into original coordinates to specify multiple system amplitudes corresponding to a the same value of external excitation frequency.

The gravity gradient investigation in future would consider torques generated by sources such as magnetism and oblateness of the earth, atmospheric drag, solar radiation

pressure, thermal bending etc. Further, nonlinearities beyond the cubic term in the LFT and TDNF cases of near identity transformation would also be analyzed.

Also, future work in gravity gradient stabilization should focus on physical implementation of the controllers and deriving TDNF based control laws. As demonstrated, all the control effort inputs are single torques per unit moment of inertia which for instance can be implemented via thrusters. Consequently, sizing and implementation of the control effort is a crucial task.

Secular perturbations should be modeled and integrated in to the future analysis of dynamics in the vicinity of small irregularly shaped bodies.

Additionally, further refinement and improvement and refinement of the developed function to model periodic perturbations is required. This would include validating the model with observed data.

In future, generalized methods to find periodic orbits in the vicinity of small irregularly shaped bodies should be explored.

Also, future work related to control of spacecraft in the vicinity of small irregular shaped bodies should investigate the physical implementation of the controllers. As demonstrated, all the control effort inputs are input accelerations which for instance can be implemented via thrusters. Consequently, sizing and implementation of the control effort is a crucial task.

REFERENCES

[1] Union of Concerned Scientists, UCS, *Satellite Database*, http://www.ucsusa.org/nuclear-weapons/space-weapons/satellite-database, Accessed: 2019-1-17.

[2] The Planetary Society, *Mission Index*, http://www.planetary.org/explore/space-topics/space-missions/, Accessed: 2019-1-17.

[3] P. M. Waswa and S. Redkar, "A survey of space mission architecture and system actualisation methodologies," *International Journal of Space Science and Engineering*, vol. 4, no. 3, pp. 234–252, Jul. 2017. DOI: 10.1504/IJSPACESE.2017.085674.

[4] W. J. Larson and J. R. Wertz, Eds., *Space Missions Analysis and Design*, 3^{rd} Edition, Space Technology Series, El Segundo, CA: Microcosm Press, 2006.

[5] B. Wie, *Space Vehicle Dynamics and Control*, 2^{nd} Edition, AIAA Education Series, Reston, VA: American Institute of Aeronautics and Astronautics, 2008.

[6] K. Alfriend, S. Vadali, P. Gurfil, J. How, and L. Breger, *Spacecraft Formation Flying: Dynamics, Control and Navigation*, ser. Elsevier Astrodynamics Series. Elsevier Science, 2009. [Online]. Available: https://books.google.com/books?id=6EidgM-aX%5C_oC.

[7] B. A. McElhoe, "An assessment of the navigation and course corrections for a manned flyby of mars or venus," *IEEE Transactions on Aerospace and Electronic Systems*, vol. AES-2, no. 4, pp. 613–623, Jul. 1966. DOI: 10.1109/TAES.1966.4501892.

[8] M. Noton, *Spacecraft Navigation and Guidance*, ser. Advances in Industrial Control. Springer London, 2012. [Online]. Available: https://books.google.com/books?id=mlPlBwAAQBAJ.

[9] T. Kubota, T. Hashimoto, J. Kawaguchi, M. Uo, and K. Shirakawa, "Guidance and navigation of hayabusa spacecraft for asteroid exploration and sample return mission," in *2006 SICE-ICASE International Joint Conference*, Oct. 2006, pp. 2793–2796. DOI: 10.1109/SICE.2006.314761.

[10] G. Deaconu, C. Louembet, and A. Théron, "Minimizing the effects of navigation uncertainties on the spacecraft rendezvous precision," eng, *Journal of Guidance, Control, and Dynamics*, vol. 37, no. 2, pp. 695–700, 2014.

[11] G. A. M. James F. Jordan and G. E. Pease, "Effects of major errors sources on planetary spacecraft navigation accuracies," eng, *Journal of Spacecraft and Rockets*, vol. 9, no. 3, pp. 196–204, 1972. DOI: https://doi.org/10.2514/3.61649.

[12] A. Suleman, "Multibody dynamics and nonlinear control of flexible space structures," *Modal Analysis*, vol. 10, no. 11, pp. 1639–1661, 2004. DOI: 10.1177/1077546304042049. eprint: https://doi.org/10.1177/1077546304042049. [Online]. Available: https://doi.org/10.1177/1077546304042049.

[13] V. V. Beletskii, *Librations on an Eccentric Orbit: NASA Technical Translation F-8504*. National Aeronautics and Space Administration: Washington DC. USA, 1963.

[14] H. A. Fujii and W. Ichiki, "Nonlinear dynamics of the tethered subsatellite system in the station keeping phase," *Journal of Guidance, Control, and Dynamics*, vol. 20, no. 2, pp. 403–406, May 2011. DOI: https://doi.org/10.2514/2.4057.

[15] V. V. Beletskii, *Motion of an Artificial Satellite About its Center of Mass: NASA Technical Translation F-429*. U.S. Dept. Commerce: Springfield, Va. USA, 1963.

[16] R. E. Sherrill, A. J. Sinclair, S. C. Sinha, and T. A. Lovell, "Lyapunov-floquet control of satellite relative motion in elliptic orbits," *IEEE Transactions on Aerospace and Electronic Systems*, vol. 51, no. 4, pp. 2800–2810, Oct. 2015. DOI: 10.1109/TAES.2015.140281.

[17] P. Massioni, T. Keviczky, E. Gill, and M. Verhaegen, "A decomposition-based approach to linear time-periodic distributed control of satellite formations," *IEEE Transactions on Control Systems Technology*, vol. 19, no. 3, pp. 481–492, May 2011. DOI: 10.1109/TCST.2010.2051228.

[18] L. Chappaz and K. C. Howell, "Trajectory design for bounded motion near uncertain binary systems comprised of small irregular bodies exploiting sliding control modes," *Acta Astronautica*, vol. 115, pp. 226–240, 2015. DOI: https://doi.org/10.1016/j.actaastro.2015.05.027. [Online]. Available: http://www.sciencedirect.com/science/article/pii/S0094576515002118.

[19] D. Lee and G. Vukovich, "Adaptive sliding mode control for spacecraft body-fixed hovering in the proximity of an asteroid," *Aerospace Science and Technology*, vol. 46, pp. 471–483, 2015. DOI: https://doi.org/10.1016/j.ast.2015.09.001. [Online]. Available: http://www.sciencedirect.com/science/article/pii/S1270963815002509X.

[20] M. Nazari, R. Wauson, T. Critz, E. A. Butcher, and D. J. Scheeres, "Observer-based body-frame hovering control over a tumbling asteroid," *Acta Astronautica*, vol. 102, pp. 124–139, 2014. DOI: https://doi.org/10.1016/j.actaastro.2014.05.016. [Online]. Available: http://www.sciencedirect.com/science/article/pii/S0094576514001763.

[21] D. L. Mingori, "Effects of energy dissipation on the attitude stability of dual-spinsatellites," *AIAA Journal*, vol. 7, no. 1, pp. 20–27, 1969. DOI: https://doi.org/10.2514/3.5029.

[22] Y. Jiang and H. Baoyin, "Periodic orbit families in the gravitational field of irregular-shaped bodies," *The Astronomical Journal*, vol. 152, no. 5, p. 137, 2016. [Online]. Available: http://stacks.iop.org/1538-3881/152/i=5/a=137.

[23] M. Vetrisano and M. Vasile, "Autonomous navigation of a spacecraft formation in the proximity of an asteroid," *Advances in Space Research*, vol. 57, no. 8, pp. 1783–1804, 2016, Advances in Asteroid and Space Debris Science and Technology - Part 2. DOI: https://doi.org/10.1016/j.asr.2015.07.024. [Online]. Available: http://www.sciencedirect.com/science/article/pii/S0273117715005268.

[24] H. Kojima, M. Iwasaki, H. A. Fujii, C. Blanksby, and P. Trivailo, "Nonlinear control of librational motion of tethered satellites in elliptic orbits," *American Institute of Aeronautics and Astronautics - Journal of Guidance, Control, and Dynamics*, vol. 27, no. 2, pp. 229–239, 2004.

[25] S. Sinha, D. Wu, V. Juneja, and P. Joseph, "Analysis of dynamic systems with periodically varying parameters via chebyshev polynomials," *Journal of Vibration and Acoustics*, vol. 115, no. 1, pp. 96–102, 1993.

[26] T. L. Vincent and W. J. Grantham, *Nonlinear and optimal control systems*. John Wiley & Sons, 1997.

[27] V. A. Yakubovich and V. M. Starzhinskii, *Linear differential equations with periodic coefficients, Vols I and II*. New York: John Wiley and Sons, 1975.

[28] W. Johnson, "Perturbation solutions for the influence of forward flight on helicopter rotor flapping stability," *NASA TM X-62*, p. 165, 1974.

[29] D. W. Jordan and P. Smith, *Nonlinear Ordinary Differential Equations: An Introduction for Scientists and Engineers*, 4^{th}. Great Clarendon Street, Oxford: Oxford University Press, 2007.

[30] M. Lovera, E. D. Marchi, and S. Bittanti, "Periodic attitude control techniques for small satellites with magnetic actuators," *IEEE Transactions on Control Systems Technology*, vol. 10, no. 1, pp. 90–95, Jan. 2002.

[31] F. D. Rossa, F. Dercole, and M. Lovera, "Attitude stability analysis for an earth pointing, magnetically controlled spacecraft," *IFAC Proceedings Volumes*, vol. 46, no. 19, pp. 518–523, 2013, 19th IFAC Symposium on Automatic Control in Aerospace.

[32] J. Sheng, O. Elbeyli, and J. Q. Sun, "Stability and optimal feedback controls for time-delayed linear periodic systems," *American Institute of Aeronautics and Astronautics Journal*, vol. 42, no. 5, pp. 908–911, 2004.

[33] H. D'Angelo, *Linear time-varying systems : analysis and synthesis*. Boston : Allyn and Bacon, 1970.

[34] S. Sinha and P. Joseph, "Control of general dynamic systems with periodically varying parameters via Liapunov-Floquet transformation," *Transanctions-American Society of Mechanical Engineers Journal of Dynamic Systems Measurement and Control*, vol. 116, pp. 650–650, 1994.

[35] R. E. Sherrill, A. J. Sinclair, S. C. Sinha, and T. A. Lovell, "Time-varying transformations for hill–clohessy–wiltshire solutions in elliptic orbits," *Celestial Mechanics and Dynamical Astronomy*, vol. 119, no. 1, pp. 55–73, May 2014. DOI: 10.1007/s10569-014-9543-x. [Online]. Available: https://doi.org/10.1007/s10569-014-9543-x.

[36] A. Gabale and S. Sinha, "A direct analysis of nonlinear systems with external periodic excitations via normal forms," *Nonlinear Dynamics*, vol. 55, no. 1-2, pp. 79–93, 2009.

[37] L. Jezequel and C. Lamarque, "Analysis of non-linear dynamical systems by the normal form theory," eng, *Journal of Sound and Vibration*, vol. 149, no. 3, pp. 429–459, 1991.

[38] A. H. Nayfeh, *Method of normal forms*, eng, ser. Wiley series in nonlinear science. New York: Wiley, 1993.

[39] S. A. Neild, A. R. Champneys, D. J. Wagg, T. L. Hill, and A. Cammarano, "The use of normal forms for analysing nonlinear mechanical vibrations," *Philosophical Transactions of the Royal Society of London A: Mathematical, Physical and Engineering Sciences*, vol. 373, no. 2051, 2015. DOI: 10.1098/rsta.2014.0404.

[40] S. A. Neild and D. J. Wagg, "Applying the method of normal forms to second-order nonlinear vibration problems," *Proceedings of the Royal Society A: Mathematical, Physical and Engineering Sciences*, vol. 467, no. 2128, pp. 1141–1163, 2011. DOI: 10.1098/rspa.2010.0270. [Online]. Available: https://royalsocietypublishing.org/doi/abs/10.1098/rspa.2010.0270.

[41] C. Touzé, O. Thomas, and A. Chaigne, "Hardening/softening behaviour in non-linear oscillations of structural systems using non-linear normal modes," *Journal of Sound and Vibration*, vol. 273, no. 1, pp. 77–101, 2004. DOI: https://doi.org/10.1016/j.jsv.2003.04.005. [Online]. Available: http://www.sciencedirect.com/science/article/pii/S0022460X03010083.

[42] C. Touzé and M. Amabili, "Nonlinear normal modes for damped geometrically nonlinear systems: Application to reduced-order modelling of harmonically forced structures," *Journal of Sound and Vibration*, vol. 298, no. 4, pp. 958–981, 2006. DOI: https://doi.org/10.1016/j.jsv.2006.06.032. [Online]. Available: http://www.sciencedirect.com/science/article/pii/S0022460X06005141.

[43] Z. Xin, Z. Zuo, H. Feng, D. Wagg, and S. A. Neild, "Higher order accuracy analysis of the second-order normal form method," *Nonlinear Dynamics*, vol. 70, pp. 2175–2185, 2012.

[44] T. Pumhössel, P. Hehenberger, and K. Zeman, "Reduced-order modelling of self-excited, time-periodic systems using the method of proper orthogonal decomposition and the floquet theory," *Mathematical and Computer Modelling of Dynamical Systems*, vol. 20, no. 6, pp. 528–545, 2014. DOI: 10.1080/13873954.2014.880181. eprint: https://doi.org/10.1080/13873954.2014.880181. [Online]. Available: https://doi.org/10.1080/13873954.2014.880181.

[45] G. Haller and S. Ponsioen, "Nonlinear normal modes and spectral submanifolds: Existence, uniqueness and use in model reduction," *Nonlinear Dynamics*, vol. 86, no. 3, pp. 1493–1534, Nov. 2016. DOI: 10.1007/s11071-016-2974-z. [Online]. Available: https://doi.org/10.1007/s11071-016-2974-z.

[46] S. Jain, P. Tiso, and G. Haller, "Exact nonlinear model reduction for a von kármán beam: Slow-fast decomposition and spectral submanifolds," *Journal of Sound and Vibration*, vol. 423, pp. 195–211, 2018. DOI: https://doi.org/10.1016/j.jsv.2018.01.049. [Online]. Available: http://www.sciencedirect.com/science/article/pii/S0022460X18300713.

[47] G. Agnes and D. Inman, "Performance of nonlinear vibration absorbers for multi-degrees-of-freedom systems using nonlinear normal modes," eng, *Nonlinear Dynamics*, vol. 25, no. 1, pp. 275–292, 2001.

[48] S. W. Shaw, C. Pierre, and E. Pesheck, "Modal analysis-based reduced-order models for nonlinear structures–an invariant manifold approach," *The Shock and Vibration Digest*, vol. 30, no. 1, pp. 3–16, 1999. DOI: 10.1177/058310249903100101.

[49] D. Jiang, C. Pierre, and S. Shaw, "Nonlinear normal modes for vibratory systems under harmonic excitation," eng, *Journal of Sound and Vibration*, vol. 288, no. 4-5, pp. 791–812, 2005.

[50] K. Avramov and Y. Mikhlin, "Review of applications of nonlinear normal modes for vibrating mechanical systems," English, *Applied Mechanics Reviews*, vol. 65, no. 2, 2013.

[51] S. Redkar and S. Sinha, "Reduced order modeling of nonlinear time periodic systems subjected to external periodic excitations," eng, *Communications in Nonlinear Science and Numerical Simulation*, vol. 16, no. 10, pp. 4120–4133, 2011.

[52] A. P. Gabale and S. Sinha, "Model reduction of nonlinear systems with external periodic excitations via construction of invariant manifolds," eng, *Journal of Sound and Vibration*, vol. 330, no. 11, pp. 2596–2607, 2011.

[53] S. Sinha, S. Redkar, and E. A. Butcher, "Order reduction of nonlinear systems with time periodic coefficients using invariant manifolds," eng, *Journal of Sound and Vibration*, vol. 284, no. 3, pp. 985–1002, 2005.

[54] R. Wisniewski and M. Blanke, "Fully magnetic attitude control for spacecraft subject to gravity gradient," *Automatica*, vol. 35, no. 7, pp. 1201–1214, 1999.

[55] C. Arduini and P. Baiocco, "Active magnetic damping attitude control for gravity gradient stabilized spacecraft," *Journal of Guidance, Control, and Dynamics*, vol. 20, no. 1, pp. 117–122, 1997, American Institute of Aeronautics and Astronautics.

[56] P. M. Waswa and S. Redkar, "Control of nonlinear spacecraft attitude motion via state augmentation, lyapunov-floquet transformation and normal forms," *Advances in Space Research*, vol. 64, no. 3, pp. 668–686, 2019. DOI: doi.org/10.1016/j.asr.2019.05.013. [Online]. Available: http://www.sciencedirect.com/science/article/pii/S0273117719303400.

[57] F. Chernous'ko, "On the motion of a satellite about its center of mass under the action of gravitational moments," *Journal of Applied Mathematics and Mechanics*, vol. 27, no. 3, pp. 708–722, 1963.

[58] T. Kane, "Attitude stability of earth-pointing satellites," *AIAA Journal*, vol. 3, pp. 726–731, Apr. 1965. DOI: 10.2514/3.2955.

[59] J. Breakwell and R. Pringle Jr, "Nonlinear resonance affecting gravity-gradient stability," in *Astrodynamics*, 16th International Astronautical Congress, Athens, Greece, 1965, pp. 305–325.

[60] Wikipedia, *List of Solar System probes*, https://en.wikipedia.org/wiki/List_of_Solar_System_probes, Accessed: 2018-1-19.

[61] National Aeronautics and Space Administration, *NASA Selects Two Missions to Explore the Early Solar System*, https://www.nasa.gov/press-release/nasa-selects-two-missions-to-explore-the-early-solar-system, Accessed: 2018-1-19.

[62] NASA, *OSIRIS-REx Asteroid Sample Return Mission*, https://www.nasa.gov/osiris-rex, Accessed: 2018-1-19.

[63] D. Scheeres, *Orbital Motion in Strongly Perturbed Environments: Applications to Asteroid, Comet and Planetary Satellite Orbiters*, ser. Springer Praxis Books. Springer Berlin Heidelberg, 2016. [Online]. Available: https://books.google.com/books?id=kAuPDAAAQBAJ.

[64] Y. Yu and H. Baoyin, "Orbital dynamics in the vicinity of asteroid 216 kleopatra," *The Astronomical Journal*, vol. 143, no. 3, p. 62, Feb. 2012. DOI: 10.1088/0004-6256/143/3/62. [Online]. Available: https://doi.org/10.1088%2F0004-6256%2F143%2F3%2F62.

[65] D. Scheeres, S. Ostro, R. Hudson, E. DeJong, and S. Suzuki, "Dynamics of orbits close to asteroid 4179 toutatis," *Icarus*, vol. 132, no. 1, pp. 53–79, 1998. DOI: https://doi.org/10.1006/icar.1997.5870. [Online]. Available: http://www.sciencedirect.com/science/article/pii/S001910359795870X.

[66] D. Scheeres, "Orbital mechanics about small bodies," *Acta Astronautica*, vol. 72, pp. 1–14, 2012. DOI: https://doi.org/10.1016/j.actaastro.2011.10.021. [Online]. Available: http://www.sciencedirect.com/science/article/pii/S0094576511003237.

[67] D. Scheeres, S. V. wal, Z. Olikara, and N. Baresi, "Dynamics in the Phobos environment," *Advances in Space Research*, vol. 63, no. 1, pp. 476–495, 2019. DOI: https://doi.org/10.1016/j.asr.2018.10.016. [Online]. Available: http://www.sciencedirect.com/science/article/pii/S0273117718307853.

[68] D. J. Scheeres, B. G. Williams, and J. K. Miller, "Evaluation of the dynamic environment of an asteroid: Applications to 433 eros," *Journal of Guidance, Control, and Dynamics*, vol. 23, no. 3, pp. 466–475, 2000. DOI: 10.2514/2.4552. eprint: https://doi.org/10.2514/2.4552. [Online]. Available: https://doi.org/10.2514/2.4552.

[69] J. Feng, R. Noomen, P. N. A. M. Visser, and J. Yuan, "Modeling and analysis of periodic orbits around a contact binary asteroid," *Astrophysics and Space Science*, vol. 357, no. 2, p. 124, May 2015. DOI: 10.1007/s10509-015-2353-0. [Online]. Available: https://doi.org/10.1007/s10509-015-2353-0.

[70] W.-D. Hu and D. J. Scheeres, "Periodic orbits in rotating second degree and order gravity fields," *Chinese Journal of Astronomy and Astrophysics*, vol. 8, no. 1, pp. 108–118, Feb. 2008. DOI: 10.1088/1009-9271/8/1/12. [Online]. Available: https://doi.org/10.1088%2F1009-9271%2F8%2F1%2F12.

[71] Y. Jiang and H. Baoyin, "Orbital mechanics near a rotating asteroid," *Journal of Astrophysics and Astronomy*, vol. 35, no. 1, pp. 17–38, Mar. 2014. DOI: 10.1007/s12036-014-9259-z. [Online]. Available: https://doi.org/10.1007/s12036-014-9259-z.

[72] H. Shang, X. Wu, and P. Cui, "Periodic orbits in the doubly synchronous binary asteroid systems and their applications in space missions," *Astrophysics and Space Science*, vol. 355, no. 1, pp. 69–87, Jan. 2015. DOI: 10.1007/s10509-014-2154-x. [Online]. Available: https://doi.org/10.1007/s10509-014-2154-x.

[73] Y. Shi, Y. Wang, and S. Xu, "Global search for periodic orbits in the irregular gravity field of a binary asteroid system," *Acta Astronautica*, 2018. DOI: https://doi.org/10.1016/j.actaastro.2018.10.014. [Online]. Available: http://www.sciencedirect.com/science/article/pii/S009457651831244X.

[74] S. B. Broschart and D. J. Scheeres, "Control of hovering spacecraft near small bodies: Application to asteroid 25143 itokawa," *Journal of Guidance, Control, and Dynamics*, vol. 28, no. 2, pp. 343–354, 2005. DOI: 10.2514/1.3890. eprint: https://doi.org/10.2514/1.3890. [Online]. Available: https://doi.org/10.2514/1.3890.

[75] S. Sinha and R. Pandiyan, "Analysis of quasilinear dynamical systems with periodic coefficients via liapunov-floquet transformation," *International Journal of Non-Linear Mechanics*, vol. 29, no. 5, pp. 687–702, 1994.

[76] E. A. Butcher and S. C. Sinha, "Normal forms and the structure of resonance sets in nonlinear time-periodic systems," *Nonlinear Dynamics*, vol. 23, no. 1, pp. 35–

55, Sep. 2000. DOI: 10.1023/A:1008312424551. [Online]. Available: https://doi.org/10.1023/A:1008312424551.

[77] G. Floquet, "Sur les équations différentielles linéaires á coefficients périodiques," fre, *Annales scientifiques de l'École Normale Supérieure*, vol. 12, pp. 47–88, 1883. [Online]. Available: http://eudml.org/doc/80895.

[78] A. Coddington and N. Levinson, *Theory of ordinary differential equations*, ser. International series in pure and applied mathematics. McGraw-Hill, 1955.

[79] A. Nayfeh and B. Balachandran, *Applied Nonlinear Dynamics: Analytical, Computational and Experimental Methods*, ser. Wiley Series in Nonlinear Science. New York, NY: Wiley & Sons Inc, 1995.

[80] S. Sinha, "On the analysis of time-periodic nonlinear dynamical systems," English, *Sadhana-Academy Proceedings In Engineering Sciences*, vol. 22, pp. 411–434, 1997.

[81] J. Mason and D. Handscomb, *Chebyshev Polynomials*. Boca Raton, Florida: CRC Press, 2003.

[82] H. Poincaré, *Les méthodes nouvelles de la mécanique céleste, Volume 1*. Paris: Gauthier-Villars, 1892.

[83] H. Dulac, "Solutions of a system of differential equations in the neighborhood of singular values," fr, *Bulletin of the Mathematical Society of France*, vol. 40, pp. 324–383, 1912. DOI: 10.24033/bsmf.910. [Online]. Available: http://www.numdam.org/item/BSMF_1912__40__324_0.

[84] G. Birkhoff, *Dynamical Systems*, ser. American Mathematical Society / Providence, Estados Unidos. American Mathematical Society, 1927. [Online]. Available: https://books.google.com/books?id=ygmWAwAAQBAJ.

[85] L. O. Chua and H. Kokubu, "Normal forms for nonlinear vector fields. i. theory and algorithm," *IEEE Transactions on Circuits and Systems*, vol. 35, no. 7, pp. 863–880, Jul. 1988. DOI: 10.1109/31.1833.

[86] C.-H. Lamarque, C. Touzé, and O. Thomas, "An upper bound for validity limits of asymptotic analytical approaches based on normal form theory," *Nonlinear Dynamics*, vol. 70, no. 3, pp. 1931–1949, Nov. 2012. DOI: 10.1007/s11071-012-0584-y. [Online]. Available: https://doi.org/10.1007/s11071-012-0584-y.

[87] V. Arnold, K. Vogtmann, and A. Weinstein, *Mathematical Methods of Classical Mechanics*, ser. Graduate Texts in Mathematics. Springer New York, 2013. [Online]. Available: https://books.google.com/books?id=UOQlBQAAQBAJ.

[88] J. Moser, *Stable and Random Motions in Dynamical Systems: With Special Emphasis on Celestial Mechanics (AM-77)*, ser. Princeton Landmarks in Mathematics and Physics. Princeton University Press, 2016. [Online]. Available: https://books.google.com/books?id=6MXdCwAAQBAJ.

[89] H. L. Smith, "Normal forms for periodic systems," eng, *Journal of Mathematical Analysis and Applications*, vol. 113, no. 2, pp. 578–600, 1986.

[90] C. Elphick, G. Iooss, and E. Tirapegui, "Normal form reduction for time-periodically driven differential equations," *Physics Letters A*, vol. 120, no. 9, pp. 459–463, 1987. DOI: https://doi.org/10.1016/0375-9601(87)90110-1. [Online]. Available: http://www.sciencedirect.com/science/article/pii/0375960187901101.

[91] D. Baleanu, J. Asad, and A. Jajarmi, "The fractional model of spring pendulum: New features within different kernels," 3/2018, vol. 19, 2018, pp. 447–454.

[92] D. Baleanu, S. Sadat Sajjadi, A. Jajarmi, and J. Asad, "New features of the fractional euler-lagrange equations for a physical system within non-singular derivative operator," *The European Physical Journal Plus*, vol. 134, no. 4, p. 181, Apr. 2019. DOI: 10.1140/epjp/i2019-12561-x. [Online]. Available: https://doi.org/10.1140/epjp/i2019-12561-x.

[93] M. S. Mahmoud, *Large scale systems modelling*, eng, 1st ed.., ser. International series on systems and control ; v. 3. Oxford [Oxfordshire] ; New York: Pergamon Press, 1981.

[94] A. Antoulas, *Approximation of large-scale dynamical systems*, eng, ser. Advances in design and control. Philadelphia: Society for Industrial and Applied Mathematics, 2005.

[95] C. Wang, H. Yu, P. Li, J. Wu, and C. Ding, "Model order reduction for transient simulation of active distribution networks," eng, *IET Generation, Transmission and Distribution*, vol. 9, no. 5, pp. 457–467, 2015.

[96] R. J. Guyan, "Reduction of stiffness and mass matrices," eng, *AIAA Journal*, vol. 3, no. 2, pp. 380–380, 1965.

[97] G. Rega and H. Troger, "Dimension reduction of dynamical systems: Methods, models, applications," eng, *Nonlinear Dynamics*, vol. 41, no. 1, pp. 1–15, 2005.

[98] A. Steindl and H. Troger, "Methods for dimension reduction and their application in nonlinear dynamics," eng, *International Journal of Solids and Structures*, vol. 38, no. 10, pp. 2131–2147, 2001.

[99] J. Guckenheimer, *Nonlinear oscillations, dynamical systems, and bifurcations of vector fields*, eng, ser. Applied mathematical sciences (Springer-Verlag New York Inc.) ; v. 42. New York: Springer-Verlag, 1983.

[100] J. Carr, *Applications of centre manifold theory*, eng, ser. Applied mathematical sciences (Springer-Verlag New York Inc.) ; v. 35. New York: Springer-Verlag, 1981.

[101] S. Sastry, *Nonlinear systems : analysis, stability, and control*, eng, ser. Interdisciplinary applied mathematics ; v. 10. New York: Springer, 1999.

[102] I. G. Malkin, *Some problems in the theory of nonlinear oscillations*, eng ; rus. U.S. Atomic Energy Commission, Technical Information Service, 1959. [Online]. Available: http://hdl.handle.net/2027/mdp.39015017402986.

[103] A. Fleig Jr., *On the Libration of a Gravity Gradient Stabilized Spacecraft in an Eccentric Orbit*, ser. NASA TECHNICAL REPORT R-350. Washington, DC, USA: National Aeronautics and Space Administration, 1970.

[104] E. Herman, *Convergence, approximation, and differential equations*. Wiley, 1986.

[105] N. H. Driscoll T. A. and L. Trefethen, Eds., *Chebfun guide: For chebfun version 5*, www.chebfun.org, 2014.

[106] S. Wiggins, *Introduction to Applied Nonlinear Dynamical Systems and Chaos*, ser. Texts in Applied Mathematics. Springer New York, 2003. [Online]. Available: https://books.google.com/books?id=RSI4RGdwnU4C.

[107] A. Dávid and S. C. Sinha, "Versal deformation and local bifurcation analysis of time-periodic nonlinear systems," *Nonlinear Dynamics*, vol. 21, no. 4, pp. 317–336, Apr. 2000. DOI: 10.1023/A:1008330023291. [Online]. Available: https://doi.org/10.1023/A:1008330023291.

[108] G. Franklin, J. Powell, and A. Emami-Naeini, *Feedback Control of Dynamic Systems, Global Edition*. Pearson Education Limited, 2015. [Online]. Available: https://books.google.com/books?id=ZV-pBwAAQBAJ.

[109] V. I. Utkin, *Sliding modes and their application in variable structure systems*, eng, Rev. from the 1974 ed.. Moscow: Mir Publishers, 1978.

[110] J. J. Slotine and S. S. Sastry, "Tracking control of non-linear systems using sliding surfaces with application to robot manipulators," in *1983 American Control Conference*, Jun. 1983, pp. 132–135. DOI: 10.23919/ACC.1983.4788090.

[111] P. Kachroo and M. Tomizuka, "Chattering reduction and error convergence in the sliding-mode control of a class of nonlinear systems," *IEEE Transactions on Automatic Control*, vol. 41, no. 7, pp. 1063–1068, Jul. 1996. DOI: 10.1109/9.508917.

[112] C. D. Murray, *Solar system dynamics*, eng. Cambridge , New York: Cambridge University Press, 1999.

[113] Y. Jiang and H. Baoyin, "Periodic orbit families in the gravitational field of irregular-shaped bodies," *The Astronomical Journal*, vol. 152, no. 5, p. 137, Oct. 2016. DOI: 10.3847/0004-6256/152/5/137. [Online]. Available: https://doi.org/10.3847%2F0004-6256%2F152%2F5%2F137.

[114] W. M. Kaula, *Theory of satellite geodesy; applications of satellites to geodesy*, eng. Waltham, Mass.: Blaisdell Pub. Co, 1966.

[115] W. D. MacMillan, *The theory of the potential,* eng, 1st ed.., ser. His Theoretical mechanics. New York [etc.: McGraw-Hill book company, inc., 1930.

[116] Y. Takahashi, D. J. Scheeres, and R. A. Werner, "Surface gravity fields for asteroids and comets," *Journal of Guidance, Control, and Dynamics*, vol. 36, no. 2, pp. 362–374, 2013. DOI: 10.2514/1.59144. eprint: https://doi.org/10.2514/1.59144. [Online]. Available: https://doi.org/10.2514/1.59144.

[117] Y. Yu, *Orbital Dynamics in the Gravitational Field of Small Bodies*, ser. Springer Theses. Springer Berlin Heidelberg, 2016. [Online]. Available: https://books.google.com/books?id=tHpBDAAAQBAJ.

[118] E. W. Hobson, *The theory of spherical and ellipsoidal harmonics,* eng. Cambridge [Eng.: The University press, 1931.

[119] R. A. Werner, "The gravitational potential of a homogeneous polyhedron or don't cut corners," *Celestial Mechanics and Dynamical Astronomy*, vol. 59, no. 3, pp. 253–278, Jul. 1994. DOI: 10.1007/BF00692875. [Online]. Available: https://doi.org/10.1007/BF00692875.

[120] G. Romain and B. Jean-Pierre, "Ellipsoidal harmonic expansions of the gravitational potential: Theory and application," *Celestial Mechanics and Dynamical Astronomy*, vol. 79, no. 4, pp. 235–275, Apr. 2001. DOI: 10.1023/A:1017555515763. [Online]. Available: https://doi.org/10.1023/A:1017555515763.

[121] R. A. Werner and D. J. Scheeres, "Exterior gravitation of a polyhedron derived and compared with harmonic and mascon gravitation representations of asteroid 4769 Castalia," *Celestial Mechanics and Dynamical Astronomy*, vol. 65, no. 3, pp. 313–344, Sep. 1996. DOI: 10.1007/BF00053511. [Online]. Available: https://doi.org/10.1007/BF00053511.

[122] P. Bartczak and S. Breiter, "Double material segment as the model of irregular bodies," *Celestial Mechanics and Dynamical Astronomy*, vol. 86, no. 2, pp. 131–141, Jun. 2003. DOI: 10.1023/A:1024115015470. [Online]. Available: https://doi.org/10.1023/A:1024115015470.

[123] J. S. Juan, A. Abad, D. Scheeres, and M. Lara, "A First Order Analytical Solution for Spacecraft Motion about (433) Eros," in *AIAA/AAS Astrodynamics Specialist Conference and Exhibit*. DOI: 10.2514/6.2002-4543. eprint: https://arc.aiaa.org/doi/pdf/10.2514/6.2002-4543. [Online]. Available: https://arc.aiaa.org/doi/abs/10.2514/6.2002-4543.

[124] W. Hu and D. Scheeres, "Numerical determination of stability regions for orbital motion in uniformly rotating second degree and order gravity fields," *Planetary and Space Science*, vol. 52, no. 8, pp. 685–692, 2004. DOI: https://doi.org/10.1016/j.pss.2004.01.003. [Online]. Available: http://www.sciencedirect.com/science/article/pii/S0032063304000315.

[125] M. Valtonen and H. Karttunen, *The Three-Body Problem*. Cambridge, New York: Cambridge University Press, 2006. [Online]. Available: https://books.google.com/books?id=dvIXkeS17bAC.

[126] S. J. Ostro, R. Hudson, K. D. Rosema, J. D. Giorgini, R. F. Jurgens, D. K. Yeomans, P. W. Chodas, R. Winkler, R. Rose, D. Choate, R. A. Cormier, D. Kelley, R. Littlefair, L. A. Benner, M. L. Thomas, and M. A. Slade, "Asteroid 4179 toutatis: 1996 radar observations," *Icarus*, vol. 137, no. 1, pp. 122–139, 1999. DOI: https://doi.org/10.1006/icar.1998.6031. [Online]. Available: http://www.sciencedirect.com/science/article/pii/S0019103598960316.

[127] R. Hudson, S. Ostro, and D. Scheeres, "High-resolution model of asteroid 4179 toutatis," *Icarus*, vol. 161, no. 2, pp. 346–355, 2003, cited By 45. DOI: 10.1016/S0019-1035(02)00042-8. [Online]. Available: https://www2.scopus.com/inwa

rd/record.uri?eid=2-s2.0-0037296750&doi=10.1016%2fS0019-1035%2802%2900042-8&partnerID=40&md5=a157441718ebe416fd2f9961f18ff454.

[128] Y. Takahashi, M. W. Busch, and D. J. Scheeres, "Spin state and moment of inertia characterization of 4179 Toutatis," *The Astronomical Journal*, vol. 146, no. 4, p. 95, Sep. 2013. DOI: 10.1088/0004-6256/146/4/95. [Online]. Available: https://doi.org/10.1088%2F0004-6256%2F146%2F4%2F95.

APPENDIX A

DETAILED EQUATIONS OF ILLUSTRATIVE EXAMPLE CASES

A.1 Sample of periodic TDNF terms in equation (2.89).

$$\begin{bmatrix} \dot{v}_1 \\ \dot{v}_2 \\ \dot{v}_3 \\ \dot{v}_4 \\ \dot{v}_5 \\ \dot{v}_6 \end{bmatrix} = \begin{bmatrix} \mathcal{V}_{11} \\ \mathcal{V}_{21} \\ -i\pi v_3 + i(2.2204 \times 10^{-16})v_4 \\ -i(2.2204 \times 10^{-16})v_3 + i\pi v_4 \\ -i4\pi v_5 \\ i4\pi v_6 \end{bmatrix}$$

where

$$\mathcal{V}_{11} = -i1.73732v_1 + i(3.33067 \times 10^{-16})v_2 + i(1.85037 \times 10^{-17})v_1^3 v_3 + i(1.11022 \times 10^{-}16)v_1^2 v_2 v_3 - i(2.31296 \times 10^{-18})v_2^3 v_3 + i(3.70074 \times 10^{-17})v_1^3 v_4 - i(9.25186 \times 10^{-18})v_1^2 v_2 v_4 + i(9.25186 \times 10^{-18})v_1 v_2^2 v_4 + i(2.31296 \times 10^{-18})v_2^3 v_4 + i(6.93889 \times 10^{-18})v_5 + i(9.03502 \times 10^{-21})v_1^2 v_3 v_5 + i(1.807 \times 10^{-20})v_1 v_2 v_3 v_5 + i(9.03502 \times 10^{-21})v_2^2 v_3 v_5 + i(1.807 \times 10^{-20})v_1 v_2 v_4 v_5 - i(9.03502 \times 10^{-21})v_2^2 v_4 v_5 - i(8.82326 \times 10^{-24})v_2 v_3 v_5^2 - i(4.41163 \times 10^{-24})v_1 v_4 v_5^2 - i(4.41163 \times 10^{-24})v_2 v_4 v_5^2 - i(2.15412 \times 10^{-27})v_3 v_5^3 + i(2.15412 \times 10^{-27})v_4 v_5^3 + i(6.93889 \times 10^{-18})v_6 - i(1.807 \times 10^{-20})v_1 v_2 v_4 v_6 + i(5.29396 \times 10^{-23})v_1 v_3 v_5 v_6 + i(1.14702 \times 10^{-22})v_2 v_3 v_5 v_6 - i(1.76465 \times 10^{-23})v_1 v_4 v_5 v_6 + i(1.76465 \times 10^{-23})v_2 v_4 v_5 v_6 + i(1.29247 \times 10^{-26})v_3 v_5^2 v_6 + i(8.61646 \times 10^{-27})v_4 v_5^2 v_6 + i(4.41163 \times 10^{-24})v_1 v_3 v_6^2 + i(4.41163 \times 10^{-24})v_2 v_3 v_6^2 - i(4.30823 \times 10^{-27})v_4 v_5 v_6^2 + (5.78241 \times 10^{-19} - i9.03502 \times 10^{-21})v_1^3 v_3 \cos(2\pi t) + i(3.75857 \times 10^{-18} - 6.32451 \times 10^{-20})v_1^2 v_2 v_3 \cos(2\pi t) + (8.67362 \times 10^{-19} + i4.51751 \times 10^{-21})v_1 v_2^2 v_3 \cos(2\pi t) + i(2.25875 \times 10^{-21})v_2^3 v_3 \cos(2\pi t) + (2.74665 \times 10^{-18} - i6.77626 \times 10^{-21})v_1^3 v_4 \cos(2\pi t) - (2.89121 \times 10^{-19} - i4.51751 \times 10^{-21})v_1^2 v_2 v_4 \cos(2\pi t) + (5.64689 \times 10^{-22} - i3.5293 \times 10^{-23})v_1^2 v_3 v_5 \cos(2\pi t) + (1.12938 \times 10^{-21} - i1.41172 \times 10^{-22})v_1 v_2 v_3 v_5 \cos(2\pi t) + i(5.64689 \times 10^{-22})v_2^2 v_3 v_5 \cos(2\pi t) + i(3.5293 \times 10^{-23})v_1^2 v_4 v_5 \cos(2\pi t) + (2.25875 \times 10^{-21} - i7.05861 \times 10^{-23})v_1 v_2 v_4 v_5 \cos(2\pi t) - (5.64689 \times 10^{-22} + i3.5293 \times 10^{-23})v_2^2 v_4 v_5 \cos(2\pi t) - (5.51454 \times 10^{-25} - i6.89317 \times 10^{-26})v_1 v_3 v_5^2 \cos(2\pi t) - i(1.10291 \times 10^{-24})v_2 v_3 v_5^2 \cos(2\pi t) - (5.51454 \times 10^{-25} - i1.37863 \times 10^{-25})v_1 v_4 v_5^2 \cos(2\pi t) + i(1.10291 \times 10^{-24})v_2 v_4 v_5^2 \cos(2\pi t) + (2.69265 \times 10^{-28} + i1.6829 \times 10^{-29})v_3 v_5^3 \cos(2\pi t) - (2.69265 \times 10^{-28} + i3.36581 \times 10^{-29})v_4 v_5^3 \cos(2\pi t) + i(4.33681 \times 10^{-19})v_6 \cos(2\pi t) - i(5.64689 \times 10^{-22})v_2^2 v_3 v_6 \cos(2\pi t) - (5.64689 \times 10^{-22} + i3.5293 \times 10^{-23})v_1^2 v_4 v_6 \cos(2\pi t) + (6.61744 \times 10^{-24} - i3.44659 \times 10^{-26})v_1 v_3 v_5 v_6 \cos(2\pi t) + (1.43378 \times 10^{-23} - i6.89317 \times 10^{-26})v_2 v_3 v_5 v_6 \cos(2\pi t) - i(2.20581 \times 10^{-24})v_1 v_4 v_5 v_6 \cos(2\pi t) + i(1.10291 \times 10^{-24})v_2 v_4 v_5 v_6 \cos(2\pi t) + (1.07706 \times 10^{-27} - i3.36581 \times 10^{-29})v_3 v_5^2 v_6 \cos(2\pi t) - i(3.36581 \times 10^{-29})v_4 v_5^2 v_6 \cos(2\pi t) + (1.10291 \times 10^{-24} + i6.89317 \times 10^{-26})v_1 v_3 v_6^2 \cos(2\pi t) + (5.51454 \times 10^{-25} + i1.03398 \times 10^{-25})v_2 v_3 v_6^2 \cos(2\pi t) + (5.51454 \times 10^{-25} + i6.89317 \times 10^{-26})v_1 v_4 v_6^2 \cos(2\pi t) + i(1.6829 \times 10^{-29})v_3 v_5 v_6^2 \cos(2\pi t) - (5.38529 \times 10^{-28} + i3.36581 \times 10^{-29})v_4 v_5 v_6^2 \cos(2\pi t) - (2.69265 \times$$

$10^{-28} - i1.6829 \times 10^{-29})v_3 v_6^3 \cos(2\pi t) - i(1.6829 \times 10^{-29})v_4 v_6^3 \cos(2\pi t) + i(8.82326 \times 10^{-24})v_1^2 v_3 v_5 \cos(2\pi t)^2 + (1.76465 \times 10^{-23} - i4.41163 \times 10^{-24})v_1 v_2 v_3 v_5 \cos(2\pi t)^2 +$
$\cdots$
$+ i(1.8684 \times 10^{-45} + i7.47359 \times 10^{-45})v_4 v_6^3 \cos(4\pi t) \sin(4\pi t)^3 \sin(2\pi t)^3 - (2.98944 \times 10^{-43} - i1.8684 \times 10^{-45})v_4 v_5^3 \sin(2\pi t) \sin(4\pi t)^3 \sin(2\pi t)^3 - (5.97887 \times 10^{-44} - i1.79366 \times 10^{-43})v_3 v_5^2 v_6 \sin(2\pi t) \sin(4\pi t)^3 \sin(2\pi t)^3$
$+ i(5.97887 \times 10^{-44})v_4 v_5^2 v_6 \sin(2\pi t) \sin(4\pi t)^3 \sin(2\pi t)^3$
$+ i(1.19577 \times 10^{-43})v_3 v_5 v_6^2 \sin(2\pi t) \sin(4\pi t)^3 \sin(2\pi t)^3$
$+ i(9.34199 \times 10^{-46})v_4 v_6^3 \sin(2\pi t) \sin(4\pi t)^3 \sin(2\pi t)^3 - (2.3355 \times 10^{-} i46 + 2.91937 \times 10^{-47})v_3 v_5^3 \sin(4\pi t)^4 \sin(2\pi t)^3 - i(4.67099 \times 10^{-46})v_3 v_5^2 v_6 \sin(4\pi t)^4 \sin(2\pi t)^3$
$+ (4.67099 \times 10^{-} i46 + 2.3355 \times 10^{-46})v_4 v_5^2 v_6 \sin(4\pi t)^4 \sin(2\pi t)^3 - (2.3355 \times 10^{-46} + i4.67099 \times 10^{-46})v_3 v_5 v_6^2 \sin(4\pi t)^4 \sin(2\pi t)^3$
$+ (4.67099 \times 10^{-46} + i2.3355 \times 10^{-46})v_4 v_5 v_6^2 \sin(4\pi t)^4 \sin(2\pi t)^3 - (1.16775 \times 10^{-46} - i2.91937 \times 10^{-47})v_3 v_6^3 \sin(4\pi t)^4 \sin(2\pi t)^3$

$\mathcal{V}_{21} = -i(3.33067 \times 10^{-}16)v_1 + i(1.73732)v_2 + i(4.62593 \times 10^{-18})v_1^3 v_3 - i(4.62593 \times 10^{-17})v_1^2 v_2 v_3 - i(9.25186 \times 10^{-17})v_1 v_2^2 v_3 + i(3.70074 \times 10^{-17})v_2^3 v_3 - i(7.17019 \times 10^{-17})v_1^3 v_4 - i(9.25186 \times 10^{-18})v_1^2 v_2 v_4 + i(9.25186 \times 10^{-18})v_1 v_2^2 v_4 + i(4.62593 \times 10^{-18})v_2^3 v_4 - i(6.93889 \times 10^{-18})v_5 - i(1.807 \times 10^{-20})v_1 v_2 v_3 v_5 - i(9.03502 \times 10^{-21})v_2^2 v_3 v_5 + i(1.807 \times 10^{-20})v_1 v_2 v_4 v_5 + i(9.03502 \times 10^{-21})v_2^2 v_4 v_5 + i(4.41163 \times 10^{-24})v_2 v_3 v_5^2 + i(4.41163 \times 10^{-24})v_1 v_4 v_5^2 + i(8.82326 \times 10^{-24})v_2 v_4 v_5^2 - i(6.93889 \times 10^{-18})v_6 + i(1.807 \times 10^{-20})v_1^2 v_3 v_6 + i(9.03502 \times 10^{-21})v_1^2 v_4 v_6 + i(1.807 \times 10^{-20})v_1 v_2 v_4 v_6 + i(9.03502 \times 10^{-21})v_2^2 v_4 v_6 - i(7.05861 \times 10^{-23})v_1 v_3 v_5 v_6 - i(9.70559 \times 10^{-23})v_2 v_3 v_5 v_6 + i(1.14702 \times 10^{-22})v_1 v_4 v_5 v_6 - i(8.61646 \times 10^{-27})v_3 v_5^2 v_6 + i(1.29247 \times 10^{-26})v_4 v_5^2 v_6 - i(4.41163 \times 10^{-24})v_2 v_3 v_6^2 - i(8.82326 \times 10^{-24})v_1 v_4 v_6^2 + i(4.30823 \times 10^{-27})v_3 v_5 v_6^2 + i(8.61646 \times 10^{-27})v_4 v_5 v_6^2 + i(2.15412 \times 10^{-27})v_3 v_6^3 - i(2.15412 \times 10^{-27})v_4 v_6^3 + (1.4456 \times 10^{-19} + i2.25875 \times 10^{-21})v_1^3 v_3 \cos(2\pi t) - (1.4456 \times 10^{-18} + i1.807 \times 10^{-20})v_1^2 v_2 v_3 \cos(2\pi t) - (3.46945 \times 10^{-18} - i4.51751 \times 10^{-21})v_1 v_2^2 v_3 \cos(2\pi t) + (1.59016 \times 10^{-18} + i2.48463 \times 10^{-20})v_2^3 v_3 \cos(2\pi t) - (2.38524 \times 10^{-18} + i2.03288 \times 10^{-20})v_1^3 v_4 \cos(2\pi t) - (1.4456 \times 10^{-18} + i4.51751 \times 10^{-21})v_1^2 v_2 v_4 \cos(2\pi t) - i(2.25875 \times 10^{-21})v_2^3 v_4 \cos(2\pi t) - i(4.33681 \times 10^{-19})v_5 \cos(2\pi t) + i(7.05861 \times 10^{-23})v_1 v_2 v_3 v_5 \cos(2\pi t) - (5.64689 \times 10^{-22} - i3.5293 \times 10^{-23})v_2^2 v_3 v_5 \cos(2\pi t) - i(5.64689 \times 10^{-22})v_1^2 v_4 v_5 \cos(2\pi t)$
$+ i(1.12938 \times 10^{-21})v_1 v_2 v_4 v_5 \cos(2\pi t)$
$-(5.64689 \times 10^{-22} - i3.5293 \times 10^{-23})v_2^2 v_4 v_5 \cos(2\pi t) + i(1.10291 \times 10^{-24})v_2 v_3 v_5^2 \cos(2\pi t) + i(5.51454 \times 10^{-25})v_1 v_4 v_5^2 \cos(2\pi t) + (1.10291 \times 10^{-24} - i3.44659 \times 10^{-26})v_2 v_4 v_5^2 \cos(2\pi t) + i(1.6829 \times 10^{-29})v_3 v_5^3 \cos(2\pi t) - i(1.6829 \times 10^{-29})v_4 v_5^3 \cos(2\pi t) - (5.64689 \times 10^{-22} - i3.5293 \times 10^{-23})v_1^2 v_3 v_6 \cos(2\pi t) - i(3.5293 \times 10^{-23})v_2^2 v_3 v_6 \cos(2\pi t) + i(5.64689 \times 10^{-22})v_1^2 v_4 v_6 \cos(2\pi t) + (2.25875 \times 10^{-21} + i1.41172 \times 10^{-22})v_1 v_2 v_4 v_6 \cos(2\pi t) + (5.64689 \times 10^{-22} + i3.5293 \times 10^{-23})v_2^2 v_4 v_6 \cos(2\pi t) - (6.61744 \times 10^{-24} + i4.30823 \times 10^{-26})v_1 v_3 v_5 v_6 \cos(2\pi t) - (1.10291 \times 10^{-23} - i3.44659 \times 10^{-26})v_2 v_3 v_5 v_6 \cos(2\pi t) + (4.41163 \times 10^{-24} + i6.89317 \times 10^{-26})v_1 v_4 v_5 v_6 \cos(2\pi t) - (5.38529 \times 10^{-28} - i1.6829 \times$

$10^{-29})v_3v_5^2v_6\cos(2\pi t)+(5.38529\times10^{-28}-i1.6829\times10^{-29})v_4v_5^2v_6\cos(2\pi t)+i(5.51454\times10^{-25})v_1v_3v_6^2\cos(2\pi t)-(5.51454\times10^{-25}+i6.89317\times10^{-26})v_2v_3v_6^2\cos(2\pi t)-(1.65436\times10^{-24}+i6.89317\times10^{-26})v_1v_4v_6^2\cos(2\pi t)-i(5.51454\times10^{-25})v_2v_4v_6^2\cos(2\pi t)+(5.38529\times10^{-28}+i3.36581\times10^{-29})v_3v_5v_6^2\cos(2\pi t)+$
$\ldots$
$-(5.97887\times10^{-43}+i1.19577\times10^{-43})v_4v_5v_6^2\sin(2\pi t)\sin(4\pi t)^3\sin(2\pi t)^3-(2.98944\times10^{-43}+i1.8684\times10^{-45})v_3v_6^3\sin(2\pi t)\sin(4\pi t)^3\sin(2\pi t)^3$
$-i(2.91937\times10^{-47})v_4v_5^3\sin(4\pi t)^4\sin(2\pi t)^3$
$-(2.3355\times10^{-46}+i4.67099\times10^{-46})v_3v_5^2v_6\sin(4\pi t)^4\sin(2\pi t)^3-(2.3355\times10^{-46}-i4.67099\times10^{-46})v_4v_5^2v_6\sin(4\pi t)^4\sin(2\pi t)^3+i(4.67099\times10^{-46})v_4v_5v_6^2\sin(4\pi t)^4\sin(2\pi t)^3-(2.3355\times10^{-46}-i2.91937\times10^{-47})v_4v_6^3\sin(4\pi t)^4\sin(2\pi t)^3$

A.2 y_7 and y_8: Parametric Equations of spring-mass-damper system (2.113)

$y_7=(8.41688-i44.0124)y_1^2y_3-(5.25571-i151.631i)y_1y_2y_3-(107.972+i145.859)y_2^2y_3+(1724.29-i6168.09)y_1y_3^2-(1939.41-i8415.1)y_2y_3^2+(20144.2-i316290)y_3^3+(57.678+i12.9645)y_1^2y_4-(75.8602+i9.05606)y_1y_2y_4+(28.043+i1.97305)y_2^2y_4+(65229.2+i41133.7)y_1y_3y_4-(31153.-i7057.42)y_2y_3y_4-(1.04042\times10^6-i3.48349\times10^6)y_3^2y_4-(5774.69+i314.841)y_1y_4^2+(4681.57+i149.413)y_2y_4^2-(1.81357\times10^6-i249610.)y_3y_4^2+(242330.+i63546.5)y_4^3-(464.764-i704.989)y_1^2y_5+(1141.9-i1870.41)y_1y_2y_5-(723.749-i1376.4)y_2^2y_5-(39182.1+i17021.2)y_1y_3y_5+(47635.7+i19690.7)y_2y_3y_5+(3.37197\times10^6-i1.28988\times10^6)y_3^2y_5-(235156.+i267773.)y_1y_4y_5+(599725.+i375592.)y_2y_4y_5-(5.4448\times10^6+i1.53458\times10^7)y_3y_4y_5-(3.92234\times10^6+i3.21059\times10^7)y_4^2y_5-(2.20416\times10^6-i2.99324\times10^6)y_1y_5^2+(2.49464\times10^6-i3.45527\times10^6)y_2y_5^2-(1.86174\times10^8+i5.35227\times10^7)y_3y_5^2-(1.91896\times10^8+i2.79952\times10^8)y_4y_5^2-(3.34833\times10^9-i5.73262\times10^9)y_5^3-(951.04-i217.566)y_1^2y_6+(1492.79-i386.165)y_1y_2y_6-(613.667-i170.879)y_2^2y_6-(155575.+i248414.)y_1y_3y_6+(120006.+i165412.)y_2y_3y_6+(3.92234\times10^6-i3.21059\times10^7)y_3^2y_6-(3016.62+i39773.6)y_1y_4y_6+(2981.09+i34252.5)y_2y_4y_6+(9.21752\times10^6+i6.8046\times10^6)y_3y_4y_6+(1.93571\times10^6-i2.32586\times10^6)y_4^2y_6-(8.77683\times10^7+i5.53469\times10^7)y_1y_5y_6+(4.19175\times10^7-i9.49602\times10^6)y_2y_5y_6+i(2.44511\times10^9+8.60461\times10^8)y_3y_5y_6-(2.39982\times10^8+i1.28299\times10^9)y_4y_5y_6+(4.22011\times10^10-i5.28005\times10^10)y_5^2y_6+(3.37462\times10^6-i1.03693\times10^6)y_1y_6^2-(3.00308\times10^6-i944483.)y_2y_6^2+(1.62331\times10^8+i2.13608\times10^8)y_3y_6^2-(8.87787\times10^6-i1.67954\times10^8)y_4y_6^2+(4.41791\times10^10-1.76106\times10^10)y_5y_6^2-(5.79082\times10^9-i1.13602\times10^9)y_6^3$

$y_8=(28.043-i1.97305)y_1^2y_3-(75.8602-i9.05606)y_1y_2y_3+(57.678-i12.9645)y_2^2y_3+(4681.57-i149.413)y_1y_3^2-(5774.69-i314.841)y_2y_3^2+(242330.-i63546.5)y_3^3-(107.972-i145.859)y_1^2y_4-(5.25571+i151.631)y_1y_2y_4+(8.41688+i44.0124)y_2^2y_4-(31153.+i7057.42)y_1y_3y_4+(65229.2-i41133.7)y_2y_3y_4-(1.81357\times10^6+i249610.)y_3^2y_4-(1939.41+i8415.1)y_1y_4^2+(1724.29+i6168.09)y_2y_4^2-(1.04042\times10^6+i3.48349\times10^6)y_3y_4^2+$

$(20144.2+i316290.)y_4^3-(613.667+i170.879)y_1^2y_5+(1492.79+i386.165)y_1y_2y_5-(951.04+i217.566)y_2^2y_5+(2981.09-i34252.5)y_1y_3y_5-(3016.62-i39773.6)y_2y_3y_5+(1.93571\times10^6+i2.32586\times10^6)y_3^2y_5+(120006.-i165412.)y_1y_4y_5-(155575.-i248414.)y_2y_4y_5+(9.21752\times10^6-i6.8046\times10^6)y_3y_4y_5+(3.92234\times10^6+i3.21059\times10^7)y_4^2y_5-(3.00308\times10^6+i944483.)y_1y_5^2+(3.37462\times10^6+i1.03693\times10^6)y_2y_5^2-(8.87787\times10^6+i1.67954\times10^8)y_3y_5^2+(1.62331\times10^8-i2.13608\times10^8)y_4y_5^2-(5.79082\times10^9+i1.13602\times10^9)y_5^3-(723.749+1376.4)y_1^2y_6+(1141.9+i1870.41)y_1y_2y_6-(464.764+i704.989)y_2^2y_6+(599725.-i375592.)y_1y_3y_6-(235156.-i267773.)y_2y_3y_6-(3.92234\times10^6-i3.21059\times10^7)y_3^2y_6+(47635.7-i19690.7)y_1y_4y_6-(39182.1-i17021.2)y_2y_4y_6-(5.4448\times10^6-i1.53458\times10^7)y_3y_4y_6+(3.37197\times10^6+i1.28988\times10^6)y_4^2y_6+(4.19175\times10^7+i9.49602\times10^6)y_1y_5y_6-(8.77683\times10^7-i5.53469\times10^7)y_2y_5y_6-(2.39982\times10^8-i1.28299\times10^9)y_3y_5y_6+(2.44511\times10^9-i8.60461\times10^8)y_4y_5y_6+(4.41791\times10^10+i1.76106\times10^10)y_5^2y_6+(2.49464\times10^6+i3.45527\times10^6)y_1y_6^2-(2.20416\times10^6+i2.99324\times10^6)y_2y_6^2-(1.91896\times10^8-i2.79952\times10^8)y_3y_6^2-(1.86174\times10^8-i5.35227\times10^7)y_4y_6^2+(4.22011\times10^10+i5.28005\times10^10)y_5y_6^2-(3.34833\times10^9+i5.73262\times10^9)y_6^3$

APPENDIX B

DETAILED EQUATIONS OF THE ISSB MOTION ANALYSIS

B.1 Elements of the state augmented autonomous system for the ISSB problem (6.9).

$$\begin{bmatrix} s_1' \\ s_2' \\ s_3' \\ s_4' \\ s_5' \\ s_6' \\ p' \\ q' \end{bmatrix} = \begin{bmatrix} f(s_1(\tau)) \\ f(s_2(\tau)) \\ f(s_3(\tau)) \\ f(s_4(\tau)) \\ f(s_5(\tau)) \\ f(s_6(\tau)) \\ q \\ -(441p)/4000000 \end{bmatrix}$$

where

$f(s_1(\tau)) = -(s_2/10000) + (9s_3)/5000 + 19.0476pq(-0.00017074\cos(\pi\tau)/148) - 0.0235514\sin(\pi\tau)/148)) + (4.97326(s_5\cos(0.0212045\tau) + 0.709s_6\sin(0.0212045\tau))^2 (s_2((-0.2419 + 0.8899\cos(0.0212045\tau) - 0.648\cos(0.042409\tau))/10000 - 0.0208\sin(0.0212045\tau)) + s_1(1.0006\cos(0.0212045\tau) + 0.0043\sin(0.0212045\tau)) + s_3(0.001 - 0.0038\cos(0.0212045\tau) + 0.0027\cos(0.042409\tau) + 0.8815\sin(0.0212045\tau)) + s_4(0.0236\cos(0.0212045\tau) + (0.101\sin(0.0212045\tau) - 0.0735\sin(0.042409\tau))/1000)) - 2.80011(s_2((-0.2419 + 0.8899\cos(0.0212045\tau) - 0.648\cos(0.042409\tau))/10000 - 0.0208\sin(0.0212045\tau)) + s_1(1.0006\cos(0.0212045\tau) + 0.0043\sin(0.0212045\tau)) + s_3(0.001 - 0.0038\cos(0.0212045\tau) + 0.0027\cos(0.042409\tau) + 0.8815\sin(0.0212045\tau)) + s_4(0.0236\cos(0.0212045\tau) + (0.101\sin(0.0212045\tau) - 0.0735\sin(0.042409\tau))/1000))^3 - 2.17315(s_2((-0.2419 + 0.8899\cos(0.0212045\tau) - 0.648\cos(0.042409\tau))/10000 - 0.0208\sin(0.0212045\tau)) + s_1(1.0006\cos(0.0212045\tau) + 0.0043\sin(0.0212045\tau)) + s_3(0.001 - 0.0038\cos(0.0212045\tau) + 0.0027\cos(0.042409\tau) + 0.8815\sin(0.0212045\tau)) + s_4(0.0236\cos(0.0212045\tau) + (0.101\sin(0.0212045\tau) - 0.0735\sin(0.042409\tau))/1000)) (-s_1(0.0013 - 0.0049\cos(0.0212045\tau) - 0.0035\cos(0.042409\tau) - 1.1357\sin(0.0212045\tau)) - s_4((0.0313 - 0.1147\cos(0.0212045\tau) - 0.0834\cos(0.042409\tau))/1000 - 0.0268\sin(0.0212045\tau)) + s_3(1.0006\cos(0.0212045\tau) + 0.0043\sin(0.0212045\tau)) - s_2(0.0236\cos(0.0212045\tau) - (0.101\sin(0.0212045\tau) + 0.0735\sin(0.042409\tau))/1000))^2) (-0.00017074\cos(\pi\tau)/148) - 0.0235514\sin(\pi\tau)/148)) + 19.0476pq(-0.0236027\cos(\pi\tau)/148) + 0.000171208\sin(\pi\tau)/148)) + (4.97326(s_5\cos(0.0212045\tau) + 0.709s_6\sin(0.0212045\tau))^2 (-s_1(0.0013 - 0.0049\cos(0.021205\tau) - 0.0035\cos(0.042409\tau) - 1.136\sin(0.0212045\tau)) + s_4((-0.0313 + 0.1147\cos(0.0212045\tau) - 0.0834\cos(0.042409\tau))/1000 - 0.0268\sin(0.0212045\tau)) + s_3(1.0006\cos(0.0212045\tau) + 0.0043\sin(0.0212045\tau)) - s_2(0.0236\cos(0.0212045\tau) + (-0.101\sin(0.0212045\tau) + 0.0735\sin(0.042409\tau))/1000)) + 2.80011(s_2((0.2419 - 0.8899\cos(0.0212045\tau) - 0.648\cos(0.042409\tau))/10000 - 0.0208\sin(0.0212045\tau)) + s_1(1.0006\cos(0.0212045\tau) + 0.0043\sin(0.0212045\tau)) + s_3(0.001 - 0.0038\cos(0.0212045\tau) + 0.0027\cos(0.042409\tau) + 0.8815\sin(0.0212045\tau)) + s_4(0.0236\cos(0.0212045\tau) + (0.101\sin(0.0212045\tau) - 0.0735\sin(0.042409\tau))/1000))^2$

$(-s_1(0.0013 - 0.005\cos(0.021\tau) - 0.0035\cos(0.042409\tau) - 1.1\sin(0.0212045\tau)) +$
$s_4((-0.0313 + 0.1147\cos(0.0212045\tau) - 0.0834\cos(0.042409\tau))/1000$
$- 0.0268\sin(0.0212045\tau)) + s_3(1.0006\cos(0.0212045\tau) + 0.0043\sin(0.0212045\tau)) -$
$s_2(0.0236\cos(0.0212045\tau) + (-0.101\sin(0.0212045\tau) + 0.0735\sin(0.043\tau))/1000)) +$
$2.17315(s_1(0.0013 - 0.005\cos(0.0212045\tau) - 0.0035\cos(0.043\tau)$
$- 1.1357\sin(0.0212045\tau)) + s_4((-0.0313 + 0.1147\cos(0.0212045\tau)$
$-0.0834\cos(0.042409\tau))/1000 - 0.0268\sin(0.0212045\tau)) + s_3(1.0006\cos(0.0212045\tau) +$
$0.0043\sin(0.0212045\tau)) - s_2(0.0236\cos(0.0212045\tau) + (-0.101\sin(0.0212045\tau) +$
$0.0735\sin(0.042409\tau))/1000))^3)(-0.0236027\cos(\pi\tau)/148) + 0.000171208\sin(\pi\tau)/148))$

$f(s_2(\tau)) = -(s_1/10000) - (23s_4)/10000 + 19.05pq(0.0023 + 1\cos(\pi\tau)/148) -$
$0.00155\cos(\pi\tau)/74) - 0.00058\cos((3\pi)\tau)/148) - 0.00030921\cos(\pi\tau)/37) -$
$0.000193188\cos((5\pi)\tau)/148) - 0.000132\cos((3\pi)\tau)/74) - 0.007\sin(\pi\tau)/148)) +$
$(4.97326(s_5\cos(0.0212045\tau) + 0.709s_6\sin(0.0212045\tau))^2(s_2((-0.2419$
$+ 0.8899\cos(0.0212045\tau) - 0.648\cos(0.042409\tau))/10000 - 0.0208\sin(0.0212045\tau)) +$
$s_1(\cos(0.0212045\tau) + 0.0043\sin(0.0212045\tau)) + s_3(0.001 - 0.0038\cos(0.0212045\tau) +$
$0.0027\cos(0.042409\tau) + 0.8815\sin(0.0212045\tau)) + s_4(0.0236\cos(0.0212045\tau) +$
$(0.101\sin(0.0212045\tau) - 0.0735\sin(0.042409\tau))/1000)) - 2.80011(s_2((-0.2419 +$
$0.8899\cos(0.0212045\tau) - 0.648\cos(0.042409\tau))/10000 - 0.0208\sin(0.0212045\tau)) +$
$s_1(\cos(0.0212045\tau) + 0.0043\sin(0.0212045\tau)) + s_3(0.001 - 0.0038\cos(0.0212045\tau) +$
$0.0027\cos(0.042409\tau) + 0.8815\sin(0.0212045\tau)) + s_4(0.0236\cos(0.0212045\tau) +$
$(0.101\sin(0.0212045\tau) - 0.0735\sin(0.042409\tau))/1000))^3 - 2.17315(s_2((-0.2419 +$
$0.8899\cos(0.0212045\tau) - 0.648\cos(0.042409\tau))/10000 - 0.0208\sin(0.0212045\tau)) +$
$s_1(\cos(0.0212045\tau) + 0.0043\sin(0.0212045\tau)) + s_3(0.001 - 0.0038\cos(0.0212045\tau) +$
$0.0027\cos(0.042409\tau) + 0.8815\sin(0.0212045\tau)) + s_4(0.0236\cos(0.0212045\tau) +$
$(0.101\sin(0.0212045\tau) - 0.0735\sin(0.042409\tau))/1000))$
$(s_1(-0.0013 + 0.0049\cos(0.0212045\tau) - 0.0035\cos(0.043\tau) - 1.1\sin(0.0212045\tau)) +$
$s_4((-0.0313 + 0.1147\cos(0.0212045\tau) - 0.0834\cos(0.042409\tau))/1000$
$- 0.0268\sin(0.0212045\tau)) + s_3(1.\cos(0.0212045\tau) + 0.0043\sin(0.0212045\tau)) -$
$s_2(0.0236\cos(0.0212045\tau) - (0.101\sin(0.0212045\tau) + 0.07\sin(0.042409\tau))/1000))^2)$
$(0.00230944 + 1.00064\cos(\pi\tau)/148) - 0.00154895\cos(\pi\tau)/74)$
$- 0.000583\cos((3\pi)\tau)/148) - 0.0003\cos(\pi\tau)/37) - 0.000193\cos((5\pi)\tau)/148) -$
$0.000132407\cos((3\pi)\tau)/74) - 0.007\sin(\pi\tau)/148)) + 19.0476pq$
$(-0.00722855\cos(\pi\tau)/148) - 0.998258\sin(\pi\tau)/148) + 0.0030905\sin(\pi\tau)/74) +$
$0.00173894\sin((3\pi)\tau)/148) + 0.00123407\sin(\pi\tau)/37) + 0.000963703\sin((5\pi)\tau)/148) +$
$0.000792617\sin((3\pi)\tau)/74) + 0.00067392\sin((7\pi)\tau)/148)) + (5(s_5\cos(0.0212045\tau) +$
$0.709s_6\sin(0.0212045\tau))^2(s_1(-0.0013 + 0.0049\cos(0.0212045\tau) - 0.0035\cos(0.042409\tau) -$
$1.1\sin(0.0212045\tau)) + s_4((-0.0313 + 0.1147\cos(0.0212045\tau)$
$-0.0834\cos(0.042409\tau))/1000 - 0.0268\sin(0.0212045\tau)) + s_3(1.0006\cos(0.0212045\tau) +$
$0.0043\sin(0.0212045\tau)) + s_2(-0.0236\cos(0.0212045\tau) - (0.101\sin(0.0212045\tau) +$
$0.0735\sin(0.042409\tau))/1000)) - 2.80011(s_2((-0.2419 + 0.8899\cos(0.0212045\tau) -$
$0.648\cos(0.042409\tau))/10000 - 0.0208\sin(0.0212045\tau)) + s_1(1.0006\cos(0.0212045\tau) +$

$0.0043\sin(0.0212045\tau))+s_3(0.001-0.0038\cos(0.0212045\tau)+0.0027\cos(0.042409\tau)+0.8815\sin(0.0212045\tau))+s_4(0.0236\cos(0.0212045\tau)+(0.101\sin(0.0212045\tau)-0.0735\sin(0.042409\tau))/1000))^2(s_1(-0.0013+0.0049\cos(0.0212045\tau)-0.0035\cos(0.042409\tau)-1.1357\sin(0.0212045\tau))-s_4((0.031-0.115\cos(0.0212045\tau)-0.0834\cos(0.042409\tau))/1000-0.0268\sin(0.0212045\tau))+s_3(1.0006\cos(0.0212045\tau)+0.0043\sin(0.0212045\tau))+s_2(-0.0236\cos(0.0212045\tau)+(-0.101\sin(0.0212045\tau)+0.0735\sin(0.042409\tau))/1000))-2.17315(s_1(-0.0013+0.0049\cos(0.0212045\tau)-0.0035\cos(0.042409\tau)-1.1357\sin(0.0212045\tau))-s_4((0.031-0.115\cos(0.0212045\tau)-0.0834\cos(0.042409\tau))/1000-0.0268\sin(0.0212045\tau))+s_3(1.0006\cos(0.0212045\tau)+0.0043\sin(0.0212045\tau))+s_2(-0.0236\cos(0.0212045\tau)+(-0.101\sin(0.0212045\tau)+0.0735\sin(0.042409\tau))/1000))^3)(-0.00722855\cos(\pi\tau)/148)-0.998258\sin(\pi\tau)/148)+0.0030905\sin(\pi\tau)/74)+0.00173894\sin((3\pi)\tau)/148)+0.00123407\sin(\pi\tau)/37)+0.000963703\sin((5\pi)\tau)/148)+0.000792617\sin((3\pi)\tau)/74)+0.00067392\sin((7\pi)\tau)/148))$

$f(s_3(\tau))=-((3s_1)/1250)-s_4/10000+19.0476pq(-0.000170573\cos(\pi\tau)/148)-0.0235491\sin(\pi\tau)/148))+(4.97326(s_5\cos(0.0212045\tau)+0.709s_6\sin(0.0212045\tau))^2(-s_1(0.0013-0.005\cos(0.0212045\tau)-0.0035\cos(0.042409\tau)-1.14\sin(0.0212045\tau))+s_4((-0.031+0.1147\cos(0.0212045\tau)-0.083\cos(0.042409\tau))/1000-0.0268\sin(0.0212045\tau))+s_3(1.0006\cos(0.0212045\tau)+0.0043\sin(0.0212045\tau))+s_2(-0.0236\cos(0.0212045\tau)+(-0.101\sin(0.0212045\tau)+0.0735\sin(0.042409\tau))/1000))-2.80011(s_2((-0.2419+0.8899\cos(0.0212045\tau)-0.648\cos(0.042409\tau))/10000-0.0208\sin(0.0212045\tau))+s_1(1.0006\cos(0.0212045\tau)+0.0043\sin(0.0212045\tau))+s_3(0.001-0.0038\cos(0.0212045\tau)+0.0027\cos(0.042409\tau)+0.8815\sin(0.0212045\tau))+s_4(0.0236\cos(0.0212045\tau)+(0.101\sin(0.0212045\tau)-0.0735\sin(0.042409\tau))/1000))^2(s_1(-0.0013+0.0049\cos(0.0212045\tau)-0.0035\cos(0.042409\tau)-1.1357\sin(0.0212045\tau))+s_4((-0.0313+0.1147\cos(0.0212045\tau)-0.0834\cos(0.042409\tau))/1000-0.0268\sin(0.0212045\tau))+s_3(1.0006\cos(0.0212045\tau)+0.0043\sin(0.0212045\tau))+s_2(-0.0236\cos(0.0212045\tau)+(-0.101\sin(0.0212045\tau)+0.0735\sin(0.042409\tau))/1000))-2.17315(s_1(-0.0013+0.0049\cos(0.0212045\tau)-0.0035\cos(0.042409\tau)-1.1357\sin(0.0212045\tau))+s_4((-0.0313+0.1147\cos(0.0212045\tau)-0.0834\cos(0.042409\tau))/1000-0.0268\sin(0.0212045\tau))+s_3(1.0006\cos(0.0212045\tau)+0.0043\sin(0.0212045\tau))+s_2(-0.0236\cos(0.0212045\tau)+(-0.101\sin(0.0212045\tau)+0.0735\sin(0.042409\tau))/1000))^3)(-0.000170573\cos(\pi\tau)/148)-0.0235491\sin(\pi\tau)/148))+19.0476pq(0.0236067\cos(\pi\tau)/148)-0.000171079\sin(\pi\tau)/148))+(4.97326(s_5\cos(0.0212045\tau)+0.709s_6\sin(0.0212045\tau))^2(s_2((-0.2419+0.8899\cos(0.0212045\tau)-0.648\cos(0.042409\tau))/10000-0.0208\sin(0.0212045\tau))+s_1(1.0006\cos(0.0212045\tau)+0.0043\sin(0.0212045\tau))+s_3(0.001-0.0038\cos(0.0212045\tau)+0.0027\cos(0.042409\tau)+0.8815\sin(0.0212045\tau))+s_4(0.0236\cos(0.0212045\tau)+(0.101\sin(0.0212045\tau)-0.0735\sin(0.042409\tau))/1000))-2.80011(s_2((-0.2419+0.8899\cos(0.0212045\tau)-0.648\cos(0.042409\tau))/10000-0.0208\sin(0.0212045\tau))+s_1(1.0006\cos(0.0212045\tau)+0.0043\sin(0.0212045\tau))+$

$s_3(0.001-0.0038\cos(0.0212045\tau)+0.0027\cos(0.042409\tau)+0.8815\sin(0.0212045\tau))+$
$s_4(0.0236\cos(0.0212045\tau)+(0.101\sin(0.0212045\tau)-0.0735\sin(0.042409\tau))/1000))^3-$
$2.17315(s_2((-0.2419+0.8899\cos(0.0212045\tau)-0.648\cos(0.042409\tau))/10000-$
$0.0208\sin(0.0212045\tau))+s_1(1.0006\cos(0.0212045\tau)+0.0043\sin(0.0212045\tau))+$
$s_3(0.001-0.0038\cos(0.0212045\tau)+0.0027\cos(0.042409\tau)+0.8815\sin(0.0212045\tau))+$
$s_4(0.0236\cos(0.0212045\tau)+(0.101\sin(0.0212045\tau)-0.0735\sin(0.042409\tau))/1000))$
$(s_1(-0.0013+0.0049\cos(0.0212045\tau)-0.0035\cos(0.042409\tau)-1.1357\sin(0.0212045\tau))+$
$s_4((-0.0313+0.1147\cos(0.0212045\tau)-0.0834\cos(0.042409\tau))/1000$
$-0.0268\sin(0.0212045\tau))+s_3(1.0006\cos(0.0212045\tau)+0.0043\sin(0.0212045\tau))+$
$s_2(-0.0236\cos(0.0212045\tau)+(-0.101\sin(0.0212045\tau)+0.0735\sin(0.042409\tau))/1000))^2)$
$(0.0236067\cos(\pi\tau)/148)-0.000171079\sin(\pi\tau)/148))$

$f(s_4(\tau))=(23s_2)/10000-s_3/10000+19.0476pq(0.00230911+1.0005\cos(\pi\tau)/148)-$
$0.00154872\cos(\pi\tau)/74)-0.000582637\cos((3\pi)\tau)/148)-0.000309167\cos(\pi\tau)/37)-$
$0.000193159\cos((5\pi)\tau)/148)-0.000132388\cos((3\pi)\tau)/74)-0.00726049\sin(\pi\tau)/148))+$
$(4.97326(s_5\cos(0.0212045\tau)+0.709s_6\sin(0.0212045\tau))^2$
$(s_1(-0.0013+0.0049\cos(0.0212045\tau)-0.0035\cos(0.042409\tau)-1.1357\sin(0.0212045\tau))+$
$s_4((-0.0313+0.1147\cos(0.0212045\tau)-0.0834\cos(0.042409\tau))/1000$
$-0.0268\sin(0.0212045\tau))+s_3(1.0006\cos(0.0212045\tau)+0.0043\sin(0.0212045\tau))+$
$s_2(-0.0236\cos(0.0212045\tau)+(-0.101\sin(0.0212045\tau)+0.0735\sin(0.042409\tau))/1000))-$
$2.80011(s_2((-0.2419+0.8899\cos(0.0212045\tau)-0.648\cos(0.042409\tau))/10000-$
$0.0208\sin(0.0212045\tau))+s_1(1.0006\cos(0.0212045\tau)+0.0043\sin(0.0212045\tau))+$
$s_3(0.001-0.0038\cos(0.0212045\tau)+0.0027\cos(0.042409\tau)+0.8815\sin(0.0212045\tau))+$
$s_4(0.0236\cos(0.0212045\tau)+(0.101\sin(0.0212045\tau)-0.0735\sin(0.042409\tau))/1000))^2$
$(s_1(-0.0013+0.0049\cos(0.0212045\tau)-0.0035\cos(0.042409\tau)$
$-1.1357\sin(0.0212045\tau))+s_4((-0.0313+0.1147\cos(0.0212045\tau)$
$-0.0834\cos(0.042409\tau))/1000-0.0268\sin(0.0212045\tau))+s_3(1.0006\cos(0.0212045\tau)$
$+0.0043\sin(0.0212045\tau))+s_2(-0.0236\cos(0.0212045\tau)+(-0.101\sin(0.0212045\tau)+$
$0.0735\sin(0.042409\tau))/1000))-2.17315(s_1(-0.0013+0.0049\cos(0.0212045\tau)-$
$0.0035\cos(0.042409\tau)-1.1357\sin(0.0212045\tau))+s_4((-0.0313+0.1147\cos(0.0212045\tau)-$
$0.0834\cos(0.042409\tau))/1000-0.0268\sin(0.0212045\tau))+s_3(1.0006\cos(0.0212045\tau)+$
$0.0043\sin(0.0212045\tau))+s_2(-0.0236\cos(0.0212045\tau)+(-0.101\sin(0.0212045\tau)+$
$0.0735\sin(0.042409\tau))/1000))^3)(0.00230911+1.0005\cos(\pi\tau)/148)$
$-0.00154872\cos(\pi\tau)/74)-0.000582637\cos((3\pi)\tau)/148)-0.000309167\cos(\pi\tau)/37)-$
$0.000193159\cos((5\pi)\tau)/148)-0.000132388\cos((3\pi)\tau)/74)-0.00726049\sin(\pi\tau)/148))+$
$19.0476pq(0.00722855\cos(\pi\tau)/148)+0.998258\sin(\pi\tau)/148)-0.0030905\sin(\pi\tau)/74)-$
$0.00173894\sin((3\pi)\tau)/148)-0.00123407\sin(\pi\tau)/37)-0.000963703\sin((5\pi)\tau)/148)-$
$0.000792617\sin((3\pi)\tau)/74)-0.00067392\sin((7\pi)\tau)/148))+(4.97326(s_5\cos(0.0212045\tau)+$
$0.709s_6\sin(0.0212045\tau))^2(s_2((-0.2419+0.8899\cos(0.0212045\tau)$
$-0.648\cos(0.042409\tau))/10000-0.0208\sin(0.0212045\tau))+s_1(1.0006\cos(0.0212045\tau)+$
$0.0043\sin(0.0212045\tau))+s_3(0.001-0.0038\cos(0.0212045\tau)+0.0027\cos(0.042409\tau)+$
$0.8815\sin(0.0212045\tau))+s_4(0.0236\cos(0.0212045\tau)+(0.101\sin(0.0212045\tau)-$

$0.0735\sin(0.042409\tau))/1000)) - 2.80011(s_2((-0.2419 + 0.8899\cos(0.0212045\tau) - 0.648\cos(0.042409\tau))/10000 - 0.0208\sin(0.0212045\tau)) + s_1(1.0006\cos(0.0212045\tau) + 0.0043\sin(0.0212045\tau)) + s_3(0.001 - 0.0038\cos(0.0212045\tau) + 0.0027\cos(0.042409\tau) + 0.8815\sin(0.0212045\tau)) + s_4(0.0236\cos(0.0212045\tau) + (0.101\sin(0.0212045\tau) - 0.0735\sin(0.042409\tau))/1000))^3 - 2.17315(s_2((-0.2419 + 0.8899\cos(0.0212045\tau) - 0.648\cos(0.042409\tau))/10000 - 0.0208\sin(0.0212045\tau)) + s_1(1.0006\cos(0.0212045\tau) + 0.0043\sin(0.0212045\tau)) + s_3(0.001 - 0.0038\cos(0.0212045\tau) + 0.0027\cos(0.042409\tau) + 0.8815\sin(0.0212045\tau)) + s_4(0.0236\cos(0.0212045\tau) + (0.101\sin(0.0212045\tau) - 0.0735\sin(0.042409\tau))/1000))(s_1(-0.0013 + 0.0049\cos(0.0212045\tau) - 0.0035\cos(0.042409\tau) - 1.1357\sin(0.0212045\tau)) + s_4((-0.0313 + 0.1147\cos(0.0212045\tau) - 0.0834\cos(0.042409\tau))/1000 - 0.0268\sin(0.0212045\tau)) + s_3(1.0006\cos(0.0212045\tau) + 0.0043\sin(0.0212045\tau)) + s_2(-0.0236\cos(0.0212045\tau) + (-0.101\sin(0.0212045\tau) + 0.0735\sin(0.042409\tau))/1000))^2)(0.00722855\cos(\pi\tau)/148) + 0.998258\sin(\pi\tau)/148) - 0.0030905\sin(\pi\tau)/74) - 0.00173894\sin((3\pi)\tau)/148) - 0.00123407\sin(\pi\tau)/37) - 0.000963703\sin((5\pi)\tau)/148) - 0.000792617\sin((3\pi)\tau)/74) - 0.00067392\sin((7\pi)\tau)/148))$

$f(s_5(\tau)) = -((73s_6)/10000) + 190.476pq(-0.00512964\cos(\pi\tau)/148) - 0.708169\sin(\pi\tau)/148) + 0.00219243\sin(\pi\tau)/74) + 0.00123671\sin((3\pi)\tau)/148) + 0.000875445\sin(\pi\tau)/37) + 0.000683641\sin((5\pi)\tau)/148) + 0.000562276\sin((3\pi)\tau)/74) + 0.00048\sin((7\pi)\tau)/148)) + (4.98(s_5\cos(0.0212\tau) + 0.709s_6\sin(0.0212045\tau))^3 - 2.80011(s_5\cos(0.0212045\tau) + 0.709s_6\sin(0.0212045\tau))(s_2((-0.2419 + 0.8899\cos(0.0212045\tau) - 0.648\cos(0.042409\tau))/10000 - 0.0208\sin(0.0212045\tau)) + s_1(1.0006\cos(0.0212045\tau) + 0.0043\sin(0.0212045\tau)) + s_3(0.001 - 0.0038\cos(0.0212045\tau) + 0.0027\cos(0.042409\tau) + 0.8815\sin(0.0212045\tau)) + s_4(0.0236\cos(0.0212045\tau) + (0.101\sin(0.0212045\tau) - 0.0735\sin(0.042409\tau))/1000))^2 - 2.17315(s_5\cos(0.0212045\tau) + 0.709s_6\sin(0.0212045\tau))(s_1(-0.0013 + 0.0049\cos(0.0212045\tau) - 0.0035\cos(0.042409\tau) - 1.1357\sin(0.0212045\tau)) + s_4((-0.0313 + 0.1147\cos(0.0212045\tau) - 0.0834\cos(0.042409\tau))/1000 - 0.0268\sin(0.0212045\tau)) + s_3(1.0006\cos(0.0212045\tau) + 0.0043\sin(0.0212045\tau)) + s_2(-0.0236\cos(0.0212045\tau) + (-0.101\sin(0.0212045\tau) + 0.0735\sin(0.042409\tau))/1000))^2)(-0.00512964\cos(\pi\tau)/148) - 0.708169\sin(\pi\tau)/148) + 0.00219243\sin(\pi\tau)/74) + 0.00123671\sin((3\pi)\tau)/148) + 0.000875445\sin(\pi\tau)/37) + 0.000683641\sin((5\pi)\tau)/148) + 0.000562276\sin((3\pi)\tau)/74) + 0.000478077\sin((7\pi)\tau)/148))$

$f(s_6(\tau)) = (29s_5)/2000 + 190.476pq(0.00231055 + 1.00113\cos(\pi\tau)/148) - 0.00154973\cos(\pi\tau)/74) - 0.000587382\cos((3\pi)\tau)/148) - 0.000309363\cos(\pi\tau)/37) - 0.000193269\cos((5\pi)\tau)/148) - 0.000132463\cos((3\pi)\tau)/74) - 0.0072671\sin(\pi\tau)/148)) + (4.97326(s_5\cos(0.0212045\tau) + 0.709s_6\sin(0.0212045\tau))^3 - 2.80011(s_5\cos(0.0212045\tau) + 0.709s_6\sin(0.0212045\tau))(s_2((-0.2419 + 0.8899\cos(0.0212045\tau) - 0.648\cos(0.042409\tau))/10000 - 0.0208\sin(0.0212045\tau)) + s_1(1.0006\cos(0.0212045\tau) + 0.0043\sin(0.0212045\tau)) + s_3(0.001 - 0.0038\cos(0.0212045\tau) + 0.0027\cos(0.042409\tau) +$

$0.8815\sin(0.0212045\tau)) + s_4(0.0236\cos(0.0212045\tau) + (0.101\sin(0.0212045\tau) - 0.0735\sin(0.042409\tau))/1000))^2 - 2.17315(s_5\cos(0.0212045\tau) + 0.709s_6\sin(0.0212045\tau))(s_1(-0.0013 + 0.0049\cos(0.0212045\tau) - 0.0035\cos(0.042409\tau) - 1.1357\sin(0.0212045\tau)) + s_4((-0.0313 + 0.1147\cos(0.0212045\tau) - 0.0834\cos(0.042409\tau))/1000 - 0.0268\sin(0.0212045\tau)) + s_3(1.0006\cos(0.0212045\tau) + 0.0043\sin(0.0212045\tau)) + s_2(-0.0236\cos(0.0212045\tau) + (-0.101\sin(0.0212045\tau) + 0.0735\sin(0.042409\tau))/1000))^2)(0.00231 + 1.00113\cos(\pi\tau)/148) - 0.0015\cos(\pi\tau)/74) - 0.00058\cos((3\pi)\tau)/148) - 0.0003\cos(\pi\tau)/37) - 0.000193269\cos((5\pi)\tau)/148) - 0.000132463\cos((3\pi)\tau)/74) - 0.0072671\sin(\pi\tau)/148))$

B.2 Full center manifold equations for the ISSB problem (6.10).

Parametric equations of the center manifold are;

$$\begin{aligned} s_1(\tau) &= P_1(\tau) \\ s_2(\tau) &= P_2(\tau) \\ s_3(\tau) &= P_3(\tau) \\ s_4(\tau) &= P_4(\tau) \end{aligned}$$

The reduced system is

$$\begin{aligned} s_5' &= P_5'(\tau) \\ s_6' &= P_6'(\tau) \\ p' &= q(\tau) \\ q' &= -\frac{(441p(\tau))}{4000000} \end{aligned}$$

where
$P_1(\tau) = -1.27476 \times 10^{-6}p^2 + 0.0100999pq + 0.0115624q^2 - (0.0574401 + 0.0564899i)p^2\cos(0.021227\tau) + (1.25218 - 1.26761i)pq\cos(0.021227\tau) + (520.999 + 512.38i)q^2\cos(0.021227\tau) - (0.0574401 - 0.0564899i)p^2\cos(0.021227\tau) + (1.25218 + 1.26761i)pq\cos(0.021227\tau) + (520.999 - 512.38i)q^2\cos(0.021227\tau) - (0.00338704 - 0.00675788i)pq\cos(0.042454\tau) - (0.00387745 + 0.00773132i)q^2$
$\cos(0.042454\tau) - (0.00338704 + 0.00675788i)pq\cos(0.042454\tau) - (0.00387745 - 0.00773132i)q^2\cos(0.042454\tau) - (0.00127421 - 0.00380249i)pq\cos(0.0636809\tau) - (0.00145872 + 0.00435022i)q^2\cos(0.0636809\tau) - (0.00127421 + 0.00380249i)pq$
$\cos(0.0636809\tau) - (0.00145872 - 0.00435022i)q^2\cos(0.0636809\tau) - (0.000676139 - 0.00269849i)pq\cos(0.0849079\tau) - (0.000774048 + 0.00308719i)q^2$
$\cos(0.0849079\tau) - (0.000676139 + 0.00269849i)pq\cos(0.0849079\tau) - (0.000774048 - 0.00308719i)q^2\cos(0.0849079\tau) - (0.000422438 - 0.0021073i)pq\cos(0.106135\tau) - (0.000483603 + 0.00241084i)q^2\cos(0.106135\tau) - (0.000422438 + 0.0021073i)pq$

$\cos(0.106135\tau) - (0.000483603 - 0.00241084i)q^2\cos(0.106135\tau) - (0.000289529 - 0.00173319i)pq\cos(0.127362\tau) - (0.000331453 + 0.00198285i)q^2\cos(0.127362\tau) - (0.000289529 + 0.00173319i)pq\cos(0.127362\tau) - (0.000331453 - 0.00198285i)q^2\cos(0.127362\tau) + (0.00147364i)pq\cos(0.148589\tau) - (0.00168591i)q^2\cos(0.148589\tau) - (0.00147364i)pq\cos(0.148589\tau) + (0.00168591i)q^2\cos(0.148589\tau) - (0.0564899 - 0.0574401i)p^2\sin(0.021227\tau) - (1.26761 + 1.25218i)pq\sin 0.021227\tau) + (512.38 - 520.999i)q^2\sin 0.021227\tau) - (0.0564899 + 0.0574401i)p^2\sin 0.021227\tau) - (1.26761 - 1.25218i)pq\sin 0.021227\tau) + (512.38 + 520.999i)q^2\sin 0.021227\tau) + (0.00675788 + 0.00338704i)pq\sin 0.042454\tau) - (0.00773132 - 0.00387745i)q^2\sin 0.042454\tau) + (0.00675788 - 0.00338704i)pq\sin 0.042454\tau) - (0.00773132 + 0.00387745i)q^2\sin 0.042454\tau) + (0.00380249 + 0.00127421i)pq\sin 0.0636809\tau) - (0.00435022 - 0.00145872i)q^2\sin 0.0636809\tau) + (0.00380249 - 0.00127421i)pq\sin 0.0636809\tau) - (0.00435022 + 0.00145872i)q^2\sin 0.0636809\tau) + (0.00269849 + 0.000676139i)pq\sin 0.0849079\tau) - (0.00308719 - 0.000774048i)q^2\sin 0.0849079\tau) + (0.00269849 - 0.000676139i)pq\sin 0.0849079\tau) - (0.00308719 + 0.000774048i)q^2\sin 0.0849079\tau) + (0.0021073 + 0.000422438i)pq\sin 0.106135\tau) - (0.00241084 - 0.000483603i)q^2\sin 0.106135\tau) + (0.0021073 - 0.000422438i)pq\sin 0.106135\tau) - (0.00241084 + 0.000483603i)q^2\sin 0.106135\tau) + (0.00173319 + 0.000289529i)pq\sin 0.127362\tau) - (0.00198285 - 0.000331453i)q^2\sin 0.127362\tau) + (0.00173319 - 0.000289529i)pq\sin 0.127362\tau) - (0.00198285 + 0.000331453i)q^2\sin 0.127362\tau) + 0.00147364pq\sin 0.148589\tau) - 0.00168591q^2\sin 0.148589\tau) + 0.00147364pq\sin 0.148589\tau) - 0.00168591q^2\sin 0.148589\tau)$

$P_2(\tau) = 0.0111306p^2 + 0.232179pq - 100.958q^2 + (2.39392 - 2.4231i)p^2\cos(0.021227\tau) + (50.6112 + 49.7665i)pq\cos(0.021227\tau) - (21713.5 - 21978.2i)q^2\cos(0.021227\tau) + (2.39392 + 2.4231i)p^2\cos(0.021227\tau) + (50.6112 - 49.7665i)pq\cos(0.021227\tau) - (21713.5 + 21978.2i)q^2\cos(0.021227\tau) - (0.00373267 - 0.0074475i)p^2\cos(0.042454\tau) - (0.077861 + 0.155359i)pq\cos(0.042454\tau) + (33.8564 - 67.551i)q^2\cos(0.042454\tau) - (0.00373267 + 0.0074475i)p^2\cos(0.042454\tau) - (0.077861 - 0.155359i)pq\cos(0.042454\tau) + (33.8564 + 67.551i)q^2\cos(0.042454\tau) - (0.00140424 - 0.00419052i)p^2\cos(0.0636809\tau) - (0.0292918 + 0.0874169i)pq\cos(0.0636809\tau) + (12.7369 - 38.0093i)q^2\cos(0.0636809\tau) - (0.00140424 + 0.00419052i)p^2\cos(0.0636809\tau) - (0.0292918 - 0.0874169i)pq\cos(0.0636809\tau) + (12.7369 + 38.0093i)q^2\cos(0.0636809\tau) - (0.000745136 - 0.00297386i)p^2\cos(0.0849079\tau) - (0.0155433 + 0.0620365i)pq\cos(0.0849079\tau) + (6.7586 - 26.9738i)q^2\cos(0.0849079\tau) - (0.000745136 + 0.00297386i)p^2\cos(0.0849079\tau) - (0.0155433 - 0.0620365i)pq\cos(0.0849079\tau) + (6.7586 + 26.9738i)q^2\cos(0.0849079\tau) - (0.000465545 - 0.00232234i)p^2\cos(0.106135\tau) - (0.00971099 + 0.0484454i)pq\cos(0.106135\tau) + (4.22263 - 21.0643i)q^2\cos(0.106135\tau) - (0.000465545 + 0.00232234i)p^2\cos(0.106135\tau) - (0.00971099 - 0.0484454i)pq\cos(0.106135\tau) + (4.22263 + 21.0643i)q^2\cos(0.106135\tau) - (0.000319074 - 0.00191005i)p^2\cos(0.127362\tau) - (0.00665574 + 0.0398449i)pq\cos(0.127362\tau) + (2.89409 - 17.3247i)q^2\cos(0.127362\tau)$

$-(0.000319074+0.00191005i)p^2\cos(0.127362\tau)-(0.00665574-0.0398449i)pq$
$\cos(0.127362\tau)+(2.89409+17.3247i)q^2\cos(0.127362\tau)+(0.00162402i)p^2$
$\cos(0.148589\tau)-(0.033878i)pq\cos(0.148589\tau)-(14.7303i)q^2\cos(0.148589\tau)-$
$(0.00162402i)p^2\cos(0.148589\tau)+(0.033878i)pq\cos(0.148589\tau)$
$+(14.7303i)q^2\cos(0.148589\tau)-(2.4231+2.39392i)p^2\sin(0.021227\tau)+(49.7665-$
$50.6112i)pq\sin(0.021227\tau)+(21978.2+21713.5i)q^2\sin(0.021227\tau)-(2.4231-$
$2.39392i)p^2\sin(0.021227\tau)+(49.7665+50.6112i)pq\sin(0.021227\tau)+(21978.2-$
$21713.5i)q^2\sin(0.021227\tau)+(0.0074475+0.00373267i)p^2\sin(0.042454\tau)-(0.155359-$
$0.077861i)pq\sin(0.042454\tau)-(67.551+33.8564i)q^2\sin(0.042454\tau)+(0.0074475-$
$0.00373267i)p^2\sin(0.042454\tau)-(0.155359+0.077861i)pq\sin(0.042454\tau)-(67.551-$
$33.8564i)q^2\sin(0.042454\tau)+(0.00419052+0.00140424i)p^2\sin(0.0636809\tau)-$
$(0.0874169-0.0292918i)pq\sin(0.0636809\tau)-(38.0093+12.7369i)q^2\sin(0.0636809\tau)+$
$(0.00419052-0.00140424i)p^2\sin(0.0636809\tau)-(0.0874169+0.0292918i)pq$
$\sin(0.0636809\tau)-(38.0093-12.7369i)q^2\sin(0.0636809\tau)+(0.00297386+$
$0.000745136i)p^2\sin(0.0849079\tau)-(0.0620365-0.0155433i)pq\sin(0.0849079\tau)-$
$(26.9738+6.7586i)q^2\sin(0.0849079\tau)+(0.00297386-0.000745136i)p^2\sin(0.0849079\tau)-$
$(0.0620365+0.0155433i)pq\sin(0.0849079\tau)-(26.9738-6.7586i)q^2\sin(0.0849079\tau)+$
$(0.00232234+0.000465545i)p^2\sin(0.106135\tau)-(0.0484454-0.00971099i)pq$
$\sin(0.106135\tau)-(21.0643+4.22263i)q^2\sin(0.106135\tau)+(0.00232234-0.000465545i)p^2$
$\sin(0.106135\tau)-(0.0484454+0.00971099i)pq\sin(0.106135\tau)-(21.0643-$
$4.22263i)q^2\sin(0.106135\tau)+(0.00191005+0.000319074i)p^2\sin(0.127362\tau)-$
$(0.0398449-0.00665574i)pq\sin(0.127362\tau)-(17.3247+2.89409i)q^2\sin(0.127362\tau)+$
$(0.00191005-0.000319074i)p^2\sin(0.127362\tau)-(0.0398449+0.00665574i)pq$
$\sin(0.127362\tau)-(17.3247-2.89409i)q^2\sin(0.127362\tau)+0.00162402p^2\sin(0.148589\tau)-$
$0.033878pq\sin(0.148589\tau)-14.7303q^2\sin(0.148589\tau)+0.00162402p^2\sin(0.148589\tau)-$
$0.033878pq\sin(0.148589\tau)-14.7303q^2\sin(0.148589\tau)$

$P_3(\tau)=0.0100666pq+0.00231649q^2+(0.0562962-0.0569785i)p^2\cos(0.021227\tau)+$
$(0.952311+0.936322i)pq\cos(0.021227\tau)-(510.623-516.811i)q^2\cos(0.021227\tau)+$
$(0.0562962+0.0569785i)p^2\cos(0.021227\tau)+(0.952311-0.936322i)pq\cos(0.021227\tau)-$
$(510.623+516.811i)q^2\cos(0.021227\tau)-(0.00337582+0.00673653i)pq\cos(0.042454\tau)-$
$(0.000776843-0.0015438i)q^2\cos(0.042454\tau)-(0.00337582-0.00673653i)pq$
$\cos(0.042454\tau)-(0.000776843+0.0015438i)q^2\cos(0.042454\tau)-(0.00127001+$
$0.00379048i)pq\cos(0.0636809\tau)-(0.00029225-0.000868659i)q^2\cos(0.0636809\tau)-$
$(0.00127001-0.00379048i)pq\cos(0.0636809\tau)-(0.00029225+0.000868659i)q^2$
$\cos(0.0636809\tau)-(0.00067391+0.00268996i)pq\cos(0.0849079\tau)-(0.000155077-$
$0.000616455i)q^2\cos(0.0849079\tau)-(0.00067391-0.00268996i)pq\cos(0.0849079\tau)-$
$(0.000155077+0.000616455i)q^2\cos(0.0849079\tau)-(0.00042104+0.00210064i)pq$
$\cos(0.106135\tau)-(0.0000968892-0.000481401i)q^2\cos(0.106135\tau)-(0.00042104-$
$0.00210064i)pq\cos(0.106135\tau)-(0.0000968892+0.000481401i)q^2\cos(0.106135\tau)-$
$(0.000288573+0.00172771i)pq\cos(0.127362\tau)-(0.0000664056-0.000395937i)q^2$
$\cos(0.127362\tau)-(0.000288573-0.00172771i)pq\cos(0.127362\tau)-(0.0000664056+$

$0.000395937i)q^2\cos(0.127362\tau) - (0.00146898i)pq\cos(0.148589\tau) + (0.000336644i)q^2$
$\cos(0.148589\tau) + (0.00146898i)pq\cos(0.148589\tau) - (0.000336644i)q^2\cos(0.148589\tau) -$
$(0.0569785 + 0.0562962i)p^2\sin(0.021227\tau) + (0.936322 - 0.952311i)pq\sin(0.021227\tau) +$
$(516.811 + 510.623i)q^2\sin(0.021227\tau) - (0.0569785 - 0.0562962i)p^2\sin(0.021227\tau) +$
$(0.936322 + 0.952311i)pq\sin(0.021227\tau) + (516.811 - 510.623i)q^2\sin(0.021227\tau) -$
$(0.00673653 - 0.00337582i)pq\sin(0.042454\tau) + (0.0015438 + 0.000776843i)q^2$
$\sin(0.042454\tau) - (0.00673653 + 0.00337582i)pq\sin(0.042454\tau) + (0.0015438 -$
$0.000776843i)q^2\sin(0.042454\tau) - (0.00379048 - 0.00127001i)pq\sin(0.0636809\tau) +$
$(0.000868659 + 0.00029225i)q^2\sin(0.0636809\tau) - (0.00379048 + 0.00127001i)pq$
$\sin(0.0636809\tau) + (0.000868659 - 0.00029225i)q^2\sin(0.0636809\tau) - (0.00268996 -$
$0.00067391i)pq\sin(0.0849079\tau) + (0.000616455 + 0.000155077i)q^2\sin(0.0849079\tau) -$
$(0.00268996 + 0.00067391i)pq\sin(0.0849079\tau) + (0.000616455 - 0.000155077i)q^2$
$\sin(0.0849079\tau) - (0.00210064 - 0.00042104i)pq\sin(0.106135\tau) + (0.000481401 +$
$0.0000968892i)q^2\sin(0.106135\tau) - (0.00210064 + 0.00042104i)pq\sin(0.106135\tau) +$
$(0.000481401 - 0.0000968892i)q^2\sin(0.106135\tau) - (0.00172771 - 0.000288573i)pq$
$\sin(0.127362\tau) + (0.000395937 + 0.0000664056i)q^2\sin(0.127362\tau) - (0.00172771 +$
$0.000288573i)pq\sin(0.127362\tau) + (0.000395937 - 0.0000664056i)q^2\sin(0.127362\tau) -$
$0.00146898pq\sin(0.148589\tau) + 0.000336644q^2\sin(0.148589\tau)$
$- 0.00146898pq\sin(0.148589\tau) + 0.000336644q^2\sin(0.148589\tau)$

$P_4(\tau) = 0.011129p^2 - 0.232193pq - 100.944q^2 + (2.42843 + 2.38811i)p^2\cos(0.021227\tau) -$
$(49.8879 - 50.5004i)pq\cos(0.021227\tau) - (22026.6 + 21660.9i)q^2\cos(0.021227\tau) +$
$(2.42843 - 2.38811i)p^2\cos(0.021227\tau) - (49.8879 + 50.5004i)pq\cos(0.021227\tau) -$
$(22026.6 - 21660.9i)q^2\cos(0.021227\tau) - (0.0037321 + 0.00744748i)p^2\cos(0.042454\tau) +$
$(0.0778665 - 0.155374i)pq\cos(0.042454\tau) + (33.8513 + 67.5509i)q^2\cos(0.042454\tau) -$
$(0.0037321 - 0.00744748i)p^2\cos(0.042454\tau) + (0.0778665 + 0.155374i)pq\cos(0.042454\tau) +$
$(33.8513 - 67.5509i)q^2\cos(0.042454\tau) - (0.00140404 + 0.00419051i)p^2\cos(0.0636809\tau) +$
$(0.0292935 - 0.0874252i)pq\cos(0.0636809\tau) + (12.7351 + 38.0092i)q^2\cos(0.0636809\tau) -$
$(0.00140404 - 0.00419051i)p^2\cos(0.0636809\tau) + (0.0292935 + 0.0874252i)pq$
$\cos(0.0636809\tau) + (12.7351 - 38.0092i)q^2\cos(0.0636809\tau) - (0.000745034 +$
$0.00297385i)p^2\cos(0.0849079\tau) + (0.0155441 - 0.0620424i)pq\cos(0.0849079\tau) +$
$(6.75768 + 26.9737i)q^2\cos(0.0849079\tau) - (0.000745034 - 0.00297385i)p^2\cos(0.0849079\tau) +$
$(0.0155441 + 0.0620424i)pq\cos(0.0849079\tau) + (6.75768 - 26.9737i)q^2\cos(0.0849079\tau) -$
$(0.000465476 + 0.00232233i)p^2\cos(0.106135\tau) + (0.00971164 - 0.04845i)pq\cos(0.106135\tau) +$
$(4.22201 + 21.0643i)q^2\cos(0.106135\tau) - (0.000465476 - 0.00232233i)p^2\cos(0.106135\tau) +$
$(0.00971164 + 0.04845i)pq\cos(0.106135\tau) + (4.22201 - 21.0643i)q^2\cos(0.106135\tau) -$
$(0.000319029 + 0.00191005i)p^2\cos(0.127362\tau) + (0.00665613 - 0.0398487i)pq$
$\cos(0.127362\tau) + (2.89369 + 17.3247i)q^2\cos(0.127362\tau) - (0.000319029 -$
$0.00191005i)p^2\cos(0.127362\tau) + (0.00665613 + 0.0398487i)pq\cos(0.127362\tau) +$
$(2.89369 - 17.3247i)q^2\cos(0.127362\tau) - (0.00162401i)p^2\cos(0.148589\tau) -$
$(0.0338812i)pq$
$\cos(0.148589\tau) + (14.7303i)q^2\cos(0.148589\tau) + (0.00162401i)p^2\cos(0.148589\tau)$

$+ \ (0.0338812i)pq\cos(0.148589\tau) \ - \ (14.7303i)q^2\cos(0.148589\tau) \ + \ (2.38811 \ - \ 2.42843i)p^2\sin(0.021227\tau) \ + \ (50.5004 \ + \ 49.8879i)pq\sin(0.021227\tau) \ - \ (21660.9 \ - \ 22026.6i)q^2\sin(0.021227\tau) \ + \ (2.38811 \ + \ 2.42843i)p^2\sin(0.021227\tau) \ + \ (50.5004 \ - \ 49.8879i)pq\sin(0.021227\tau) \ - \ (21660.9 + 22026.6i)q^2\sin(0.021227\tau) \ - \ (0.00744748 \ - \ 0.0037321i)p^2\sin(0.042454\tau) - (0.155374 + 0.0778665i)pq\sin(0.042454\tau) + (67.5509 \ - \ 33.8513i)q^2\sin(0.042454\tau) - (0.00744748 + 0.0037321i)p^2\sin(0.042454\tau) - (0.155374 \ - \ 0.0778665i)pq\sin(0.042454\tau) + (67.5509 + 33.8513i)q^2\sin(0.042454\tau) \ - \ (0.00419051 \ - \ 0.00140404i)p^2\sin(0.0636809\tau) \ - \ (0.0874252 \ + \ 0.0292935i)pq\sin(0.0636809\tau) \ + \ (38.0092 - 12.7351i)q^2\sin(0.0636809\tau) - (0.00419051 + 0.00140404i)p^2\sin(0.0636809\tau) - \ (0.0874252 - 0.0292935i)pq\sin(0.0636809\tau) + (38.0092 + 12.7351i)q^2\sin(0.0636809\tau) - \ (0.00297385 - 0.000745034i)p^2\sin(0.0849079\tau) - (0.0620424 + 0.0155441i)pq \ \sin(0.0849079\tau) \ + \ (26.9737 \ - \ 6.75768i)q^2\sin(0.0849079\tau) \ - \ (0.00297385 \ + \ 0.000745034i)p^2\sin(0.0849079\tau) \ - \ (0.0620424 \ - \ 0.0155441i)pq\sin(0.0849079\tau) \ + \ (26.9737 + 6.75768i)q^2\sin(0.0849079\tau) - (0.00232233 - 0.000465476i)p^2\sin(0.106135\tau) - \ (0.04845 \ + \ 0.00971164i)pq\sin(0.106135\tau) \ + \ (21.0643 \ - \ 4.22201i)q^2\sin(0.106135\tau) \ - \ (0.002 + 0.000465i)p^2\sin(0.106135\tau) - (0.04845 - 0.0097i)pq\sin(0.106135\tau) + (21.0643 + \ 4.222i)q^2\sin(0.106135\tau) \ - \ (0.0019 \ - \ 0.00032i)p^2\sin(0.127362\tau) \ - \ (0.0398487 \ + \ 0.00665613i)pq\sin(0.127362\tau) + (17.3247 - 2.89369i)q^2\sin(0.127362\tau) - (0.00191005 + \ 0.000319029i)p^2\sin(0.127362\tau) - (0.0398487 - 0.00665613i)pq \ \sin(0.127362\tau) + (17.3247 + 2.89369i)q^2\sin(0.127362\tau) - 0.00162401p^2\sin(0.148589\tau) - \ 0.0338812pq\sin(0.148589\tau) + 14.7303q^2\sin(0.148589\tau) - 0.00162401p^2 \ \sin(0.148589\tau) - 0.0338812pq\sin(0.148589\tau) + 14.7303q^2\sin(0.148589\tau)$

$P_5'(\tau) = -((73s_6)/10000) + 190.476pq(-0.00512964\cos(\pi\tau)/148) - 0.708169 \ \sin(\pi\tau)/148) + 0.00219243\sin(\pi\tau)/74) + 0.00123671\sin((3\pi)\tau)/148) \ +0.000875445\sin(\pi\tau)/37) + 0.000683641\sin((5\pi)\tau)/148) + 0.000562276\sin((3\pi)\tau)/74) + \ 0.000478077\sin((7\pi)\tau)/148)) + (4.97326(s_5\cos(0.0212045\tau) + 0.709s_6\sin(0.0212045\tau))^3 - \ 2.80011(s_5\cos(0.0212045\tau) + 0.709s_6\sin(0.0212045\tau))((0.001 - 0.0038\cos(0.0212045\tau) + \ 0.0027\cos(0.042409\tau) + 0.8815\sin(0.0212045\tau))(p^2((0.0562962 - 0.0569785i) \ (\cos(0.021227\tau) \ - \ i\sin(0.021227\tau)) \ + \ (0.0562962 \ + \ 0.0569785i)(\cos(0.021227\tau) \ + \ i\sin(0.021227\tau))) \ + \ q^2(0.00231649 \ - \ (510.623 \ - \ 516.811i)(\cos(0.021227\tau) \ - \ i\sin(0.021227\tau)) \ - \ (510.623 \ + \ 516.811i)(\cos(0.021227\tau) \ + \ i\sin(0.021227\tau)) \ - \ (0.000776843 \ - \ 0.0015438i)(\cos(0.042454\tau) \ - \ i\sin(0.042454\tau)) \ - \ (0.000776843 \ + \ 0.0015438i)(\cos(0.042454\tau) + i\sin(0.042454\tau)) - (0.00029225 - 0.000868659i) \ (\cos(0.0636809\tau) - i\sin(0.0636809\tau)) - (0.00029225 + 0.000868659i)(\cos(0.0636809\tau) + \ i\sin(0.0636809\tau)) - (0.000155077 - 0.000616455i)(\cos(0.0849079\tau) - i\sin(0.0849079\tau)) - \ (0.000155077 + 0.000616455i)(\cos(0.0849079\tau) + i\sin(0.0849079\tau)) - (0.0000968892 - \ 0.000481401i)(\cos(0.106135\tau) - i\sin(0.106135\tau)) - (0.0000968892 + 0.000481401i) \ (\cos(0.106135\tau) + i\sin(0.106135\tau)) - (0.0000664056 - 0.000395937i)(\cos(0.127362\tau) - \ i\sin(0.127362\tau)) - (0.0000664056 + 0.000395937i)(\cos(0.127362\tau) + i\sin(0.127362\tau)) + \ (0.000336644i)(\cos(0.148589\tau) - i\sin(0.148589\tau)) - (0.000336644i)(\cos(0.148589\tau) + \ i\sin(0.148589\tau))) \ + \ pq(0.0100666 \ + \ (0.952311 \ + \ 0.936322i)(\cos(0.021227\tau) \ -$

$i\sin(0.021227\tau)) + (0.952311 - 0.936322i)(\cos(0.021227\tau) + i\sin(0.021227\tau)) - (0.00337582 + 0.00673653i)(\cos(0.042454\tau) - i\sin(0.042454\tau)) - (0.00337582 - 0.00673653i)(\cos(0.042454\tau) + i\sin(0.042454\tau)) - (0.00127001 + 0.00379048i)(\cos(0.0636809\tau) - i\sin(0.0636809\tau)) - (0.00127001 - 0.00379048i)(\cos(0.0636809\tau) + i\sin(0.0636809\tau)) - (0.00067391 + 0.00268996i)(\cos(0.0849079\tau) - i\sin(0.0849079\tau)) - (0.00067391 - 0.00268996i)(\cos(0.0849079\tau) + i\sin(0.0849079\tau)) - (0.00042104 + 0.00210064i)(\cos(0.106135\tau) - i\sin(0.106135\tau)) - (0.00042104 - 0.00210064i)(\cos(0.106135\tau) + i\sin(0.106135\tau)) - (0.000288573 + 0.00172771i)(\cos(0.127362\tau) - i\sin(0.127362\tau)) - (0.000288573 - 0.00172771i)(\cos(0.127362\tau) + i\sin(0.127362\tau)) - (0.00146898i)(\cos(0.148589\tau) - i\sin(0.148589\tau)) + (0.00146898i)(\cos(0.148589\tau) + i\sin(0.148589\tau)))) + (1.0006\cos(0.0212045\tau) + 0.0043\sin(0.0212045\tau))(p^2(-1.27476 \times 10^{-6} - (0.0574401 + 0.0564899i)(\cos(0.021227\tau) - i\sin(0.021227\tau)) - (0.0574401 - 0.0564899i)(\cos(0.021227\tau) + i\sin(0.021227\tau))) + pq(0.0100999 + (1.25218 - 1.26761i)(\cos(0.021227\tau) - i\sin(0.021227\tau)) + (1.25218 + 1.26761i)(\cos(0.021227\tau) + i\sin(0.021227\tau)) - (0.00338704 - 0.00675788i)(\cos(0.042454\tau) - i\sin(0.042454\tau)) - (0.00338704 + 0.00675788i)(\cos(0.042454\tau) + i\sin(0.042454\tau)) - (0.00127421 - 0.00380249i)(\cos(0.0636809\tau) - i\sin(0.0636809\tau)) - (0.00127421 + 0.00380249i)(\cos(0.0636809\tau) + i\sin(0.0636809\tau)) - (0.000676139 - 0.00269849i)(\cos(0.0849079\tau) - i\sin(0.0849079\tau)) - (0.000676139 + 0.00269849i)(\cos(0.0849079\tau) + i\sin(0.0849079\tau)) - (0.000422438 - 0.0021073i)(\cos(0.106135\tau) - i\sin(0.106135\tau)) - (0.000422438 + 0.0021073i)(\cos(0.106135\tau) + i\sin(0.106135\tau)) - (0.000289529 - 0.00173319i)(\cos(0.127362\tau) - i\sin(0.127362\tau)) - (0.000289529 + 0.00173319i)(\cos(0.127362\tau) + i\sin(0.127362\tau)) + (0.00147364i)(\cos(0.148589\tau) - i\sin(0.148589\tau)) - (0.00147364i)(\cos(0.148589\tau) + i\sin(0.148589\tau))) + q^2(0.0115624 + (520.999 + 512.38i)(\cos(0.021227\tau) - i\sin(0.021227\tau)) + (520.999 - 512.38i)(\cos(0.021227\tau) + i\sin(0.021227\tau)) - (0.00387745 + 0.00773132i)(\cos(0.042454\tau) - i\sin(0.042454\tau)) - (0.00387745 - 0.00773132i)(\cos(0.042454\tau) + i\sin(0.042454\tau)) - (0.00145872 + 0.00435022i)(\cos(0.0636809\tau) - i\sin(0.0636809\tau)) - (0.00145872 - 0.00435022i)(\cos(0.0636809\tau) + i\sin(0.0636809\tau)) - (0.000774048 + 0.00308719i)(\cos(0.0849079\tau) - i\sin(0.0849079\tau)) - (0.000774048 - 0.00308719i)(\cos(0.0849079\tau) + i\sin(0.0849079\tau)) - (0.000483603 + 0.00241084i)(\cos(0.106135\tau) - i\sin(0.106135\tau)) - (0.000483603 - 0.00241084i)(\cos(0.106135\tau) + i\sin(0.106135\tau)) - (0.000331453 + 0.00198285i)(\cos(0.127362\tau) - i\sin(0.127362\tau)) - (0.000331453 - 0.00198285i)(\cos(0.127362\tau) + i\sin(0.127362\tau)) - (0.00168591i)(\cos(0.148589\tau) - i\sin(0.148589\tau)) + (0.00168591i)(\cos(0.148589\tau) + i\sin(0.148589\tau)))) + (0.0236\cos(0.0212045\tau) + (0.101\sin(0.0212045\tau) - 0.0735\sin(0.042409\tau))/1000)(p^2(0.011129 + (2.42843 + 2.38811i)(\cos(0.021227\tau) - i\sin(0.021227\tau)) + (2.42843 - 2.38811i)(\cos(0.021227\tau) + i\sin(0.021227\tau)) - (0.0037321 + 0.00744748i)(\cos(0.042454\tau) - i\sin(0.042454\tau)) - (0.0037321 - 0.00744748i)(\cos(0.042454\tau) + i\sin(0.042454\tau)) - (0.00140404 + 0.00419051i)(\cos(0.0636809\tau) - i\sin(0.0636809\tau)) - (0.00140404 - 0.00419051i)(\cos(0.0636809\tau) + i\sin(0.0636809\tau)) - (0.000745034 + 0.00297385i)(\cos(0.0849079\tau) - i\sin(0.0849079\tau)) - (0.000745034 - 0.00297385i)(\cos(0.0849079\tau) + i\sin(0.0849079\tau)) - (0.000465476 +$

$0.00232233i)(\cos(0.106135\tau) - i\sin(0.106135\tau)) - (0.000465476 - 0.00232233i)$
$(\cos(0.106135\tau) + i\sin(0.106135\tau)) - (0.000319029 + 0.00191005i)(\cos(0.127362\tau) -$
$i\sin(0.127362\tau)) - (0.000319029 - 0.00191005i)(\cos(0.127362\tau) + i\sin(0.127362\tau)) -$
$(0.00162401i)(\cos(0.148589\tau) - i\sin(0.148589\tau)) + (0.00162401i)(\cos(0.148589\tau) +$
$i\sin(0.148589\tau))) + pq(-0.232193 - (49.8879 - 50.5004i)(\cos(0.021227\tau) -$
$i\sin(0.021227\tau)) - (49.8879 + 50.5004i)(\cos(0.021227\tau) + i\sin(0.021227\tau)) +$
$(0.0778665 - 0.155374i)(\cos(0.042454\tau) - i\sin(0.042454\tau)) + (0.0778665 +$
$0.155374i)(\cos(0.042454\tau) + i\sin(0.042454\tau)) + (0.0292935 - 0.0874252i)$
$(\cos(0.0636809\tau) - i\sin(0.0636809\tau)) + (0.0292935 + 0.0874252i)(\cos(0.0636809\tau) +$
$i\sin(0.0636809\tau)) + (0.0155441 - 0.0620424i)(\cos(0.0849079\tau) - i\sin(0.0849079\tau)) +$
$(0.0155441 + 0.0620424i)(\cos(0.0849079\tau) + i\sin(0.0849079\tau)) + (0.00971164 -$
$0.04845i)(\cos(0.106135\tau) - i\sin(0.106135\tau)) + (0.00971164 + 0.04845i)(\cos(0.106135\tau) +$
$i\sin(0.106135\tau)) + (0.00665613 - 0.0398487i)(\cos(0.127362\tau) - i\sin(0.127362\tau)) +$
$(0.00665613 + 0.0398487i)(\cos(0.127362\tau) + i\sin(0.127362\tau)) - (0.0338812i)$
$(\cos(0.148589\tau) - i\sin(0.148589\tau)) + (0.0338812i)(\cos(0.148589\tau) + i\sin(0.148589\tau))) +$
$q^2(-100.944 - (22026.6 + 21660.9i)(\cos(0.021227\tau) - i\sin(0.021227\tau)) - (22026.6 -$
$21660.9i)(\cos(0.021227\tau) + i\sin(0.021227\tau)) + (33.8513 + 67.5509i)$
$(\cos(0.042454\tau) - i\sin(0.042454\tau)) + (33.8513 - 67.5509i)(\cos(0.042454\tau) +$
$i\sin(0.042454\tau)) + (12.7351 + 38.0092i)(\cos(0.0636809\tau) - i\sin(0.0636809\tau)) +$
$(12.7351 - 38.0092i)(\cos(0.0636809\tau) + i\sin(0.0636809\tau)) + (6.75768 + 26.9737i)$
$(\cos(0.0849079\tau) - i\sin(0.0849079\tau)) + (6.75768 - 26.9737i)(\cos(0.0849079\tau) +$
$i\sin(0.0849079\tau)) + (4.22201 + 21.0643i)(\cos(0.106135\tau) - i\sin(0.106135\tau)) +$
$(4.22201 - 21.0643i)(\cos(0.106135\tau) + i\sin(0.106135\tau)) + (2.89369 + 17.3247i)$
$(\cos(0.127362\tau) - i\sin(0.127362\tau)) + (2.89369 - 17.3247i)(\cos(0.127362\tau) +$
$i\sin(0.127362\tau)) + (14.7303i)(\cos(0.148589\tau) - i\sin(0.148589\tau)) - (14.7303i)$
$(\cos(0.148589\tau) + i\sin(0.148589\tau)))) + ((-0.2419 + 0.8899\cos(0.0212045\tau) -$
$0.648\cos(0.042409\tau))/10000 - 0.0208\sin(0.0212045\tau))(p^2(0.0111306 + (2.39392 -$
$2.4231i)(\cos(0.021227\tau) - i\sin(0.021227\tau)) + (2.39392 + 2.4231i)(\cos(0.021227\tau) +$
$i\sin(0.021227\tau)) - (0.00373267 - 0.0074475i)(\cos(0.042454\tau) - i\sin(0.042454\tau)) -$
$(0.00373267 + 0.0074475i)(\cos(0.042454\tau) + i\sin(0.042454\tau)) - (0.00140424 -$
$0.00419052i)(\cos(0.0636809\tau) - i\sin(0.0636809\tau)) - (0.00140424 + 0.00419052i)$
$(\cos(0.0636809\tau) + i\sin(0.0636809\tau)) - (0.000745136 - 0.00297386i)(\cos(0.0849079\tau) -$
$i\sin(0.0849079\tau)) - (0.000745136 + 0.00297386i)(\cos(0.0849079\tau) + i\sin(0.0849079\tau)) -$
$(0.000465545 - 0.00232234i)(\cos(0.106135\tau) - i\sin(0.106135\tau)) - (0.000465545 +$
$0.00232234i)(\cos(0.106135\tau) + i\sin(0.106135\tau)) - (0.000319074 - 0.00191005i)$
$(\cos(0.127362\tau) - i\sin(0.127362\tau)) - (0.000319074 + 0.00191005i)(\cos(0.127362\tau) +$
$i\sin(0.127362\tau)) + (0.00162402i)(\cos(0.148589\tau) - i\sin(0.148589\tau)) - (0.00162402i)$
$(\cos(0.148589\tau) + i\sin(0.148589\tau))) + pq(0.232179 + (50.6112 + 49.7665i)(\cos(0.021227\tau) -$
$i\sin(0.021227\tau)) + (50.6112 - 49.7665i)(\cos(0.021227\tau) + i\sin(0.021227\tau)) - (0.077861 +$
$0.155359i)(\cos(0.042454\tau) - i\sin(0.042454\tau)) - (0.077861 - 0.155359i)$
$(\cos(0.042454\tau) + i\sin(0.042454\tau)) - (0.0292918 + 0.0874169i)(\cos(0.0636809\tau) -$
$i\sin(0.0636809\tau)) - (0.0292918 - 0.0874169i)(\cos(0.0636809\tau) + i\sin(0.0636809\tau)) -$

$(0.0155433 + 0.0620365i)(\cos(0.0849079\tau) - i\sin(0.0849079\tau)) - (0.0155433 - 0.0620365i)$
$(\cos(0.0849079\tau) + i\sin(0.0849079\tau)) - (0.00971099 + 0.0484454i)(\cos(0.106135\tau) - i\sin(0.106135\tau)) - (0.00971099 - 0.0484454i)(\cos(0.106135\tau) + i\sin(0.106135\tau)) - (0.00665574 + 0.0398449i)(\cos(0.127362\tau) - i\sin(0.127362\tau)) - (0.00665574 - 0.0398449i)(\cos(0.127362\tau) + i\sin(0.127362\tau)) - (0.033878i)(\cos(0.148589\tau) - i\sin(0.148589\tau)) + (0.033878i)(\cos(0.148589\tau) + i\sin(0.148589\tau))) + q^2(-100.958 - (21713.5 - 21978.2i)(\cos(0.021227\tau) - i\sin(0.021227\tau)) - (21713.5 + 21978.2i)$
$(\cos(0.021227\tau) + i\sin(0.021227\tau)) + (33.8564 - 67.551i)(\cos(0.042454\tau) - i\sin(0.042454\tau)) + (33.8564 + 67.551i)(\cos(0.042454\tau) + i\sin(0.042454\tau)) + (12.7369 - 38.0093i)(\cos(0.0636809\tau) - i\sin(0.0636809\tau)) + (12.7369 + 38.0093i)(\cos(0.0636809\tau) + i\sin(0.0636809\tau)) + (6.7586 - 26.9738i)(\cos(0.0849079\tau) - i\sin(0.0849079\tau)) + (6.7586 + 26.9738i)(\cos(0.0849079\tau) + i\sin(0.0849079\tau)) + (4.22263 - 21.0643i)$
$(\cos(0.106135\tau) - i\sin(0.106135\tau)) + (4.22263 + 21.0643i)(\cos(0.106135\tau) + i\sin(0.106135\tau)) + (2.89409 - 17.3247i)(\cos(0.127362\tau) - i\sin(0.127362\tau)) + (2.89409 + 17.3247i)(\cos(0.127362\tau) + i\sin(0.127362\tau)) - (14.7303i)(\cos(0.148589\tau) - i\sin(0.148589\tau)) + (14.7303i)(\cos(0.148589\tau) + i\sin(0.148589\tau)))))^2 - 2.17315$
$(s_5\cos(0.0212045\tau) + 0.709s_6\sin(0.0212045\tau))((1.0006\cos(0.0212045\tau)$
$+ 0.0043\sin(0.021\tau))(p^2((0.056 - 0.056i)(\cos(0.021227\tau) - i\sin(0.021\tau)) + (0.056 + 0.056i)(\cos(0.021227\tau) + i\sin(0.021227\tau))) + q^2(0.00231649 - (510.623 - 516.811i)(\cos(0.021227\tau) - i\sin(0.021227\tau)) - (510.623 + 516.811i)$
$(\cos(0.021227\tau) + i\sin(0.021227\tau)) - (0.000776843 - 0.0015438i)(\cos(0.042454\tau) - i\sin(0.042454\tau)) - (0.000776843 + 0.0015438i)(\cos(0.042454\tau) + i\sin(0.042454\tau)) - (0.00029225 - 0.000868659i)(\cos(0.0636809\tau) - i\sin(0.0636809\tau)) - (0.00029225 + 0.000868659i)(\cos(0.0636809\tau) + i\sin(0.0636809\tau)) - (0.000155077 - 0.000616455i)$
$(\cos(0.0849079\tau) - i\sin(0.0849079\tau)) - (0.000155077 + 0.000616455i)(\cos(0.0849079\tau) + i\sin(0.0849079\tau)) - (0.0000968892 - 0.000481401i)(\cos(0.106135\tau) - i\sin(0.106135\tau)) - (0.0000968892 + 0.000481401i)(\cos(0.106135\tau) + i\sin(0.106135\tau)) - (0.0000664056 - 0.000395937i)(\cos(0.127362\tau) - i\sin(0.127362\tau)) - (0.0000664056 + 0.000395937i)$
$(\cos(0.127362\tau) + i\sin(0.127362\tau)) + (0.000336644i)(\cos(0.148589\tau) - i\sin(0.148589\tau)) - (0.000336644i)(\cos(0.148589\tau) + i\sin(0.148589\tau))) + pq(0.0100666 + (0.952311 + 0.936322i)(\cos(0.021227\tau) - i\sin(0.021227\tau)) + (0.952311 - 0.936322i)(\cos(0.021227\tau) + i\sin(0.021227\tau)) - (0.00337582 + 0.00673653i)(\cos(0.042454\tau) - i\sin(0.042454\tau)) - (0.00337582 - 0.00673653i)(\cos(0.042454\tau) + i\sin(0.042454\tau)) - (0.00127001 + 0.00379048i)(\cos(0.0636809\tau) - i\sin(0.0636809\tau)) - (0.00127001 - 0.00379048i)$
$(\cos(0.0636809\tau) + i\sin(0.0636809\tau)) - (0.00067391 + 0.00268996i)(\cos(0.0849079\tau) - i\sin(0.0849079\tau)) - (0.00067391 - 0.00268996i)(\cos(0.0849079\tau) + i\sin(0.0849079\tau)) - (0.00042104 + 0.00210064i)(\cos(0.106135\tau) - i\sin(0.106135\tau)) - (0.00042104 - 0.00210064i)(\cos(0.106135\tau) + i\sin(0.106135\tau)) - (0.000288573 + 0.00172771i)$
$(\cos(0.127362\tau) - i\sin(0.127362\tau)) - (0.000288573 - 0.00172771i)(\cos(0.127362\tau) + i\sin(0.127362\tau)) - (0.00146898i)(\cos(0.148589\tau) - i\sin(0.148589\tau)) + (0.00146898i)$
$(\cos(0.148589\tau) + i\sin(0.148589\tau)))) + (-0.0013 + 0.0049\cos(0.0212045\tau) -$

$0.0035\cos(0.042409\tau) - 1.1357\sin(0.0212045\tau))(p^2(-1.27476 \times 10^{-6} - (0.0574401 + 0.056i)(\cos(0.021227\tau) - i\sin(0.021227\tau)) - (0.057 - 0.056i)(\cos(0.021227\tau) + i\sin(0.021227\tau))) + pq(0.0100999 + (1.25218 - 1.26761i)(\cos(0.021227\tau) - i\sin(0.021227\tau)) + (1.25218 + 1.26761i)(\cos(0.021227\tau) + i\sin(0.021227\tau)) - (0.00338704 - 0.00675788i)(\cos(0.042454\tau) - i\sin(0.042454\tau)) - (0.00338704 + 0.00675788i)(\cos(0.042454\tau) + i\sin(0.042454\tau)) - (0.00127421 - 0.00380249i)(\cos(0.0636809\tau) - i\sin(0.0636809\tau)) - (0.00127421 + 0.00380249i)(\cos(0.0636809\tau) + i\sin(0.0636809\tau)) - (0.000676139 - 0.00269849i)(\cos(0.0849079\tau) - i\sin(0.0849079\tau)) - (0.000676139 + 0.00269849i)(\cos(0.0849079\tau) + i\sin(0.0849079\tau)) - (0.000422438 - 0.0021073i)(\cos(0.106135\tau) - i\sin(0.106135\tau)) - (0.000422438 + 0.0021073i)(\cos(0.106135\tau) + i\sin(0.106135\tau)) - (0.000289529 - 0.00173319i)(\cos(0.127362\tau) - i\sin(0.127362\tau)) - (0.000289529 + 0.00173319i)(\cos(0.127362\tau) + i\sin(0.127362\tau)) + (0.00147364i)(\cos(0.148589\tau) - i\sin(0.148589\tau)) - (0.00147364i)(\cos(0.148589\tau) + i\sin(0.148589\tau))) + q^2(0.0115624 + (520.999 + 512.38i)(\cos(0.021227\tau) - i\sin(0.021227\tau)) + (520.999 - 512.38i)(\cos(0.021227\tau) + i\sin(0.021227\tau)) - (0.00387745 + 0.00773132i)(\cos(0.042454\tau) - i\sin(0.042454\tau)) - (0.00387745 - 0.00773132i)(\cos(0.042454\tau) + i\sin(0.042454\tau)) - (0.00145872 + 0.00435022i)(\cos(0.0636809\tau) - i\sin(0.0636809\tau)) - (0.00145872 - 0.00435022i)(\cos(0.0636809\tau) + i\sin(0.0636809\tau)) - (0.000774048 + 0.00308719i)(\cos(0.0849079\tau) - i\sin(0.0849079\tau)) - (0.000774048 - 0.00308719i)(\cos(0.0849079\tau) + i\sin(0.0849079\tau)) - (0.000483603 + 0.00241084i)(\cos(0.106135\tau) - i\sin(0.106135\tau)) - (0.000483603 - 0.00241084i)(\cos(0.106135\tau) + i\sin(0.106135\tau)) - (0.000331453 + 0.00198285i)(\cos(0.127362\tau) - i\sin(0.127362\tau)) - (0.000331453 - 0.00198285i)(\cos(0.127362\tau) + i\sin(0.127362\tau)) - (0.00168591i)(\cos(0.148589\tau) - i\sin(0.148589\tau)) + (0.00168591i)(\cos(0.148589\tau) + i\sin(0.148589\tau))))+((-0.0313+0.1147\cos(0.0212045\tau)-0.0834\cos(0.042409\tau))/1000-0.0268\sin(0.0212045\tau))(p^2(0.011129 + (2.42843 + 2.38811i)(\cos(0.021227\tau) - i\sin(0.021227\tau)) + (2.42843 - 2.38811i)(\cos(0.021227\tau) + i\sin(0.021227\tau)) - (0.0037321 + 0.00744748i)(\cos(0.042454\tau) - i\sin(0.042454\tau)) - (0.0037321 - 0.00744748i)(\cos(0.042454\tau) + i\sin(0.042454\tau)) - (0.00140404 + 0.00419051i)(\cos(0.0636809\tau) - i\sin(0.0636809\tau)) - (0.00140404 - 0.00419051i)(\cos(0.0636809\tau) + i\sin(0.0636809\tau)) - (0.000745034 + 0.00297385i)(\cos(0.0849079\tau) - i\sin(0.0849079\tau)) - (0.000745034 - 0.00297385i)(\cos(0.0849079\tau) + i\sin(0.0849079\tau)) - (0.000465476 + 0.00232233i)(\cos(0.106135\tau) - i\sin(0.106135\tau)) - (0.000465476 - 0.00232233i)(\cos(0.106135\tau) + i\sin(0.106135\tau)) - (0.000319029 + 0.00191005i)(\cos(0.127362\tau) - i\sin(0.127362\tau)) - (0.000319029 - 0.00191005i)(\cos(0.127362\tau) + i\sin(0.127362\tau)) - (0.00162401i)(\cos(0.148589\tau) - i\sin(0.148589\tau)) + (0.00162401i)(\cos(0.148589\tau) + i\sin(0.148589\tau))) + pq(-0.232193 - (49.8879 - 50.5004i)(\cos(0.021227\tau) - i\sin(0.021227\tau)) - (49.8879 + 50.5004i)(\cos(0.021227\tau) + i\sin(0.021227\tau)) + (0.0778665 - 0.155374i)(\cos(0.042454\tau) - i\sin(0.042454\tau)) + (0.0778665 + 0.155374i)(\cos(0.042454\tau) + i\sin(0.042454\tau)) + (0.0292935 - 0.0874252i)(\cos(0.0636809\tau) - i\sin(0.0636809\tau)) + (0.0292935 + 0.0874252i)(\cos(0.0636809\tau) + i\sin(0.0636809\tau)) + (0.0155441 - 0.0620424i)(\cos(0.0849079\tau) - i\sin(0.0849079\tau)) +$

$(0.0155441 + 0.0620424i)(\cos(0.0849079\tau) + i\sin(0.0849079\tau)) + (0.00971164 - 0.04845i)(\cos(0.106135\tau) - i\sin(0.106135\tau)) + (0.00971164 + 0.04845i)(\cos(0.106135\tau) + i\sin(0.106135\tau)) + (0.00665613 - 0.0398487i)(\cos(0.127362\tau) - i\sin(0.127362\tau)) + (0.00665613 + 0.0398487i)(\cos(0.127362\tau) + i\sin(0.127362\tau)) - (0.0338812i)(\cos(0.148589\tau) - i\sin(0.148589\tau)) + (0.0338812i)(\cos(0.148589\tau) + i\sin(0.148589\tau))) + q^2(-100.944 - (22026.6 + 21660.9i)(\cos(0.021227\tau) - i\sin(0.021227\tau)) - (22026.6 - 21660.9i)(\cos(0.021227\tau) + i\sin(0.021227\tau)) + (33.8513 + 67.5509i)(\cos(0.042454\tau) - i\sin(0.042454\tau)) + (33.8513 - 67.5509i)(\cos(0.042454\tau) + i\sin(0.042454\tau)) + (12.7351 + 38.0092i)(\cos(0.0636809\tau) - i\sin(0.0636809\tau)) + (12.7351 - 38.0092i)(\cos(0.0636809\tau) + i\sin(0.0636809\tau)) + (6.75768 + 26.9737i)(\cos(0.0849079\tau) - i\sin(0.0849079\tau)) + (6.75768 - 26.9737i)(\cos(0.0849079\tau) + i\sin(0.0849079\tau)) + (4.22201 + 21.0643i)(\cos(0.106135\tau) - i\sin(0.106135\tau)) + (4.22201 - 21.0643i)(\cos(0.106135\tau) + i\sin(0.106135\tau)) + (2.89369 + 17.3247i)(\cos(0.127362\tau) - i\sin(0.127362\tau)) + (2.89369 - 17.3247i)(\cos(0.127362\tau) + i\sin(0.127362\tau)) + (14.7303i)(\cos(0.148589\tau) - i\sin(0.148589\tau)) - (14.7303i)(\cos(0.148589\tau) + i\sin(0.148589\tau)))) + (-0.0236\cos(0.0212045\tau) + (-0.101\sin(0.0212045\tau) + 0.0735\sin(0.042409\tau))/1000)(p^2(0.0111306 + (2.39392 - 2.4231i)(\cos(0.021227\tau) - i\sin(0.021227\tau)) + (2.39392 + 2.4231i)(\cos(0.021227\tau) + i\sin(0.021227\tau)) - (0.0037 - 0.007i)(\cos(0.042454\tau) - i\sin(0.042\tau)) - (0.0037 + 0.007i)(\cos(0.042454\tau) + i\sin(0.042454\tau)) - (0.00140424 - 0.0042i)(\cos(0.064\tau) - i\sin(0.0636809\tau)) - (0.0014 + 0.004i)(\cos(0.0636809\tau) + i\sin(0.0636809\tau)) - (0.00075 - 0.003i)(\cos(0.0849079\tau) - i\sin(0.0849079\tau)) - (0.000745136 + 0.00297386i)(\cos(0.0849079\tau) + i\sin(0.0849079\tau)) - (0.000465545 - 0.00232234i)(\cos(0.106135\tau) - i\sin(0.106135\tau)) - (0.000465545 + 0.00232234i)(\cos(0.106135\tau) + i\sin(0.106135\tau)) - (0.000319074 - 0.00191005i)(\cos(0.127362\tau) - i\sin(0.127362\tau)) - (0.000319074 + 0.00191005i)(\cos(0.127362\tau) + i\sin(0.127362\tau)) + (0.00162402i)(\cos(0.148589\tau) - i\sin(0.148589\tau)) - (0.00162402i)(\cos(0.148589\tau) + i\sin(0.148589\tau))) + pq(0.232179 + (50.6112 + 49.7665i)(\cos(0.021227\tau) - i\sin(0.021227\tau)) + (50.6112 - 49.7665i)(\cos(0.021227\tau) + i\sin(0.021227\tau)) - (0.077861 + 0.155359i)(\cos(0.042454\tau) - i\sin(0.042454\tau)) - (0.077861 - 0.155359i)(\cos(0.042454\tau) + i\sin(0.042454\tau)) - (0.0292918 + 0.0874169i)(\cos(0.0636809\tau) - i\sin(0.0636809\tau)) - (0.0292918 - 0.0874169i)(\cos(0.0636809\tau) + i\sin(0.0636809\tau)) - (0.0155433 + 0.0620365i)(\cos(0.0849079\tau) - i\sin(0.0849079\tau)) - (0.0155433 - 0.0620365i)(\cos(0.0849079\tau) + i\sin(0.0849079\tau)) - (0.00971099 + 0.0484454i)(\cos(0.106135\tau) - i\sin(0.106135\tau)) - (0.00971099 - 0.0484454i)(\cos(0.106135\tau) + i\sin(0.106135\tau)) - (0.00665574 + 0.0398449i)(\cos(0.127362\tau) - i\sin(0.127362\tau)) - (0.00665574 - 0.0398449i)(\cos(0.127362\tau) + i\sin(0.127362\tau)) - (0.033878i)(\cos(0.148589\tau) - i\sin(0.148589\tau)) + (0.033878i)(\cos(0.148589\tau) + i\sin(0.148589\tau))) + q^2(-100.958 - (21713.5 - 21978.2i)(\cos(0.021227\tau) - i\sin(0.021227\tau)) - (21713.5 + 21978.2i)(\cos(0.021227\tau) + i\sin(0.021227\tau)) + (33.8564 - 67.551i)(\cos(0.042454\tau) -$

$i\sin(0.042454\tau))+(33.8564+67.551i)(\cos(0.042454\tau)+i\sin(0.042454\tau))+(12.7369-38.0093i)(\cos(0.0636809\tau)-i\sin(0.0636809\tau))+(12.7369+38.0093i)(\cos(0.0636809\tau)+i\sin(0.0636809\tau))+(6.7586-26.9738i)(\cos(0.0849079\tau)-i\sin(0.0849079\tau))+(6.7586+26.9738i)(\cos(0.0849079\tau)+i\sin(0.0849079\tau))+(4.22263-21.0643i)(\cos(0.106135\tau)-i\sin(0.106135\tau))+(4.22263+21.0643i)(\cos(0.106135\tau)+i\sin(0.106135\tau))+(2.89409-17.3247i)(\cos(0.127362\tau)-i\sin(0.127362\tau))+(2.89409+17.3247i)(\cos(0.127362\tau)+i\sin(0.127362\tau))-(14.7303i)(\cos(0.148589\tau)-i\sin(0.148589\tau))+(14.7303i)(\cos(0.148589\tau)+i\sin(0.148589\tau)))))^2)(-0.00512964\cos(\pi\tau)/148)-0.708169\sin(\pi\tau)/148)+0.00219243\sin(\pi\tau)/74)+0.00123671\sin((3\pi)\tau)/148)+0.000875445\sin(\pi\tau)/37)+0.000683641\sin((5\pi)\tau)/148)+0.000562276\sin((3\pi)\tau)/74)+0.000478077\sin((7\pi)\tau)/148))$

$P_6'(\tau)=(29s_5)/2000+190.476pq(0.00231055+1.00113\cos(\pi\tau)/148)-0.00154973\cos(\pi\tau)/74)-0.000587382\cos((3\pi)\tau)/148)-0.000309363\cos(\pi\tau)/37)-0.000193269\cos((5\pi)\tau)/148)-0.000132463\cos((3\pi)\tau)/74)-0.0072671\sin(\pi\tau)/148))+(4.97326(s_5\cos(0.0212045\tau)+0.709s_6\sin(0.0212045\tau))^3-2.80011(s_5\cos(0.0212045\tau)+0.709s_6\sin(0.0212045\tau))((0.001-0.0038\cos(0.0212045\tau)+0.0027\cos(0.042409\tau)+0.8815\sin(0.0212045\tau))(p^2((0.0562962-0.0569785i)(\cos(0.021227\tau)-i\sin(0.021227\tau))+(0.0562962+0.0569785i)(\cos(0.021227\tau)+i\sin(0.021227\tau)))+q^2(0.00231649-(510.623-516.811i)(\cos(0.021227\tau)-i\sin(0.021227\tau))-(510.623+516.811i)(\cos(0.021227\tau)+i\sin(0.021227\tau))-(0.000776843-0.0015438i)(\cos(0.042454\tau)-i\sin(0.042454\tau))-(0.000776843+0.0015438i)(\cos(0.042454\tau)+i\sin(0.042454\tau))-(0.00029225-0.000868659i)(\cos(0.0636809\tau)-i\sin(0.0636809\tau))-(0.00029225+0.000868659i)(\cos(0.0636809\tau)+i\sin(0.0636809\tau))-(0.000155077-0.000616455i)(\cos(0.0849079\tau)-i\sin(0.0849079\tau))-(0.000155077+0.000616455i)(\cos(0.0849079\tau)+i\sin(0.0849079\tau))-(0.0000968892-0.000481401i)(\cos(0.106135\tau)-i\sin(0.106135\tau))-(0.0000968892+0.000481401i)(\cos(0.106135\tau)+i\sin(0.106135\tau))-(0.0000664056-0.000395937i)(\cos(0.127362\tau)-i\sin(0.127362\tau))-(0.0000664056+0.000395937i)(\cos(0.127362\tau)+i\sin(0.127362\tau))+(0.000336644i)(\cos(0.148589\tau)-i\sin(0.148589\tau))-(0.000336644i)(\cos(0.148589\tau)+i\sin(0.148589\tau)))+pq(0.0100666+(0.952311+0.936322i)(\cos(0.021227\tau)-i\sin(0.021227\tau))+(0.952311-0.936322i)(\cos(0.021227\tau)+i\sin(0.021227\tau))-(0.00337582+0.00673653i)(\cos(0.042454\tau)-i\sin(0.042454\tau))-(0.00337582-0.00673653i)(\cos(0.042454\tau)+i\sin(0.042454\tau))-(0.00127001+0.00379048i)(\cos(0.0636809\tau)-i\sin(0.0636809\tau))-(0.00127001-0.00379048i)(\cos(0.0636809\tau)+i\sin(0.0636809\tau))-(0.00067391+0.00268996i)(\cos(0.0849079\tau)-i\sin(0.0849079\tau))-(0.00067391-0.00268996i)(\cos(0.0849079\tau)+i\sin(0.0849079\tau))-(0.00042104+0.00210064i)(\cos(0.106135\tau)-i\sin(0.106135\tau))-(0.00042104-0.00210064i)(\cos(0.106135\tau)+i\sin(0.106135\tau))-(0.000288573+0.00172771i)(\cos(0.127362\tau)-i\sin(0.127362\tau))-(0.000288573-0.00172771i)(\cos(0.127362\tau)+i\sin(0.127362\tau))-(0.00146898i)(\cos(0.148589\tau)-i\sin(0.148589\tau))+(0.00146898i)(\cos(0.148589\tau)+i\sin(0.148589\tau))))+(1.0006\cos(0.0212045\tau)+0.0043\sin(0.0212045\tau))(p^2(-1.27476\times10^{-6}-(0.0574401+0.0564899i)(\cos(0.021227\tau)-i\sin(0.021227\tau))-$

$(0.0574401 - 0.0564899i)(\cos(0.021227\tau) + i\sin(0.021227\tau))) + pq(0.0100999 +$
$(1.25218 - 1.26761i)(\cos(0.021227\tau) - i\sin(0.021227\tau))$
$+ (1.25218 + 1.26761i)(\cos(0.021227\tau) + i\sin(0.021227\tau)) - (0.00338704 -$
$0.00675788i)(\cos(0.042454\tau) - i\sin(0.042454\tau)) - (0.00338704 + 0.00675788i)$
$(\cos(0.042454\tau) + i\sin(0.042454\tau)) - (0.00127421 - 0.00380249i)(\cos(0.0636809\tau) -$
$i\sin(0.0636809\tau)) - (0.00127421 + 0.00380249i)(\cos(0.0636809\tau) + i\sin(0.0636809\tau)) -$
$(0.000676139 - 0.00269849i)(\cos(0.0849079\tau) - i\sin(0.0849079\tau)) - (0.000676139 +$
$0.00269849i)(\cos(0.0849079\tau) + i\sin(0.0849079\tau)) - (0.000422438 - 0.0021073i)$
$(\cos(0.106135\tau) - i\sin(0.106135\tau)) - (0.000422438 + 0.0021073i)(\cos(0.106135\tau) +$
$i\sin(0.106135\tau)) - (0.000289529 - 0.00173319i)(\cos(0.127362\tau) - i\sin(0.127362\tau)) -$
$(0.000289529 + 0.00173319i)(\cos(0.127362\tau) + i\sin(0.127362\tau)) + (0.00147364i)$
$(\cos(0.148589\tau) - i\sin(0.148589\tau)) - (0.00147364i)(\cos(0.148589\tau) + i\sin(0.148589\tau))) +$
$q^2(0.0115624 + (520.999 + 512.38i)(\cos(0.021227\tau) - i\sin(0.021227\tau)) + (520.999 -$
$512.38i)(\cos(0.021227\tau) + i\sin(0.021227\tau)) - (0.00387745 + 0.00773132i)(\cos(0.042454\tau) -$
$i\sin(0.042454\tau)) - (0.00387745 - 0.00773132i)(\cos(0.042454\tau) + i\sin(0.042454\tau)) -$
$(0.00145872 + 0.00435022i)(\cos(0.0636809\tau) - i\sin(0.0636809\tau)) - (0.00145872 -$
$0.00435022i)(\cos(0.0636809\tau) + i\sin(0.0636809\tau)) - (0.000774048 + 0.00308719i)$
$(\cos(0.0849079\tau) - i\sin(0.0849079\tau)) - (0.000774048 - 0.00308719i)(\cos(0.0849079\tau) +$
$i\sin(0.0849079\tau)) - (0.000483603 + 0.00241084i)(\cos(0.106135\tau) - i\sin(0.106135\tau)) -$
$(0.000483603 - 0.00241084i)(\cos(0.106135\tau) + i\sin(0.106135\tau)) - (0.000331453 +$
$0.00198285i)(\cos(0.127362\tau) - i\sin(0.127362\tau)) - (0.000331453 - 0.00198285i)$
$(\cos(0.127362\tau) + i\sin(0.127362\tau)) - (0.00168591i)(\cos(0.148589\tau) - i\sin(0.148589\tau)) +$
$(0.00168591i)(\cos(0.148589\tau) + i\sin(0.148589\tau)))) + (0.0236\cos(0.0212045\tau) +$
$(0.101\sin(0.0212045\tau) - 0.0735\sin(0.042409\tau))/1000)(p^2(0.011129 + (2.42843 +$
$2.38811i)(\cos(0.021227\tau) - i\sin(0.021227\tau)) + (2.42843 - 2.38811i)(\cos(0.021227\tau) +$
$i\sin(0.021227\tau)) - (0.0037321 + 0.00744748i)(\cos(0.042454\tau) - i\sin(0.042454\tau)) -$
$(0.0037321 - 0.00744748i)(\cos(0.042454\tau) + i\sin(0.042454\tau)) - (0.00140404 +$
$0.00419051i)(\cos(0.0636809\tau) - i\sin(0.0636809\tau)) - (0.00140404 - 0.00419051i)$
$(\cos(0.0636809\tau) + i\sin(0.0636809\tau)) - (0.000745034 + 0.00297385i)(\cos(0.0849079\tau) -$
$i\sin(0.0849079\tau)) - (0.000745034 - 0.00297385i)(\cos(0.0849079\tau) + i\sin(0.0849079\tau)) -$
$(0.000465476 + 0.00232233i)(\cos(0.106135\tau) - i\sin(0.106135\tau)) - (0.000465476 -$
$0.00232233i)(\cos(0.106135\tau) + i\sin(0.106135\tau)) - (0.000319029 + 0.00191005i)$
$(\cos(0.127362\tau) - i\sin(0.127362\tau)) - (0.000319029 - 0.00191005i)(\cos(0.127362\tau) +$
$i\sin(0.127362\tau)) - (0.00162401i)(\cos(0.148589\tau) - i\sin(0.148589\tau)) + (0.00162401i)$
$(\cos(0.148589\tau) + i\sin(0.148589\tau))) + pq(-0.232193 - (49.8879 - 50.5004i)(\cos(0.021227\tau) -$
$i\sin(0.021227\tau)) - (49.8879 + 50.5004i)(\cos(0.021227\tau) + i\sin(0.021227\tau)) +$
$(0.0778665 - 0.155374i)(\cos(0.042454\tau) - i\sin(0.042454\tau)) + (0.0778665 +$
$0.155374i)(\cos(0.042454\tau) + i\sin(0.042454\tau)) + (0.0292935 - 0.0874252i)(\cos(0.0636809\tau) -$
$i\sin(0.0636809\tau)) + (0.0292935 + 0.0874252i)(\cos(0.0636809\tau) + i\sin(0.0636809\tau)) +$
$(0.0155441 - 0.0620424i)(\cos(0.0849079\tau) - i\sin(0.0849079\tau)) + (0.0155441 +$
$0.0620424i)(\cos(0.0849079\tau) + i\sin(0.0849079\tau)) + (0.00971164 - 0.04845i)(\cos(0.106135\tau) -$
$i\sin(0.106135\tau)) + (0.00971164 + 0.04845i)(\cos(0.106135\tau) + i\sin(0.106135\tau)) +$

$(0.00665613 - 0.0398487i)(\cos(0.127362\tau) - i\sin(0.127362\tau)) + (0.00665613 + 0.0398487i)(\cos(0.127362\tau) + i\sin(0.127362\tau)) - (0.0338812i)(\cos(0.148589\tau) - i\sin(0.148589\tau)) + (0.0338812i)(\cos(0.148589\tau) + i\sin(0.148589\tau))) + q^2(-100.944 - (22026.6 + 21660.9i)(\cos(0.021227\tau) - i\sin(0.021227\tau)) - (22026.6 - 21660.9i)(\cos(0.021227\tau) + i\sin(0.021227\tau)) + (33.8513 + 67.5509i)(\cos(0.042454\tau) - i\sin(0.042454\tau)) + (33.8513 - 67.5509i)(\cos(0.042454\tau) + i\sin(0.042454\tau)) + (12.7351 + 38.0092i)(\cos(0.0636809\tau) - i\sin(0.0636809\tau)) + (12.7351 - 38.0092i)(\cos(0.0636809\tau) + i\sin(0.0636809\tau)) + (6.75768 + 26.9737i)(\cos(0.0849079\tau) - i\sin(0.0849079\tau)) + (6.75768 - 26.9737i)(\cos(0.0849079\tau) + i\sin(0.0849079\tau)) + (4.22201 + 21.0643i)(\cos(0.106135\tau) - i\sin(0.106135\tau)) + (4.22201 - 21.0643i)(\cos(0.106135\tau) + i\sin(0.106135\tau)) + (2.89369 + 17.3247i)(\cos(0.127362\tau) - i\sin(0.127362\tau)) + (2.89369 - 17.3247i)(\cos(0.127362\tau) + i\sin(0.127362\tau)) + (14.7303i)(\cos(0.148589\tau) - i\sin(0.148589\tau)) - (14.7303i)(\cos(0.148589\tau) + i\sin(0.148589\tau)))) + ((-0.2419 + 0.8899\cos(0.0212045\tau) - 0.648\cos(0.042409\tau))/10000 - 0.0208\sin(0.0212045\tau)) (p^2(0.0111306 + (2.39392 - 2.4231i)(\cos(0.021227\tau) - i\sin(0.021227\tau)) + (2.39392 + 2.4231i)(\cos(0.021\tau) + i\sin(0.02\tau)) - (0.004 - 0.007i)(\cos(0.042\tau) - i\sin(0.042\tau)) - (0.004 + 0.007i)(\cos(0.042454\tau) + i\sin(0.042454\tau)) - (0.00140424 - 0.00419052i)(\cos(0.0636809\tau) - i\sin(0.0636809\tau)) - (0.0014 + 0.0042i)(\cos(0.0636809\tau) + i\sin(0.0636809\tau)) - (0.00075 - 0.003i)(\cos(0.0849079\tau) - i\sin(0.0849079\tau)) - (0.000745136 + 0.00297386i)(\cos(0.0849079\tau) + i\sin(0.0849079\tau)) - (0.000465545 - 0.00232234i)(\cos(0.106135\tau) - i\sin(0.106135\tau)) - (0.000465545 + 0.00232234i)(\cos(0.106135\tau) + i\sin(0.106135\tau)) - (0.000319074 - 0.00191005i)(\cos(0.127362\tau) - i\sin(0.127362\tau)) - (0.000319074 + 0.00191005i)(\cos(0.127362\tau) + i\sin(0.127362\tau)) + (0.00162402i)(\cos(0.148589\tau) - i\sin(0.148589\tau)) - (0.00162402i)(\cos(0.148589\tau) + i\sin(0.148589\tau))) + pq(0.232179 + (50.6112 + 49.7665i)(\cos(0.021227\tau) - i\sin(0.021227\tau)) + (50.6112 - 49.7665i)(\cos(0.021227\tau) + i\sin(0.021227\tau)) - (0.077861 + 0.155359i)(\cos(0.042454\tau) - i\sin(0.042454\tau)) - (0.077861 - 0.155359i)(\cos(0.042454\tau) + i\sin(0.042454\tau)) - (0.0292918 + 0.0874169i)(\cos(0.0636809\tau) - i\sin(0.0636809\tau)) - (0.0292918 - 0.0874169i)(\cos(0.0636809\tau) + i\sin(0.0636809\tau)) - (0.0155433 + 0.0620365i)(\cos(0.0849079\tau) - i\sin(0.0849079\tau)) - (0.0155433 - 0.0620365i)(\cos(0.0849079\tau) + i\sin(0.0849079\tau)) - (0.00971099 + 0.0484454i)(\cos(0.106135\tau) - i\sin(0.106135\tau)) - (0.00971099 - 0.0484454i)(\cos(0.106135\tau) + i\sin(0.106135\tau)) - (0.00665574 + 0.0398449i)(\cos(0.127362\tau) - i\sin(0.127362\tau)) - (0.00665574 - 0.0398449i)(\cos(0.127362\tau) + i\sin(0.127362\tau)) - (0.033878i)(\cos(0.148589\tau) - i\sin(0.148589\tau)) + (0.033878i)(\cos(0.148589\tau) + i\sin(0.148589\tau))) + q^2(-100.958 - (21713.5 - 21978.2i)(\cos(0.021227\tau) - i\sin(0.021227\tau)) - (21713.5 + 21978.2i)(\cos(0.021227\tau) + i\sin(0.021227\tau)) + (33.8564 - 67.551i)(\cos(0.042454\tau) - i\sin(0.042454\tau)) + (33.8564 + 67.551i)(\cos(0.042454\tau) + i\sin(0.042454\tau)) + (12.7369 - 38.0093i)(\cos(0.0636809\tau) - i\sin(0.0636809\tau)) + (12.7369 + 38.0093i)(\cos(0.0636809\tau) + i\sin(0.0636809\tau)) + (6.7586 - 26.9738i)(\cos(0.0849079\tau) - i\sin(0.0849079\tau)) + (6.7586 + 26.9738i)(\cos(0.0849079\tau) +$

$i\sin(0.0849079\tau))+(4.22263-21.0643i)(\cos(0.106135\tau)-i\sin(0.106135\tau))+(4.22263+$
$21.0643i)(\cos(0.106135\tau)+i\sin(0.106135\tau))+(2.89409-17.3247i)$
$(\cos(0.127362\tau)-i\sin(0.127362\tau))+(2.89409+17.3247i)(\cos(0.127362\tau)+$
$i\sin(0.127362\tau))-(14.7303i)(\cos(0.148589\tau)-i\sin(0.148589\tau))+(14.7303i)$
$(\cos(0.148589\tau)+i\sin(0.148589\tau)))))^2-2.17315(s_5\cos(0.0212045\tau)$
$+0.709s_6\sin(0.0212045\tau))((1.0006\cos(0.0212045\tau)+0.0043\sin(0.0212045\tau))$
$(p^2((0.0562962-0.0569785i)(\cos(0.021227\tau)-i\sin(0.021227\tau))+(0.0562962+$
$0.0569785i)(\cos(0.021227\tau)+i\sin(0.021227\tau)))+q^2(0.00231649-(510.623-$
$516.811i)(\cos(0.021227\tau)-i\sin(0.021227\tau))-(510.623+516.811i)(\cos(0.021227\tau)+$
$i\sin(0.021227\tau))-(0.000776843-0.0015438i)(\cos(0.042454\tau)-i\sin(0.042454\tau))-$
$(0.000776843+0.0015438i)(\cos(0.042454\tau)+i\sin(0.042454\tau))-(0.00029225-$
$0.000868659i)(\cos(0.0636809\tau)-i\sin(0.0636809\tau))-(0.00029225+0.000868659i)$
$(\cos(0.0636809\tau)+i\sin(0.0636809\tau))-(0.000155077-0.000616455i)(\cos(0.0849079\tau)-$
$i\sin(0.0849079\tau))-(0.000155077+0.000616455i)(\cos(0.0849079\tau)+i\sin(0.0849079\tau))-$
$(0.0000968892-0.000481401i)(\cos(0.106135\tau)-i\sin(0.106135\tau))-(0.0000968892+$
$0.000481401i)(\cos(0.106135\tau)+i\sin(0.106135\tau))-(0.0000664056-0.000395937i)$
$(\cos(0.127362\tau)-i\sin(0.127362\tau))-(0.0000664056+0.000395937i)(\cos(0.127362\tau)+$
$i\sin(0.127362\tau))+(0.000336644i)(\cos(0.148589\tau)-i\sin(0.148589\tau))-(0.000336644i)$
$(\cos(0.148589\tau)+i\sin(0.148589\tau)))+pq(0.0100666+(0.952311+0.936322i)$
$(\cos(0.021227\tau)-i\sin(0.021227\tau))+(0.952311-0.936322i)(\cos(0.021227\tau)+$
$i\sin(0.021227\tau))-(0.00337582+0.00673653i)(\cos(0.042454\tau)-i\sin(0.042454\tau))-$
$(0.00337582-0.00673653i)(\cos(0.042454\tau)+i\sin(0.042454\tau))-(0.00127001+$
$0.00379048i)(\cos(0.0636809\tau)-i\sin(0.0636809\tau))-(0.00127001-0.00379048i)$
$(\cos(0.0636809\tau)+i\sin(0.0636809\tau))-(0.00067391+0.00268996i)(\cos(0.0849079\tau)-$
$i\sin(0.0849079\tau))-(0.00067391-0.00268996i)(\cos(0.0849079\tau)+i\sin(0.0849079\tau))-$
$(0.00042104+0.00210064i)(\cos(0.106135\tau)-i\sin(0.106135\tau))-(0.00042104-$
$0.00210064i)(\cos(0.106135\tau)+i\sin(0.106135\tau))-(0.000288573+0.00172771i)$
$(\cos(0.127362\tau)-i\sin(0.127362\tau))-(0.000288573-0.00172771i)(\cos(0.127362\tau)+$
$i\sin(0.127362\tau))-(0.00146898i)(\cos(0.148589\tau)-i\sin(0.148589\tau))+(0.00146898i)$
$(\cos(0.148589\tau)+i\sin(0.148589\tau))))+(-0.0013+0.0049\cos(0.0212045\tau)-$
$0.0035\cos(0.042409\tau)-1.1357\sin(0.0212045\tau))(p^2(-1.27476\times10^{-6}-(0.0574401+$
$0.0564899i)(\cos(0.021227\tau)-i\sin(0.021227\tau))-(0.0574401-0.0564899i)(\cos(0.021227\tau)+$
$i\sin(0.021227\tau)))+pq(0.0100999+(1.25218-1.26761i)(\cos(0.021227\tau)-$
$i\sin(0.021227\tau))+(1.25218+1.26761i)(\cos(0.021227\tau)+i\sin(0.021227\tau))-$
$(0.00338704-0.00675788i)(\cos(0.042454\tau)-i\sin(0.042454\tau))-(0.00338704+$
$0.00675788i)(\cos(0.042454\tau)+i\sin(0.042454\tau))-(0.00127421-0.00380249i)$
$(\cos(0.0636809\tau)-i\sin(0.0636809\tau))-(0.00127421+0.00380249i)(\cos(0.0636809\tau)+$
$i\sin(0.0636809\tau))-(0.000676139-0.00269849i)(\cos(0.0849079\tau)-i\sin(0.0849079\tau))-$
$(0.000676139+0.00269849i)(\cos(0.0849079\tau)+i\sin(0.0849079\tau))-(0.000422438-$
$0.0021073i)(\cos(0.106135\tau)-i\sin(0.106135\tau))-(0.000422438+0.0021073i)$
$(\cos(0.106135\tau)+i\sin(0.106135\tau))-(0.000289529-0.00173319i)(\cos(0.127362\tau)-$
$i\sin(0.127362\tau))-(0.000289529+0.00173319i)(\cos(0.127362\tau)+i\sin(0.127362\tau))+$

$(0.00147364i)(\cos(0.148589\tau) - i\sin(0.148589\tau)) - (0.00147364i)(\cos(0.148589\tau) + i\sin(0.148589\tau))) + q^2(0.0115624 + (520.999 + 512.38i)(\cos(0.021227\tau) - i\sin(0.021227\tau)) + (520.999 - 512.38i)(\cos(0.021227\tau) + i\sin(0.021227\tau)) - (0.00387745 + 0.00773132i)(\cos(0.042454\tau) - i\sin(0.042454\tau)) - (0.00387745 - 0.00773132i)(\cos(0.042454\tau) + i\sin(0.042454\tau)) - (0.00145872 + 0.00435022i)(\cos(0.0636809\tau) - i\sin(0.0636809\tau)) - (0.00145872 - 0.00435022i)(\cos(0.0636809\tau) + i\sin(0.0636809\tau)) - (0.000774048 + 0.00308719i)(\cos(0.0849079\tau) - i\sin(0.0849079\tau)) - (0.000774048 - 0.00308719i)(\cos(0.0849079\tau) + i\sin(0.0849079\tau)) - (0.000483603 + 0.00241084i)(\cos(0.106135\tau) - i\sin(0.106135\tau)) - (0.000483603 - 0.00241084i)(\cos(0.106135\tau) + i\sin(0.106135\tau)) - (0.000331453 + 0.00198285i)(\cos(0.127362\tau) - i\sin(0.127362\tau)) - (0.000331453 - 0.00198285i)(\cos(0.127362\tau) + i\sin(0.127362\tau)) - (0.00168591i)(\cos(0.148589\tau) - i\sin(0.148589\tau)) + (0.00168591i)(\cos(0.148589\tau) + i\sin(0.148589\tau))) + ((-0.0313 + 0.1147\cos(0.0212045\tau) - 0.0834\cos(0.042409\tau))/1000 - 0.0268\sin(0.0212045\tau))(p^2(0.011129 + (2.42843 + 2.38811i)(\cos(0.021227\tau) - i\sin(0.021227\tau)) + (2.42843 - 2.38811i)(\cos(0.021227\tau) + i\sin(0.021227\tau)) - (0.0037321 + 0.00744748i)(\cos(0.042454\tau) - i\sin(0.042454\tau)) - (0.0037321 - 0.00744748i)(\cos(0.042454\tau) + i\sin(0.042454\tau)) - (0.00140404 + 0.00419051i)(\cos(0.0636809\tau) - i\sin(0.0636809\tau)) - (0.00140404 - 0.00419051i)(\cos(0.0636809\tau) + i\sin(0.0636809\tau)) - (0.000745034 + 0.00297385i)(\cos(0.0849079\tau) - i\sin(0.0849079\tau)) - (0.000745034 - 0.00297385i)(\cos(0.0849079\tau) + i\sin(0.0849079\tau)) - (0.000465476 + 0.00232233i)(\cos(0.106135\tau) - i\sin(0.106135\tau)) - (0.000465476 - 0.00232233i)(\cos(0.106135\tau) + i\sin(0.106135\tau)) - (0.000319029 + 0.00191005i)(\cos(0.127362\tau) - i\sin(0.127362\tau)) - (0.000319029 - 0.00191005i)(\cos(0.127362\tau) + i\sin(0.127362\tau)) - (0.00162401i)(\cos(0.148589\tau) - i\sin(0.148589\tau)) + (0.00162401i)(\cos(0.148589\tau) + i\sin(0.148589\tau))) + pq(-0.232193 - (49.8879 - 50.5004i)(\cos(0.021227\tau) - i\sin(0.021227\tau)) - (49.8879 + 50.5004i)(\cos(0.021227\tau) + i\sin(0.021227\tau)) + (0.0778665 - 0.155374i)(\cos(0.042454\tau) - i\sin(0.042454\tau)) + (0.0778665 + 0.155374i)(\cos(0.042454\tau) + i\sin(0.042454\tau)) + (0.0292935 - 0.0874252i)(\cos(0.0636809\tau) - i\sin(0.0636809\tau)) + (0.0292935 + 0.0874252i)(\cos(0.0636809\tau) + i\sin(0.0636809\tau)) + (0.0155441 - 0.0620424i)(\cos(0.0849079\tau) - i\sin(0.0849079\tau)) + (0.0155441 + 0.0620424i)(\cos(0.0849079\tau) + i\sin(0.0849079\tau)) + (0.00971164 - 0.04845i)(\cos(0.106135\tau) - i\sin(0.106135\tau)) + (0.00971164 + 0.04845i)(\cos(0.106135\tau) + i\sin(0.106135\tau)) + (0.00665613 - 0.0398487i)(\cos(0.127362\tau) - i\sin(0.127362\tau)) + (0.00665613 + 0.0398487i)(\cos(0.127362\tau) + i\sin(0.127362\tau)) - (0.0338812i)(\cos(0.148589\tau) - i\sin(0.148589\tau)) + (0.0338812i)(\cos(0.148589\tau) + i\sin(0.148589\tau))) + q^2(-100.944 - (22026.6 + 21660.9i)(\cos(0.021227\tau) - i\sin(0.021227\tau)) - (22026.6 - 21660.9i)(\cos(0.021227\tau) + i\sin(0.021227\tau)) + (33.8513 + 67.5509i)(\cos(0.042454\tau) - i\sin(0.042454\tau)) + (33.8513 - 67.5509i)(\cos(0.042454\tau) + i\sin(0.042454\tau)) + (12.7351 + 38.0092i)(\cos(0.0636809\tau) - i\sin(0.0636809\tau)) + (12.7351 - 38.0092i)(\cos(0.0636809\tau) + i\sin(0.0636809\tau)) + (6.75768 + 26.9737i)(\cos(0.0849079\tau) - i\sin(0.0849079\tau)) + (6.75768 - 26.9737i)(\cos(0.0849079\tau) + i\sin(0.0849079\tau)) + (4.22201 + 21.0643i)$

$(\cos(0.106135\tau) - i\sin(0.106135\tau)) + (4.22201 - 21.0643i)(\cos(0.106135\tau) + i\sin(0.106135\tau)) + (2.89369 + 17.3247i)(\cos(0.127362\tau) - i\sin(0.127362\tau)) + (2.89369 - 17.3247i)(\cos(0.127362\tau) + i\sin(0.127362\tau)) + (14.7303i)(\cos(0.148589\tau) - i\sin(0.148589\tau)) - (14.7303i)(\cos(0.148589\tau) + i\sin(0.148589\tau))))$
$- (0.0236\cos(0.0212045\tau) + (-0.101\sin(0.0212045\tau) + 0.0735\sin(0.042409\tau))/1000)$
$(p^2(0.0111306 + (2.39392 - 2.4231i)(\cos(0.021227\tau) - i\sin(0.021227\tau)) + (2.39392 + 2.4231i)(\cos(0.021227\tau) + i\sin(0.021\tau)) - (0.004 - 0.007i)(\cos(0.042\tau) - i\sin(0.042\tau)) - (0.004 + 0.007i)(\cos(0.042\tau) + i\sin(0.042454\tau)) - (0.00140424 - 0.00419052i)(\cos(0.0636809\tau) - i\sin(0.063\tau)) - (0.0014 + 0.004i)(\cos(0.0636809\tau) + i\sin(0.0636809\tau)) - (0.000745136 - 0.00297386i)$
$(\cos(0.0849079\tau) - i\sin(0.0849079\tau)) - (0.000745136 + 0.00297386i)(\cos(0.0849079\tau) + i\sin(0.0849079\tau)) - (0.000465545 - 0.00232234i)(\cos(0.106135\tau) - i\sin(0.106135\tau)) - (0.000465545 + 0.00232234i)(\cos(0.106135\tau) + i\sin(0.106135\tau)) - (0.000319074 - 0.00191005i)(\cos(0.127362\tau) - i\sin(0.127362\tau)) - (0.000319074 + 0.00191005i)$
$(\cos(0.127362\tau) + i\sin(0.127362\tau)) + (0.00162402i)(\cos(0.148589\tau) - i\sin(0.148589\tau)) - (0.00162402i)(\cos(0.148589\tau) + i\sin(0.148589\tau))) + pq(0.232179 + (50.6112 + 49.7665i)(\cos(0.021227\tau) - i\sin(0.021227\tau)) + (50.6112 - 49.7665i)(\cos(0.021227\tau) + i\sin(0.021227\tau)) - (0.077861 + 0.155359i)(\cos(0.042454\tau) - i\sin(0.042454\tau)) - (0.077861 - 0.155359i)(\cos(0.042454\tau) + i\sin(0.042454\tau)) - (0.0292918 + 0.0874169i)(\cos(0.0636809\tau) - i\sin(0.0636809\tau)) - (0.0292918 - 0.0874169i)$
$(\cos(0.0636809\tau) + i\sin(0.0636809\tau)) - (0.0155433 + 0.0620365i)(\cos(0.0849079\tau) - i\sin(0.0849079\tau)) - (0.0155433 - 0.0620365i)(\cos(0.0849079\tau) + i\sin(0.0849079\tau)) - (0.00971099 + 0.0484454i)(\cos(0.106135\tau) - i\sin(0.106135\tau)) - (0.00971099 - 0.0484454i)(\cos(0.106135\tau) + i\sin(0.106135\tau)) - (0.00665574 + 0.0398449i)$
$(\cos(0.127362\tau) - i\sin(0.127362\tau)) - (0.00665574 - 0.0398449i)(\cos(0.127362\tau) + i\sin(0.127362\tau)) - (0.033878i)(\cos(0.148589\tau) - i\sin(0.148589\tau)) + (0.033878i)$
$(\cos(0.148589\tau) + i\sin(0.148589\tau))) + q^2(-100.958 - (21713.5 - 21978.2i)(\cos(0.021227\tau) - i\sin(0.021227\tau)) - (21713.5 + 21978.2i)(\cos(0.021227\tau) + i\sin(0.021227\tau)) + (33.8564 - 67.551i)(\cos(0.042454\tau) - i\sin(0.042454\tau)) + (33.8564 + 67.551i)(\cos(0.042454\tau) + i\sin(0.042454\tau)) + (12.7369 - 38.0093i)(\cos(0.0636809\tau) - i\sin(0.0636809\tau)) + (12.7369 + 38.0093i)(\cos(0.0636809\tau) + i\sin(0.0636809\tau)) + (6.7586 - 26.9738i)$
$(\cos(0.0849079\tau) - i\sin(0.0849079\tau)) + (6.7586 + 26.9738i)(\cos(0.0849079\tau) + i\sin(0.0849079\tau)) + (4.22263 - 21.0643i)(\cos(0.106135\tau) - i\sin(0.106135\tau)) + (4.22263 + 21.0643i)(\cos(0.106135\tau) + i\sin(0.106135\tau)) + (2.89409 - 17.3247i)$
$(\cos(0.127362\tau) - i\sin(0.127362\tau)) + (2.89409 + 17.3247i)(\cos(0.127362\tau) + i\sin(0.127362\tau)) - (14.7303i)$
$(\cos(0.148589\tau) - i\sin(0.148589\tau)) + (14.7303i)(\cos(0.148589\tau) + i\sin(0.148589\tau)))))^2)$
$(0.00231055 + 1.00113\cos(\pi\tau)/148) - 0.00154973\cos(\pi\tau)/74)$
$-0.000587382\cos((3\pi)\tau)/148) - 0.000309363\cos(\pi\tau)/37) - 0.000193269\cos((5\pi)\tau)/148)$
$- 0.000132463\cos((3\pi)\tau)/74) - 0.0072671\sin(\pi\tau)/148))$

attitude motion
control and stabilization
3-axis stabilization, 7
spin stabilization, 7
stability, 7

Bennu, 9
bifurcation
see gravity gradient stabilization
bifurcation, 91

Callisto, 9
center manifold reduction, 3, 6, 11, 30
constant coefficients, 36, 59, 64
eigenvalues, 177
examples, 60
external periodic excitation, 53, 177
periodic coefficients, 56, 60, 177
reducability condition, 36, 66
reduced order model, 178
time periodic, 32
center of mass, 7
Chebfun, 84
Chebyshev polynomials, 16, 82, 84
conclusions and discussions
Dissertation, 187
controllability, 112, 114
controllability matrix, 112

dissertation contributions, 187
dissertation scope and overview, 10
Duffing's equation, 43

eccentricity, 79
effective gravitational potential, 148
ellipsoidal harmonics models
orthogonal ellipsoidal coordinates, 142
external periodic excitation, 37

feedback control
control input, 112, 125, 128
linear control
L-F transformed system, 114
state augmented system, 112
nonlinear control, 179
bifurcation control, 121, 126
sliding mode control, 115, 119
proportional gain, 125
Floquet constant matrix, 18, 101, 109
Floquet multipliers
see gravity gradient stabilization
Floquet multipliers, 164
see nonlinear control bifurcation control
Floquet multiplier location, 129
seegravity gradient stabilization
Floquet multipliers, 84
Floquet Theory, 18, 79
Floquet theory, 11
Floquet Transition Matrix (FTM), 82, 84, 96, 101, 109, 164
trace, 87
forcing
see periodic
external excitation, 2
Fourier series
see LFT matrix, 18, 21, 98, 111, 172
future research directions, 194

Ganymede, 9
gravitational potential
ellipsoidal harmonics models, 142
gravity field harmonic coefficients, 137
logarithmic potential, 147
mascons, 146
polyhedron models, 144
configuration, 145

spherical harmonics models, 136, 138
spherical harmonicsmodels
moments of inertia, 140
gravity gradient stabilization, 7, 8
assumptions, 76
augmented coordinates, 82
bifurcation, 91
bifurcation controlled, 125
chaos, 86
control input, 112, 125, 128
controlled augmented states system, 126
controlled L-F transformed system, 129
dynamical model, 76, 79
feedback control, 105
Floquet multiplier location, 84, 129
L-F transformed system, 126, 128
Lyapunov exponents, 86
Lyapunov stability, 84
normalized augmented coordinates, 125
original coordinates, 79, 109
pitch planar motion, 76
pitch planar motion analysis, 79
Poincaré map, 86
principal period normalization, 84
resonance, 91
roll-yaw, 76
simplicity, 76
stability and chaos, 82
stability chart, 87, 90
state space representation, 84
time history analysis, 79
versal deformation, 93, 95, 103

intuitive state augmentation, 38, 39, 51, 56, 174
L-F transformed system, 98
state space representation, 101
original coordinates system, 79

Io, 9
Irregularly Shaped Small Bodies, 9

Jacobi integral, 148, 150
Jordan canonical form, 93, 101

L-F transformed system
Normal Forms, 103, 178
closed form solution, 105
state space representation, 119
versal deformation, 96
limit cycle, 105
versal deformation parameter, 103
Laplace's equation, 137
Legendre Functions, 137
LFT matrix, 20, 21
Elements as Fourier series, 18, 21, 34, 111
periodic elements, 98, 101, 111, 172, 174
LUCY, 9
Lyapunov Exponents
see gravity gradient stabilization
chaos, 86
Lyapunov function, 117, 120
Lyapunov-Floquet transformation, 3, 16, 171
theory, 20, 21

Mathieu-Duffing equation, 49
MATLAB, 84
modal matrix, 93, 101
Model Order Reduction, 15, 16, 171
moments of inertia, 79, 140, 155
MOR
seeModel Order Reduction, 31
motion in the vicinity of irregularly shaped small bodies
see motion in the vicinity of ISSB, 134
motion in the vicinity of ISSB, 9, 134, 135
center manifold reduction, 174

chaos, 165
controlled orbit, 182
controlled states response, 182
equation of motion, 147, 157
controlled orbit, 182
Floquet multiplier location, 164
Floquet Transition Matrix (FTM), 164
gravity field harmonic coefficients , 153
motion analysis, 150
motion control, 170
motion nonlinear control, 179, 182
periodic body angular velocity, 150
periodic perturbations, 151
Poincaré map, 166
stability, 163
state space model, 152
time history analysis, 158, 159
time scaling, 151
Toutatis
angular velocity variation, 156
orbital parameters, 153
shape and coordinate axes, 155
uncontrolled orbit, 162
uncontrolled states response, 158, 159

nonlinear control
bifurcation control, 125
Floquet multiplier location, 129
L-F transformed system, 126, 129
state augmented system, 121, 126
motion in the vicinity of ISSB, 179
sliding mode control, 115
L-F transformed system, 119, 120
state augmented system, 115, 117
Normal Forms
L-F transformed system, 103
reduced order system, 178
state augmented system, 93
normal forms
constant coefficients, 39, 43
examples, 43
external periodic excitation, 37
periodic coefficients, 42, 49
resonant condition, 29, 41
solvability condition, 26, 28, 42
Normal Forms theory, 3, 5, 10, 11, 16, 23, 171

orbit radius, 79, 147
OSIRIS-REx, 9

parameter versal deformation
see L-F transformed system
versal deformation parameter, 103
see state augmented system
versal deformation parameter, 95
periodic
coefficients, 2
elements of LFT matrix, 98, 101, 111, 172
external excitation, 2
Poincaré map, 86
see gravity gradient stabilization
Poincaré map, 86
principle moments of inertia, 79, 140
PYSCHE, 9

resonance
see gravity gradient stabilization
resonance, 91

sigmoid function, 117
space systems
minimally excited, 3
operation, 2
perturbations, 2
spacecraft
see space systems, 9–11
see space systems, 3, 7
spacecraft angular velocity, 79
spherical harmonics models

second degree and order, 140, 149, 153
sectoral harmonics, 138
tesseral harmonics, 138
zonal harmonics, 138
stability chart
see gravity gradient stabilization stability chart, 90
see gravity gradient stabilization, stability chart, 87
state augmented system
bifurcation analysis, 93
Normal Forms, 93
closed form solution, 95
versal deformation, 93
limit cycle, 96
versal deformation parameter, 95
State Transition Matrix (STM), 82, 109
Stokes coefficients
seegravitational potential gravity field harmonic coefficients, 137
summary and discussions
Chapter 2, 70
Chapter 3, 106
Chapter 4, 130
Chapter 5, 166
Chapter 6, 185
switching function, 115, 119
system state augmentation, 3, 16, 171

TDNF, 27, 29, 103, 178
the potential, 135
TINF, 25, 29, 103, 126, 178
Titan , 9
Toutatis, 13
motion analysis, 150
true anomaly, 79

versal deformation
see gravity gradient stabilization versal deformation, 95, 103
see L-F transformed system versal deformation, 96
see state augmented system versal deformation, 93